

# **PHYSICO-CHEMICAL PROPERTIES OF POLYPROPYLENE GLYCOLS**

**BY**

**SALONI GUPTA [B.Sc. (Hons)]**

A thesis submitted in partial fulfilment of the requirements of the  
University of Greenwich for the Degree of Doctor of Philosophy

January, 2015

Department of Chemical, Pharmaceutical & Environmental Sciences  
Faculty of Engineering & Science,  
University of Greenwich (Medway Campus),  
Chatham Maritime,  
Kent ME4 4TB, UK



**UNIVERSITY  
of  
GREENWICH**

# DECLARATION

*I certify that this work has not been accepted in substance for any degree, and is not concurrently being submitted for any degree other than that of Doctor of Philosophy being studied at the University of Greenwich. I also declare that the work is the result of my own investigations except where otherwise identified by references and that I have not plagiarised the work of others.*

Saloni Gupta (Candidate):

.....

## **PhD Supervisors**

Dr A. P. Mendham:

Prof. S. A. Leharne:

Prof. B. Z. Chowdhry:

Date: January 15<sup>th</sup>, 2015

# ACKNOWLEDGEMENTS

I would like to express my sincere thanks to Prof. Stephen A. Leharne, Prof. Babur Z. Chowdhry and Dr Andrew P. Mendham for the invaluable guidance, support and encouragement they have given me as my supervisors throughout my PhD journey. They have always believed in me and encouraged me to do better.

I am indebted to everyone who has assisted and encouraged me in the course of my studies, particularly Prof. Peter Griffiths, Dr Samuel Owusu-Ware, Dr Milan Antonijevic, Dr Beatrice Cattoz and Dr Joanna Thorne. The technical support I have received from staff members, particularly, Devyani, Atiya, Mark Allen, Steve Williams and the Link laboratory technicians has been invaluable.

Most importantly thank you to my wonderful parents, my sisters (Sanya and Mannat) and my brother (Yatharth) for their love and encouragement. My parents are the two most hard-working people I know and they have been my inspiration and the driving force to complete this doctoral thesis. None of this would have been possible without them. My little sister Sanya has always set an example for me to never give up no matter what the circumstances are. I cannot thank my husband Sunny Goyal enough for his love, support and patience. He has always pushed me to perform better. I am grateful to all my friends and family who have supported me emotionally throughout this process.

I also believe that having the opportunity to undertake and complete this PhD has been a complete blessing from God. God has constantly blessed me with miracles when I thought I could not do it.

# ABSTRACT

## *Physico-chemical properties of polypropylene glycols*

Poly(propylene glycol) (PPG) samples of different molecular mass were characterized using differential scanning calorimetry, modulated differential scanning calorimetry, thermogravimetry and thermally stimulated current (TSC) spectroscopy. It was shown, by TSC, that the glass transition temperature and the degree of molecular mobility increased with increasing molecular mass of PPG. Additional experiments showed that PPGs of molecular mass 425, 1000 and 2000 Da undergo one global relaxation process; however, PPG 2700 (Da) undergoes an additional relaxation process after the glass transition which has been attributed either to the release of the excess charge delocalised in the polymer structure or a liquid-liquid transition.

Thermally induced phase separation in aqueous solutions of PPG has been examined using a variety of techniques including high sensitivity scanning calorimetry (HSDSC), hot stage microscopy, small angle neutron scattering, and turbidity measurements. The data suggest that phase separation is a consequence of PPG aggregation (droplets); the aggregates grow in size, as the temperature is raised further. It is postulated that phase separation occurs *via* nucleation and growth, which is corroborated by model fitting the calorimetric data using a mass action aggregation model. It is concluded that phase separation of PPG occurs as a result of the disruption of a hydrogen bonded network between water and PPG.

The effect of five sugars (mannitol, maltose, raffinose, sucrose and trehalose) on the  $T_m$  (transition temperature) of aqueous PPG 1000 solutions was studied by HSDSC and turbidity measurements. All the sugars decreased the phase separation temperature of the PPG solutions, with trehalose and maltose showing the greatest effect.

A series of experiments, using HPLC, showed that phase separated PPG (1000 Da) increased the apparent aqueous solubility of naphthalene.

*SALONI GUPTA [B.Sc. (Hons)]*

# OVERVIEW

Chapter 1 provides a brief background to the subject area of the research reported in the thesis and the project objectives.

Chapter 2 gives a general introduction to polymers, in particular PPG, and the phase-separation behaviour of PPG is discussed.

Chapter 3 provides the theory and the principles underlying the experimental techniques used in the research reported herein.

In Chapter 4 the experimental thermal properties of five different molecular weight PPG samples obtained using different techniques are discussed.

In Chapter 5 the experimental phase-separation behaviour of aqueous samples of PPG 1000, using different techniques, as a function of concentration, is reported and discussed.

In Chapter 6 the effect of the presence of five sugars, at different concentrations, on the phase-separation behaviour of aqueous PPG solutions is reported.

In Chapter 7 the use of aqueous PPG solutions as a solubilizing medium using a model hydrophobic compound, naphthalene, is reported.

# CONTENTS

<b>DECLARATION.....</b>	<b>II</b>
<b>ACKNOWLEDGEMENTS .....</b>	<b>III</b>
<b>ABSTRACT.....</b>	<b>IV</b>
<b>OVERVIEW.....</b>	<b>V</b>
<b>FIGURES.....</b>	<b>IX</b>
<b>TABLES.....</b>	<b>XVIII</b>
<b>ABBREVIATIONS AND SYMBOLS.....</b>	<b>XX</b>
<b>CONFERENCE/SEMINAR PRESENTATIONS AND PUBLICATIONS.....</b>	<b>XXVI</b>
Chapter 1 : Project Overview.....	1
1.1 Project Background.....	1
1.2 Project Objectives .....	5
Chapter 2 : Polymers and their Phase-Separation in Aqueous Solutions .....	8
2.1 Polymers.....	8
2.1.1 Classification of Polymers.....	8
2.1.2 Polymer Architecture.....	10
2.1.3 Molar Mass of Polymers.....	15
2.2 Glass-Transition and Melting: Important Polymer Properties .....	16
2.3 Poly(Propylene Glycol) (PPG).....	19
2.3.1 Properties .....	21
2.3.2 Applications.....	21
2.3.3 PPG as a Thermosensitive/Thermoresponsive Polymer.....	22
2.4 Thermodynamics of Phase-Separation in Polymer Solutions .....	22
2.4.1 Phase Diagrams .....	27
Chapter 3 : Principal Experimental Techniques: Theory, Instrumentation and Applications .43	
3.1 Introduction .....	43
3.2 Calorimetric Analysis.....	43
3.2.1 Definition of Calorimetry .....	43
3.2.2 Classification of Calorimeters .....	44
3.2.3 Differential Scanning Calorimetry .....	44
3.2.4 High Sensitivity Differential Scanning Calorimetry (HSDSC).....	46
3.3 Thermogravimetric Analysis (TGA).....	53
3.4 Hot Stage Microscopy (HSM).....	55

3.5 Thermally Stimulated Current (TSC) Spectroscopy .....	56
3.6 Turbidity Measurement (UV-Visible Spectrometer) .....	62
3.7 Dynamic Light Scattering (DLS) .....	65
3.8 Small Angle Neutron Scattering (SANS).....	68
3.9 High Performance Liquid Chromatography (HPLC).....	70
Chapter 4 : Study of Some Physical-Chemical Properties of Different Molecular Mass PPGs .....	76
4.1 Introduction .....	76
4.2 Experimental .....	76
4.2.1 Materials .....	76
4.2.2 Methods .....	77
4.2.2.1 Thermogravimetric Analysis .....	77
4.2.2.2 Differential Scanning Calorimetry.....	79
4.2.2.3 Thermally Stimulated Current Spectroscopy.....	80
4.2.2.4 High Sensitivity Differential Scanning Calorimetry.....	82
4.2.2.5 UV-Visible Spectroscopy .....	84
4.3 Results and Discussion.....	84
4.3.1 Thermogravimetric Analysis .....	84
4.3.2 Differential Scanning Calorimetry .....	86
4.3.3 Thermally Simulated Current Spectroscopy.....	89
4.3.4 High Sensitivity Differential Scanning Calorimetry .....	96
4.3.5 Turbidity Measurements using UV-Visible Spectrometry .....	102
4.4 Conclusions .....	104
Chapter 5 : Investigation of Phase Separation in Aqueous Solutions of PPG.....	106
5.1 Introduction .....	106
5.2 Experimental .....	107
5.2.1 Materials .....	107
5.2.2 Methods .....	107
5.2.2.1 High Sensitivity Differential Scanning Calorimetry.....	107
5.2.2.2 Hot Stage Microscopy.....	107
5.2.2.3 UV-Visible Spectroscopy .....	108
5.2.2.4 Small-Angle Neutron Scattering.....	108
5.2.2.5 Dynamic Light Scattering .....	109
5.3 Results and Discussion.....	109

5.3.1 High Sensitivity Differential Scanning Calorimetry .....	109
5.3.2 Hot Stage Microscopy .....	125
5.3.3 Turbidity Measurements using UV-Visible Spectrometer .....	127
5.3.4 Small-Angle Neutron Scattering .....	129
5.3.5 Dynamic Light Scattering.....	130
5.4 Data Analysis .....	131
5.5 Conclusions .....	141
Chapter 6 Effect of Sugars on the Phase-Transition Temperature of PPG.....	143
6.1 Introduction .....	143
6.1.1 Sugars and their Effect on the Dielectric Constant.....	148
6.2 Experimental .....	153
6.2.1 Materials .....	153
6.2.2 Methods .....	153
6.3 Results and Discussion.....	153
6.4 Conclusions .....	168
Chapter 7 : Use of PPG as a Solubilising Agent for Naphthalene.....	170
7.1 Introduction .....	170
7.2 Experimental .....	173
7.2.1 Materials .....	173
7.2.2 Methods .....	174
7.2.2.1 High Performance Liquid Chromatography .....	174
7.3 Results and Discussion.....	175
7.4 Conclusions .....	182
<b>CONCLUSIONS .....</b>	<b>183</b>
<b>FUTURE WORK.....</b>	<b>187</b>
<b>REFERENCES.....</b>	<b>189</b>
<b>APPENDICES .....</b>	<b>202</b>



# FIGURES

## Chapter 2

<b>Figure 2.1</b> A general classification of polymers. ....	8
<b>Figure 2.2</b> Basic structure of polymers (Qiu & Bae 2006). ....	11
<b>Figure 2.3</b> A sketch showing a linear drug-polymer conjugate (Qiu & Bae 2006). ....	14
<b>Figure 2.4</b> Types of micelles formed by linear block copolymer; .....	15
<b>Figure 2.5</b> Glass-transition temperatures upon heating and cooling of a sample using a plot of change in specific volume as a function of temperature. ....	18
<b>Figure 2.6</b> The change in specific volume of polymer with the temperature for (i) rapid cooling of the material (A-C-D), (ii) slow cooling (A-E-F) (Alfrey & Gurnee 1967). ....	19
<b>Figure 2.7</b> Structure of poly(propylene) glycol. ....	21
<b>Figure 2.8</b> A lattice model for solvent-solute (similar size) and for solvent-polymer molecules. ....	26
<b>Figure 2.9</b> Hydrogen bonding between PPG and water. ....	29
<b>Figure 2.10</b> Phase-separation model suggested by Carlsson et al (1991). ....	31
<b>Figure 2.11</b> A typical temperature-composition diagram showing the LCST and UCST for a weakly interacting polymer solution (Robeson 2007). ....	32
<b>Figure 2.12</b> Change in Gibbs free energy for the combination of pure A and pure B as a function of the change in composition. ....	33
<b>Figure 2.13</b> Change in entropy with the change in composition upon mixing of two components. ....	34
<b>Figure 2.14</b> Change in Gibbs free energy with composition upon mixing of the two components when $\Delta H_{mixing} = 0$ . ....	34

<b>Figure 2.15</b> Total Gibbs free energy of the solution as a function of composition when $\Delta H_{mixing} = 0$ .....	35
<b>Figure 2.16</b> Set of phase-diagrams showing the change in Gibbs free energy as a function of composition.....	37
<b>Figure 2.17</b> Change in Gibbs free energy at different temperatures as a function of composition showing the critical point, spinodal curve and the binodal curve. ....	37
<b>Figure 2.18</b> Phase-diagram showing stable, metastable and unstable regions as the Gibbs free energy changes at different temperatures as a function of the composition. ....	38
<b>Figure 2.19</b> Different phase-diagrams showing LCST, UCST and systems showing both LCST and UCST behaviour (Galaev & Mattiasson 2007). ....	39
<b>Figure 2.20</b> Large composition fluctuations (dotted line) in the metastable region of the phase-diagram. ....	40
<b>Figure 2.21</b> Small composition fluctuations (dotted line) in the unstable region of the phase-diagram. ....	41

## Chapter 3

<b>Figure 3.1</b> Classification of calorimeters. ....	44
<b>Figure 3.2</b> A typical DSC thermogram. ....	45
<b>Figure 3.3</b> A typical HSDSC output. ....	49
<b>Figure 3.4</b> Typical TGA output showing the thermal gravimetric or TG curve (navy plot) and the derivative thermal gravimetric or DTG curve (red plot).....	54
<b>Figure 3.5</b> Schematic of the response of molecules during a typical TSC spectroscopy experiment (Owusu-Ware 2013).....	57
<b>Figure 3.6</b> Typical TSC output obtained using TSDC.....	58
<b>Figure 3.7</b> Deflection of light beam by undissolved particles in a sample. ....	62

<b>Figure 3.8</b> Effect of the particle size on the scattering of an incident light beam (Brumberger, H., Stein, R.S., and Powell 1968). .....	62
<b>Figure 3.9</b> A sketch showing the effect of the presence of dispersed particles on the turbidity of a suspension and the light transmittance. ....	63
<b>Figure 3.10</b> A sketch showing the effect of the particle size on the intensity of fluctuation of the laser light using DLS.....	66
<b>Figure 3.11</b> A simple diagram showing the influence of the particle size on the scattering angle.....	70

## Chapter 4

<b>Figure 4.1</b> SETARAM TSC II calibration kit set up (SETERAM TSC II manual). ....	81
<b>Figure 4.2</b> Calibration results showing the onsets of crystallisation and melting processes (SETERAM TSC II manual). ....	81
<b>Figure 4.3</b> Derivative Thermogravimetric (DTG) curve overlay of different PPG samples heated from ambient temperature to 600°C at 10°C min <sup>-1</sup> . ....	85
<b>Figure 4.4</b> Thermogravimetric (TG) curve overlay of different PPG samples. ....	86
<b>Figure 4.5</b> Total heat flow using DSC for the five different PPG samples.....	88
<b>Figure 4.6</b> Reversing heat flow signal obtained using DSC for the five different PPG samples showing the glass transition which is under equilibrium control i.e. it is reversible.....	88
<b>Figure 4.7</b> Non-reversing heat flow signal obtained using DSC for the five different PPG samples showing that enthalpy relaxation is not reversible.....	89
<b>Figure 4.8</b> Global TSDC curve overlay of PPG 425, 1000, 2000 and 2700 polarized at -70°C with a polarizing field of 350 V mm <sup>-1</sup> . ....	90
<b>Figure 4.9</b> Plots of normalised polarization values against PPG molecular mass .....	92

<b>Figure 4.10</b> The TW results obtained for PPG 425 (left) and PPG 1000 (right), (a) the TW experimental output showing each discrete relaxation mode under the global TSDC output and (b) the distribution of relaxation times obtained for each TW experimental output.....	93
<b>Figure 4.11</b> The TW results obtained for PPG 2000 (left) and 2700 (right), (a) the TW experimental output showing each discrete relaxation mode under the global TSDC output and (b) the distribution of relaxation times obtained for each TW experimental output.....	94
<b>Figure 4.12</b> HSDSC output for the change in heat capacity for different molecular mass PPGs as a function of temperature.....	97
<b>Figure 4.13</b> Relationship between the optimised calorimetric enthalpy values and molecular mass of PPG, obtained using the model fitting procedure.....	99
<b>Figure 4.14</b> Relationship between the optimised van't Hoff enthalpy values and molecular mass of PPG, obtained using the model fitting procedure.....	100
<b>Figure 4.15</b> Relationship between the optimised $T_{1/2}$ values and molecular mass of PPG, obtained using the model fitting procedure. ....	100
<b>Figure 4.16</b> Relationship between the optimised heat capacity change values and molecular mass of PPG, obtained using the model fitting procedure.....	101
<b>Figure 4.17</b> Relationship between the optimised n values and molecular mass of PPG, obtained using the model fitting procedure. ....	101
<b>Figure 4.18</b> Increase in absorbance of PPG solutions with temperature. ....	102
<b>Figure 4.19</b> Cloud-point at the beginning of the phase-transition peak obtained from the HSDSC data.....	103
<b>Figure 4.20</b> Plot of cloud-points obtained using turbidity and HSDSC measurements.....	103

## Chapter 5

<b>Figure 5.1</b> HSDSC output for different concentrations of aqueous PPG solutions as a function of temperature.....	110
<b>Figure 5.2</b> HSDSC outputs for different concentrations of PPG solutions prepared in D <sub>2</sub> O as a function of temperature.....	113
<b>Figure 5.3</b> HSDSC data output for the reheating scans for 5 mg mL <sup>-1</sup> PPG in H <sub>2</sub> O and D <sub>2</sub> O solutions at 1°C min <sup>-1</sup> as a function of temperature.....	114
<b>Figure 5.4</b> The absence and presence of creaming in PPG in H <sub>2</sub> O and D <sub>2</sub> O solutions, respectively upon heating. ....	115
<b>Figure 5.5</b> HSDSC data for nine different PPG concentrations in water solutions upon heating at 1°C min <sup>-1</sup> . ....	116
<b>Figure 5.6</b> An example of a model fit for the HSDSC output for an aqueous PPG solution obtained using Scientist. ....	117
<b>Figure 5.7</b> Concentration dependence of PPG on the optimised aggregation number obtained using the model fitting procedure. ....	118
<b>Figure 5.8</b> Concentration dependence of PPG on the optimised van't Hoff enthalpy values obtained using the model fitting procedure. ....	119
<b>Figure 5.9</b> Concentration dependence of PPG on the optimised calorimetric enthalpy values obtained using the model fitting procedure. ....	119
<b>Figure 5.10</b> Relationship between the optimised values of T <sub>1/2</sub> and the heat capacity change values obtained for PPG, using the model fitting procedure. ....	120
<b>Figure 5.11</b> Relationship between the optimised van't Hoff enthalpy values and T <sub>1/2</sub> of PPG obtained using the model fitting procedure. ....	120

<b>Figure 5.12</b> Relationship between the optimised calorimetric enthalpy values and $T_{1/2}$ of PPG obtained using the model fitting procedure. ....	121
<b>Figure 5.13</b> Relationship between the optimised van't Hoff enthalpy values and $T_{1/2}$ of PPG in $D_2O$ solutions obtained using the model fitting procedure. ....	122
<b>Figure 5.14</b> Relationship between the optimised calorimetric enthalpy values and $T_{1/2}$ of PPG in $D_2O$ solutions obtained using the model fitting procedure. ....	123
<b>Figure 5.15</b> Concentration dependence of the optimised van't Hoff enthalpy values of PPG in $D_2O$ solutions obtained using the model fitting procedure. ....	123
<b>Figure 5.16</b> Concentration dependence of the optimised calorimetric enthalpy values of PPG in $D_2O$ solutions obtained using the model fitting procedure. ....	124
<b>Figure 5.17</b> Concentration dependence of the optimised aggregation number of PPG in $D_2O$ solutions obtained using the model fitting procedure. ....	124
<b>Figure 5.18</b> Relationship between the optimised heat capacity values and $T_{1/2}$ of PPG in $D_2O$ solutions obtained using the model fitting procedure. ....	125
<b>Figure 5.19</b> Hot stage microscopy images obtained for $20 \text{ mg mL}^{-1}$ aqueous PPG solution when heated at $1^\circ\text{C min}^{-1}$ . ....	126
<b>Figure 5.20</b> Graph of absorbance against temperature for a number of solutions with different PPG concentrations to measure the cloud-point of the solutions. ....	127
<b>Figure 5.21</b> Absorbance change with temperature for PPG solutions in different solvents. ....	128
<b>Figure 5.22</b> Plots for cloud points using two techniques: HSDSC and turbidity (UV-Visible spectroscopy). ....	128
<b>Figure 5.23</b> SANS plot for $20 \text{ mg mL}^{-1}$ PPG solution in a mixture of 80% $D_2O$ and 20% $H_2O$ at 6 different temperatures. ....	129
<b>Figure 5.24</b> Size of particles as a function of temperature for $1 \text{ mg mL}^{-1}$ and $2 \text{ mg mL}^{-1}$ aqueous PPG solutions. ....	130

<b>Figure 5.25</b> Cloud point data showing a plot of temperature at which phase separation is first detected optically. ....	134
<b>Figure 5.26</b> Fit of the computed $\alpha$ values to the temperature (cloud-point) data.....	135
<b>Figure 5.27</b> Plot of simulated HSDSC signal using the cloud-point data (solid line) and the actual HSDSC data (dashed line) obtained at 30 mg mL <sup>-1</sup> (in black), 15 mg mL <sup>-1</sup> (in red) and 5 mg mL <sup>-1</sup> (in blue). ....	136
<b>Figure 5.28</b> Plot of phase-separated PPG ( $\alpha$ ) as a function of temperature for different concentrations of PPG (dashed lines) along with the cloud-point curve (solid line).....	138
<b>Figure 5.29</b> HSDSC simulations (solid line) for 15 mg mL <sup>-1</sup> (in red) and 30 mg mL <sup>-1</sup> (in black) using 5 mg mL <sup>-1</sup> (in blue) (the original HSDSC data is shown in dashed line). ....	139
<b>Figure 5.30</b> HSDSC simulations (solid line) for 5 mg mL <sup>-1</sup> (in blue) and 30 mg mL <sup>-1</sup> (in black) using 15 mg mL <sup>-1</sup> (in red) (the original HSDSC data is shown in dashed line). ....	140
<b>Figure 5.31</b> HSDSC simulations (solid line) for 5 mg mL <sup>-1</sup> (in blue) and 15 mg mL <sup>-1</sup> (in red) using 30 mg mL <sup>-1</sup> (in black) (the original HSDSC data is shown in dashed line).....	140

## Chapter 6

<b>Figure 6.1</b> Hofmeister series showing typical ordering of the anion series and some of its related properties (Zhang & Cremer 2006).....	145
<b>Figure 6.2</b> Change in heat capacity of 10 mg mL <sup>-1</sup> PPG solution with the change in the mannitol concentration.....	154
<b>Figure 6.3</b> Change in heat capacity of 10 mg mL <sup>-1</sup> PPG solution with the change in the maltose concentration. ....	154
<b>Figure 6.4</b> Change in heat capacity of 10 mg mL <sup>-1</sup> PPG solution with the change in the sucrose concentration.....	155
<b>Figure 6.5</b> Change in heat capacity of 10 mg mL <sup>-1</sup> PPG solution with the change in the trehalose concentration. ....	155

<b>Figure 6.6</b> Change in heat capacity of 10 mg mL <sup>-1</sup> PPG solution with the change in the raffinose concentration.....	156
<b>Figure 6.7</b> Change in the T <sub>m</sub> of 10 mg mL <sup>-1</sup> PPG solution upon addition of sugars at different concentrations. ....	159
<b>Figure 6.8</b> Change in absorbance of the cloud-point data for different concentrations of maltose in 10 mg mL <sup>-1</sup> aqueous PPG solution as a function of temperature. ....	160
<b>Figure 6.9</b> Change in absorbance of the cloud-point data for different concentrations of mannitol in 10 mg mL <sup>-1</sup> aqueous PPG solution as a function of temperature. ....	160
<b>Figure 6.10</b> Change in absorbance of the cloud-point data for different concentrations of sucrose in 10 mg mL <sup>-1</sup> aqueous PPG solution as a function of temperature. ....	161
<b>Figure 6.11</b> Change in absorbance of the cloud-point data for different concentrations of trehalose in 10 mg mL <sup>-1</sup> aqueous PPG solution as a function of temperature. ....	161
<b>Figure 6.12</b> Change in absorbance of the cloud-point data for different concentrations of raffinose in 10 mg mL <sup>-1</sup> aqueous PPG solution as a function of temperature. ....	162
<b>Figure 6.13</b> Change in the cloud-point obtained using turbidity and HSDSC measurements of the aqueous PPG solutions with the addition of different concentrations of sugars.....	164
<b>Figure 6.14</b> Amount of phase-separated PPG ( $\alpha$ ) for different sugars with the change in the total sugar concentration. ....	167

## Chapter 7

<b>Figure 7.1</b> Structure of naphthalene. ....	171
<b>Figure 7.2</b> Data obtained for naphthalene solubilisation in 1 mg mL <sup>-1</sup> solution of PPG.....	176
<b>Figure 7.3</b> Data obtained for naphthalene solubilisation in 3 mg mL <sup>-1</sup> solution of PPG. The data point at 30°C is part of the low temperature pre-phase separation data.....	176
<b>Figure 7.4</b> Data obtained for naphthalene solubilisation in 5 mg mL <sup>-1</sup> solution of PPG. The data point at 70°C was treated as an outlier. ....	177



**Figure 7.5** A simulated output for the effect of temperature on the apparent aqueous solubility of naphthalene in the two-phase system for 1 mg mL<sup>-1</sup> PPG solution using the two-state aggregation model. .... 180

# TABLES

## Chapter 2

<b>Table 2.1</b> Classification of polymers and their general properties (Nicholson, 2012).....	9
<b>Table 2.2</b> Polymer classification and their general pharmaceutical properties (Qiu & Bae, 2006). .....	12
<b>Table 2.3</b> Experimental methods to determine the average relative molar mass of polymers (Nicholson, 2012). .....	16
<b>Table 2.4</b> Some general characteristics of PPG (Burdock, 1997; Cheremisinoff, 2003).....	21

## Chapter 3

<b>Table 3.1</b> Characteristics of different types of polarisations upon application of $E_p$ .....	58
<b>Table 3.2</b> Comparison of the major techniques used in this research. ....	73

## Chapter 4

<b>Table 4.1</b> Some properties of different molecular mass PPGs .....	77
<b>Table 4.2</b> The peak temperatures for the weight loss change for different PPG samples upon heating.....	86
<b>Table 4.3</b> Change in the enthalpy relaxation and $T_g$ with the change in the molecular mass of PPGs.....	89
<b>Table 4.4</b> Glass transition temperatures obtained for PPG 425, 1000, 2000 and 2700 by DSC and TSC .....	96

## Chapter 5

<b>Table 5.1</b> Change of $T_m$ with the change in concentration of PPG in water solution.....	112
<b>Table 5.2</b> Change of $T_m$ with the change in the PPG concentration in the presence of $D_2O$ ....	113
<b>Table 5.3</b> HSDSC parameters obtained for aqueous solutions of PPG as a function of concentration.....	118
<b>Table 5.4</b> HSDSC parameters obtained for aqueous PPG solutions in $D_2O$ as a function of concentration.....	122

## Chapter 6

<b>Table 6.1</b> Physiochemical properties of the investigated sugars.....	151
<b>Table 6.2</b> Effect of different sugars in varying concentrations on $T_m$ of aqueous PPG solution .....	158
<b>Table 6.3</b> Cloud-points measured using turbidity for different sugar concentrations in PPG solutions. ....	163
<b>Table 6.4</b> Cloud-points measured using data obtained from HSDSC for different sugar concentrations in PPG solutions. ....	164
<b>Table 6.5</b> Change in aggregation number with the change in sugar concentration in aqueous PPG solutions.....	166
<b>Table 6.6</b> Change in $\alpha$ value for different sugars with the change in the sugar concentration. .....	167

## Chapter 7

<b>Table 7.1</b> Apparent naphthalene concentration in aqueous PPG solutions as a function of PPG concentration and temperature.....	175
---	-----

# ABBREVIATIONS AND SYMBOLS

<b>Abbreviation</b>	<b>Meaning</b>
<b>ACN</b>	Acetonitrile
<b>ATP</b>	Adenosine triphosphate
<b>ASTM</b>	American Society for Testing and Materials
<b>BHT</b>	Butylated hydroxytoluene
<b>CP</b>	Cloud point
<b>CMC</b>	Critical micelle concentration
<b>DP</b>	Degree of polymerisation
<b>DNA</b>	Deoxyribonucleic acid
<b>DTG/TG</b>	Derivative thermogravimetric/thermogravimetric
<b>DSC</b>	Differential scanning calorimetry
<b>DMSO</b>	Dimethyl sulfoxide
<b>DLS</b>	Dynamic light scattering
<b>EPR</b>	Enhanced permeation and retention
<b>EO</b>	Ethylene oxide
<b>GPC</b>	Gel-permeation chromatography
<b>GRAS</b>	Generally recognized as safe
<b>gP</b>	Glycoprotein
<b>HPLC</b>	High performance liquid chromatography
<b>HVLP</b>	High volume low pressure
<b>HSDSC</b>	High-sensitivity differential scanning calorimetry
<b>HSM</b>	Hot-stage microscopy
<b>HLB</b>	Hydrophile-lipophile balance
<b>HOC</b>	Hydrophobic organic compound
<b>IPN</b>	Interpenetrating polymer networks
<b>LCST</b>	Lower critical solution temperature
<b>MDSC</b>	Modulated differential scanning calorimetry
<b>MSR</b>	Molar solubilisation ratio
<b>MDR</b>	Multi-drug resistant
<b>NDI</b>	Naphthalenediimide
<b>NMR</b>	Nuclear magnetic resonance

<b>PCS</b>	Photon correlation spectroscopy
<b>PEG</b>	Poly(ethylene glycol)
<b>PEO</b>	Poly(ethylene oxide)
<b>PPG</b>	Poly(propylene glycol)
<b>PPO</b>	Poly(propylene oxide)
<b>PEI</b>	Polyethylenimine
<b>PIC</b>	Polyion complex
<b>PNIPA</b>	Poly- <i>N</i> -isopropylacrylamide
<b>PTFE</b>	Polytetrafluoroethylene
<b>PO</b>	Propylene oxide
<b>QELS</b>	Quasi-elastic light scattering
<b>RID</b>	Refractive index detector
<b>RCS</b>	Refrigerated cooling system
<b>RES</b>	Reticuloendothelial system
<b>SANS</b>	Small-angle neutron scattering
<b>THF</b>	Tetrahydrofuran
<b>TM</b>	Thermal microscopy
<b>TW</b>	Thermal windowing
<b>TIPS</b>	Thermally induced phase-separation
<b>TMDSC</b>	Thermally modulated differential scanning calorimetry
<b>TSC</b>	Thermally stimulated current
<b>TSDC</b>	Thermally stimulated depolarisation current
<b>TGA</b>	Thermogravimetric analysis
<b>UV-Visible</b>	Ultraviolet-Visible
<b>UCST</b>	Upper critical solution temperature
<b>VWD</b>	Variable wavelength detector

<b>Symbol</b>	<b>Meaning</b>
<b>e</b>	Absorptivity
<b>n</b>	Aggregation number
<b>C<sub>P,xs</sub></b>	Apparent excess heat capacity
<b>S<sub>aq</sub></b>	Aqueous saturated solubility of naphthalene

<b>G<sub>2</sub></b>	Autocorrelation function
<b>A</b>	Background term designated as the baseline value
<b>k</b>	Boltzmann's constant
<b>ΔH<sub>cal</sub></b>	Calorimetric enthalpy
<b>ΔH</b>	Change in enthalpy
<b>ΔT</b>	Change in temperature
<b>ΔQ</b>	Change in the heat
<b>μ<sup>0</sup>X<sub>n</sub></b>	Chemical potential of aggregates in pure state
<b>μ<sup>0</sup>X</b>	Chemical potential of unimers in pure state
<b>μ<sub>X</sub></b>	Chemical potential of unimers in solution
<b>μ<sub>X<sub>n</sub></sub></b>	Chemical potential of aggregates in solution
<b>[X<sub>n</sub>]</b>	Concentration of n unimer aggregates
<b>[X]<sup>n</sup></b>	Concentration of unimeric chains
<b>T<sub>c</sub></b>	Crystallisation temperature
<b>Γ</b>	Decay constant
<b>I(T)</b>	Depolarisation current
<b>D</b>	Diameter of particles
<b>q</b>	Difference in the magnitude of charge between either ends of dipole
<b>D</b>	Diffusion coefficient
<b>α</b>	Dimensionless particle size parameter
<b>d</b>	Distance between the centres of positive and the negative charge.
<b>μ</b>	Electric dipole moment
<b>δ</b>	Electronegativity
<b>ΔH<sub>mixing</sub></b>	Enthalpy of mixing
<b>S</b>	Entropy
<b>ΔS<sub>mixing</sub></b>	Entropy of mixing
<b>K</b>	Equilibrium constant
<b>K<sub>p</sub></b>	Equilibrium constant or partition coefficient for the equilibrium distribution of naphthalene between water and the separated PPG phase
<b>P<sub>e</sub></b>	Equilibrium polarisation at infinite time
<b>T<sub>f</sub></b>	Final temperature upon heating of the sample
<b>k<sub>f</sub></b>	Final wavevector
<b>χ<sub>AB</sub></b>	Flory-Huggins interaction parameter

$\Delta G_{dil,A}$	Free energy of dilution of molecules A
$\Delta G_{mixing}$	Free energy of mixing
$G_B$	Free energy of molecules B
$G_A$	Free energy of molecules A
$G_2$	Free energy of solute
$G_1$	Free energy of solvent
$R$	Gas constant
$T_M$	Glass transition temperature obtained by TSC
$T_g$	Glass-transition temperature obtained by DSC
$T_g'$	Glass-transition temperature when polymer is heated from glassy-state
$\Delta C_P$	Heat capacity change
$C_P$	Heat capacity of the system at constant pressure
$T_i$	Initial temperature
$k_i$	Initial wavevectors
$B$	Instrument-dependent factor
$I_0$	Intensity of the incident light
$I$	Intensity of the transmitted light
$l$	Length of the optical path
$\beta$	Linear heating rate
$T_m$	Melting-point temperature
$q$	Modulus of the scattering vector
$M_i$	Molar mass of the molecular species i
$n_A$	Mole fraction of A
$n_B$	Mole fraction of B
$X_A$	Mole fraction of molecules A
$X_B$	Mole fraction of molecules B
$x_2$	Mole fraction of solute
$x_1$	Mole fraction of solvent
$n_{PPG}$	Mole of phase separated PPG
$Q$	Momentum transfer
$G_1$	First order autocorrelation function
$M_n$	Number Average molar mass
$W$	Number of different arrangements of arranging molecules in the lattice

$N_A$	Number of molecules of A
$N_B$	Number of molecules of B
$N_i$	Number of molecules of i
$N$	Number of scattering particles per unit volume
$T_m$	Phase-transition temperature
$T_p$	Polarisation temperature
$r$	Radius of the particles
$m$	Ratio of the refractive index of the particles and the medium
$C_{ref}$	Reference concentration
$T_{ref}$	Reference temperature
$n$	Refractive index of the dispersion medium
$n_m$	Refractive index of the medium
$n_p$	Refractive index of the particles
$\tau$	Relaxation time
$P(t)$	Remaining polarization at time t
$I$	Scattered intensity
$\theta$	Scattering angle
$E_p$	Static electric field
$T$	Temperature
$T_d$	Temperature a few degree below polarisation temperature
$T_o$	Temperature at quench cooling of dipoles
$T_{1/2}$	Temperature at which half the molecules have formed a separate phase
$T_w$	Temperature of thermal windowing experiments
$S^*$	The apparent aqueous solubility of naphthalene in the aqueous two-phase system
$d$	The apparent Stokes-Einstein particle diameter
$\alpha$	The extent of conversion of unimeric polymer chains into aggregates
$S_{PPG}$	The solubility of naphthalene in the separated PPG phase
$t$	Time
$t_w$	Time for which the sample is held isothermal without any external electric field
$t_w$	Time of windowing
$t_p$	Time static electric field is applied for
$t$	Time-of-flight



$C_{\text{Total}}$	Total concentration
$C$	Total concentration of the polymer
$L$	Total flight path
$Q$	Total Mie scattering coefficient
$N$	Total number of sites in the lattice
$D_T$	Translational diffusion coefficient
$\tau$	Turbidity
$\Delta H_{vH}$	van't Hoff enthalpy
$pA^\circ$	Vapour pressure of A in pure state
$pA$	Vapour pressure of substance A in a solution
$t'$	Very small time interval
$\eta$	Viscosity
$V$	Volume
$\Phi_A$	Volume fraction of A
$\Phi_B$	Volume fraction of B
$V_A$	Volume occupied by each molecule of A
$V_B$	Volume occupied by each molecule of B
$V_W$	Volume of water
$\lambda_m$	Wavelength of the incident light in the dispersion medium
$\lambda_0$	Wavelength of the incident light in vacuum
$\lambda$	Wavelength of the incident neutron beam
$M_w$	Weight average molar mass
$M_z$	z-Average molar mass

# CONFERENCE/SEMINAR PRESENTATIONS AND PUBLICATIONS

## Conference/Seminar Presentations

**Title** Characterization of Poly(propylene glycol) and analysis of its phase-separation behaviour

**Conference** CALCON The 69<sup>th</sup> North American Calorimetry Conference, July 6<sup>th</sup>-10<sup>th</sup>, 2014, Santa Fe, New Mexico, USA.

**Type** Oral Presentation

**Title** Characterization of Poly(propylene glycol)s

**Conference** Second faculty research symposium, 24<sup>th</sup> June, 2014

**Type** Poster Presentation

**Title** Characterization of aqueous solutions of Poly(propylene glycol)

**Conference** Second faculty research symposium, 24<sup>th</sup> June, 2014

**Type** Poster Presentation

**Title** Analysis of the phase-transition behaviour of poly(propylene glycol)

**Conference** PhD Lunch Time Research Seminar, 26<sup>th</sup> June, 2013

**Type** Oral Presentation

## Publications

**Title:** A high-sensitivity differential scanning calorimetry (HSDSC) study of phase-separation behaviour of aqueous poly(propylene glycol) (PPG) solution

**Authors:** Saloni Gupta, Babur Z. Chowdhry, Peter C Griffiths, Beatrice Cattoz, Andrew P. Mendham and Stephen A. Leharne,

**Status:** In progress (Jan. 2015)

**Title:** Physico-chemical characterisation of different molecular mass poly(propylene glycols) (PPGs) in pure and solution states

**Authors:** Saloni Gupta, Samuel K. Owusu-Ware, Babur Z. Chowdhry, Stephen A. Leharne, Andrew P. Mendham and Milan D. Antonijevic

- Status:** In progress (Jan. 2015)
- Title:** Thermally stimulated current (TSC) study of the influence of molecular weight on the glass-transition behaviour poly(propylene glycol) (PPG)
- Authors:** Samuel K. Owusu-Ware, Saloni Gupta, Babur Z. Chowdhry, Stephen A. Leharne, Andrew P. Mendham and Milan D. Antonijevic
- Status:** In progress (Jan. 2015)
- Title:** Study of the effect of different sugars on the phase-separation behaviour of aqueous poly(propylene glycol) (PPG) solution.
- Authors:** Saloni Gupta, Andrew P. Mendham, Babur Z. Chowdhry and Stephen A. Leharne
- Status:** In progress (Jan. 2015)
- Title:** Study of the use of phase-separated aqueous poly(propylene glycol) (PPG) in the solubilisation of naphthalene.
- Authors:** Saloni Gupta, Babur Z. Chowdhry, Andrew. P. Mendham and Stephen A. Leharne
- Status:** In progress (Jan. 2015)

## Chapter 1 : Project Overview

### 1.1 Project Background

Folkman and Long, in 1964, discovered that small hydrophobic drug molecules diffuse at a controlled rate through silicon tubing which then revolutionised the use of polymer systems for controlled drug release (Freiberg & Zhu 2004). Since then, polymers have been utilised in drug and gene delivery for example in the form of films, tablets, microspheres and implantation devices. Polymeric micelles are becoming increasingly popular for use as vehicles for the delivery of therapeutic and diagnostic agents (Alivisatos 1996; Sutherland 2002). They are preferred over the traditional surfactants because the CMC of polymeric micelles is in the order of  $10^{-7}$  to  $10^{-6}$  M while that of surfactant molecules is in the order of  $10^{-4}$  to  $10^{-3}$  M (Rijcken et al. 2007). This suggests that polymeric micelles are less prone to dissociation at low concentrations (for example, with blood volume upon intravenous administration) (Torchilin 2001) and so they have longer circulation times in the body and hence greater bioavailability. Their size is similar to the size of many natural carriers such as viruses and serum lipoproteins, which make these particles easily recognizable in the body and enhances their interaction with specific cells in the body. These materials include polymer micelles, polymer-DNA complexes, nanogels and liposomes which are, all collectively, designated “nanomedicines” (Batrakova & Kabanov 2008). Polymer therapeutics is another term commonly used for linear or branched polymer chains acting either as a bioactive (a polymeric drug) or an inert carrier to which the drug is covalently attached (Liechty et al. 2010). These materials offer increased bioavailability of the drug, improved release kinetics and intracellular transport. They can exhibit temporal control which aims to achieve pre-determined drug release kinetics and spatial distribution control; the purpose being targeted drug delivery in the body. Most of the polymer conjugates are designed for anticancer therapeutics but some other diseases have also been targeted including rheumatoid arthritis, diabetes, ischemia and hepatitis B and C (Liechty et al. 2010).

Their popularity in cancer drug delivery is due to the passive tumour targeting phenomenon, first stated by Maeda and Matsumura, called enhanced permeation and retention (EPR) (Maeda & Matsumura 1988). It has been shown that when anticancer drugs are transported as polymer conjugates, they accumulate in tumour cells by up to 70-fold compared with “normal” cells (Liechty et al. 2010). They can help to circumvent the reticuloendothelial system (RES), renal clearance and other natural defence mechanisms in the body which is of considerable interest for drug delivery purposes (Batrakova & Kabanov 2008). Conjugation of polypeptide drugs with some synthetic polymers is known to improve many biological properties of drugs such as bioavailability, cell adhesion, stability, dissolution and plasma half-lives.

## Rationale

Pluronics are amphiphilic ABA block copolymers comprising of two ethylene oxide (EO), A, blocks separated by a central propylene oxide (PO), B, block. They are used in a wide variety of industrial formulations/processes and are becoming increasingly popular for the formulation of drug delivery systems. Structurally they may be described by the following formula  $EO_y-PO_x-EO_y$ , where y has a chain length of 2-130 EO units and x from 16-70 PO units (Kabanov et al. 2002). The amphiphilic pluronic copolymers can be characterized by their hydrophile-lipophile balance (HLB). This is determined by the relative sizes of the EO and PO blocks and determines their potential to interact with hydrophobic surfaces and biomembranes. The most widely investigated copolymers are the tri-block copolymers PEO-PPO-PEO consisting of two polyethylene oxide (PEO) (also called poly(ethylene glycol) PEG) chains and a poly(propylene oxide) (PPO) (also called poly(propylene glycol) PPG) chain (Kabanov et al. 2002). They are also called poloxamers. These copolymers form aggregates that can be rod-like, spherical, ellipsoidal or cylindrical depending on the concentration, the temperature, the molecular weight and the ratio of the EO and PO blocks in the copolymer (Kadam et al. 2011). In aqueous solutions (water) the core of the micelles/aggregates is occupied by the hydrophobic PPG chain

and the shell consists of hydrated, hydrophilic PEG chains. The core of these micelles can act as a “cargo hold” for the insertion of hydrophobic therapeutic agents, usually in amounts of 20-30% by weight (Batrakova & Kabanov 2008). The shell prevents any interaction between the drugs inserted inside the core and the proteins and other cell components outside these micelles, leading to the relatively high bioavailability of these drugs inside cells of the body. The critical micelle concentration (CMC) is a concentration above which amphiphilic molecules begin to self-associate to form aggregates termed micelles. The CMC for these block copolymers is temperature dependent and it decreases with an increase in temperature.

More recently these block copolymers have been used to increase the therapeutic effectiveness of many anticancer agents such as carboplatin, camptothecin, paclitaxel, and cisplatin since once translocated into the cell, they affect various cellular functions including mitochondrial respiration, ATP synthesis, and drug efflux transporters (Zahedi et al. 2012). All these effects are the result of the unimers (non-aggregated polymer chains) which exist below the CMC. The first anti-cancer micellar formulation to reach clinical evaluation was SP1049C which comprises of pluronics L61 and F127 containing the drug doxorubicin (Dox) in the mixed micelles of these pluronics. The pharmacokinetic and the biodistribution data obtained demonstrated more efficient accumulation of the micellar drug in the tumour cells compared with the free drug (Batrakova & Kabanov 2008). Another study reported increased carboplatin toxicity, in experimental carcinoma, of the drug in micelles constituted of pluronic L61 and P85 compared with the free drug (Krupka et al. 2007).

A good understanding of the micellisation process is necessary to enable the use of any block copolymers, or polymers, for drug delivery purposes. The micellisation process is entropy-driven and involves the dehydration of the PPG chains at elevated temperatures. The dehydration of the PPG leads to an increase in hydrophobicity, which results in the aggregation of the PPG blocks, whilst at the same time the PEG chains remain hydrophilic. However, with

any further increase in temperature PEG chains become dehydrated which leads to phase separation. Phase separation is detected as a clouding phenomenon (Inoue & Yamashita 2006). Therefore, the sequence of transformation is unimer  $\rightarrow$  micelle  $\rightarrow$  phase separation.

The aim of this study is to closely study the aggregation behaviour of PPG chains without any hydrophilic attachments (unlike the presence of hydrophilic PEG chains in poloxamers) since PPG might be the driving force for the micellisation process. The aggregation behaviour of poly(propylene oxide) (PPO) with positive charges at both ends has been investigated in aqueous solution; the positive charges were produced by protonation of terminal  $\text{NH}_2$  groups attached to the polymer composed of 33 PO units. It was found that the aggregation behaviour is quite sensitive to temperature. At low temperature, the polymer dissolves in water as a unimer. When temperature is increased, the unimer solution undergoes a phase separation to give a turbid solution. Further increase in temperature produces a transparent micellar solution (Inoue & Yamashita 2006). This behaviour is similar to that of pluronic L62 reported by Bahadur and co-workers. They reported two cloud-points for aqueous L62 solutions. The first cloud-point reported in aqueous solutions of L62 is due to the presence of polydispersity and, because the short PPG chains are unable to form micelles when heated, they phase separate. The second cloud-point, however, is due to the dehydration of PEG chains (Inoue & Yamashita 2006; Zahedi et al. 2012). However, PPG containing terminal  $\text{NH}_2$  groups has only one cloud point due to the absence of PEG chains. Apart from the foregoing research, researchers have studied systems with PPG 400 +  $(\text{NH}_4)_2\text{SO}_4$  in water (Kato et al. 1990), PPG 425 in NaCl at three different temperatures and PPG 725 in NaCl at two different temperatures (Cheluget et al. 1994). Zafarani-Moattar et al., examined the liquid-liquid equilibria data for aqueous PPG in the presence of tri-potassium citrate at different temperatures (Zafarani-Moattar et al. 2008). The effect of sodium di-hydrogen phosphate on aqueous PPG system has also been studied (Sadeghi & Jamehbozorg 2008). Many other research studies have been conducted by other

researchers in order to examine the phase-separation of PPG by the addition of salts or other moieties but the phase-separation of PPG solutions in water with changing temperature has not, to date, been examined in detail.

Previous researchers have reported the use of pluronics in promoting drug penetration across cell membranes (Kabanov et al. 1992; Slepnev et al. 1992), the blood-brain barrier (Kabanov et al. 1989) and skin. It has been shown that pluronics L61 and P85 enhance the sensitivity of multi-drug resistant (MDR) cells. L61 and P85 have hypersensitizing effect on cytotoxic effect of doxorubicin and daunorubicin in MDR cells respectively (Alakhov et al. 1996; Venne et al. 1996). Melik-Nubarov et al., suggested that the ability of pluronics to bind to cell membranes results in the promotion of drug penetration across biological barriers. They examined the binding to cells of two copolymers, P85 and L61, and showed that pluronic L61 with higher hydrophobic PPG content bounds to cells 1.5-2.5 times better than pluronic P85 with a higher hydrophilic, PEG, content (Melik-Nubarov et al. 1999). This difference in binding abilities of the two different pluronics to the cell membrane is because of the difference in their hydrophobicities (HLB index). Their findings were comparable to the work undertaken by other researchers suggesting the greater therapeutic effect of L61 compared with P85 (Batrakova et al. 1996). This suggests that PPG greatly enhances the binding of drugs to certain cells and hence the current research is aimed at analysing the physico-chemical properties and phase-separation behaviour of PPG and investigating its potential as a solubilizing agent, as PPG might have the potential to be used for drug delivery purposes.

## 1.2 Project Objectives

The research reported herein has the following objectives.

- Since a detailed study of the physico-chemical properties of PPG is missing in the scientific literature, a study has been conducted on the thermal properties of pure PPG



samples of different molecular weight using three different techniques: thermogravimetric analysis (TGA), differential scanning calorimetry (DSC) and thermally stimulated depolarisation current (TSDC) spectroscopy (including thermal windowing (TW)). A study was also performed to analyse the effect of the molecular weight of PPG on the phase-transition temperature ( $T_m$ ) of aqueous solutions of PPGs using high sensitivity differential scanning calorimetry (HSDSC) together with turbidity measurements undertaken using UV-Visible spectroscopy to measure cloud-points of PPG solutions.

- As a result of changes in temperature, PPGs in pluronics are the cause of micellisation. So, an investigation to study the phase-separation behaviour of PPG becomes necessary. The phase-separation of one PPG (out of the five different molecular PPGs) as a function of temperature and concentration has been studied in more detail. The foregoing studies were undertaken-using HSDSC together with turbidity measurements, dynamic light scattering (DLS), small angle neutron scattering (SANS) and hot stage microscopy (HSM)-to help investigate the mechanism of phase-separation in detail.
- The effect of five different sugars on the phase separation of PPG has been investigated. Sugars decrease the phase-transition temperature of PPG solutions. To formulate a drug in the body, the aggregates encapsulating a drug need to be stable at room temperature and hence sugars were used to reduce the phase-transition temperature of aqueous PPG solutions. The effect of different sugars as a function of varying concentration of sugar and temperature was investigated using HSDSC studies together with turbidity data obtained using turbidity measurements.

- Solubilisation of hydrophobic drugs is a major issue in the pharmaceutical industry.

Use of aqueous PPG as a solubilizing agent to increase the solubility of a model hydrophobic compound, naphthalene, was examined using HPLC measurements.

## Chapter 2 : Polymers and their Phase-Separation in Aqueous Solutions

### 2.1 Polymers

A polymer is a large molecule composed of various smaller units called monomers. The word polymer is derived from two Greek words, ‘poly’ meaning many and ‘meros’ meaning part (Gedde 1995). The term polymerism when originated applied to molecules with identical empirical formulae but different chemical and physical properties. In the 1920’s, Herman Staudinger introduced another term ‘macromolecule’ which is another Greek word meaning a ‘large molecule’ which is now interchangeably used with the word polymer (Nicholson 2012). Polymers can be linear, branched or have a highly interconnected three-dimensional network. The size of the polymer can be defined by its mass or the degree of polymerisation (number of repeat units in that polymer). The relative molar mass of a polymer can be calculated by multiplying the relative molar mass of the monomer and its degree of polymerisation (DP). Generally molecules with a relative molar mass of 1000 Da or above or a DP of 1000 or above are considered to be polymers (Nicholson 2012).

#### 2.1.1 Classification of Polymers

Polymers are classified into different types and subtypes (Fig. 2.1 and Table 2.1).

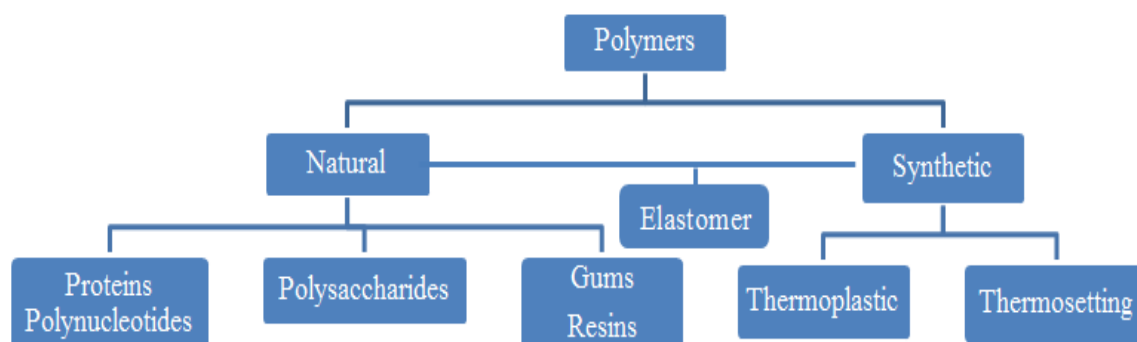


**Figure 2.1** A general classification of polymers.

**Table 2.1** Classification of polymers and their general properties (Nicholson 2012).

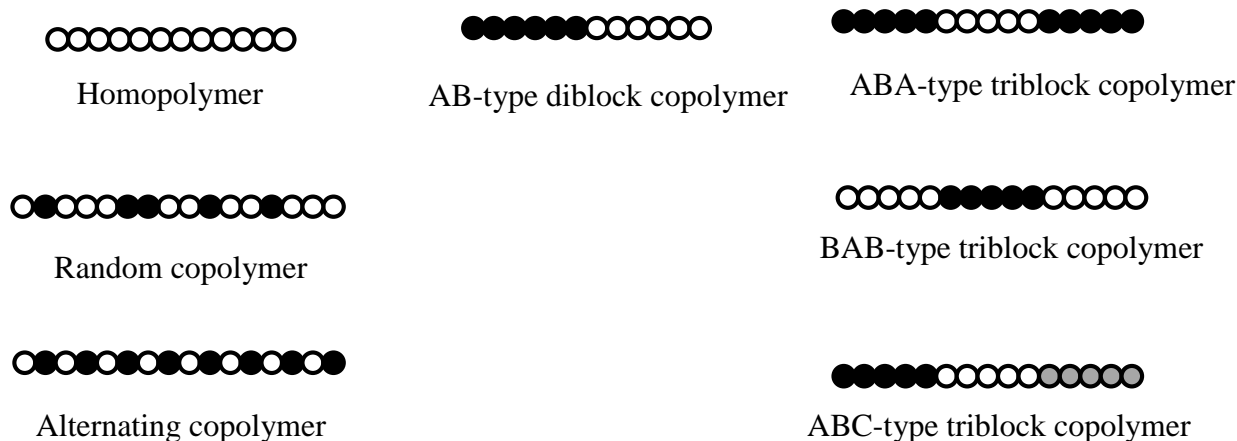
<b>On the basis of thermal treatment</b>		
<b>Thermoplastics</b>	<b>Thermosets</b>	
They melt when heated and re-solidify when cooled.	Do not melt when heated but decompose irreversibly at very high temperatures.	
Have linear or lightly branched structure.	Highly branched with extensive three-dimensional network of covalent chemical bonds.	
<b>On the basis of the type of reaction involved in their formation</b>		
<b>Condensation polymers</b>	<b>Addition polymers</b>	
Synthesis involves loss of a small molecular weight molecule, usually a water molecule, e.g. formation of polyesters.	Formed by the addition reaction of an unsaturated monomer, e.g. formation of vinyl chloride.	
<b>On the basis of the mechanism involved in the polymerisation reactions</b>		
<b>Step reactions</b>	<b>Chain reactions</b>	
Similar to condensation reactions but does not involve the loss of the small molecule, e.g., synthesis of polyurethanes.	Involves the activation of a few sites within the reacting medium and a build-up of a few high relative molar mass molecules while the rest of the monomer remains unreacted.	
Large molecules do not appear until towards the end of the reaction.	Large molecules appear and the monomers are present during the most of the reaction.	
Form simple linear molecules or heavily cross-linked network.	Form linear or lightly branched molecules.	
Lead to the formation of either thermoplastics or thermosets.	Most of these reactions lead to the formation of thermoplastics.	
<b>On the basis of existence in nature</b>		
<b>Natural polymers</b>	<b>Synthetic polymers</b>	
They are present naturally in nature.	They are man-made organic polymers and are usually based on covalent compounds of carbon.	
They are, usually, structurally more complex than synthetic polymers.	Can have elements that are capable of covalent bonding with carbon like hydrogen, oxygen, chlorine, fluorine, phosphorus and sulphur.	
Examples include proteins, nucleic acids and carbohydrates.	Examples include poly(ethylene), poly(propylene), poly(styrene), poly(vinyl chloride) etc.	
<b>On the basis of stereochemistry</b>		
<b>Isotactic</b>	<b>Syndiotactic</b>	<b>Atactic</b>
The substituents are attached on the same side of the backbone polymer chain.	The pendant groups are on the opposite side of the polymer backbone.	Do not have any regularity in the arrangement of the carbon atoms.

## 2.1.2 Polymer Architecture

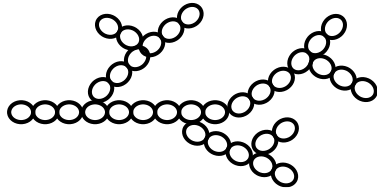
Polymer architecture, also known as topology, describes the shape of a single polymer molecule. Polymer structure influences the physiochemical properties of the polymer. The structure/sequence/number of monomer(s), the backbone stability and water solubility (as well as many other factors) affect polymer properties and are taken into consideration when selecting polymers for drug delivery. Linear polymers and block copolymers have different properties to branched polymers. They display different melt rheology, physical behaviour and solution properties. Polymers have been classified based on their structure (Table 2.2).

Figure 2.2 shows the basic structure of different polymers.

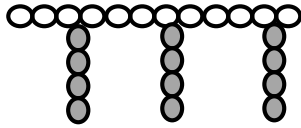
### a. Linear Polymers



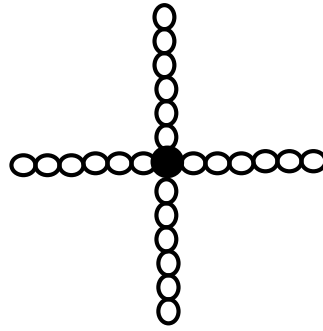
**b. Branched polymers**



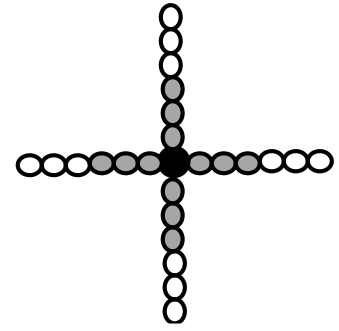
Hyper-branched polymer



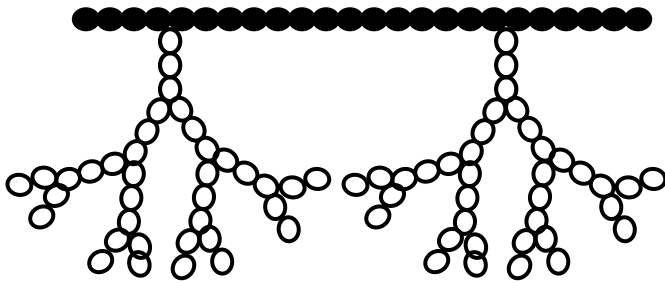
Graft copolymer



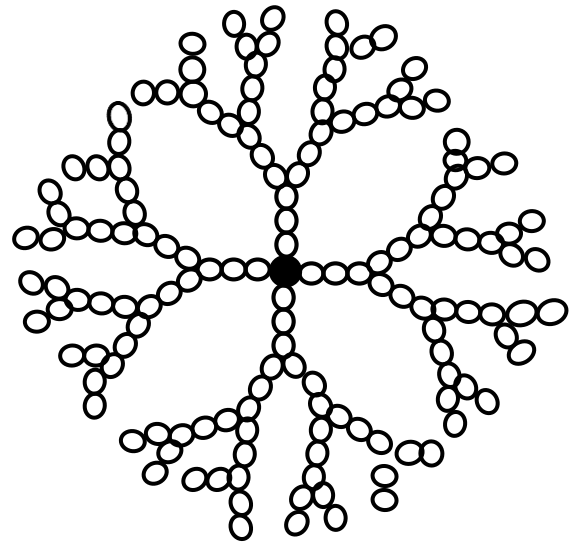
Star-shaped polymer



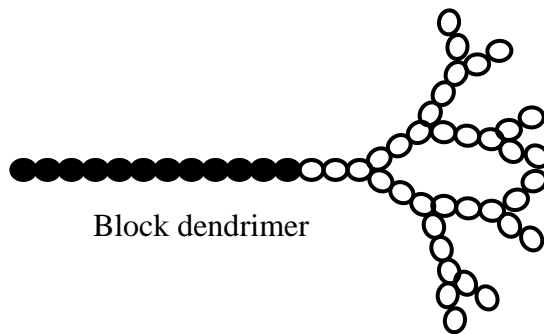
Star-shaped block copolymer



Dendri-graft copolymer

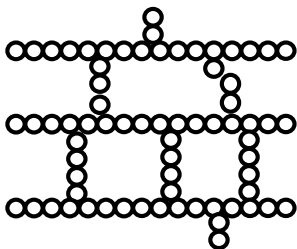


Dendrimer

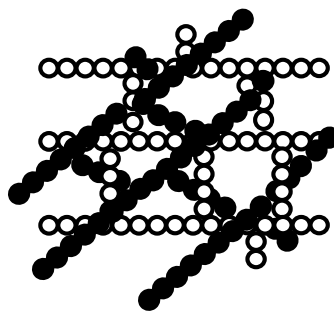


Block dendrimer

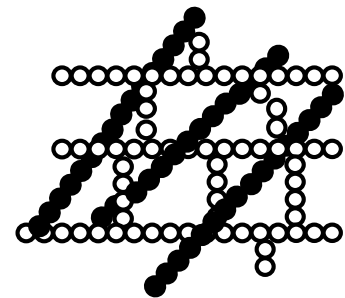
**c. Cross-linked polymers**



Polymer networks



Interpenetrating polymer networks (IPN)



Semi - IPN

**Figure 2.2** Basic structure of polymers (Qiu & Bae 2006).

**Table 2.2** Polymer classification and their general pharmaceutical properties (Qiu & Bae 2006).

Type of Polymer	Properties
Linear Polymers	<ul style="list-style-type: none"> <li>➤ The polymer-drug conjugation model was proposed by Ringsdorf in 1975, which consists of polymeric backbone, spacer, drug, targeting group and the solubilizing moiety (Ringsdorf 1975). This model is used to design these conjugates and target them in the subcellular compartments.</li> <li>➤ When dissolved in solvents can form random coil structures of 5-15 nm in size.</li> <li>➤ Can also be tailored to have multivalency by addition of comonomers to the polymer backbone and therapeutic drugs can be linked to these polymers.</li> </ul>
Block copolymers	<ul style="list-style-type: none"> <li>➤ Linear polymers having two or more blocks possessing both a soluble and an insoluble block.</li> <li>➤ They can be AB type diblock, ABA- or BAB- type triblock or multiblock polymers. The A block represents the solvent soluble block and the B is the insoluble block.</li> <li>➤ Are being used for the delivery of anticancer, anti-inflammatory, antiviral, antibacterial and DNA drugs.</li> <li>➤ When dissolved in a solvent, they can self-assemble to form one of the following:               <ul style="list-style-type: none"> <li>○ common block copolymer micelle</li> <li>○ drug-conjugated block copolymer micelle</li> <li>○ block ionomer complex micelle.</li> </ul> </li> </ul>
Branched polymers	
Hyper-branched polymers	<ul style="list-style-type: none"> <li>➤ A common example is polyethylenimine (PEI), are water-soluble polyamines with different molecular weights and degrees of chemical modification.</li> <li>➤ Form spheroid-shaped molecules with primary, secondary and tertiary charged amine groups which can act</li> </ul>

	as a cationic polyelectrolyte and are used for DNA delivery.
Graft polymers	<ul style="list-style-type: none"> <li>➤ Contain an extensive branching along the linear polymer backbone and are also called comb-type copolymers.</li> <li>➤ Can act as thermosensitive hydrogels when added to aqueous solutions for drug delivery purposes.</li> </ul>
Star polymers	<ul style="list-style-type: none"> <li>➤ Three-dimensional hyperbranched structures having a central core and different molecular weight linear arms emerging from the core.</li> <li>➤ Are used as drug vectors, they have a benefit over linear polymers because of a smaller hydrodynamic radius and low solution viscosity which helps in complete renal excretion.</li> </ul>
Dendrimers	<ul style="list-style-type: none"> <li>➤ Three-dimensional structures having layered branches, called generations, extending from the central core.</li> <li>➤ Have a multifunctional central core, branched units and surface groups.</li> <li>➤ Internal cavity for non-covalent drug encapsulation of hydrophobic drugs.</li> <li>➤ Controlled multivalency of the dendrimers can serve as points for attaching combination of drug molecules, targeting and solubilizing groups.</li> </ul>



The basic structure of linear and block copolymers in drug delivery systems is explained below.

**Linear polymers:** Each individual component of the linear polymer-conjugate model can be individually optimised/ selected to enhance the efficiency of drug transport in the body. Figure 2.3 shows a sketch of a linear drug-polymer conjugate.

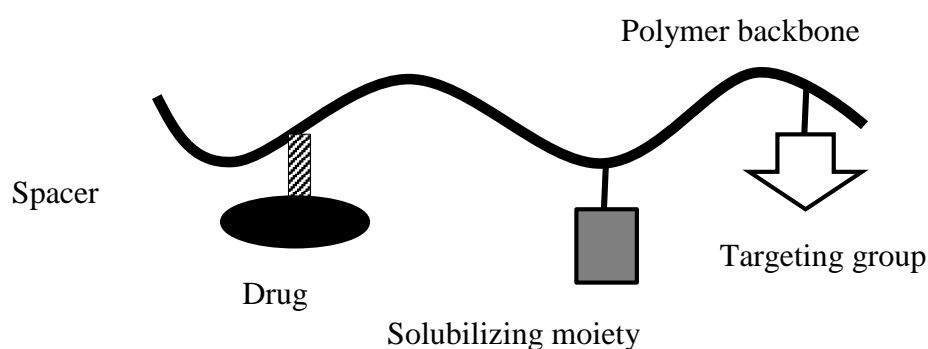


**Figure 2.3** A sketch showing a linear drug-polymer conjugate (Qiu & Bae 2006).

**Block copolymers:** PEG usually acts as the hydrophilic block in most of the block copolymers because of its low toxicity and high water solubility. In drug conjugated micelles, the drug interacts with the hydrophobic block to form a hydrophobic core, so the drug remains out of contact with water and the hydrophilic block helps in the dissolution of this conjugate. There are three major types of micelles based on linear block copolymers; common block copolymer micelles, drug-conjugated block copolymer micelles and block ionomer complex micelles. A polyion complex (PIC) is comprised of two block copolymers of opposite charge (Qiu & Bae 2006). Figure 2.4 shows the structure of the three types of micelles formed by linear block copolymers.

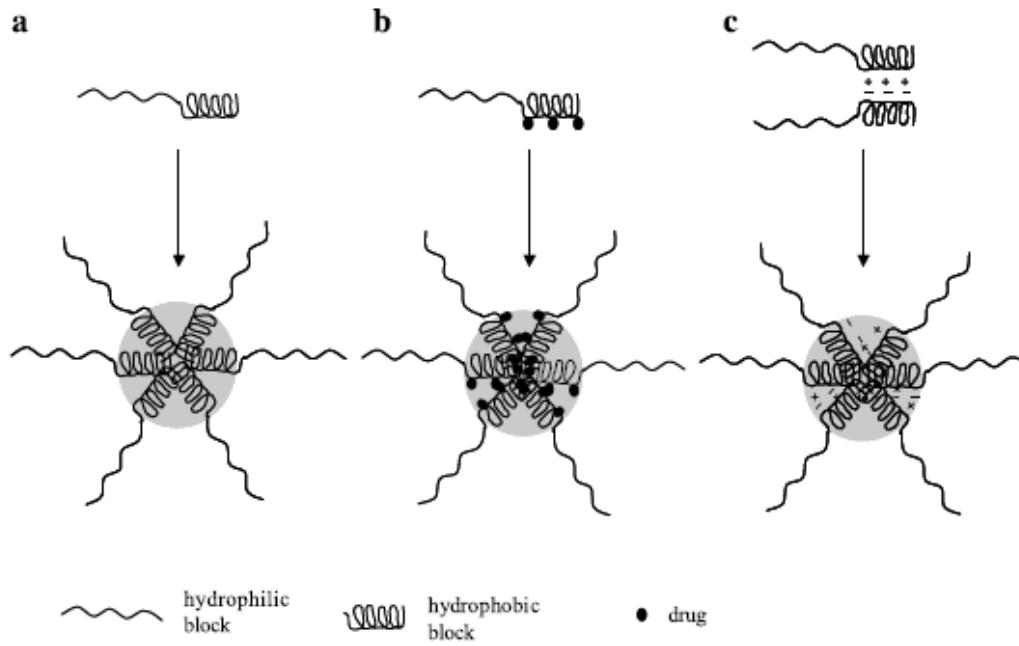


**Figure 2.4** Types of micelles formed by linear block copolymer;

(a) common block copolymer micelle, (b) drug-conjugated block copolymer micelle, and (c) block ionomer complex micelle (Qiu & Bae 2006).

### 2.1.3 Molar Mass of Polymers

Polymers when produced result in a mixture of molecular sizes and the properties of these polymers depend on the average size of the molecules present. There are three types of molar mass distributions (Nicholson 2012).

1. Number average,

$$M_n = \frac{\sum_{i=1}^{\infty} N_i M_i}{\sum_{i=1}^{\infty} N_i} \quad (2.1)$$

$M_i$  is the molar mass of the molecular species  $i$  and  $N_i$  is the number of molecules of  $i$  in the sample.

2. Weight average,

$$M_w = \frac{\sum_{i=1}^{\infty} N_i M_i^2}{\sum_{i=1}^{\infty} N_i M_i} \quad (2.2)$$

For polymers with all molecules of the same molar mass,  $M_n = M_w$ , the ratio  $M_w : M_n = 1$  which is termed as the polydispersity of the sample. Such a sample is said to be homo- or mono-dispersed.

3. The third distribution is called the z-average,  $M_z$ , given by:

$$M_z = \frac{\sum_{i=1}^{\infty} N_i M_i^3}{\sum_{i=1}^{\infty} N_i M_i^2} \quad (2.3)$$

There are various experimental methods that are used to determine the average relative molar mass of polymers (Table 2.3).

**Table 2.3** Experimental methods to determine the average relative molar mass of polymers (Nicholson 2012).

<b>Molar mass distribution type</b>	<b>Experimental Method</b>
$M_n$	Gel-permeation chromatography (GPC)
	Membrane osmometry
	Vapour phase osmometry
	End group analysis
$M_w$	Light scattering and GPC
$M_z$	Ultracentrifugation

## 2.2 Glass-Transition and Melting: Important Polymer Properties

The glass-transition is a property present in amorphous polymers and it is a process whereby the polymer goes from a glassy state to a rubbery state. During this transition, it passes through the glass-transition temperature ( $T_g$ ). It is the temperature on the specific volume vs temperature plot where the slope of the glassy and the rubbery region intersect.

Since polymers are never perfectly crystalline, in crystalline polymers, the surrounding amorphous regions undergo a glass-transition. Such polymers display both a  $T_g$  and a melting point ( $T_m$ ) corresponding to the disordered and the ordered regions of the polymer, respectively.  $T_m$  is the temperature at which the material undergoes a phase-change from solid to liquid. It is contributed by the crystalline part of the polymer and the polymer loses its crystalline structure at this temperature. The  $T_m$  usually represents a melting range because of the presence of various polymer chain lengths and crystallites of various sizes with many defects. These defects lead to the depression of the melting temperature (Cowie 1991).

The glass-transition temperature ( $T_g$ ) is not a specific transition temperature but a range of temperatures over which the mobility of a polymer changes. It is very important because a lot of polymer properties change in this region. A plot of specific volume measured as a function of temperature can be used to determine the  $T_g$ . When the specific volume is plotted against the temperature, both the glassy and the rubbery region show a linear change in specific volume with the temperature but the slopes of the two states are different, with the slope of the rubbery state being greater than that of the glassy state.  $T_g$  is at a higher temperature when the polymer is cooled from a rubber state than if the polymer is heated from a glassy state which is designated as  $T_g'$  (Daniels 1989). Fig. 2.5 shows the two glass-transition temperatures, one upon heating and the other upon cooling of the sample.

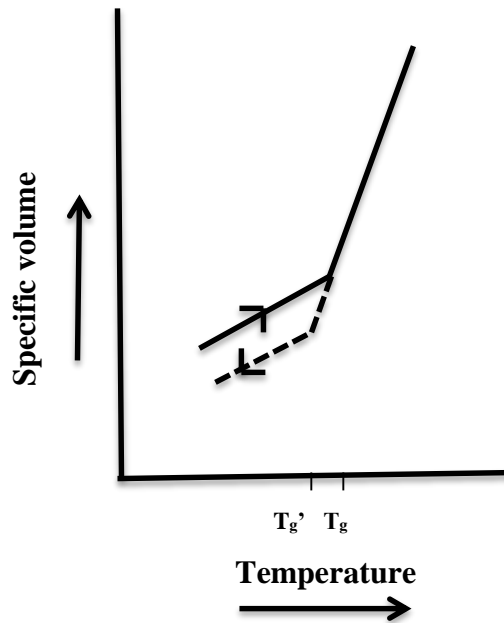


**Figure 2.5** Glass-transition temperatures upon heating and cooling of a sample using a plot of change in specific volume as a function of temperature.

The  $T_g$  of polymers change with change in molecular weight; it increases with an increase in the molecular weight of the polymer. A larger molecular weight polymer would have a restricted mobility and hence a higher energy needed to move the molecules.

All polymers are rigid solids at very low temperatures but as the temperature is increased, they gain thermal energy and the polymer chains start to move freely and they become viscous liquids. Solid polymers can have a crystalline or a non-crystalline structure which depends upon the cooling rate from its melting temperature ( $T_m$ ) to  $T_g$  (Fig. 2.6). A linear polymer is a viscous liquid at temperatures above  $T_m$  (A). On rapid cooling, it goes through a rubbery region (C) which upon further cooling below the  $T_g$  vitrifies into an amorphous glassy-state (D). However, upon slow cooling below the  $T_m$  crystallites form in a rubbery matrix (E) which upon further slow cooling forms a glassy matrix (F) (Gerdeen & Rorrer 2011). The glassy state is a persistent non-equilibrium state (Dissado & Fothergill 1992).

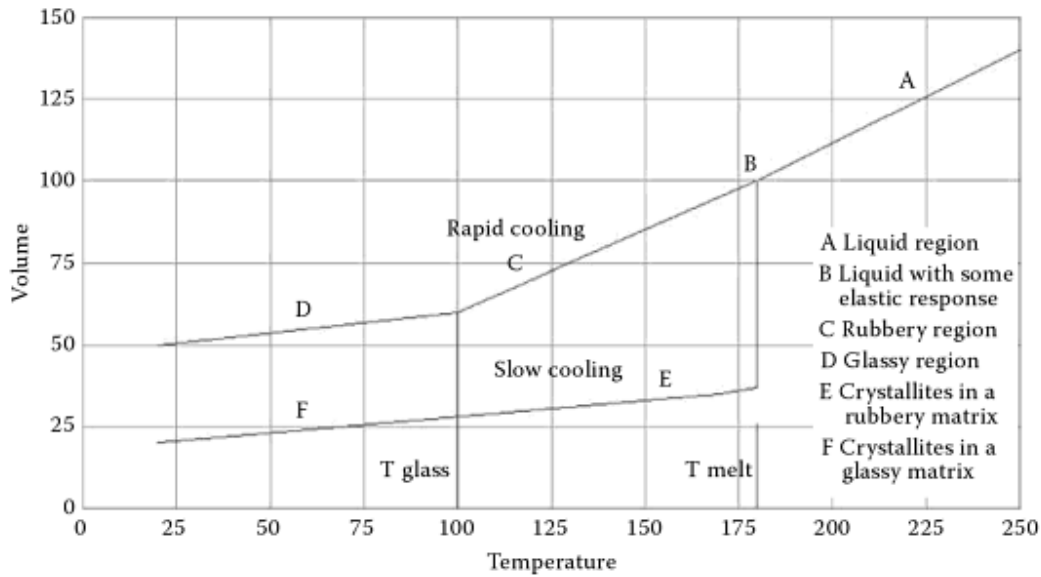


**Figure 2.6** The change in specific volume of polymer with the temperature for (i) rapid cooling of the material (A-C-D), (ii) slow cooling (A-E-F) (Alfrey & Gurnee 1967).

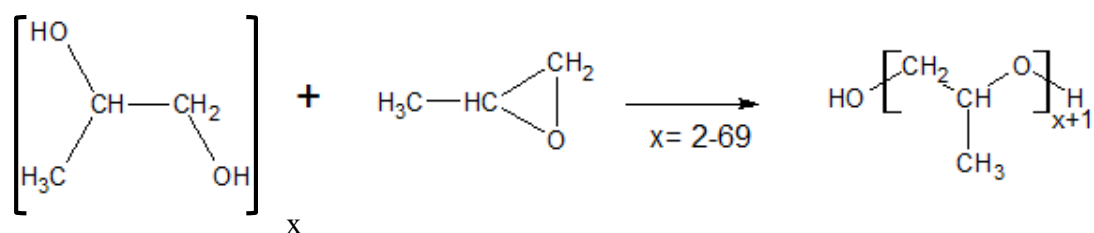
The glass transition temperature,  $T_g$ , is very important as it marks the point where the mechanical properties of the polymer change and it becomes deformed after this temperature. At temperatures below the  $T_g$ , the polymer is more brittle and so this temperature determines the applications for the polymer use. Generally, polymers with a  $T_g$  below room temperature are defined as elastomers and a  $T_g$  above room temperature defines rigid polymers with defined structures (thermoplastics) (Hempstead & Worthington 2005).

### 2.3 Poly(Propylene Glycol) (PPG)

PPG is a polymer of propylene oxide monomers and is also called poly(propylene oxide) or poly(propane-1,2-diol). The term “oxide” is used for high molar mass polymers whereas “glycol” is used for low to medium range molar mass (500-3500) polymers (Chanda & Roy 2006). They are clear, viscous liquids and have a low pour point. Increasing molecular weight is directly proportional to the increase in viscosity and inversely proportional to solubility (Dow Chemical Company, Codex 2003). These polymers are synthesised by the base-catalyzed addition of propylene oxide to 1,2-propylene glycol initiator at temperatures of 100-200°C and

pressures between 2000 and 6000 hPa (Dege et al. 1959; MAK 1998), as shown in Scheme 2.1.

They have allyl and *cis*-propenyl end groups.



**Scheme 2.1** The production of PPG using propylene oxide.

The toxicity of PPG is moderate to low and depends on the molecular weight of PPG. It reaches its maximum toxicity at PPG 600 and PPG 750 (MAK 1998). The content of antioxidants such as tert-butylhydroxytoluene (BHT) present in PPG is very low; less than 0.09% (Dow Chemical Company). Propylene glycol is used in the automotive coolant industries because of its favourable toxicological and environmental properties compared with ethylene glycol (Beal & Coolants 1986).

The use of ethylene glycol in antifreeze agents is being substituted by propylene glycol in breweries and other industries because it is considered less toxic. Antifreeze agents traditionally manufactured using ethylene glycols are considered highly toxic and poisonous. It is substituted for ethylene glycol and glycerol, in the manufacture of synthetic resins, an emulsifier in foods and solvent for food colours and flavours (NIH U.S. National Library of Medicine). The Food and Drug Administration (FDA) has considered propylene glycol as GRAS, “generally recognized as safe”, making it acceptable for use in flavourings, drugs, and cosmetics, and as a direct food additive (Agency for Toxic Substances and Disease Registry). Ethylene oxide however is not considered GRAS by the FDA. Comparing the toxicity of ethylene glycol with that of propylene glycol, LaKind *et al.* stated that “From the standpoint of lethality, acute effects, and reproductive, developmental, and kidney toxicity, the toxicity of

ethylene glycol exceeds that of propylene glycol. Further, localized dermal effects from ethylene glycol and propylene glycol are both mild, with data suggesting that propylene glycol may have a skin contact sensitization potential. Finally, propylene glycol exposure in laboratory animals has been associated with reversible haematological changes; no data was provided for ethylene glycol from which to draw a toxicological comparison” (LaKind et al. 1999).

### 2.3.1 Properties

Table 2.4 gives some important properties of PPG. The basic structure of PPG is shown in Figure 2.7. The molecular weight of each repeat unit in PPG is 58 g/mol.

**Table 2.4** Some general characteristics of PPG (Cheremisinoff 2003; Burdock 1997).

Characteristics	Values
Appearance	Clear to lightly coloured liquid
Odour	None; slight sweet; faint ether-like
Propylene oxide, max	0.02%
pH	6-9
Specific gravity at 20°C	1.012
Boiling point at 1 atm	Decomposes

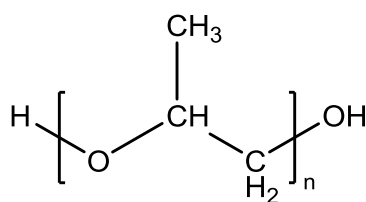


**Figure 2.7** Structure of poly(propylene) glycol.

### 2.3.2 Applications

- PPG offers a wide range of formulating properties. It can be used as functional fluid since it has excellent solvency and lubricity.
- It is used as a raw material or additive for the production of spin finish lubricants for synthetic fibres due to their excellent lubricant properties.



- It can act as defoamer in the textile industry.
- It is also used in fermentation foam control by acting as a defoamer.
- It offers a variety of uses in metalworking including its use as a lubricant and paper processing (defoaming & deinking agents) applications.
- It has a wide role in personal care products because it can dissolve many cosmetic ingredients and has low toxicity, causes no skin irritation and has no odour.
- Its other applications include its use in water and wastewater treatment (foam control agents), heat-transfer/hydraulic fluids (because they have low vapour pressure and high thermal conductivity).
- Also has application as industrial surfactants and synthetic lubricants.

(Dow Chemical Company)

### **2.3.3 PPG as a Thermosensitive/Thermoresponsive Polymer**

Thermoresponsive polymers in solutions respond to temperature. Thermoresponsive polymer solutions can either show lower critical solution temperature (LCST) or upper critical solution temperature (UCST) behaviour.

LCST and UCST are the temperatures below and above which the polymer-solvent mixture is completely miscible. PPG is a thermosensitive polymer (Ward & Georgiou 2011). Cloud point (CP) is a good determinant of LCST for linear thermosensitive polymers (Cao et al. 2007). The CP of most thermosensitive polymers can be modulated by copolymerising with hydrophobic or hydrophilic co-monomers. Hydrophobic co-monomers decrease the CP and hydrophilic co-monomers increase it (Ward & Georgiou 2011; Rijcken et al. 2007).

### **2.4 Thermodynamics of Phase-Separation in Polymer Solutions**

The solubility of a solute in a solvent depends upon the interaction between the solute and the solvent. Polar polymers dissolve easily in polar solvents while the non-polar polymers prefer

organic solvents. A solute will dissolve in a solvent if the intermolecular forces between the polymer and the solvent are greater than or equal to the forces between the polymer-polymer and the solvent-solvent molecules. Whilst if any of the other two forces are greater than the polymer-solvent interaction, they will remain immiscible. A polymer can be solubilized in a solvent when the free energy of mixing,  $\Delta G_{mixing}$ , is negative, which depends on the enthalpy,  $\Delta H_{mixing}$ , and entropy,  $\Delta S_{mixing}$ , of mixing given by:

$$\Delta G_{mixing} = \Delta H_{mixing} - T\Delta S_{mixing} \quad (2.4)$$

The free energy is strongly dependent on the enthalpy of mixing because the entropy of mixing is always positive.

Formally, Raoult's law states that the vapour pressure of a solution of a non-volatile solute is equal to the vapour pressure of the pure solvent at that temperature multiplied by its mole fraction. It accounts for the mixing and behaviour of small molecules with comparable sizes of solvent and solute. The Flory-Huggins model, however, provides a better description for systems containing macromolecules. When the disparity between the sizes of the two components present in a system is great, the value for the entropy of mixing of the system starts to deviate from the "ideal behaviour" because Raoult's law uses mole fraction to estimate the solute activity in solvents. Raoult's law assumes the solution to be ideal and in reality only solutes at extreme dilution obey ideality. Flory-Huggins however uses volume fraction instead of the mole fraction to estimate the solute activity in solvents and provides a better model for predicting the solubility of higher molecular weight solutes (Chiou & Manes 1986; Flory 1942).

## Raoult's Law and Flory-Huggins Theory

Binary mixtures where the enthalpy of mixing,  $\Delta H_{mixing}$ , is zero (because when the components are mixed, the interactions in the individual components are same as the interactions between the mixed components, no thermal energy is released or taken during mixing) and the entropy is ideal are called ideal mixtures and follow Raoult's law. These are either very dilute mixtures or mixtures of similar sized molecules. The free energy of dilution of A is given by (Nicholson 2012; Dill & Bromberg 2010):

$$\Delta G_{dil,A} = kT \ln(p_A/p_A^\circ) \quad (2.5)$$

Where  $p_A$  is the vapour pressure of substance A in a solution and  $p_A^\circ$  is the vapour pressure of A in the pure state. Raoult showed that for molecules of two dissimilar types, A and B, but similar size, the vapour pressure of substance A in the mixtures is related to the mole fraction of molecules of A in the mixture, *i.e.*,

$$p_A = p_A^\circ \frac{N_A}{N_A + N_B} = p_A^\circ n_A \quad (2.6)$$

Where  $n_A$  is the mole fraction of A.  $N_A$  and  $N_B$  are the number of molecules of A and B, respectively.

Substituting back into equation 2.5, Raoult's law shows that the free energy of mixing or dilution is given by:

$$\Delta G_{dil,A} = kT \ln n_A \quad (2.7)$$

To calculate the entropy of mixing of such systems, the liquid is modelled on a lattice arrangement. For low molar mass solutes, each point in the lattice is either occupied by a solute

or a solvent molecule. The possible number of arrangements of a solute and solvent molecule in a lattice will be very large. According to the Boltzmann equation (Eq. 2.8), the greater the number of arrangements of molecules in a system, the greater the entropy.

$$S = k \ln W \quad (2.8)$$

Where  $S$  is the entropy and  $W$  is the number of different combinations of arranging  $N_A$  and  $N_B$  in a lattice of total number of sites  $N = N_A + N_B$ .

$$W = \frac{N!}{N_A! N_B!} \quad (2.9)$$

Sterling's approximation yields:

$$\ln N! = N \ln N - N \quad (2.10)$$

Substituting Eq. 2.9 and 2.10 into Eq. 2.8 gives:

$$\Delta S_{mixing} = k(N \ln N - N_A \ln N_A - N_B \ln N_B) = -k(N_A \ln n_A + N_B \ln n_B) \quad (2.11)$$

Equation 2.11 is only valid for equal sized low molecular weight molecules. Polymer solutions do not follow this law other than at extreme dilutions because of their large sizes compared with solvent molecules. In polymer solutions, where the molecular weight of polymer is a lot larger than the size of the solvent molecules, the mole fraction of solvent turns out to be close to unity. Therefore the partial pressure of the solvent (which is dependent upon the mole fraction of solvent in the solution) and the vapour pressure are equal according to Raoult's law. However experiments do not confirm the validity of Raoult's law for polymer solutions (Canuto 2010). Raoult's model presupposes that the effect that a large a polymer solute has on the solvent is the same as any ordinary solute molecule which is not usually true because each

polymeric segment might be larger than an ordinary solute molecule (Flory 1953). This is why, for such systems, the Flory-Huggins theory provides a better understanding of the entropy of these systems since it uses volume fraction instead of mole fraction.

Figure 2.8 shows a lattice arrangement for ordinary solute molecules with solvent, and polymer in a solvent system. The number of possible arrangements in a polymer-solvent system would be less than a typical solute-solvent lattice arrangement. We assume that the polymer molecules consist of a large number of chain segments of equal length joined together by flexible links. Each link then occupies a site on the lattice. The solution has to be sufficiently concentrated so that the occupied lattice sites are distributed at random, rather than having the clustered structure in a non-random way.

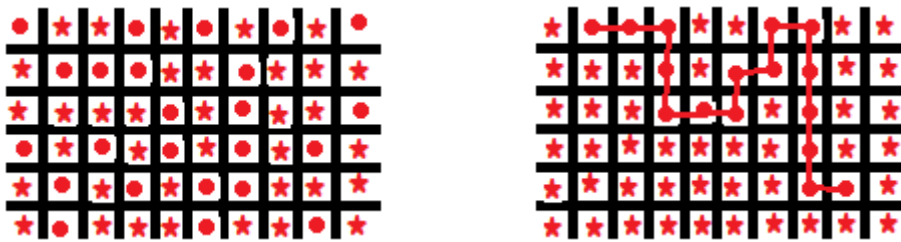


**Figure 2.8** A lattice model for solvent-solute (similar size) and for solvent-polymer molecules. For polymers, the assumption is made that the lattice is comprised of  $N$  cells, with a total volume of  $V$ . Each polymer and solvent molecule occupies volumes  $V_A$  and  $V_B$ , respectively, with each monomer unit occupying a volume,  $V_{mer}$ . The molecular volume,  $V_i$ , is equal to the product of  $V_{mer}$  and the number of monomer units. For solvents, the number of monomer unit is 1. The volume fractions for A and B are represented by the equations:

$$\Phi_A = \frac{V_A N_A}{V_A N_A + V_B N_B}; \Phi_B = \frac{V_B N_B}{V_A N_A + V_B N_B}; V = V_A N_A + V_B N_B \quad (2.12)$$

Substituting Eq. 2.12 in Eq. 2.11:

$$\Delta S_{mixing} = -k(N_A \ln \phi_A + N_B \ln \phi_B) = -kV \left( \frac{\phi_A}{V_A} \ln \phi_A + \frac{\phi_B}{V_B} \ln \phi_B \right) \quad (2.13)$$

$\phi_A$  and  $\phi_B$  are the volume of fractions A and B, respectively.

P.J. Flory (Flory 1942) and M.L. Huggins (Huggins 1942), worked independently to arrive at the Flory-Huggins theory. Both the models were based on the idea of a lattice in which the components of a mixture are placed. Flory-Huggins theory gives the value for the free energy of mixing for a polymer solution:

$$\Delta G_{mixing} = kTV \left[ \frac{\phi_A}{V_A} \ln \phi_A + \frac{\phi_B}{V_B} \ln \phi_B \right] + \frac{\phi_A \phi_B \chi_{AB} kTV}{v_r} \quad (2.14)$$

$v_r$  = molecular volume of a specific segment and  $\chi_{AB}$  = Flory-Huggins interaction parameter;

$v_r$  is often calculated as the square root of the product of the individual segmental unit molecular volumes of the polymeric components,  $v_r = \sqrt{V_A V_B}$ .

#### 2.4.1 Phase Diagrams

There are two major reasons why polymers may be soluble in water: (i) the presence of polar functional groups which interact with the water molecules and (ii) the presence of relatively non-polar groups which makes the structure of the polymer less regular and hence allows the water entry into the material. The presence of an organic non-polar backbone in polymers causes hydrophobic interactions when dissolved in water which causes the water molecules to adopt a cage-like structure, held together by hydrogen-bonds, around the non-polar part of the polymer chains. An increase in the temperature of polymer solutions showing LCST behaviour leads to the phase-separation of a system. So phase-separation in LCST polymers is entropy driven because the polymer is “not in solution” and water is less ordered and has high entropy; this effect is called the “hydrophobic interaction”. But for UCST polymers, the phase-

separation is enthalpy driven (Kulshreshtha & Vasile 2003). A variety of phase-diagrams are possible for a binary polymer solution other than the typical temperature-composition phase diagrams exhibiting LCST or UCST behaviour. Before we start discussing the phase-diagrams, it is important to study the phase-separation models proposed by various researchers.

### **Models Explaining the Phase-Separation Phenomenon in Poly(ethers)**

Water has a tetrahedral coordination in the liquid state that is well established, by the use of X-ray and neutron diffraction data (Narten 1972), and has a large interstitial space. Kjellander and Florin analysed the phase behaviour of aqueous solutions of poly(ethylene oxide), PEG. When PEG is dissolved in water, the ether oxygen atoms of PEG form hydrogen bonds with water molecules and the methylene group of the PEG gets trapped in the interstitial voids of the tetrahedral water molecules. This increases the structuring of the system and decreases the entropy of the solution. The completion of this cage structure depends on the solute size, geometry and other properties of the solute molecules.

At low temperatures, the effect of unfavourable entropy due to the enhanced structuring of water around the PEG molecules is dominated by the effect of the combinatorial entropy gain (it has the largest value for small molecules) and the decrease in enthalpy due to structuring. This leads to complete miscibility of water and PEG. However, when the temperature is raised, if the extensive hydrogen-bonded structure does not break down rapidly enough, the unfavourable entropy factor starts to play a significant role leading to phase-separation and a decrease in the extent of hydrogen-bonding. If the temperature is further increased, because the structure has mainly disappeared at this stage, the role of combinatorial entropy starts to dominate. This allows the components to mix again to form a one-phase system (Kjellander & Florin 1981). When PPG is added to water (Fig. 2.9), it too forms an enhanced hydrogen-

bonded structure, similar to that encountered in the PEG/water system and is characterised by a negative excess entropy and enthalpy of mixing.

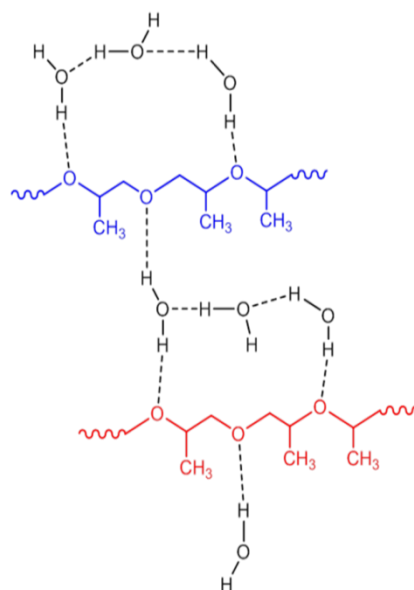


**Figure 2.9** Hydrogen bonding between PPG and water.

The difference between PEG and PPG in water is that the structuring is not optimal in PPG because of the steric hindrance due to the methyl groups in PPG. The strain of the water structure leads to a smaller hydrogen-bond energy than in the case of PEG leading to a lower phase-separation temperature. And this is the reason why some copolymers of ethylene oxide and propylene oxide have a lower phase-separation temperature than PEG because of the hydrogen-bond strain due to the methyl groups of PPG (Kjellander & Florin 1981).

Goldstein proposed a model, which is an extension of Flory-Huggins model, where he suggests the segment-solvent interaction parameter to be temperature dependent. He assumes that the polymer segments can be either hydrogen bonded or non-hydrogen bonded to the water molecules. The hydrogen bonded state would be energetically favoured but not entropically favoured; however, for the non-hydrogen bonded state the opposite would hold. So when the temperature is increased, the polymer-water interaction becomes more unfavourable leading to



phase-separation. This is because the hydrogen bonded regions between the polymer-solvent are strongly attractive while the non-hydrogen bonded regions are strongly repulsive. Goldstein suggested that at high temperatures the probability of the polymer-solvent interaction is dominated by the non-bonded interaction. So he proposed that the phase-separation occurs due to a reduction of the hydration of the PEG chains whereas Kjellander suggests that the phase-separation is the consequence of hydration (Goldstein 1984; Binks & Furlong 1999; Alexandridis & Lindman 2000).

A different model has been proposed by Karlström. His proposed mechanism is based upon the idea that the conformation of the PEG polymer segment varies with temperature in water. They assumed that each PEG segment exists in two forms due to the rotations around C-C and C-O bonds. So with the change in temperature and polymer conformation, the interaction of different segments with the adjacent polymer segments or the solvent molecules changes (Karlstrom 1985). He proposed that one of these conformations exists in a high energy state and another in a low energy state. The conformation with the lowest energy has the oxygen atoms in *gauche* orientation around the C-C bond and a *trans* conformation is preferred around the C-O bond (Bailey & Koleske 1976). This gives rise to a large dipole moment that is responsible for the interaction of polymer molecules with water. But at higher temperatures, the less-polar conformer of PEG chains become dominant. This increases the importance of the repulsive (non-polar) domains leading to phase-separation (Karlstrom 1985; Binks & Furlong 1999).

The advantage of the Karlström model is that it defines the temperature dependence on the solubility of EO based polymers in both aqueous and non-aqueous solutions. This model is consistent with observed NMR chemical shifts of PEG in aqueous solution, in organic solvents and in pure PEG (Bjoerling et al. 1991). The data supports conformational changes with

temperature. The Kjellander and Goldstein models can be used for other polymers and surfactants undergoing phase-separation in aqueous solutions (Binks & Furlong 1999).

A model was suggested by Carlsson for the phase-separation behaviour of poly(propylene oxide) in aqueous solutions (Carlsson et al. 1995). They proposed that the presence of the two conformations of the –OCCO– segments of the polyether depended on the temperature as well as the polarity of the environment; one with a small number of more-polar (lower internal energy) conformations and one comprising of the more numerous less-polar (higher internal energy) conformations. At low temperature, the polar state dominates, which leads to less unfavourable polymer-water interactions. But at elevated temperatures, the non-polar state becomes more populated, which results in more unfavourable polymer-water interactions (Fig. 2.10).

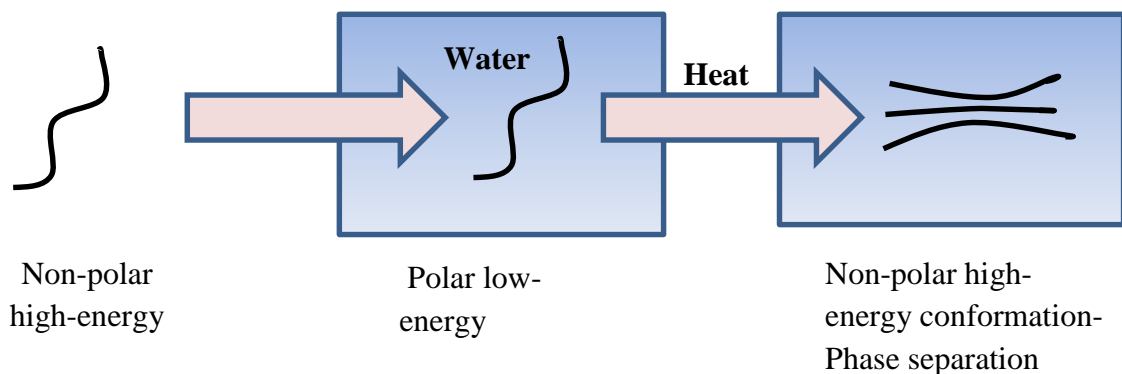


**Figure 2.10** Phase-separation model suggested by Carlsson et al (1991).

### Process of Phase Separation

A polymer solution can separate into two phases as a function of temperature; one with high polymer concentration and another one with low polymer concentration. There are several ways in which phase separation can occur. Phase separation induced thermally is called thermally induced phase separation (TIPS). Binary phase diagrams showing phase boundaries as a function of temperature and composition can provide information about the TIPS process (van de Witte et al. 1996). The thermodynamics of the phase separation helps

determine the possibility of the occurrence of a phase transition. For any system to be thermodynamically stable, the free energy of the system has to be minimal. And if a system is at high energy, it would undergo phase-separation to reduce the free energy of the system.

Phase separation may involve liquid-liquid de-mixing, crystallisation of the polymer from solution, gelation of the polymer solution or association between the components in a solution/aggregate structure. When temperature is plotted against the concentration of a particular molecular species a phase-diagram is obtained with phase-boundaries.

For homopolymer solutions or polymer blends, two phase-boundaries can be detected; the lower one corresponding to thermally induced mixing and the upper one corresponding to thermally induced demixing (Fig. 2.11). The maximum temperature of the lower boundary, where thermally induced mixing occurs, is the UCST and the maximum temperature, where thermally induced demixing occurs, is the LCST. The other phase boundaries in Fig. 2.11 will be discussed later in the chapter.

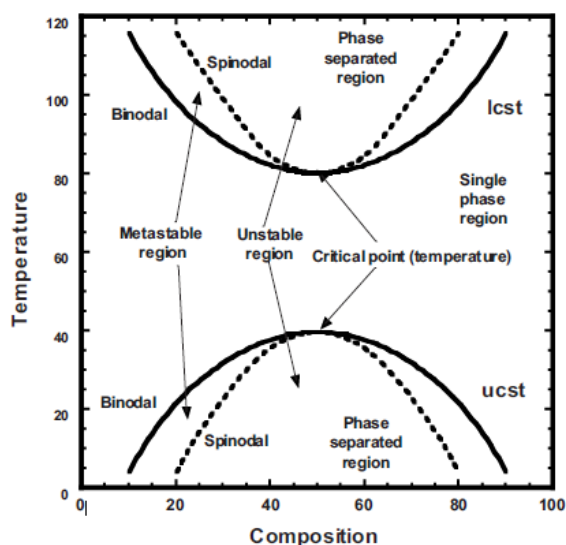


**Figure 2.11** A typical temperature-composition diagram showing the LCST and UCST for a weakly interacting polymer solution (Robeson 2007).

## Physics of the LCST and UCST

The total Gibbs free energy for a mixture of non-interacting molecules A and B of respective molar free energy  $G_A$  and  $G_B$  is given by:

$$G(\text{pure, combined}) = G_A \cdot X_A + G_B \cdot X_B \quad (2.15)$$

$X_A$  and  $X_B$  are the mole fractions of A and B, respectively.

A plot of the change in the Gibbs free energy for the combination of pure A and pure B as a function of the change in the composition is shown in Fig. 2.12.

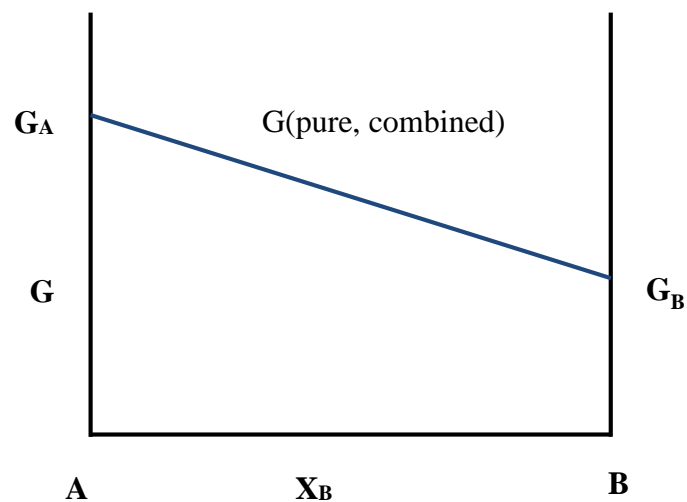


**Figure 2.12** Change in Gibbs free energy for the combination of pure A and pure B as a function of the change in composition.

The change in Gibbs free energy after mixing these two components, when there is an interaction between the two components, is given by the expression:

$$\Delta G_{\text{mixing}} = \Delta H_{\text{mixing}} - T\Delta S_{\text{mixing}} \quad (2.16)$$

Where  $\Delta H_{mixing}$  is the enthalpy change upon mixing and  $\Delta S_{mixing}$  is the entropy change upon mixing.  $\Delta H_{mixing}$  depends on the chemical interactions between the two and  $\Delta S_{mixing}$  is the increase in the randomness as the two components come in close contact with each other. For ideal solutions,  $\Delta H_{mixing} = 0$ . The change in the entropy of the mixture as the two components are mixed with each other is shown in Figure 2.13.

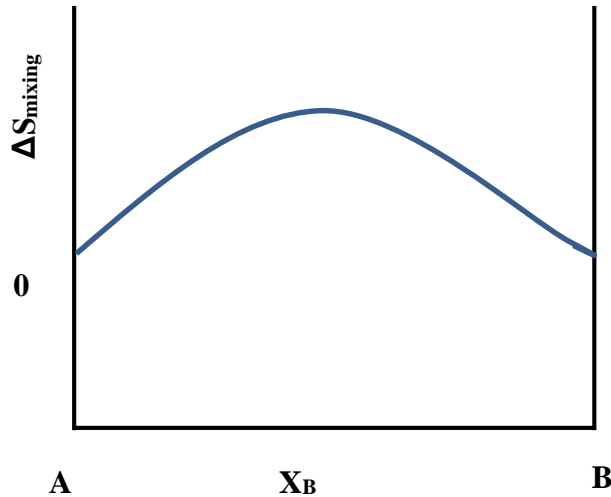


**Figure 2.13** Change in entropy with the change in composition upon mixing of two components.

Hence, the Gibbs free energy due to mixing (Fig. 2.14) can be derived using Eq. 2.16:

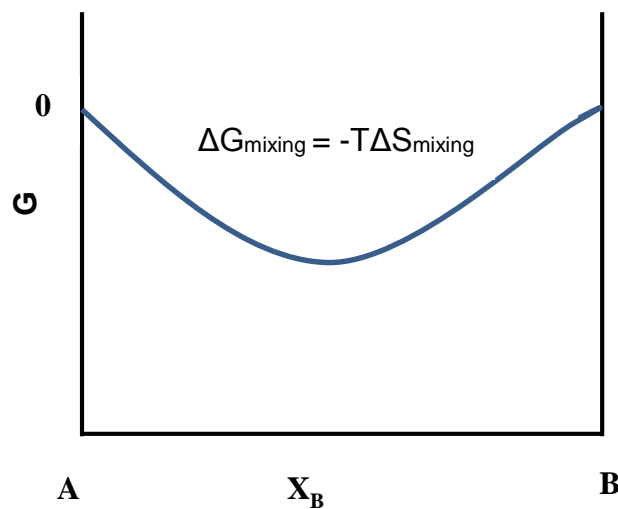


**Figure 2.14** Change in Gibbs free energy with composition upon mixing of the two components when  $\Delta H_{mixing} = 0$ .

From Figs. 2.13 and 2.14, the total Gibbs free energy for a solution (Fig. 2.15) can be derived by adding the Gibbs free energy of the pure, combined, and the change in Gibbs free energy upon mixing.

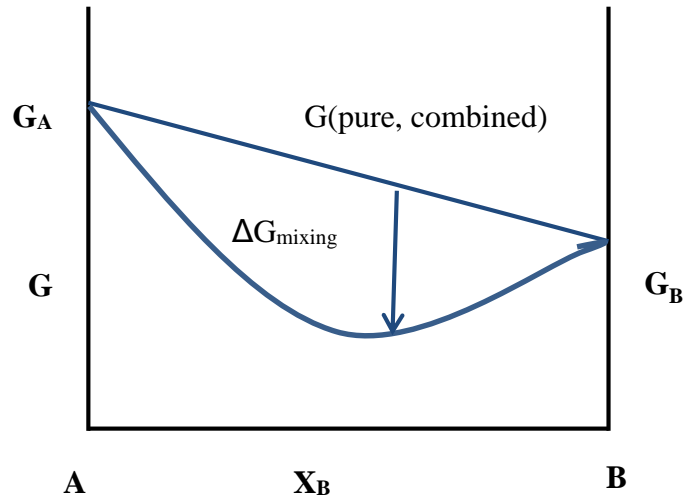


**Figure 2.15** Total Gibbs free energy of the solution as a function of composition when  $\Delta H_{mixing} = 0$ .

The above curves are for binary systems which result in ideal or close to ideal solutions.

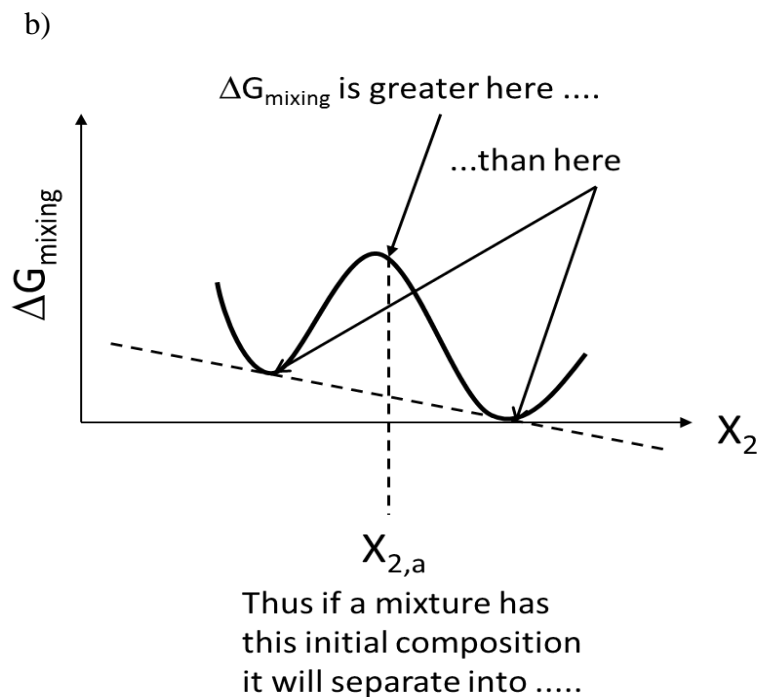
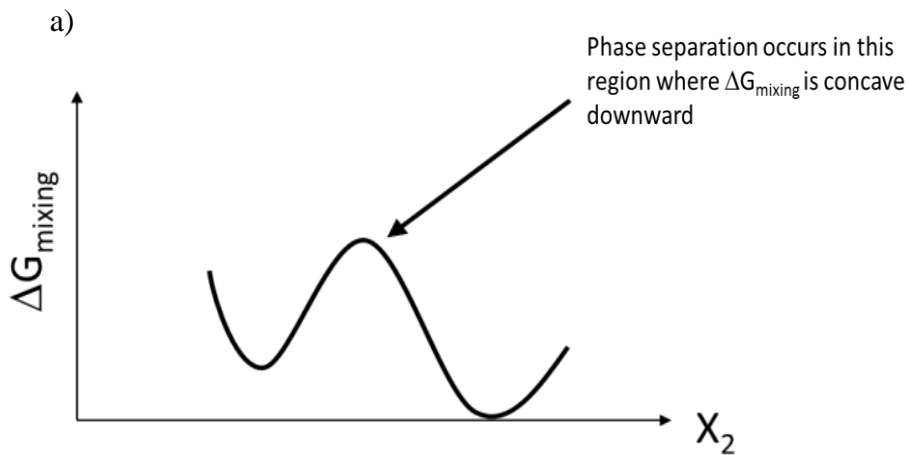
For non-ideal solutions, the enthalpy of mixing is never zero.

For a polymer mixture to be stable, the Gibbs free energy of the mixed system has to be lower than the free energies of the individual components. If  $x_1$  is the mole fraction of solvent and  $x_2$  is the mole fraction of solute (polymer), then for a mixture to be stable, the free energy of the mixture must be:

$$\Delta G_{mixing} < x_1 \Delta G_1 + x_2 \Delta G_2 \quad (2.17)$$

So for a system with a high value of  $\Delta G_{mixing}$  (top of the concave down curve as shown in Fig. 2.16a), it would separate into two phases with the minimum  $\Delta G_{mixing}$  value (bottom ends of the curve; Fig. 2.16b) and the composition of each phase corresponding to two minima of the

$\Delta G_{mixing}$  value (Fig. 2.16b). Fig. 2.16c shows the spinodal boundary which marks the limit of the stability of a solution. Within this curve, infinitesimally small fluctuations in composition will lead to phase-separation. The binodal curve denotes the condition at which two distinct phases may coexist. It also marks a boundary between the set of conditions for which it is thermodynamically favourable for the system to be fully mixed and the set of conditions for which it is thermodynamically favourable for a system to phase-separate.



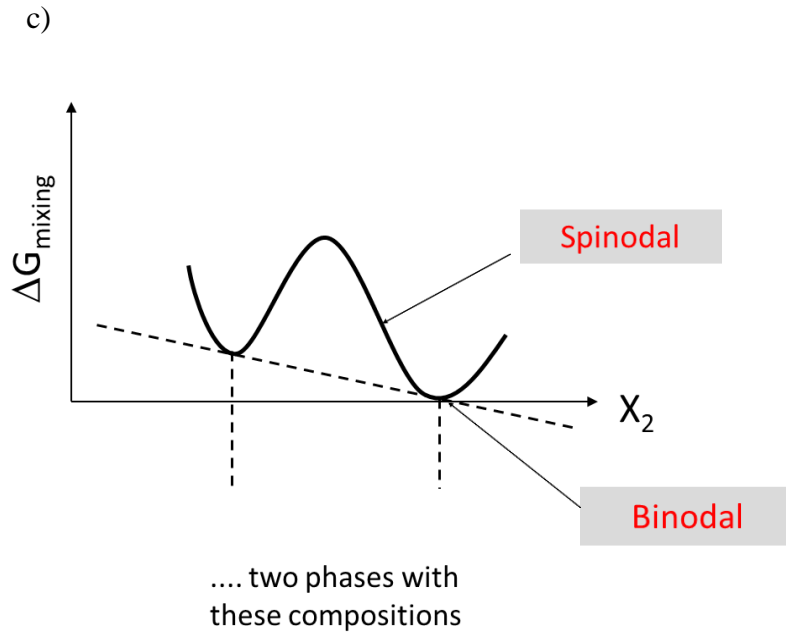


**Figure 2.16** Set of phase-diagrams showing the change in Gibbs free as a function of composition.

A plot of Gibbs free energy as a function of the composition  $x_2$  at different temperatures yields the UCST curve showing the binodal curve, spinodal curve and the critical point (Fig. 2.17).

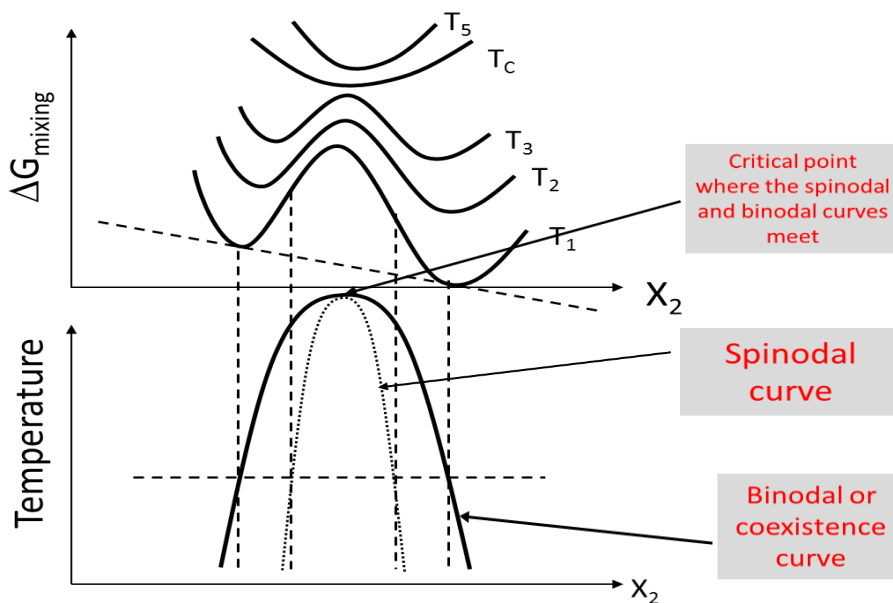


**Figure 2.17** Change in Gibbs free energy at different temperatures as a function of composition showing the critical point, spinodal curve and the binodal curve.



Figure 2.18 shows the stable, metastable and the unstable regions in the phase-diagram.

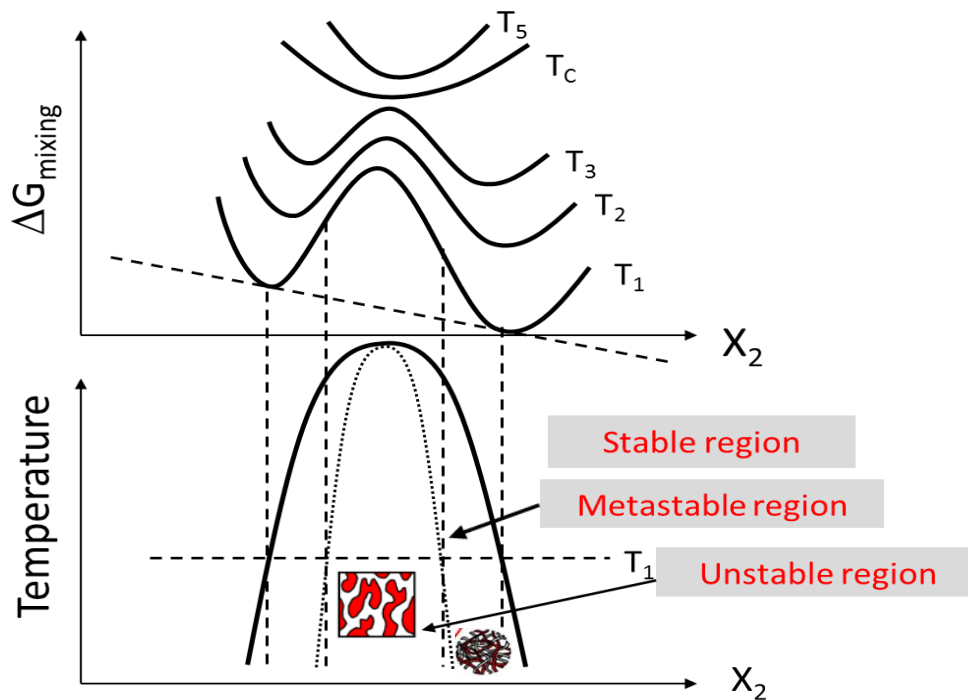


**Figure 2.18** Phase-diagram showing stable, metastable and unstable regions as the Gibbs free energy changes at different temperatures as a function of the composition.

The binodal curve also known as the cloud-point curve (for polydisperse systems) marks the boundary of the liquid-liquid coexistence curve. There exists another region bounded by the spinodal curve. Phase separation occurs by a nucleation and growth mechanism in the area between the binodal and the spinodal curve. The point where these two curves meet is called the critical point and at this point the amount and the composition of the polymer-rich and polymer-poor phase is similar. The area between the spinodal and the binodal is referred to as the metastable region. In this region, the solutions are stable depending on the composition fluctuations, if the fluctuations are small, the solution is stable and would not phase separate, but if they are large, demixing will occur. The region enclosed by the spinodal curve represents the unstable region (van de Witte et al. 1996).

In other words, the binodal curve is a phase transition line between a homogenous phase and a phase separated region in the phase diagram and the spinodal curve is the deeper part of the phase-separated region (Dill & Bromberg 2010).

Polymer mixtures that separate via cooling are characterized by an Upper Critical Solution Temperature (UCST) or the upper consolute temperature and those that separate upon heating are characterized by Lower Critical Solution Temperature (LCST) or the lower consolute temperature. Some polymers however have a combination of both UCST and LCST and can form a closed-loop miscibility gap (Fig. 2.19).

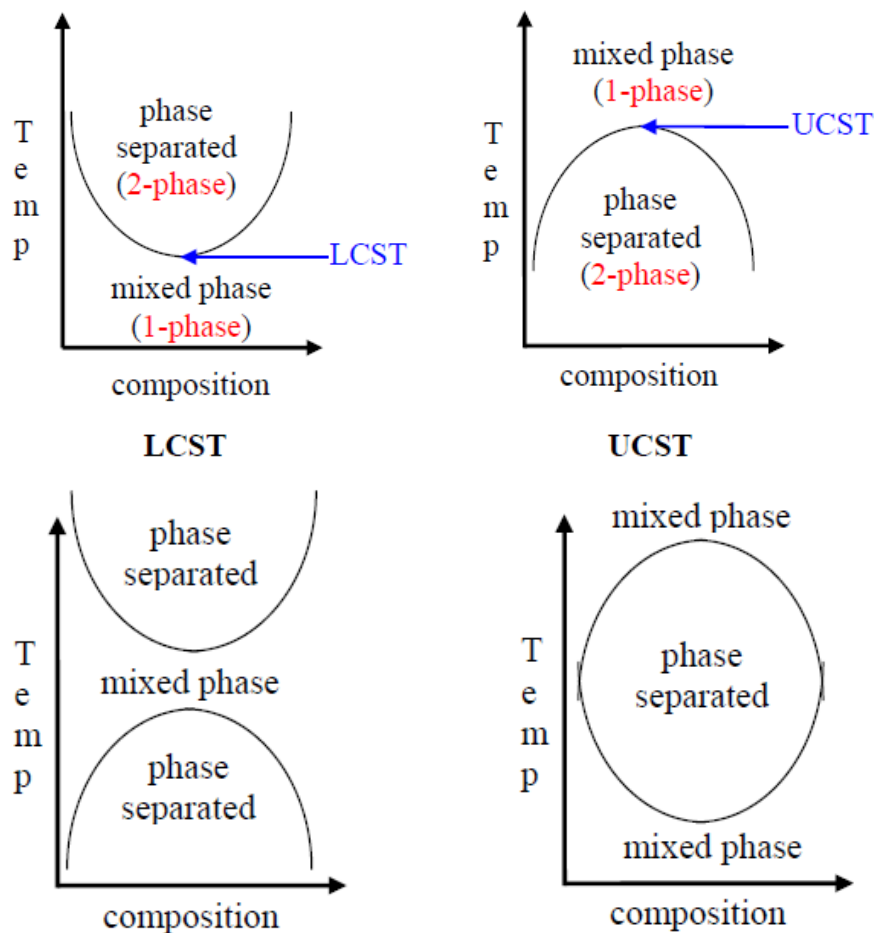


**Figure 2.19** Different phase-diagrams showing LCST, UCST and systems showing both LCST and UCST behaviour (Galaev & Mattiasson 2007).

As mentioned earlier, the stability of a system in the metastable region depends on the fluctuations in the system. There are two mechanisms for a system to undergo phase-separation: nucleation and growth or by spinodal decomposition.

- a) Nucleation and growth: The metastable region corresponds to a region where the system is only stable with respect to small composition fluctuations but for very large fluctuations, it becomes unstable. Large composition fluctuations lead to nucleus formation and the phenomenon is called nucleation. This formed nucleus then starts growing and the whole process together is called nucleation and growth. Phase-separation by nucleation and growth requires an energy barrier to be crossed. The separation appears as small spherical regions of the phase 2 that grow over time.

Fig. 2.20 shows the part of the phase-diagram where the curvature is positive but inside the miscibility gap. The free energy change here increases which means any small fluctuations would be stable against the phase-separation. So the system needs large composition fluctuations, still inside the miscibility gap but outside the spinodal curve to decrease the energy and phase separate by nucleation (Jiang & Wen 2011).

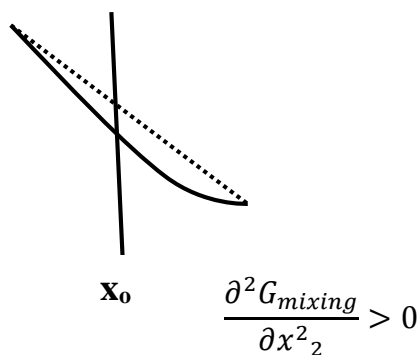


**Figure 2.20** Large composition fluctuations (dotted line) in the metastable region of the phase-diagram.

b) Spinodal decomposition: A small change in the composition within the unstable spinodal curve reduces the free energy and any small fluctuations are amplified. This decomposition does not have any energy barrier. The separation is an interconnected domain of the two phases that appear as overlapping “worms” which coarsen overtime to form spheroid domains (Sperling 2005) .

Fig. 2.21 shows the part of the free energy curve where the curvature is negative. Any small fluctuations in composition shown by the dotted line will lead to phase-separation because the free energy change is negative (Hannay 2013).

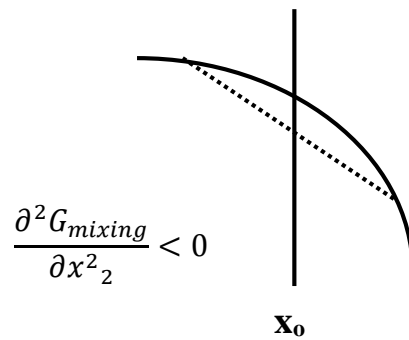


**Figure 2.21** Small composition fluctuations (dotted line) in the unstable region of the phase-diagram.

The aim of this work is to study the phase-separation behaviour of aqueous PPG solutions using different experimental techniques. In order to understand the mechanism of this phase-separation, it is necessary to understand/take into account the phase diagrams and the models proposed by different researchers for phase-separation discussed in this chapter. The data from the HSDSC and turbidity measurements will be used to obtain the phase diagram for aqueous solutions of PPG. The effect of concentration, temperature, scan rate and molecular weight of PPG on the phase-separation temperature will be studied using the two techniques. The data

obtained from other experimental techniques will be used to assess the hypothesis proposed for the phase-separation mechanism. The phase-separation models will be used to explain the data obtained. Further to that, the effect of the addition of sugars on phase-diagrams will also be reported using HSDSC and turbidity measurements. Furthermore, studies of the use of phase-separated PPG for solubilisation of a model hydrophobic compound, naphthalene, using HPLC will be described.

## **Chapter 3 : Principal Experimental Techniques: Theory, Instrumentation and Applications**

### **3.1 Introduction**

This chapter discusses the instrumentation, applications and the theory behind the principal experimental techniques used in this project. The data obtained from these techniques will then be presented and discussed in the subsequent chapters.

### **3.2 Calorimetric Analysis**

Calorimetry is the primary technique used for the determination of the thermal properties of materials. It is the only known method for the direct determination of the enthalpy associated with thermally induced processes. The thermal properties obtained using this technique helps to provide an understanding of the effect of temperature on the specific physical properties of the samples. It measures the heat flow (power) associated with thermal transitions as a function of time and temperature.

Lavoisier and Laplace in 1780, designed an ice calorimeter wherein they measured the amount of ice melted/water produced by the metabolism of a guinea pig which indirectly helped in the measurement of the heat produced by the guinea pig (Fenby 1987). These experiments marked the foundation of the field of thermochemistry. Since then calorimetry has become a popular technique to monitor the heat changes involved in reactions.

#### **3.2.1 Definition of Calorimetry**

Calorimetry is the measurement of the heat changes occurring during a chemical or physical process. The experiments are performed under controlled conditions such as constant temperature, volume or pressure.

### 3.2.2 Classification of Calorimeters

Fig. 3.1 shows the general classification of calorimeters. They can be classified on the basis of: the principle of the measurement of heat (e.g. heat compensating or heat accumulating); or on the method of operation (e.g. static, flow or scanning); or on the principle of their construction (e.g. single or twin cell) (Haines 2002).

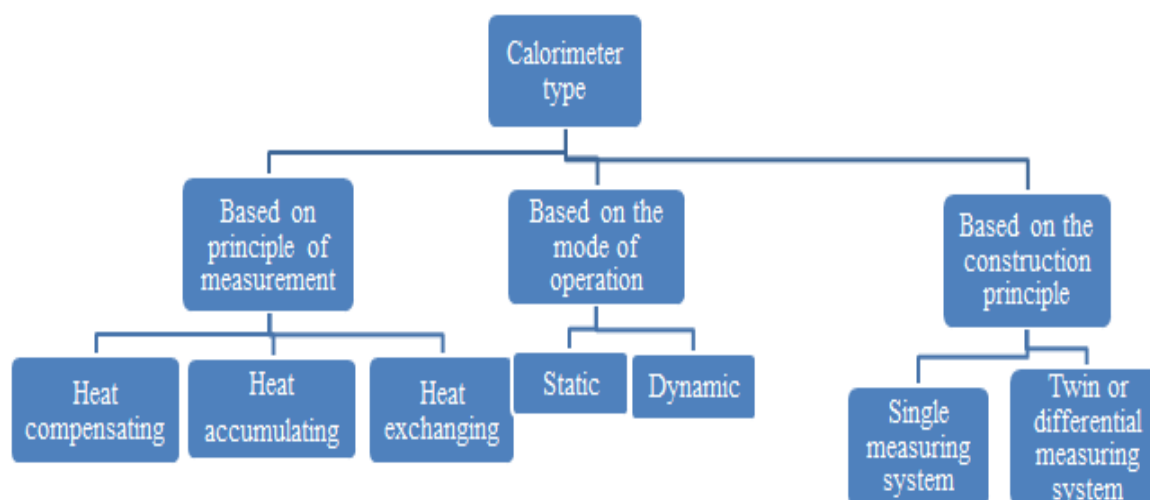


**Figure 3.1** Classification of calorimeters.

### 3.2.3 Differential Scanning Calorimetry

Differential scanning calorimetry (DSC) was first developed in the early 1960's (Schick 2009). It is used to measure the thermodynamic properties of thermally induced phase-transitions and conformational changes in polymers and biopolymers. DSC measures the characteristic temperatures and the heat flow associated with thermal transitions (including both chemical and physical reactions). Heat flow is the extra power provided by the instrumental heaters to maintain the same temperature between the reference and the sample pan/cell.

The change in the heat ( $\Delta Q$ ) of a system is proportional to the change in temperature ( $\Delta T$ ) and is dependent upon the heat capacity of the system at constant pressure ( $C_P$ ). Heat capacity is

defined as the heat required to raise the temperature of unit mass of sample by 1K. The expression defining the relationship between the three terms is given as:

$$\Delta Q = C_p \Delta T \quad (3.1)$$

In this technique, the heat flow difference between the sample and the inert reference (usually an empty pan) is measured at a constant heating rate. The heat going in and out of the sample is dependent upon the heat capacity, and the size of the endothermic for example melting, evaporation, decomposition, protein denaturation or the exothermic for example crystallization) processes taking place in the system. The heat flow signal for the DSC output is given by:

$$\frac{dQ}{dt} = C_p \frac{dT}{dt} + f(T, t) \quad (3.2)$$

Where  $dQ/dt$  is the heat flow rate,  $dT/dt$  is the heating rate and  $f(T, t)$  is the kinetic component of the heat flow at absolute temperature and time. A typical DSC curve is shown in Fig. 3.2.

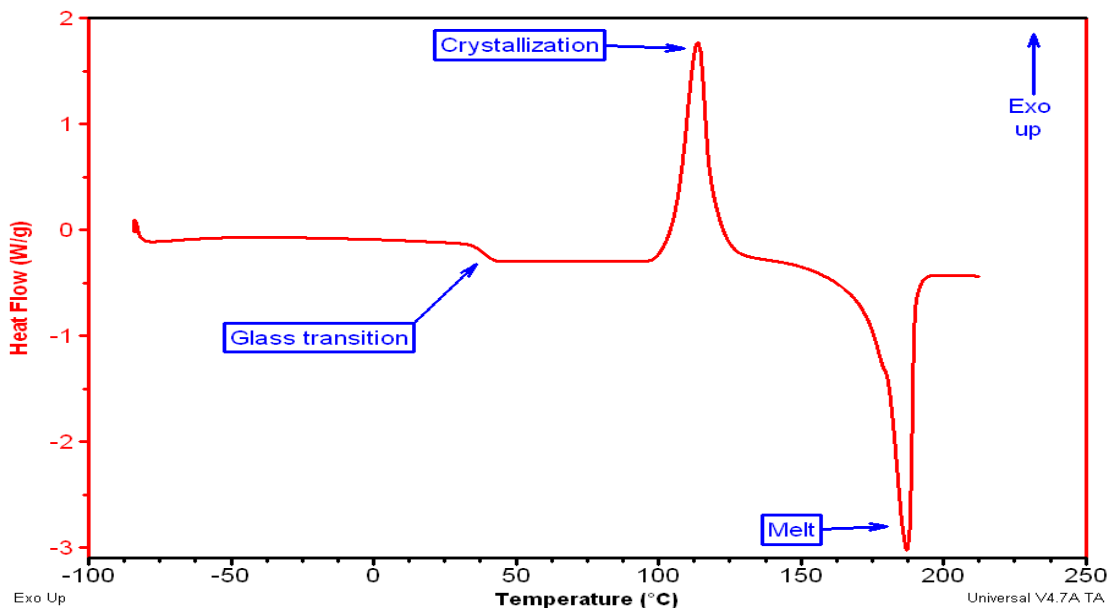


**Figure 3.2** A typical DSC thermogram.



$T_g$  in DSC studies is the temperature at the mid-point of the step change in the baseline of the heat flow signal (Gabbott 2008). First-order transitions such as melting and crystallization are detected by the peak maximum temperature. The enthalpy change ( $\Delta H$ ) can be found by integration of the area under the first-order transition peaks and is a measure of the energy difference between the initial and final states of the system under examination.

Modulated DSC (MDSC) is performed these days in order to achieve a better understanding of the calorimetric signals. MDSC permits separation of the total heat flow signal into its thermodynamic and kinetic components. It improves the resolution of overlapping events that are otherwise difficult to characterise using standard DSC.

Sensitivity in standard DSC can be improved for the detection of weak transitions by either increasing the sample mass or decreasing the scan rate. But if better resolution is needed, then this is achieved by increasing the sample mass and/or by using faster scan rates, which is always at the expense of sensitivity. MDSC is therefore used to increase the resolution of thermal transitions without losing sensitivity. In MDSC, a sinusoidal modulation of temperature is overlaid on a linear heating ramp, which changes a constant heating rate to a periodic function (Verdonck et al. 1999).

**Applications:** DSC can be employed to examine phenomena such as glass-transitions, phase-changes, melting, crystallization, thermal stability, the onset of oxidation processes, polymorphic transitions and biopolymer denaturation /melting transitions.

### 3.2.4 High Sensitivity Differential Scanning Calorimetry (HSDSC)

HSDSC is used to directly study the reactions occurring in solution. The sensitivity of the HSDSC instrument used for these experiments is  $\pm 0.028 \mu\text{W}$  and operates at relatively lower scan rates ( $0.05\text{-}2^\circ\text{C min}^{-1}$ ) than traditional DSC instruments. This technique permits the study of a range of systems including the denaturation of proteins, phase changes in lipid bilayers,

and phase transitions in dilute synthetic polymer solutions. Besides heating and cooling experiments, isothermal experiments can also be performed using HSDSC.

HSDSC instrument consists of two cells, one containing the sample and the other containing the reference. These cells are heated at a constant controlled rate by heaters, which are designed to maintain a zero temperature difference between the two cells. When a thermal process takes place in the sample cell, a temperature differential is detected between the sample cell and the reference cell by using very sensitive thermocouples; feedback systems are then used to control thermistors which compensate for the temperature differential to maintain the same temperature in both the reference and sample cells. The temperature differential between the two cells is measured as an excess power function and is recorded as a function of temperature.

The initial output from an HSDSC experiment is a power-temperature output which is converted into an excess heat capacity,  $C_p$ , (the difference between the sample and the reference heat capacity) vs temperature output.  $C_p$  is the heat capacity measured at a constant pressure; it is the amount of heat required to raise the temperature of a certain amount of substance by one degree centigrade (Myers 2003). A thermogram consists of 3 regions, a pre-transition baseline, an endothermic transition and a post-transition baseline. At temperatures below the phase-transition temperature ( $T_m$ ), the  $C_p$  indicates the difference in the heat capacity between the solution and the solvent. The endothermic transition reaches its maximum at  $T_m$ , and the post-transition baseline represents the relative heat capacity of the product(s).

Liquid water has a high  $C_p$  due to its hydrogen bonded structure. Entropy is the measure of the disorder in system; the higher the disorder, the higher the entropy. Entropy can also be defined as the number of ways the molecules in a system can take up energy without an increase in the temperature. The magnitude of the heat capacity depends on the number of ways of distributing the added heat energy to the system. So a system with fewer ways of distributing the added

energy will require less energy to raise the temperature and hence will have a lower  $C_p$ . However, a system where energy can be added in a lot of different ways will require greater energy to raise the temperature of the system and will have a higher  $C_p$ . So adding heat to a system will increase its entropy by giving the molecules more energy to explore more ways of rearranging themselves. Water however, because of the presence of hydrogen bonds, has a greater tendency to resist the temperature change. HSDSC can be used to measure the heat absorbed by the solute molecules in a solution despite the high  $C_p$  of water; thus demonstrating its sensitivity.

The calorimetric enthalpy,  $\Delta H_{cal}$ , is the total integrated area under the thermogram. After baseline correction, the signal represents the total heat energy change in the sample undergoing a transition.  $\Delta H_{cal}$  is a model-free measure of enthalpy and only depends on the amount of sample present in the cell. However it must be emphasised that the measurement of  $\Delta H_{cal}$  presupposes that all the molecules in solution undergo the observed transition. In a phase separation process not all the molecules will phase separate as indicated by reference to any relevant phase diagram (Atkins and de Paula, 2014)

The van't Hoff enthalpy,  $\Delta H_{vH}$ , however, is an estimation of enthalpy based on an assumed model for the process. At any temperature, the area under the  $C_p$  curve divided by the total area is the measure of the extent to which a process has occurred. Since the van't Hoff enthalpy value is based on a model, the purity, polydispersity, concentration and the volume of sample does not impact on the value of  $\Delta H_{vH}$ . Ideally the values of  $\Delta H_{cal}$  and  $\Delta H_{vH}$  should be the same for a two state process but any deviations gives information about the purity and concentration of the sample, the mechanism involved during the transition and the reversibility of the reaction (Cooper et al. 2000).

There are two types of baselines that need to be taken into account for the estimation of calorimetric and van't Hoff enthalpies, since both the area under the thermogram and the shape of thermogram are affected by the baseline. There is an “instrumental” baseline and a “sample” baseline. The instrumental baseline can simply be obtained by obtaining a scan of the reference sample in both cells of the calorimeter, but retaining the same parameters as the sample vs reference scan. The sample baseline, however, is not as straightforward because of the effects of the change in heat capacity as a function of temperature. Usually a sigmoidal baseline is fitted to the data in order to obtain the area under the thermogram and hence the value of  $\Delta H_{\text{cal}}$ .

A typical HSDSC output is shown in Fig. 3.3 and a sigmoidal baseline has been fitted to subtract from the sample scan.

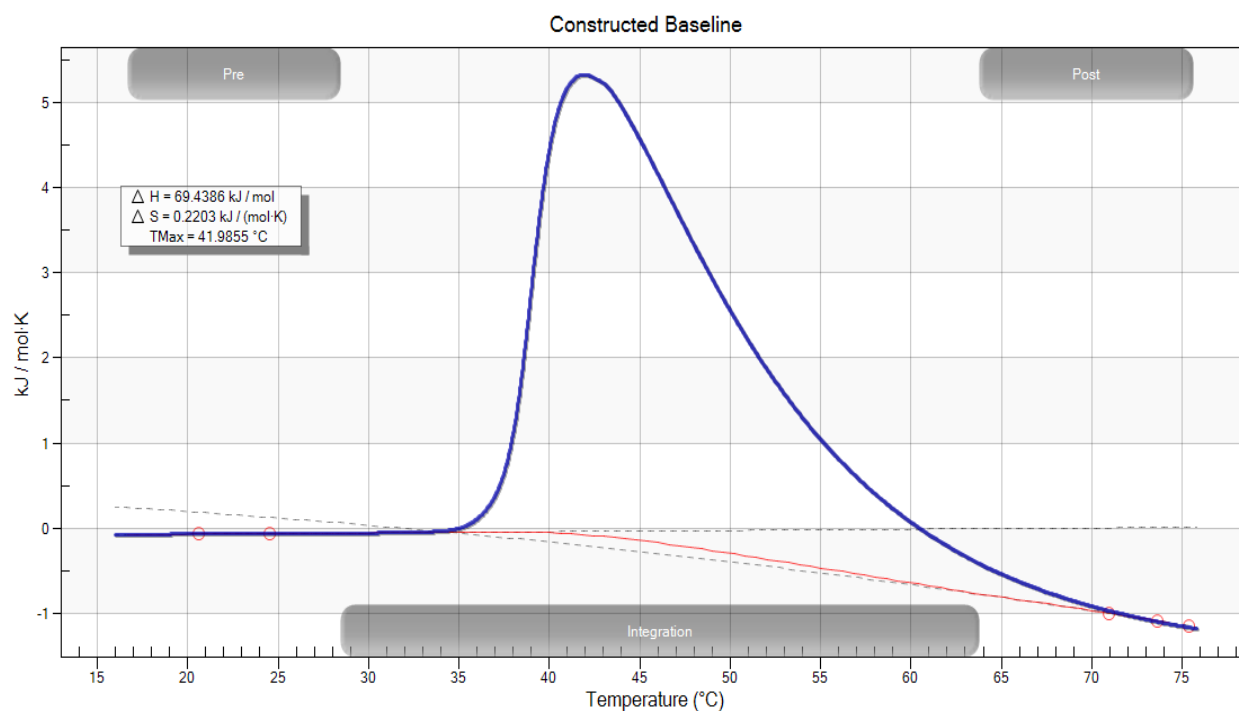


**Figure 3.3** A typical HSDSC output.

In the experiments conducted by HSDSC in this research, the sample baseline is obtained by fitting the pre-transition part of the thermogram to either a polynomial or a linear fit; whichever fits the pre-transition part of the baseline the best. This is then subtracted from the output to obtain the actual value of  $\Delta H_{\text{cal}}$ .

The pre- and post-transitional baselines have a different excess heat capacity. This is due to the change in the heat capacity of the solute after interaction with water. In the case of aqueous PPG solutions, the pre-transitional excess heat capacity is greater than the post-transitional excess heat capacity indicating the weakening of hydrogen bonds. The stronger the hydrogen bonds, the greater the heat capacity of the system (e.g. pure water). This is due to the loss of structuring and hence higher entropy in the system associated with the weakening of the hydrogen-bonded structure.

### **Analysis of the Data**

Kirchhoff's law is used in the determination of the temperature dependence of the specific enthalpy of a process obtained using a calorimeter (Association 1999):

$$\Delta H(T) = \Delta H(T_m) + \Delta C_p(T - T_m) \quad (3.3)$$

There are a few assumptions made for the analysis of the HSDSC data. The system is presumed to be a two-state process wherein no significantly populated intermediate states are observed, so all the reactant molecules undergo change to form product molecules/ensemble structures. In order for the phase-separation to occur in the metastable region, small fluctuations in composition do not cause an instability in the system such that phase-separation is irreversible. The data obtained using HSDSC (discussed further on in the thesis), confirms the idea that system comprises of a hydrogen-bonded network which collapses on heating and is reformed on cooling. So the phase-separation observed in the aqueous PPG system is *via* nucleation and

growth and we use a mass-action description of nucleation and growth. The equilibrium constant for aggregation is given by the ratio of the total concentrations of aggregates to unimeric chains.



$[X]^n$  = Concentration of unimeric chains

$[X_n]$  = Concentration of n unimer chains

$n$  = Aggregation number

HSDSC records the power required to maintain the reference and sample cells at the same temperature as the temperature is increased linearly as a function of time, so  $dT/dt$  is constant. The output of the calorimeter is recorded as  $(dq/dt)_P$  versus  $t$  (time). This can then be converted into a plot of apparent excess heat capacity ( $C_{p,xs}$ ) versus temperature,  $T$ , by multiplying the X-axis by the scan rate and the Y-axis by the reciprocal of the scan rate. This process is called scan rate normalisation.

$C_{p,xs}$  at any point is related to the measured calorimetric enthalpy ( $\Delta H_{cal}$ ) by the equation:

$$C_{p, xs} = \Delta H_{cal} \frac{d\alpha}{dT} \quad (3.5)$$

The van't Hoff isochore equation describes the temperature dependence of the equilibrium constant.

$$\frac{\partial \ln(K(T))}{\partial T} = \frac{\Delta H_{vH}(T)}{RT^2} \quad (3.6)$$

$\Delta H_{vH}$  = Change in van't Hoff enthalpy

$R$  = Gas constant

The temperature dependence of the van't Hoff enthalpy is given by Equation 3.7:

$$\Delta H_{vH}(T) = \Delta H_{vH}(T_{1/2}) + \Delta C_p(T - T_{1/2}) \quad (3.7)$$

$T_{1/2}$  is the temperature where half the polymer chains are aggregated.

If  $\alpha$  is the extent of conversion of unimeric chains into aggregates, then  $K(T)$  can be rewritten in terms of  $\alpha$  as:

$$K(T) = \frac{[X_n]}{[X]^n} = \frac{\frac{\alpha C}{n}}{((1 - \alpha)C)^n} \quad (3.8)$$

$C$  is the total concentration of the polymer.

Integrating the van't Hoff isochore equation gives:

$$\frac{K(T)}{K(T_{1/2})} = \exp\left(\frac{\Delta H_{vH}(T_{1/2})}{R}\left(\frac{1}{T_{1/2}} - \frac{1}{T}\right) + \frac{\Delta C_p(T_{1/2})}{R}\left(\ln\left(\frac{T}{T_{1/2}}\right) + \frac{T_{1/2}}{T} - 1\right)\right) \quad (3.9)$$

Substituting  $K(T)$  in the Eq. 3.9 with  $\alpha$  from Eq. 3.8:

$$\frac{\alpha(T)0.5^{n-1}}{(1 - \alpha(T))^n} = \exp\left(\frac{\Delta H_{vH}(T_{1/2})}{R}\left(\frac{1}{T_{1/2}} - \frac{1}{T}\right) + \frac{\Delta C_p(T_{1/2})}{R}\left(\ln\left(\frac{T}{T_{1/2}}\right) + \frac{T_{1/2}}{T} - 1\right)\right) \quad (3.10)$$

Since all the parameters in the above equation apart from  $\alpha$  are known,  $\alpha$  can be calculated using Eq. 3.10.

The value of  $\alpha$  can then be used to calculate  $C_{p,xs}$ :

$$C_{p,xs} = \frac{d}{dT} (\alpha(T)\Delta H_{cal}(T)) \quad (3.11)$$

Software called “Scientist” is then used for the data modelling purposes and a signal is simulated using the above calculations to fit the calorimetric signal by reducing the sum of square residuals to a minimum value possible as shown in the Eq. 3.12.

$$(C_{p,xs,data} - C_{p,xs,calc})^2 = \text{sum of square residuals} \quad (3.12)$$

## Applications

HSDSC has many pharmaceutical and biochemical applications. It can be utilised in protein conformational studies, DNA binding studies to protein (Privalov & Gill 1987) and lipid phase-transitions and lipid-protein interaction studies (McElhaney 1982; Sturtevant 1987; Freire 1995). Phase transitions obtained using HSDSC have been used to determine values for binding interactions, purity, stability, and drug-release mechanisms for drug delivery purposes (Chiu & Prenner 2011).

### 3.3 Thermogravimetric Analysis (TGA)

This thermal technique measures the change in the mass of a sample as a function of time or temperature under a controlled atmosphere. Conventional thermogravimetry (TG) was undertaken by heating samples to a certain temperature and then removing them at regular time intervals to weigh the sample out (Keattch 1969). The technique was then refined so that the samples could be weighed while heating. Urbain and Boulanger first used the technique in 1912 (Urbain & Boulanger 1912). Isothermal studies can also be conducted sometimes where the change in mass is recorded as a function of time. TGA can be used to record/detect various



processes including the study of adsorption or absorption, sublimation, dehydration/desolvation, vaporization, desorption and decomposition.

A typical TGA curve is displayed in Fig. 3.4. A derivative curve (DTG) can also be obtained from the first derivative of the weight as a function of temperature. This curve helps identify the onset, the peak and the endpoint of the processes that are poorly resolved by the weight (%) curve.

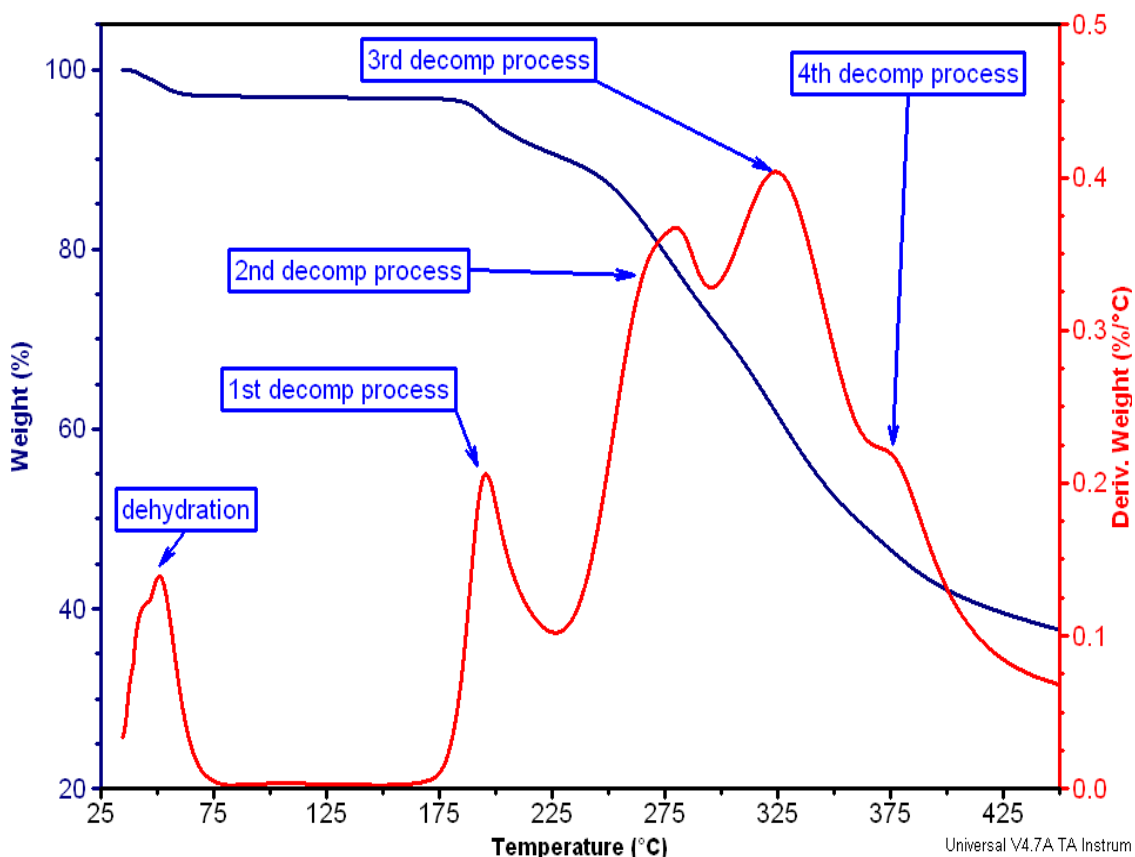


**Figure 3.4** Typical TGA output showing the thermal gravimetric or TG curve (navy plot) and the derivative thermal gravimetric or DTG curve (red plot).

TGA is one of the most important techniques for the assessment of solid-state kinetic behaviour (Vyazovkin et al. 2011) to provide an insight into dehydration/hydration kinetics (Alkhamis et al., 2006). TGA is used in this study to determine the stability of PPGs of different molecular mass.

## **Main applications**

The main applications of TGA are material characterization, performing thermal stability studies, kinetic studies & product lifetime estimation, corrosion studies, compositional analysis and determination of filler, moisture and volatile content in materials

### **3.4 Hot Stage Microscopy (HSM)**

Hot stage microscopy also known as thermal microscopy (TM) or thermo-microscopy is a technique to monitor the dynamic and kinetic changes in materials as the temperature is raised or cooled down (Maniar & Abrams 1974). It is a simple and inexpensive technique that involves the combination of microscopy and thermal analysis. It consists of a polarized microscope with x20 objective, or higher magnification, and a hot-stage where the sample is mounted. For kinetic studies, the events are recorded with a motion picture camera. The samples are heated under vacuum or under an inert gas atmosphere. The heating rate is controlled by varying the current applied to the stage. The cooling rate is controlled by gradually decreasing the current or by introducing a blast of an inert gas such as helium, at a certain pressure. Sample transformations are examined under bright-field illumination, phase-contrast, interference contrast or polarized-light illumination. Visual examination provides information about the melting-point and other transformations that take place during the heating or the cooling process. It also allows the determination of particle size and morphology.

## **Applications**

HSM is used to study decomposition, polymorphism, compound morphology, sublimation, evaporation, different type of transformations, melting, solidification upon cooling and crystal growth.

### 3.5 Thermally Stimulated Current (TSC) Spectroscopy

TSC spectroscopy is a technique used to detect slow molecular mobility in solid state materials and used to measure the changes in the dipole orientation in polar molecules as a function of time or temperature, when an external static electric field is applied to samples. It has applications in the characterization of low molecular weight organic materials in the pharmaceutical, biotechnology and healthcare industries. It is the change in the orientation of dipoles due to rotational movement of parts or the whole of molecules or the movement of charged species which generates the current that is recorded in TSC. There are several experimental modes of TSC spectroscopy but the most commonly used mode is thermally stimulated depolarisation current (TSDC).

#### **Thermally Stimulated Depolarisation Current**

The sample is heated to a polarisation temperature ( $T_p$ ). The polarisation temperature is the temperature at which the sample is excited when placed between the electrodes of a parallel plane capacitor. A static electric field ( $E_p$ ) is applied to the sample for a time period ( $t_p$ ) that is long enough to obtain the saturation of various polarisations at that temperature. This orients the dipoles in the sample and aligns them to their respective opposite charges. The dipoles are then frozen in their polarised position by quench cooling to a temperature ( $T_o$ ) which is substantially lower than the polarisation temperature ( $T_p$ ) and held isothermally for a short period of time, usually 1 min, before removing the externally applied electrical field. The sample is then heated from  $T_o$  to a final temperature ( $T_f$ ) which is higher than the  $T_p$  at a linear heating rate ( $\beta$ ). The increasing molecular mobility provided by heating the sample permits the dipoles to relax to a more random distribution of orientations. Higher temperatures decrease the relaxation time for the movement of dipoles back to their equilibrium distribution. The relaxation time is the time taken for the dipoles to relax back to the equilibrium state. The equilibrium state is a random distribution of dipole orientations.

This process generates current which is measured using an extremely sensitive electrometer ( $10^{-14}$  A). The current generated is measured as a function of temperature.

The TSDC output is complex, consisting of several different dipole relaxation modes. Greater detail can be acquired by using the thermal windowing (TW) experiments which are explained later which isolates a series of current signals, each corresponding to groups of dipoles occurring within the global TSDC output. This is achieved by employing narrow temperature windows of polarisation.

The behaviour of dipoles during a TSDC experiment is shown in Fig. 3.5.

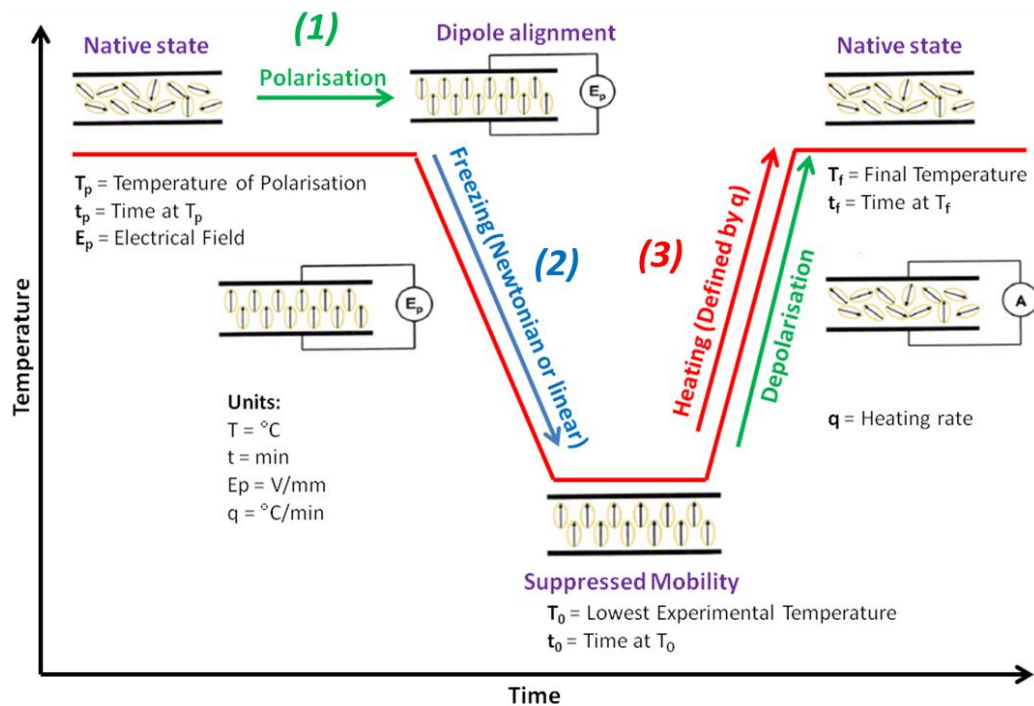


**Figure 3.5** Schematic of the response of molecules during a typical TSC spectroscopy experiment (Owusu-Ware 2013).

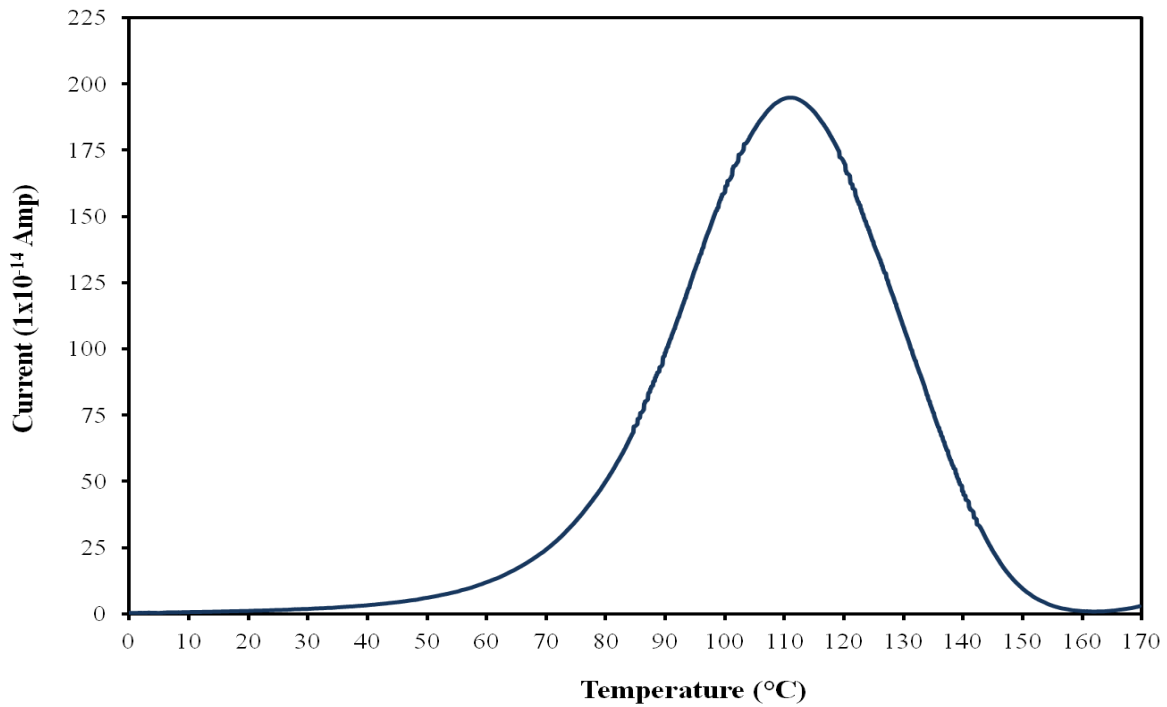


**Figure 3.6** Typical TSC output obtained using TSDC.

The difference in electronegativity of the atoms due to existence of partial positive ( $\delta^+$ ) and partial negative ( $\delta^-$ ) regions creates a dipole in the system. The electric dipole moment,  $\mu$ , can be defined as  $\mu = q \times d$ , where  $q$  is the difference in the magnitude of charge between either ends of the dipole and  $d$  is the distance between the centres of positive and the negative charge (Tripathy & De 2008).

Table 3.1 shows the characteristics of the different types of polarisations in a sample when an external electric field is applied.

**Table 3.1** Characteristics of different types of polarisations upon application of  $E_p$ .

Type of polarisation	Characteristics
Electronic	<ul style="list-style-type: none"> <li>• Involves distortion of electronic shell</li> <li>• Fastest (<math>\leq 10^{-15}</math>s) because of the small distances required for the electronic displacement</li> </ul>
Atomic	<ul style="list-style-type: none"> <li>• Polarisation due to the hetero-polar bonds leading to atomic displacement.</li> <li>• Second fastest (<math>10^{-14} - 10^{-12}</math> s)</li> </ul>
Space charge	<ul style="list-style-type: none"> <li>• Results from high voltage field or insufficient contact between electrodes and the sample</li> </ul>

Interfacial	<ul style="list-style-type: none"> <li>• Similar to space charge but occurs because of the different ohmic conductivity of different phases</li> <li>• The charge is accumulated near the interface of different phases</li> </ul>
Orientalional or dipole	<ul style="list-style-type: none"> <li>• Caused due to the orientation of permanent or induced molecular or ionic dipoles</li> <li>• Dependent upon viscosity due to restricted movement of parts of the molecules</li> <li>• Most important for TSC experiments</li> <li>• Time scale is <math>10^{-12}</math> s</li> </ul>

Orientalional polarisation provides information about the rotational freedom of the molecules and about the viscosity of the materials. They exhibit depolarisation that is directly proportional to the strength of the applied electric field.

### **Thermal Windowing**

TW is another common experiment performed in TSC analysis. The sample is heated or cooled to a polarisation temperature where a direct electrical current is applied for a time period. The polarised sample is then cooled to a few degrees ( $T_d$ ) below the initial  $T_p$ , where the electrical field is cut off and held isothermally for a time ( $t_w$ ) to allow the dipoles with the shorter relaxation time to relax to their temperature dependent equilibrium orientations. The sample is then quench cooled to  $T_0$  and the depolarisation current is measured as the sample is heated to the  $T_f$  at a controlled rate.

In the TW experiment only a fraction of the full spectrum (a few dipoles with shorter relaxation times) is polarised and this is repeated across the whole temperature range of the global relaxation process, ideally resulting in the deconvolution of the complex relaxation process into elementary Debye relaxation processes.

## Theoretical Background

The widely accepted model describing the TSDC relaxation process is Debye's theory of dipole relaxation. This theory makes three major assumptions: (1) that polarisation of dielectric materials is homogeneous, (2) dipoles have a single relaxation time, and (3) that there are no interactions between the dipoles during the polarisation processes. The decay of polarisation is therefore generally expressed as:

$$P(t) = P_e \left[ \exp \left( - \int_0^t \frac{dt}{\tau} \right) \right] \quad (3.13)$$

Where  $P(t)$  is the remaining polarization at time  $t$ ,  $P_e$  is equilibrium polarisation at infinite time and  $\tau$  is the relaxation time.

Assuming that depolarisation is the direct opposite of the polarising process i.e. dipoles exhibit the same relaxation time and no interactions between dipoles occur, then the rate of depolarisation in TSDC experiments is given by:

$$\frac{dP(t)}{dt} = - \frac{P(t)}{\tau(T)} \quad (3.14)$$

During an experiment, depolarisation is induced by the application of a constant heating rate ( $\beta$ ); hence there is a well-defined relationship between temperature and time so that  $T(t) = T_i + \beta t$ , where  $T_i$  is the initial temperature. Incorporation of the heating rate into Eq. 3.14 gives:

$$\frac{dP(T)}{dT} = - \frac{1}{\beta} \frac{P(T)}{\tau(T)} \quad (3.15)$$

The depolarisation current ( $I(T)$ ), which is the experimental output, is therefore given by:

$$I(T) = -\frac{dP(t)}{dt} = -\beta \frac{dP(T)}{dT} \quad (3.16)$$

Values for the polarisation in the samples are given by taking the integral of Eq. 3.16 to give Eq. 3.17:

$$P(T) = \frac{1}{\beta} \int_T^{T_f} I(T') dT' \quad (3.17)$$

Where  $T_f$  is the final temperature i.e. the temperature at which the sample is completely depolarised.

The temperature dependent relaxation time is therefore given by the expression:

$$\tau(T) = \frac{\frac{1}{\beta} \int_T^{T_f} I(T') dT'}{I(T)} \quad (3.18)$$

The TSDC output of the distribution of relaxation time is usually presented in the logarithmic form as:

$$\ln[\tau(T)] = \ln \left[ \frac{1}{\beta} \int_T^{T_f} I(T') dT' \right] - \ln I(T) \quad (3.19)$$

## Applications

TSC studies are usually conducted to provide additional information about molecular mobility in the solid state and to characterise thermal transitions in the crystalline and amorphous phases in pharmaceutical drugs and excipients (Craig & Reading 2014; Antonijević 2012).



### 3.6 Turbidity Measurement (UV-Visible Spectrometer)

Turbidity is an optical property that measures the scattering of a light beam by particles dispersed in a fluid (normally liquid) medium when passed through a suspension (Fig. 3.7). It is also called photoextinction or total light scattering and gives information about flocculation, coagulation, sedimentation, particle concentration and particle size in a sample (Kissa 1999). Turbidity can be measured using a single or a double beam spectrometer or a nephelometer.

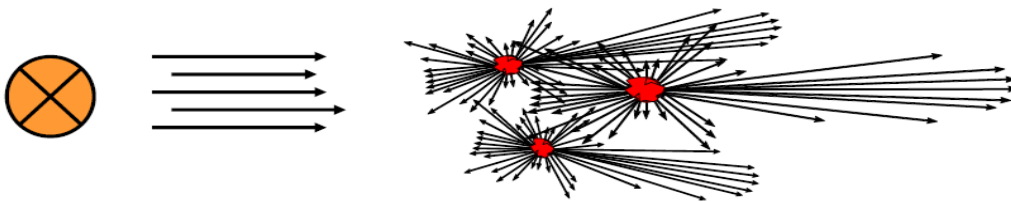


**Figure 3.7** Deflection of light beam by undissolved particles in a sample.

The light transmittance in turbidity measurement depends on the type, size (Fig. 3.8), shape and concentration of the particles in the solution, the wavelength (colour) of the incident light and the angle of measurement.

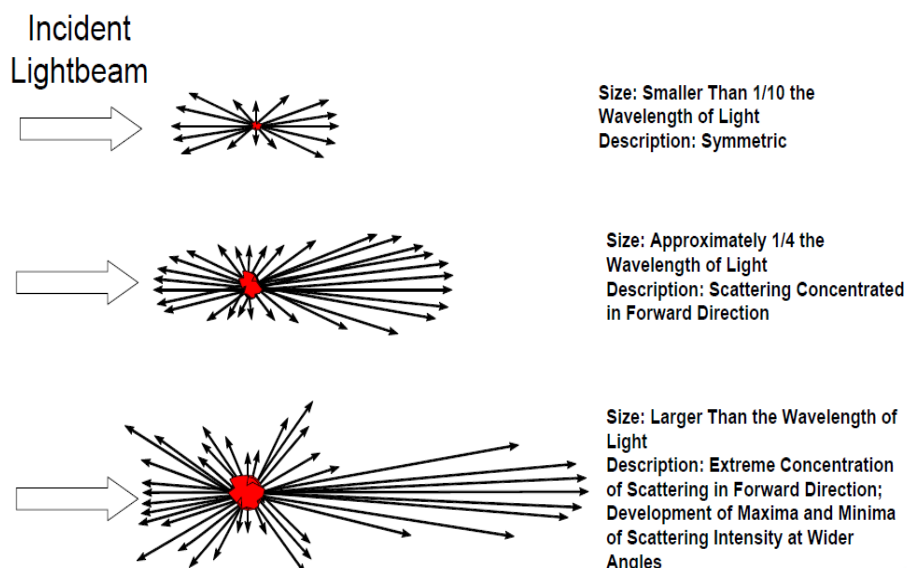


**Figure 3.8** Effect of the particle size on the scattering of an incident light beam (Brumberger, H., Stein, R.S., and Powell 1968).

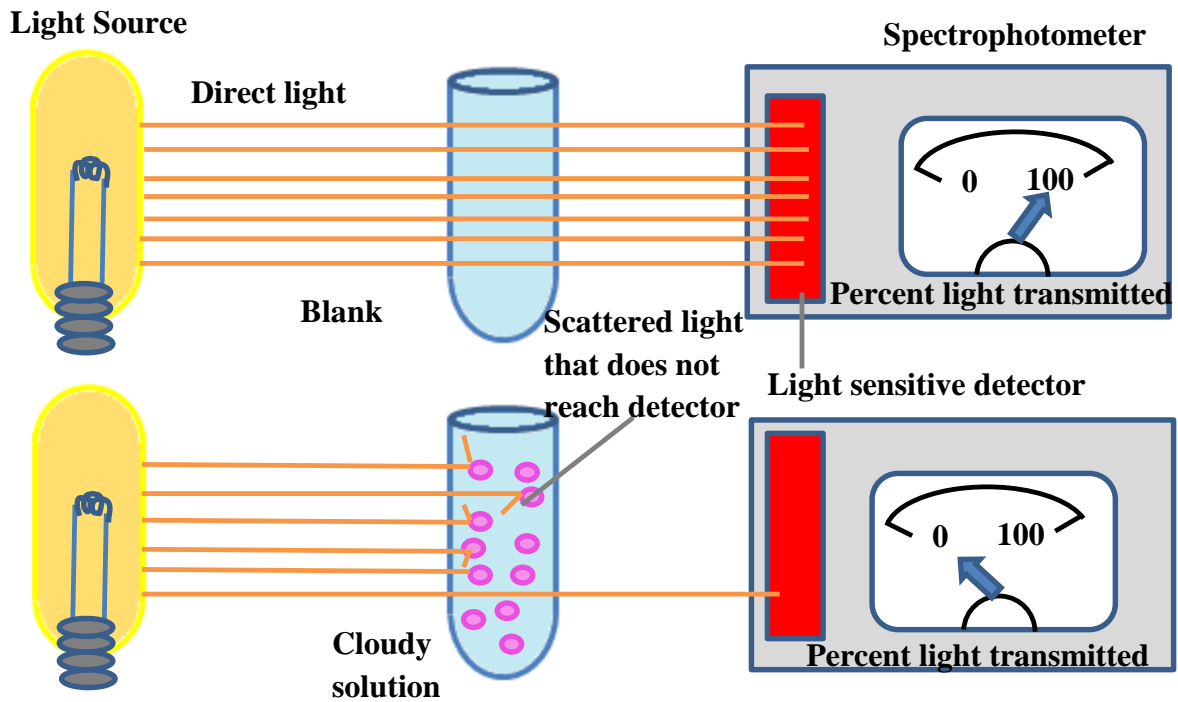


**Figure 3.9** A sketch showing the effect of the presence of dispersed particles on the turbidity of a suspension and the light transmittance.

Fehrenbacher and co-workers reported the use of UV-Visible spectrometers for turbidity measurements (Fehrenbacher et al. 2000). Turbidity,  $\tau$ , is defined as the attenuation of the beam of light according to the equation:

$$\tau = \left(\frac{1}{l}\right) \ln \left(\frac{I_0}{I}\right) \quad (3.20)$$

Where  $l$  is the length of the optical path and  $I_0$  and  $I$  are the intensities of the incident and the transmitted light respectively. If absorbance can be excluded, the turbidity is solely due to the scattering of the light by the particles. So the measurement of  $\tau$  as a function of incident wavelength can be used to determine the optical properties of a solution (Anon 2012b). Using the relationship, turbidity,  $\tau = e c$  where  $e$  is the molar absorptivity coefficient and  $c$  is the total concentration of the solution, molar absorptivity constant can be found out when the turbidity of solution is known. The theory of light scattering by isotropic monodisperse spherical

particles has been given by Mie and can be used to find the turbidity by monodisperse spherical particles (Kissa 1999).

The decrease in light transmission due to light scattering depends on the number of scattering particles,  $N$ , per unit volume and their scattering cross-section,  $\pi r^2$ .

$$\tau = Q\pi r^2 N \quad (3.21)$$

Where  $Q$  is the total Mie scattering coefficient and  $r$  is the radius of the particles.

The scattering coefficient,  $Q$ , is defined as the ratio of the scattering cross-section to the geometrical cross-section.  $Q$  is the function of two parameters  $\alpha$  and  $m$ , where  $\alpha$  is a dimensionless particle size parameter (Eq. 3.22);  $m$  is the ratio of refractive index of the particles,  $n_p$ , and refractive index of the medium,  $n_m$ . This indicates that particles with bigger diameter will scatter more compared to the particles with a smaller diameter.

$$\alpha = \frac{2\pi r}{\lambda_m} = \frac{\pi D}{\lambda_m} \quad (3.22)$$

Where  $\lambda_m$  is the wavelength of the incident light in the dispersion medium and  $D$  is the diameter of the particles. The wavelength  $\lambda_m$  is related to the refractive index,  $n_m$ , of the medium by Eq. 3.23:

$$\lambda_m = \frac{\lambda_0}{n_m} \quad (3.23)$$

Where  $\lambda_0$  is the wavelength of the incident light in vacuum.

$$m = \frac{n_p}{n_m} \quad (3.24)$$

Equation 3.22 states that  $\alpha$  is inversely proportional to  $\lambda_m$ , which is the wavelength of the incident light. So using a shorter wavelength of incident light would give higher scattering efficiency. This can be used to help determine the incident wavelength to be used for the experiments.

## **Applications**

Turbidity measurements are most commonly undertaken for wastewater treatment to determine the effectiveness of the treatment method. It can be used to monitor and increase the efficiency of precipitation and the filtration process (Staff 2011).

### **3.7 Dynamic Light Scattering (DLS)**

Dynamic light scattering (DLS) is a technique used to measure the time-dependent fluctuations of scattered light and is also called photon correlation spectroscopy (PCS) or quasi-elastic light scattering (QELS) (Kissa 1999). It is a non-invasive technique for measuring the size and the size distribution of particles and molecules of submicron size (Goldburg 1999). In this technique, monochromatic light, e.g. a laser light is passed through a sample. The Brownian motion of particles or molecules in suspensions or emulsions causes the laser light to be scattered at different intensities due to the Doppler Shift which changes the wavelength of the incoming light. An interference pattern is created and each bright spot represents a speckle. The speckle pattern changes as the particle moves and this is called flickering. The study of these intensity fluctuations yields the velocity of the Brownian motion which can then be used to determine the particle size using the Stokes-Einstein equation (Goldburg 1999). The velocity of the scatterer is measured in order to calculate the diffusion coefficient which is then used to calculate the size of the particles. Larger particles move less rapidly than the smaller particles. If the Brownian motion is not interrupted by sedimentation or particle-particle interactions (usually due to high concentrations), the movement of particles is random. The fluctuations in

the scattered light intensity are detected and measured by a photomultiplier and the data obtained is processed by a correlator.

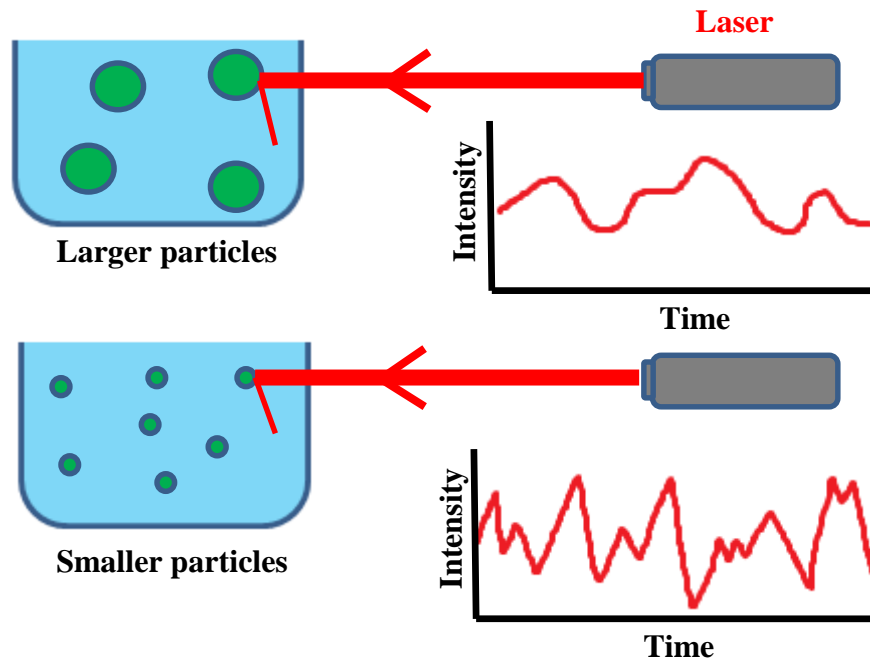


**Figure 3.10** A sketch showing the effect of the particle size on the intensity of fluctuation of the laser light using DLS.

A correlator is used to compare the intensity of scattered light at time  $t$  to the intensity observed at a very small time interval  $t'$  and construct a second order autocorrelation function  $G_2(t')$  of the scattered intensity:

$$G_2(t') = \frac{\langle I(t)I(t+t') \rangle}{\langle I(t) \rangle^2} \quad (3.25)$$

The experimentally measured intensity autocorrelation function  $G_2(t')$  depends only on the time interval  $t'$ , and is independent of  $t$ , at which the measurement was started.

This  $G_2(t')$ , can be related to the normalized field autocorrelation function  $G_1(t')$  by the Siegert relation, if the number of particles in the measure volume is adequate.

$$G_2(t') = A + B[G_1(t')]^2 \quad (3.26)$$

Where  $A$  is the background term designated as the baseline value,  $B$  an instrument-dependant factor.

It can be shown that the autocorrelation function  $G_1(t')$  of a monodisperse sample decays exponentially:

$$G_1(t') = \exp(-\Gamma t') \quad (3.27)$$

where  $\Gamma$  is the decay constant ( $s^{-1}$ ).

Substitution of the above two equations yields the measured intensity autocorrelation function:

$$G_2(t') = A + B \exp(-2\Gamma t') \quad (3.28)$$

The decay constant  $\Gamma$  is linearly related to the translational diffusion coefficient,  $D_T$ , of the particle:

$$\Gamma = D_T q^2 \quad (3.29)$$

The modulus,  $q$ , of the scattering vector is given by:

$$q = \frac{4\pi n}{\lambda_0} \sin(\theta/2) \quad (3.30)$$

Where  $n$  is the refractive index of the dispersion medium,  $\theta$  is the scattering angle and  $\lambda_0$  is the incident light wavelength in vacuum.

DLS measures the diffusion coefficient  $D$ , which can be used in the calculation of particle size using the Stokes-Einstein equation:

$$D = \frac{kT}{3\pi\eta d} \quad (3.31)$$

Where  $k$  is the Boltzmann's constant,  $T$  is the absolute temperature,  $\eta$  is the viscosity and  $d$  is the apparent Stokes-Einstein particle diameter. This equation is though only valid for non-interacting, spherically shaped, smooth and rigid particles.

One of the advantages of using this technique is that it allows the analysis of samples with broad molecular mass distribution (e.g. proteins in their native form and different size aggregates or polymers in their unaggregated and aggregated states).

## **Applications**

This technique has a range of applications; it is used to for macromolecular characterization and to study the interactions in proteins, nucleic acids, micelles, viruses and polysaccharides and has many physiological and biomedical applications (Pecora 1985).

### **3.8 Small Angle Neutron Scattering (SANS)**

Neutron scattering gives detailed information about the microscopic behaviour of condensed matter and plays a major role in shaping the experimental and theoretical understanding of materials ranging from magnetism and superconductivity to chemical surfaces and interfaces. Neutrons are generated by two main mechanisms; either by using a beam of neutrons derived by fission of  $^{235}\text{U}$  nuclei or a more recent approach where a beam of high energy charged particles is fired at the target to produce high energy neutrons. A moderator then slows these neutrons down. These types of neutron sources are called accelerator-based sources of neutrons. Traditional accelerator-based systems used an electron source to accelerate the electron beam and then fired at a dense target made of heavy element like uranium to produce neutrons by a two-stage process. But in the more recent approach, also used at ISIS, the sources use a linear accelerator together with a synchrotron to accelerate a beam of protons to high energy ( $\sim 800$  MeV) which is then fired at a heavy metal target for example tantalum, uranium or tungsten. Neutrons are produced by the spallation process, these types of sources are usually

pulsed and so a pulsed neutron flux is produced and is ideally suited for the time-of-flight neutron diffraction technique. This involves measuring the time-of-flight ( $t$ ) taken for a neutron to travel the total flight path ( $L$ ) from the moderator to the detector via the sample. The neutrons scatter from the sample, changing their energy and direction and are then intercepted by the detector. The momentum transfer ( $Q$ ) to the sample involved in this process is given by the equation:

$$Q^2 = k_i^2 + k_f^2 - 2 \cdot k_i \cdot k_f \cdot \cos\theta \quad (3.32)$$

Where  $k_i$  and  $k_f$  are the initial and the final wavevectors respectively and  $\theta$  is the scattering angle.

Small-angle neutron scattering (SANS) has become one of the key techniques to study the large scale structures and the bulk properties of materials (such as size, polydispersity, structure and particle interaction). The length scale probed by this technique ranges from tens to hundreds of nanometers making them ideal to study surfactants, colloids and polymers.

In SANS, different length scales are explored in reciprocal space by detecting the number of scattered neutrons as a function of the wavevector,  $Q$ , which is inversely proportional to the distance,  $d$  (where  $d = 2\pi/Q$ ) and is related to the wavelength of the incident neutron beam,  $\lambda$  and the scattering angle,  $\theta$  by the relationship:

$$Q = \frac{4\pi \sin(\theta/2)}{\lambda} \quad (3.33)$$

The value of  $Q$  hence can be varied by altering  $\theta$  or  $\lambda$ .

SANS beam has a 2-D area detector in a vacuum tank between 2-20 m of the sample.



SANS measurements were performed on time of flight LOQ diffractometer at ISIS Spallation Neutron Source, Oxfordshire, UK. Neutron wavelengths spanning 2.2-10 Å were used to access a  $Q$  range ( $Q = 4\pi \sin(\theta/2)/\lambda$ ) of approximately 0.008-0.25 Å<sup>-1</sup> (25 Hz), with a fixed sample-detector distance of 4.1 m.

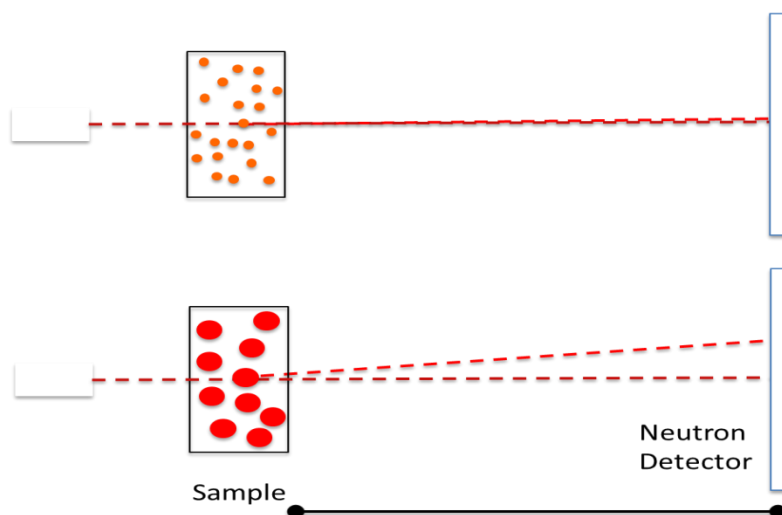


**Figure 3.11** A simple diagram showing the influence of the particle size on the scattering angle.

## Applications

SANS is used to study the bulk properties of a material (such as size, polydispersity, structure and particle interaction). The length scales probed by this technique ranges from tens to hundreds of nanometres which makes it ideal for studying materials such as surfactants, colloids, polymers, liquid crystals, protein solutions and lipid bilayers (ISIS).

## 3.9 High Performance Liquid Chromatography (HPLC)

HPLC is one of the most powerful chromatographic techniques for the separation and analysis of mixtures. The selectivity and the efficiency of the system can be altered by utilising stationary and mobile phase interactions. Classical liquid chromatography was evolved into highly efficient liquid chromatography in the 1960's (Horvath et al. 1967; Huber & Hulsman

1967; Kirkland 1968; Kirkland 1969). The high performance version of this technique is a result of the use of high operating pressures and small and uniform packing particle sizes, where individual components are moved down the column with the mobile phase forced through the column by high pressure using a pump. The mixture is then resolved into its individual components by the column packing due to the chemical/physical interactions between the mixture molecules and the column particles. These are then detected at the end of the column by a detector. The high performance refers to the narrowness of the peaks due to the extremely high plate numbers per unit length which is related to the small particle sizes in the packed column. High pressure is necessary to drive the fluid through the small pore sizes which creates an enormous back pressure. High performance also relates to the good resolution (separation) of peaks that is achievable.

In chromatography, the mobile phase retards components in relation to the degree of interaction they have with the stationary phase in competition with the mobile phase. The commonly used separation mechanisms in HPLC are reversed phase chromatography, normal phase and adsorption chromatography, ion exchange chromatography and size exclusion chromatography. Reversed phase chromatography is the most popular mode with the non-polar packing material in which silica gel is modified by attaching long hydrocarbon chains to them and a polar mobile phase is used. A strong attraction between the polar solvent and polar molecules in the mixture being passed through the column will lead to shorter retention time of these molecules. Non-polar compounds in the mixture however will tend to form attractions with the hydrocarbon groups attached to the silica gel because of van der Waals dispersion forces. They therefore spend less time in solution in the solvent and so they will travel through the column slowly.

For normal phase chromatography, a polar stationary phase e.g. silica is used with aliphatic or aromatic hydrocarbons as a mobile phase. Polar compounds in the mixture being passed

through the column will stick longer to the polar silica than the non-polar compounds which will pass through the column quickly and hence detected first by the detector.

### **Applications**

HPLC can be used for both qualitative and quantitative analysis of pure samples and complex mixtures of molecules. It has applications in virtually all fields of science for fundamental and applied research including biotechnology, biochemistry and pharmaceutical industries. Table 3.2 shows the basic principles of the major techniques used in this project and the advantages and the disadvantages of each technique.

**Table 3.2** Comparison of the major techniques used in this research.

Analytical Technique	Basic principal	Information	Advantages	Disadvantages
<b>Thermal Analytical techniques</b>				
Differential Scanning Calorimetry (DSC)	The instrument measures the heat flow into and out of a sample and an empty reference pan in a single furnace, as a function of temperature or time. The sample and the reference are heated at a controlled rate or held isothermally for a time period.	<ul style="list-style-type: none"> <li>Thermally activated processes associated heat exchange i.e. melting, evaporation, decomposition sublimation and glass transition</li> </ul>	<ul style="list-style-type: none"> <li>Small sample mass</li> <li>Easy to use</li> <li>Very little sample preparation</li> <li>Temperature variability</li> <li>Various sample types can be analysed</li> </ul>	<ul style="list-style-type: none"> <li>Cannot capture transitions that are associated with small changes in enthalpy</li> <li>No gold standard for baseline type to use for integration</li> </ul>
High Sensitivity Differential Scanning Calorimetry (HSDSC)	The instrument measures the difference between the heat flow into the sample solution and the blank solution, as a function of temperature or time.	<ul style="list-style-type: none"> <li>Thermally activated processes involving heat exchange in the solution samples, e.g. phase-transitions and aggregation processes.</li> </ul>	<ul style="list-style-type: none"> <li>Small sample volume</li> <li>Easy to use</li> <li>Temperature variability</li> <li>Protein analysis and other analysis with small heat changes can be detected</li> </ul>	<ul style="list-style-type: none"> <li>Air bubble and contaminants present in samples can affect the heat measurements.</li> <li>No gold standard for baseline type to use for integration</li> </ul>
Thermal Gravimetric Analysis (TGA)	Sample in a crucible is heated in an enclosed furnace under inert or oxidative atmosphere suspended on a highly sensitive balance. The weight of the sample is measured as a function of temperature or time.	<ul style="list-style-type: none"> <li>Thermally activated processes associated with weight change i.e. decomposition, sublimation and evaporation</li> </ul>	<ul style="list-style-type: none"> <li>Small sample mass</li> <li>Easy to use</li> <li>Very little sample preparation</li> <li>Temperature variability</li> </ul>	<ul style="list-style-type: none"> <li>Destructive</li> <li>Limited to transitions with associated weight change</li> </ul>
Hot-stage microscopy (HSM)	A beam of visible light is passed through a condenser onto the sample. Transmission, refraction and reflection of the light by the sample is then magnified and focused onto the ocular. The attached heating block heats the sample at a controlled rate, allowing the assessment of the optical properties of the sample as a function of temperature or time. The attachment of cross- polarisers below and above the sample, which rotates the plane of a polarised light, allows the analysis of the birefringence of crystalline solids due to their anisotropic properties.	<ul style="list-style-type: none"> <li>Birefringent properties (crystallinity)</li> <li>Crystal habits</li> <li>Morphology</li> </ul>	<ul style="list-style-type: none"> <li>Small sample mass</li> <li>Easy to use</li> <li>Very little sample preparation</li> <li>Temperature variability</li> </ul>	<ul style="list-style-type: none"> <li>Destructive method</li> <li>Does not provide quantitative information</li> </ul>

Spectroscopic Techniques				
Thermally stimulated current (TSC) spectroscopy	Measures the current generated by the orientation/reorientation of dipoles under the influence of static electrical field. Secondary relaxations appear at temperatures below primary processes.	<ul style="list-style-type: none"> <li>• Direct determination of relaxation times and their distribution</li> <li>• Able to distinguish between primary and secondary relaxation process</li> </ul>	<ul style="list-style-type: none"> <li>• Provides better resolution and higher sensitivity to secondary relaxation in comparison to DSC</li> </ul>	<ul style="list-style-type: none"> <li>• Problems with reproducibility</li> </ul>
Turbidity measurements (UV-Visible spectroscopy)	Absorption spectroscopy or reflectance spectroscopy in the ultraviolet-visible spectral region. Works on the principle of Beer-Lambert law, absorbance is directly proportional to the concentration of the absorbing species in the sample. This absorption corresponds to the excitation of the outer electrons in the molecules.	<ul style="list-style-type: none"> <li>• Provides qualitative and quantitative information for identification and concentration analysis.</li> <li>• Analysis of mixtures</li> </ul>	<ul style="list-style-type: none"> <li>• Easy to use</li> <li>• Non-destructive method</li> <li>• Temperature variability</li> <li>• Various sample types can be analysed</li> </ul>	<ul style="list-style-type: none"> <li>• Spectra not highly specific</li> <li>• Mixtures of molecules can be a problem due to overlap</li> </ul>
Dynamic light scattering (DLS)	A technique to measure the time-dependant fluctuations of scattering light and use that to measure the size and size distribution of molecules and particles typically in the submicron region.	<ul style="list-style-type: none"> <li>• Helps characterization of particles, emulsions or molecules, which have been dispersed or dissolved in suspensions.</li> </ul>	<ul style="list-style-type: none"> <li>• Capable of absolute measurements of several parameters of interest; <i>e.g.</i> molecular weight, mean square radius of gyration.</li> <li>• Useful over wide range of molecular weight.</li> </ul>	<ul style="list-style-type: none"> <li>• Only useful for transparent samples</li> <li>• Requires removal of extraneous scattering moieties; <i>e.g.</i> dust.</li> <li>• Requires solvent with a different refractive index than the solute.</li> </ul>
Small angle neutron scattering (SANS)	SANS is a neutron scattering technique that enables the study of materials on the nanometre to micrometre length scales. The experiment consists of a well collimated beam of neutrons being passed through a sample and detectors to count the number of neutrons scattered as a function of angle and neutron wavelength. This data can then be used to extract information about the shape, size, arrangement, and interactions of the components of the sample.	<ul style="list-style-type: none"> <li>• SANS is used in a wide range of scientific fields, but finds particular use in the study of soft matter (<i>e.g.</i> colloids and polymers), biophysics (<i>e.g.</i> lipids and lipid-protein complexes), biology (<i>e.g.</i> solution structures of proteins) and hard condensed</li> </ul>	<ul style="list-style-type: none"> <li>• Can be used to distinguish neighbouring elements in the periodic Table and isotopes of elements because they have substantially different scattering cross-sections.</li> </ul>	<ul style="list-style-type: none"> <li>• Expensive to build and maintain the site</li> <li>• Have relatively low flux and limited investigations in rapid time dependent processes</li> </ul>

		matter (e.g. superconductors and magnetic materials).	<ul style="list-style-type: none"> <li>• Neutrons are highly penetrating making them useful for the investigation of the interior of materials.</li> </ul>	
<b>Chromatography Techniques</b>				
High performance liquid chromatography (HPLC)	Sample is passed through a liquid mobile phase to separate the components of a mixture through a stationary column under high pressure. Components interacting with the stationary phase come out of the column slower than the non-interacting components and get detected at different times.	<ul style="list-style-type: none"> <li>• Can separate minute amounts of peptides and proteins.</li> <li>• Have applications in many industries including pharmaceutical and biotechnology industries.</li> </ul>	<ul style="list-style-type: none"> <li>• Powerful, high resolution and automated process.</li> <li>• Needs small amount of sample for analysis.</li> </ul>	<ul style="list-style-type: none"> <li>• Can be expensive to set up.</li> <li>• Low-sensitivity for some compounds.</li> </ul>

## **Chapter 4 : Study of Some Physical-Chemical Properties of Different Molecular Mass PPGs**

### **4.1 Introduction**

Previous investigations have shown greater effectiveness of pluronics with higher PPG content in changing the membrane microviscosity. L61 which has 90% PPG content induces a greater change in the plasma membrane microviscosity of tumor cells compared with P85 which has 50% PPG content (Melik-Nubarov et al. 1999). These observations provide, in part, the rationale for the project which is to investigate whether PPG can be used as a solubilizing agent for the drug delivery purposes.

The purpose of this chapter is to report investigations of the physico-chemical properties of PPG in its “pure” liquid form using TGA, DSC, TSDC and TW. The TGA study was undertaken to understand the thermal stability of the polymers by examining any weight loss processes as a function of temperature. Thermal properties were ascertained using DSC and MDSC. The focus of the TSDC and TW investigation was to elucidate the relationship between the PPG molecular mass and the molecular mobility. The cloud-point temperature and the phase-transition temperature ( $T_m$ ) of PPG upon heating were also analysed and compared using HSDSC and turbidity measurements.

### **4.2 Experimental**

#### **4.2.1 Materials**

Five different molecular mass PPG samples  $M_n \sim 425$ ,  $M_n \sim 725$ ,  $M_n \sim 1000$ ,  $M_n \sim 2000$  and  $M_n \sim 2700$  were purchased from Sigma-Aldrich UK and used as received. Double deionized water was used (supplied by the laboratories at the University of Greenwich).

The molecular mass of PPGs are between 150-4000 with the commercially available PPGs having a low polydispersity ( $M_w/M_n = 1.11-1.25$ ) and are soluble in ketones,

chlorohydrocarbons and aromatic hydrocarbons (Salamone 1996). Solubility in water at 20°C varies with molecular mass. PPG 425 is completely miscible in all proportions with water but PPG 1025 has a limited solubility of 1.5 g/100 g solution in water (Anon 2012a). Some important properties of different molecular mass PPGs are shown in Table 4.1.

**Table 4.1** Some properties of different molecular mass PPGs (Sigma-Aldrich).

Average Molecular mass	Refractive index (nD20)	Viscosity (cSt) (25°C)	Hydroxyl value (mg KOH/g)	Density (g mL <sup>-1</sup> ) at 25°C
425	1.447	80	263	1.004
725	1.449	115	147	1.007
1000	1.449	150	111	1.005
2000	1.451	300	56	1.005
2700	1.451	630	37	1.004

## 4.2.2 Methods

### 4.2.2.1 Thermogravimetric Analysis

Instrument: Q5000-IR Thermogravimetric Analyser

Manufacturer: TA Instruments, UK

Cooling system (internal): Compressed air cooling/water circulator

Software (control): TA Q Series (TA Instruments, UK)

Software (analysis): TA Universal Analysis (TA Instruments, UK)

### Calibration

Temperature calibrations were performed using the Curie point of a ferromagnetic metal as described by the ASTM E1582 method. A magnet is placed beneath the furnace in this calibration to increase the apparent weight of the certified reference materials, which in this case are alumel and nickel. After the stabilisation of the apparent weight under the influence of



the magnet, the sample is heated at usually 5 and 10°C min<sup>-1</sup>. The sample loses magnetism at the Curie point resulting in a sharp drop in the loss of the apparent weight. The extrapolated end point temperature is calculated. The expected Curie points for the certified alumel and nickel materials are 152.26 and 358.28°C, respectively. The instrumental software automatically computes the offset between the experimental and reference Curie point temperatures and stores the value in a calibration temperature table.

Weight calibration is performed using known calibration weights provided by the manufacturer. For this calibration an empty sample pan and 100 mg standard weight are weighed and automatic adjustments of the balance are performed until the weight reading matches that of the standard weight.

All samples were introduced into the furnace in a Tzero™ hermetically sealed aluminium sample pan with a single pinhole in the lid. Samples were heated under a nitrogen atmosphere at a flow rate of 25 ml min<sup>-1</sup> from ambient temperature to a maximum of 600°C at a specified heating rate.

### **Instrumentation and Experimental Protocol**

The main components of a thermobalance are: a sensitive recording balance, a furnace with a controlled environment and a data recorder and plotter. The change in mass is recorded by a null-balance when the beam carrying the sample and the counterweight moves leading to a variation in current in the photodetector. The sample usually hangs down from the balance into the furnace. The furnace is designed to withstand high temperatures and is purged with air or nitrogen to maintain inert atmosphere inside the furnace (Price et al. 2000).

A sample mass of 15.00 ± 1 mg was used for all PPG samples. Samples were heated to 600°C in hermetically sealed aluminium pans with a single pinhole in the lid, at a heating rate of 10°C min<sup>-1</sup>.

#### 4.2.2.2 Differential Scanning Calorimetry

Instrument:	DSC Q2000
Manufacturer:	TA Instruments, UK
Cooling system (internal):	Refrigerated cooling system (RCS)
Software (control):	TA Q Series (TA Instruments, UK)
Software (analysis):	TA Universal Analysis (TA Instruments, UK)

#### Calibration

The calibration of the TA Instruments Q2000 instrument is performed in two parts. The first part is the determination of the cell resistance and capacitance. For this calibration two experiments are performed. The first experiment is the determination of the cell resistance and this is performed with an empty cell. During this experiment the cell is equilibrated at a temperature of  $-90^{\circ}\text{C}$  for 5 minutes, followed by a heating ramp from  $-90$  to  $400^{\circ}\text{C}$  at  $20^{\circ}\text{C min}^{-1}$ . It is important to note that a preheating experiment using the same parameters is usually performed. The second part of the calibration is to determine the cell capacitance, which involves the same experimental method as the cell resistance but with the use of sapphire discs of known weight and heat capacity in the reference and sample cell.

The next calibration involves the determination of the cell constant and temperature calibration, which are obtained from a single experiment.

In this experiment 1-5 mg of an indium standard is pre-heated to a temperature above the melting transition temperature i.e.  $180^{\circ}\text{C}$  and then held at this selected temperature. The sample is then cooled to  $100^{\circ}\text{C}$  held under isothermal conditions and then subjected to a heating ramp (usually  $10^{\circ}\text{C min}^{-1}$ ) to a temperature above the melting transition. The enthalpy of fusion is determined by integration and compared with the known value ( $28.71 \text{ J g}^{-1}$ ). The cell constant

is the ratio between the experimentally determined and expected value and should be between 1 and 1.2. The melting temperature is determined using the extrapolated onset temperature, and this is also compared with the known value (56.6°C) and the difference is calculated for the temperature calibration.

### **Instrumentation and Experimental Protocol**

DSC studies were performed using hermetically sealed Tzero™ aluminium pans with a pinhole in the lid. DSC studies were performed under a nitrogen atmosphere at a flow of 50 mL min<sup>-1</sup>. Sample masses of 10 ± 1 mg were equilibrated at -90°C, held isothermally for 5 min and then heated to -40°C at 2°C min<sup>-1</sup>.

#### **4.2.2.3 Thermally Stimulated Current Spectroscopy**

Instrument: TSCII/RMA, Thermally Stimulated Current spectrometer

Manufacturer: SETARAM Instrumentation, France

Electrometer (internal): 6517A electrometer/high-resistance meter (Keithley, UK)

Cooling system (external): 900 series LN2 microdosing system (Norhof, Netherlands)

Software: TSC/RMA software (SETARAM Instrumentation, France)

### **Calibration**

The only calibration that is needed before analysis is a temperature calibration using an indium standard. The objective of the calibration is to compensate for the temperature difference between the temperature sensor and the sample area. The instrument comes with a special calibration kit (Fig. 4.1) that consists of a calibration electrode probe, which holds the indium sample firmly in place against the PTFE cup. The dimple in the electrode absorbs the molten indium upon heating to prevent it from flowing out to the edge of the electrode. This is important as it lowers the noise generated during the melting of indium.

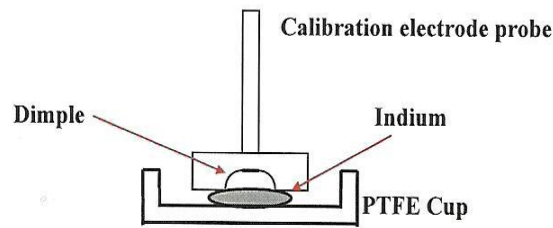


**Figure 4.1** SETARAM TSC II calibration kit set up (SETERAM TSC II manual).

In the calibration experiment the indium sample is initially heated to 190°C, which is about 40°C above the melting point. This preheating process removes any internal stress. A polarisation voltage of 1 V mm<sup>-1</sup> is applied as the sample is kept at 190°C for 3 min. The response of the indium sample is then recorded as the sample cooled and heated at the same rate, allowing the determination of the temperature onsets for the crystallisation ( $T_c$ ) and melting ( $T_m$ ) processes (Fig. 4.2).

The offset is calculated by comparing the experimentally determined onsets with expected values ( $T_m = 156.6^\circ\text{C}$  and  $T_c = 155.0^\circ\text{C}$ ) i.e. the offset is given by the subtraction of the experimental onsets from the expected values.

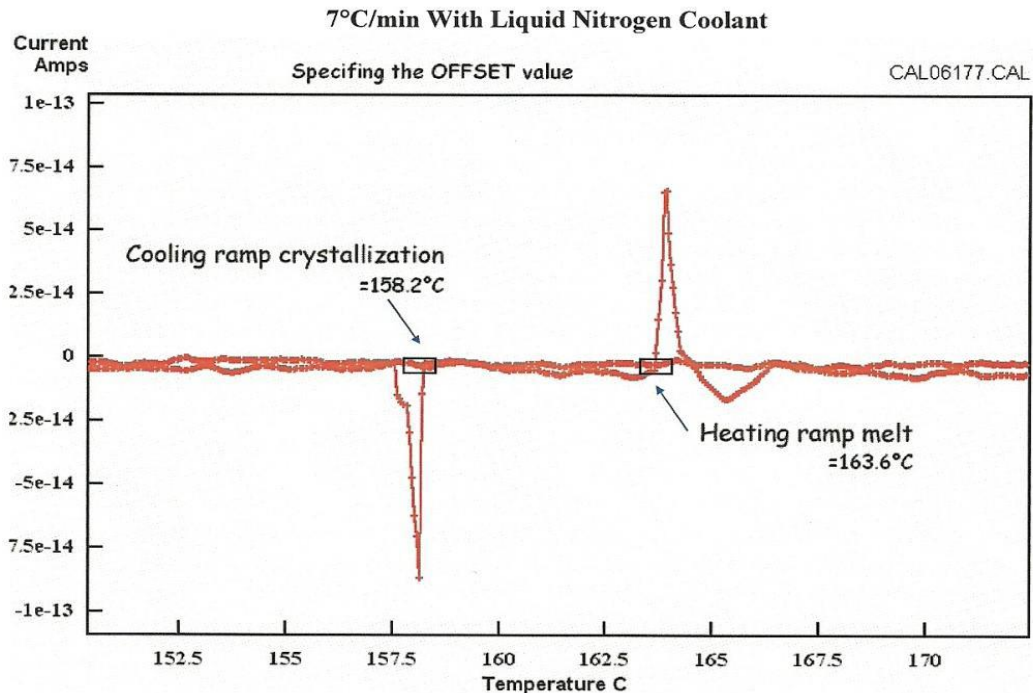


**Figure 4.2** Calibration results showing the onsets of crystallisation and melting processes (SETERAM TSC II manual).

## **Instrumentation and Experimental Protocol**

Experiments were performed using a liquid electrode arrangement that consists of a bottom and upper electrode with a PTFE ring spacer, the sample in this arrangement has an effective surface area of 50 mm<sup>2</sup>. The sample size used was in the range of 60 – 80 mg. Prior to each experimental run, the sample chamber was evacuated to 10<sup>-4</sup> mbar and flushed several times with high purity helium (1.1 bars) prior to the analysis. The global TSDC spectra were obtained by polarising the sample at -70°C with a polarisation field ( $E_p$ ) ranging from 50 to 350 V mm<sup>-1</sup> for 2 min ( $t_p$ ). In the case of thermal windowing experiments, the samples were polarised with  $E_p = 350$  V mm<sup>-1</sup> at  $T_p$  of -94 to -65°C in increments of 1°C.  $T_w$  was set at 1°C, whilst  $t_p$  and  $t_w$  were set at 2 min for all four samples.

### **4.2.2.4 High Sensitivity Differential Scanning Calorimetry**

Instrument:	NanoDSC
Manufacturer:	TA Instruments, UK
Heat Measurement System	Power Compensation
Software (control):	Nano DSC Run (TA Instruments, UK)
Software (analysis):	NanoAnalyze (TA Instruments, UK)

## **Instrumentation and Experimental Protocol**

No calibration is needed. But the balancing of cells is occasionally performed. The balance and residual scans are run to obtain flat baselines. When baseline scans are subtracted from sample scans, the baseline shifts cancel out. The balance run creates a baseline for the calorimeter, which yields a heat flow signal that is near zero when both cells contain solutions with near identical heat capacity. To further flatten the baseline across the entire temperature range, a residual scan is run to correct the instrument baseline and is generally used for cosmetic

reasons only. To perform the balance and the residual scan, deionized and degassed water is filled in the reference and the sample cells and is scanned from 0-130°C at 1°C min<sup>-1</sup>.

This instrument can measure microwatt levels of power input into the appropriate cell in order to maintain the cells at the same temperature. The cells have a fixed capillary design which minimizes aggregation and precipitation of samples in the cells. This design has another benefit; these capillary tubes have a high surface-to-volume ratio that helps provide an even heat supply to the samples and reduces the temperature gradient and viscosity effects. It has a small cell volume of 300 µL. This small volume helps in minimizing the temperature gradient that occurs in large sample volumes and also helps in the elimination of the need of constant stirring of the sample to avoid the presence of any air bubbles entering the cells. The small cell volume also prevents the production of heat due to the stirring of variable viscosity liquids that can produce uncontrollable heat, which is a lot greater than the measured heat effect. The fixed cells system helps reproducibility and stability between the subsequent scans.

2 mg mL<sup>-1</sup> aqueous solutions of PPG samples were prepared in deionised water. All the samples were degassed in the degassing station (TA Instruments) for 10 min at 25°C under a vacuum of 20 mmHg to minimise gas bubble formation during scanning. This process is necessary in order to prevent noisy scans as bubble formation can cause abrupt changes in heat capacity data. The reference cell was filled with deionised water and the sample cell with the degassed sample and the cells were pressurised up to 3 atm using the software control. The samples were scanned up and down from 10-85°C at a scan rate of 1°C min<sup>-1</sup> and equilibrated at the temperature for 30 minutes before the start of each scan.

#### 4.2.2.5 UV-Visible Spectroscopy

Instrument:	Cary 100 UV-Vis
Manufacturer:	Agilent Technologies, UK
Software (control):	Cary WinUV (Agilent Technologies, UK)
Software (analysis):	Cary WinUV (Agilent Technologies, UK)

#### Calibration

There is no need for calibration. In-built tests in the software are available for the optimization of the settings and validation of the accuracy of Cary 100. The tests are pre-set with default parameters that comply with international standards for Good Laboratory Practices.

#### Experimental Protocol

Aqueous solutions of PPGs ( $2 \text{ mg mL}^{-1}$ ) were prepared in deionised water and the blank used was deionised water. The samples were heated from 10-85°C at  $2^\circ\text{C min}^{-1}$  and the measurements were taken at every  $2^\circ\text{C}$ . The temperature was held at 10 and 85°C for 5 min to allow the sample to equilibrate. Measurements were taken at 532 nm wavelength and optically matched glass cuvettes were used for the experiments with plastic lids to cover the cuvettes.

### 4.3 Results and Discussion

#### 4.3.1 Thermogravimetric Analysis

TGA results for the different PPG samples (Fig. 4.3) show a significant difference in the temperature of decomposition between PPG 425 and the other PPG samples analysed as the samples were heated from ambient to 600°C. We propose the reaction in the pans was a decomposition reaction because of the PPG decomposes upon heating due to the appearance of tiny black residues at the end of the experiment. It has also been reported in the literature

that heating of PPG at 1 atm causes it to decompose (Cheremisinoff 2003). The derivative weight-loss curve (Fig. 4.3) shows that there is a single weight-loss process involved because of the presence of only one peak for each PPG samples in the thermogram. The derivative peak temperature (Table 4.2) shows the peak weight loss temperature for different PPGs. Furthermore, no water content was detected for the PPGs except for PPG 425 which exhibited a very low moisture content of  $1.2 \pm 0.3\%$  (Fig. 4.4). TGA gives information about the stability of the PPG samples. The decomposition temperatures for the five PPGs indicate the lowest stability of PPG 425 because of lower decomposition temperature compared with the other PPGs. The difference between the decomposition temperatures of PPG 425 compared with the other PPGs is probably due to the lower entanglement and intramolecular interactions between the lower molecular mass PPGs.

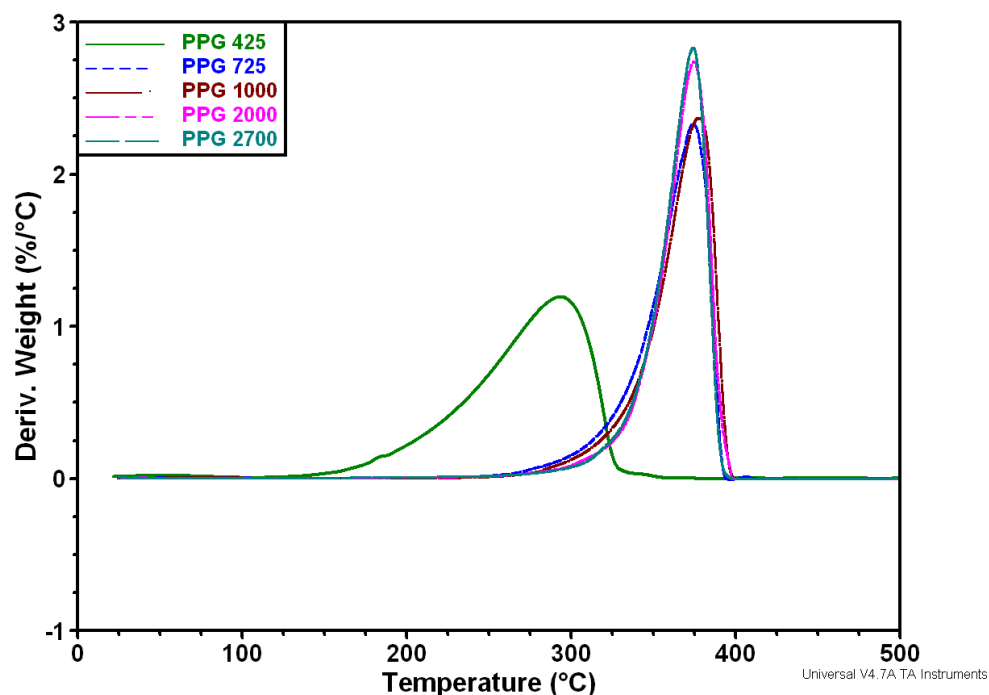


**Figure 4.3** Derivative Thermogravimetric (DTG) curve overlay of different PPG samples heated from ambient temperature to 600°C at 10°C min<sup>-1</sup>.



**Table 4.2** The peak temperatures for the weight loss change for different PPG samples upon heating.

Molecular mass of PPG	Peak temperature (°C)
425	293 ± 1
725	374 ± 2
1000	379 ± 2
2000	374 ± 2
2700	374 ± 2

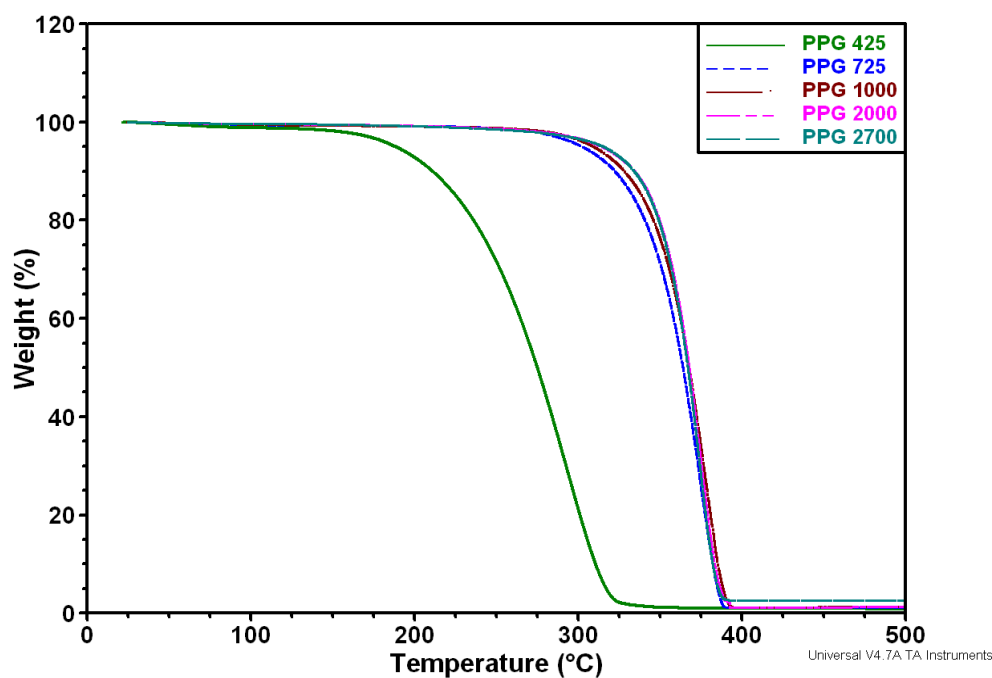


**Figure 4.4** Thermogravimetric (TG) curve overlay of different PPG samples.

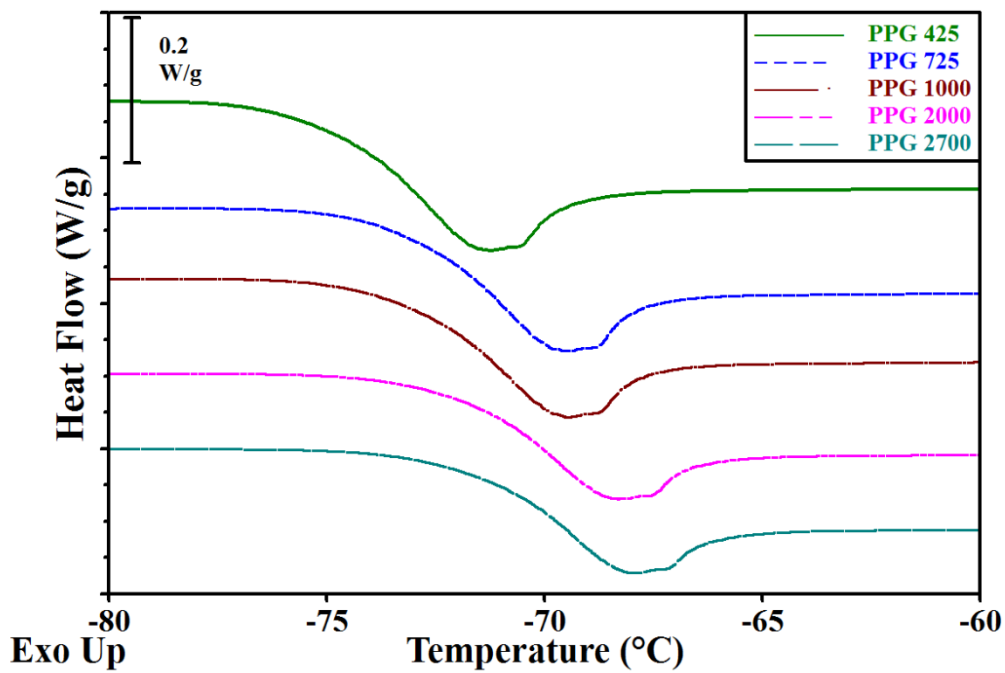
### 4.3.2 Differential Scanning Calorimetry

MDSC was performed on the samples. PPG samples are liquid at room temperature and the DSC results show that cooling the sample to  $-90^{\circ}\text{C}$  generates an amorphous form. Enthalpy relaxation was observed in the heat flow step-change during the glass transition (Fig. 4.5). Normally this phenomenon is due to non-equilibrium cooling producing free volume. The molecular motion of the chains has been frozen and the chains are not in their preferred equilibrium positions (Hutchinson 1995). On warming above  $T_g$ , the chains can move and relax into their preferred positions thereby giving rise to the enthalpic signal superimposed upon the  $T_g$  step.

The  $T_g$  was determined by the temperature mid-point of the transitions (Fig. 4.6). Fig. 4.5 shows the total heat flow obtained using DSC. This graph shows that there is a step change in the heat flow baseline obtained for the 5 PPG samples that overlaps with a small endothermic signal (enthalpy relaxation). Data obtained from the temperature modulated DSC (TMDSC) (Fig. 4.6 and Fig. 4.7) separates the total heat flow into two parts; a reversible or thermodynamic component, reflecting the temperature changes of vibrational amplitudes and an irreversible or kinetic process, so-called enthalpy relaxation.

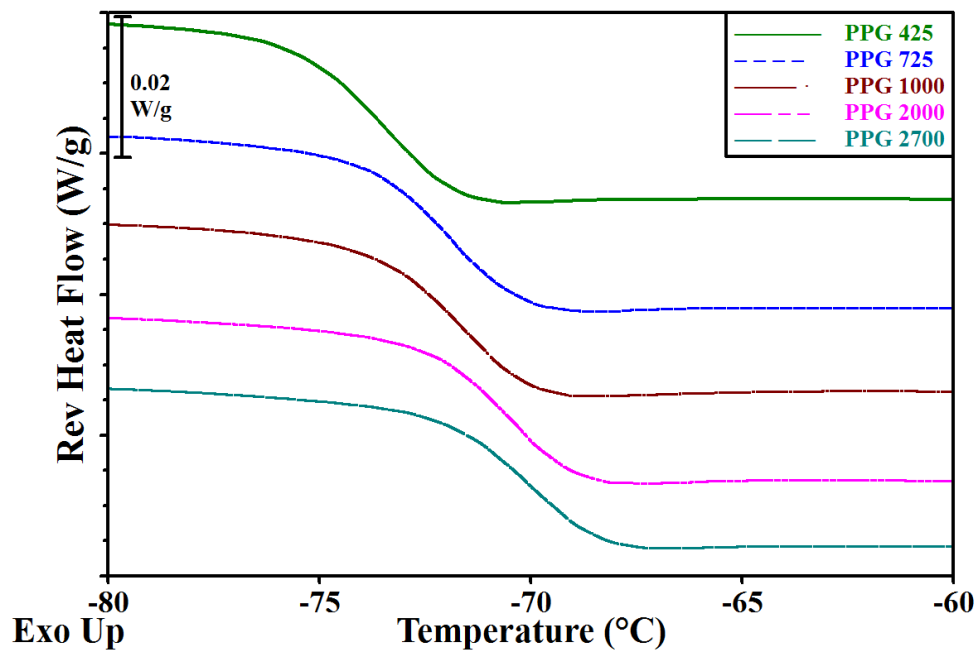
The reversing heat flow signal, (Fig. 4.6) gives information about the glass-transition temperature.  $T_g$  increases with an increase in the molecular mass of PPG (Table 4.3).

The non-reversing heat flow signal (Fig. 4.7) shows recovery of excess energy (enthalpy relaxation) lost during the glass formation process for different molecular mass PPGs. Table 4.3 shows that the enthalpy relaxation decreases with the increase in molecular mass. The difference between these enthalpy relaxation values for the different PPGs is very small (Table 4.3). This decrease is possibly due to the fact that mobility is more sluggish for larger molecular mass compounds; and as such the loss in excess energy due to molecular rearrangement is limited by viscous factors. This certainly seems a reasonable explanation given the scale of the increase in viscosity when PPG 425 is compared to PPG 2700, as shown in Table 4.1.



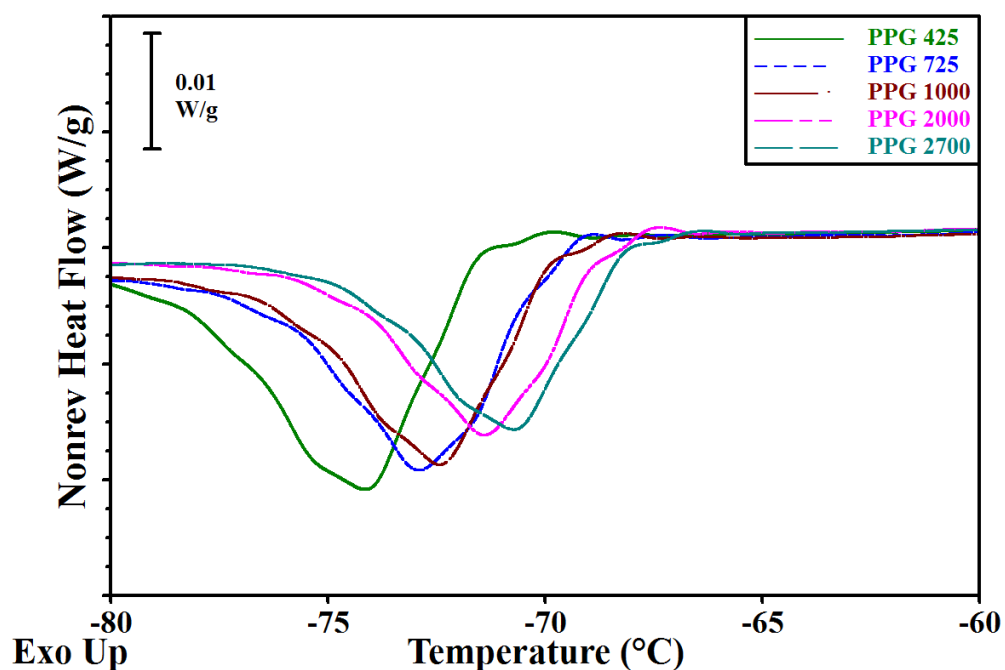
**Figure 4.5** Total heat flow using DSC for the five different PPG samples.

Fig. 4.6 shows the glass transition that is under equilibrium control, i.e. it is reversible. Fig. 4.7 shows that enthalpy relaxation is not reversible due to PPG chains in their non-preferred orientations and positions.



**Figure 4.6** Reversing heat flow signal obtained using DSC for the five different PPG

samples showing the glass transition which is under equilibrium control i.e. it is reversible.



**Figure 4.7** Non-reversing heat flow signal obtained using DSC for the five different PPG samples showing that enthalpy relaxation is not reversible.

**Table 4.3** Change in the enthalpy relaxation and  $T_g$  with the change in the molecular mass of PPGs.

Molecular mass of PPG	Enthalpy Relaxation change, $\Delta H$ ( $J g^{-1}$ )	Glass-transition temperature, $T_g$ ( $^{\circ}C$ )
425	2.7	$-74 \pm 1$
725	2.5	$-73 \pm 1$
1000	2.3	$-72 \pm 1$
2000	2.1	$-71 \pm 1$
2700	1.9	$-70 \pm 1$

### 4.3.3 Thermally Simulated Current Spectroscopy

TSDC and TW experiments were conducted to study the movement of dipoles in the samples. Four PPG samples were analysed using TSC covering the molecular mass between 425-2700. PPG 425, 1000, 2000 and 2700 were chosen for the detailed TSC study.

### TSDC analysis

The TSDC output for the PPGs after polarisation at  $-70^{\circ}\text{C}$  using a voltage of  $350\text{ V mm}^{-1}$  is presented in Fig. 4.8. The global dipole relaxation processes observed for the PPG samples that is attributed to the glass transition relaxation process are observed in the temperature range analysed. The current intensity and the temperature of the current maxima ( $T_m$ ) exhibit small but consistent differences between consecutive PPG's. The current intensity decreases but the  $T_m$  increases with the increasing molecular mass. The temperature and magnitude of the currents generated provide information about the degree of dipole mobility, which is an indication of the molecular mobility.

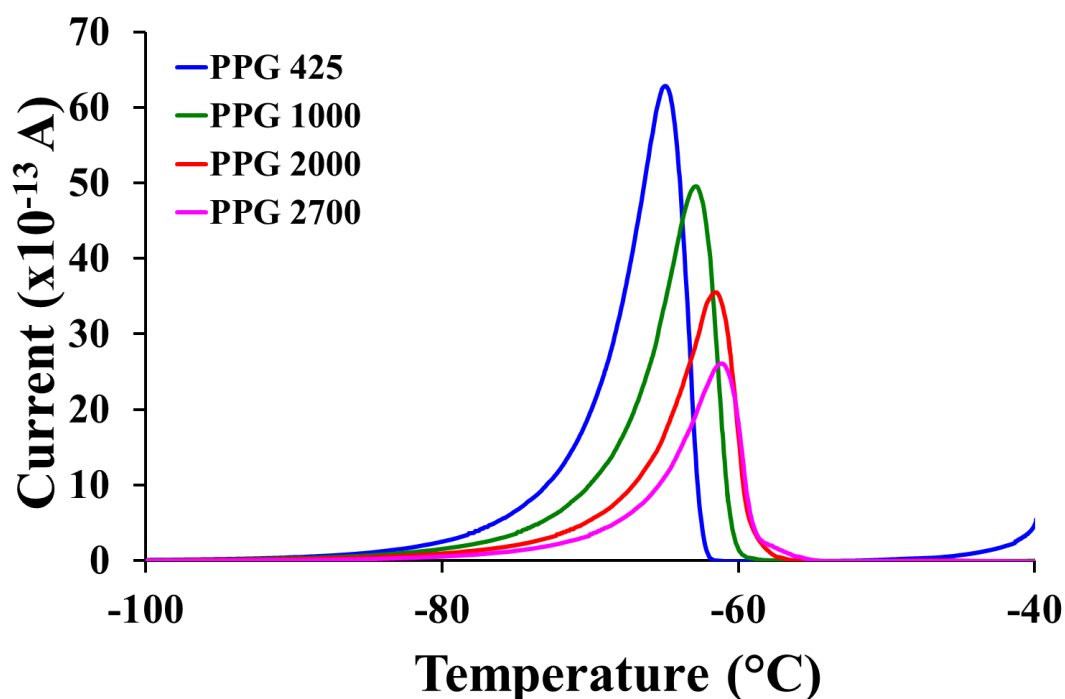


**Figure 4.8** Global TSDC curve overlay of PPG 425, 1000, 2000 and 2700 polarized at  $-70^{\circ}\text{C}$  with a polarizing field of  $350\text{ V mm}^{-1}$ .

For related polymer materials, interpretation of the TSDC spectrum in terms of the degree of molecular mobility can be difficult, since the current generated from TSDC experiments can result from a multitude of contributing factors such as space charge and interfacial polarisations, sample mass and number of dipoles per unit volume present in the sample (Turnhout 1975; Ibar 1993). However, with careful experimentation, the contributions from space and interfacial charges can be removed, and by normalising the polarisation acquired, it is possible to extract important information about the nature and the degree of the molecular mobility.

In this study the polarisation values, obtained using  $350 \text{ V mm}^{-1}$  at  $-70^\circ\text{C}$ , were normalised with respect to the mass (g) and the number of moles. When polarisation is normalised in relation to mass (g), an inverse linear relationship ( $R^2 > 0.999$ ) with increasing PPG molecular mass was observed (Fig. 4.9a). The decrease in polarisation detected with increasing PPG molecular mass is attributed to the hydroxyl value, which form the major polarisable units in the PPG polymers. PPG 425, which undergoes greater polarisation, has the highest hydroxyl value, whilst PPG 2700 which has the lowest hydroxyl value exhibits the lowest polarisation of the PPG samples analysed (Table 4.1).

The next approach leads to the polarisation being normalised based on the number of moles, to account for the effect of the amount of hydroxide groups/permanent dipoles present in each sample on the magnitude of polarisation (it is assumed that each PPG molecule is linear and contains only two OH groups located on the ends of the polymer chain). Polarisation increases with increasing molecular mass ( $R^2 > 0.9$ ) (Fig. 4.9b). If we consider the magnitude of polarisation to be indicative of the amount of molecular motion the sample undergoes, then it can be stated that increasing molecular mass increases the degree of molecular mobility. This demonstrates that mobility does not only arise from the OH groups but involves the movement of the molecular backbone which is full of oxygen in its structure. An increase in PPG

molecular mass leads to a decrease in the intra- and inter- molecular interactions which then lead to an increase in the chain flexibility. Larger molecular mass PPGs exhibit greater degrees of motional freedom and, therefore, a greater number of motional modes can be activated during the polarisation process. The degree of molecular mobility of polymer segments (once activated) is therefore enhanced in larger molecular mass PPGs, which is reflected in the relationship found between polarisation per molecule ( $C \text{ mol}^{-1}$ ) and the molecular mass of the PPGs analysed (Fig. 4.9b).

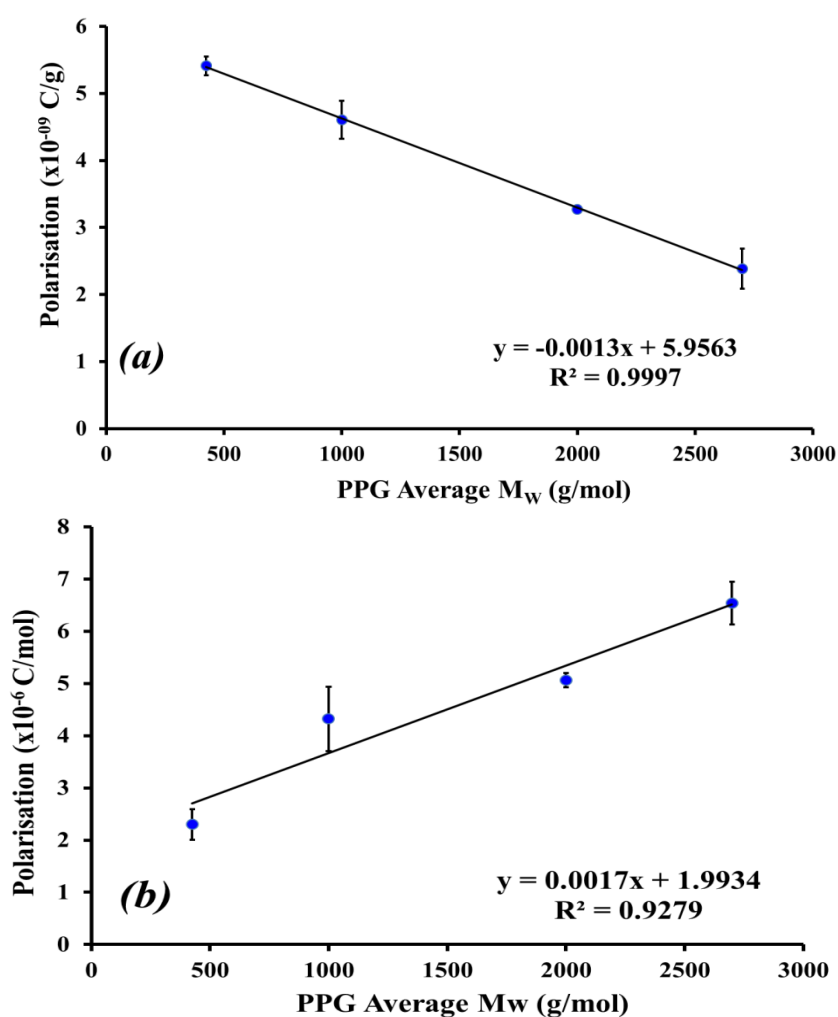


**Figure 4.9** Plots of normalised polarization values against PPG molecular mass

(a) normalised to the mass of sample used and (b) normalised using the number of molecules.

## TW Analysis

The thermal windowing experiments were performed to provide greater detail about the nature of the molecular mobility detected in the glass transition region for the PPG samples. Figs. 4.10 and 4.11 show the results obtained from the TW experiments conducted on the PPG samples together with the distribution of the relaxation times for each elementary process isolated.

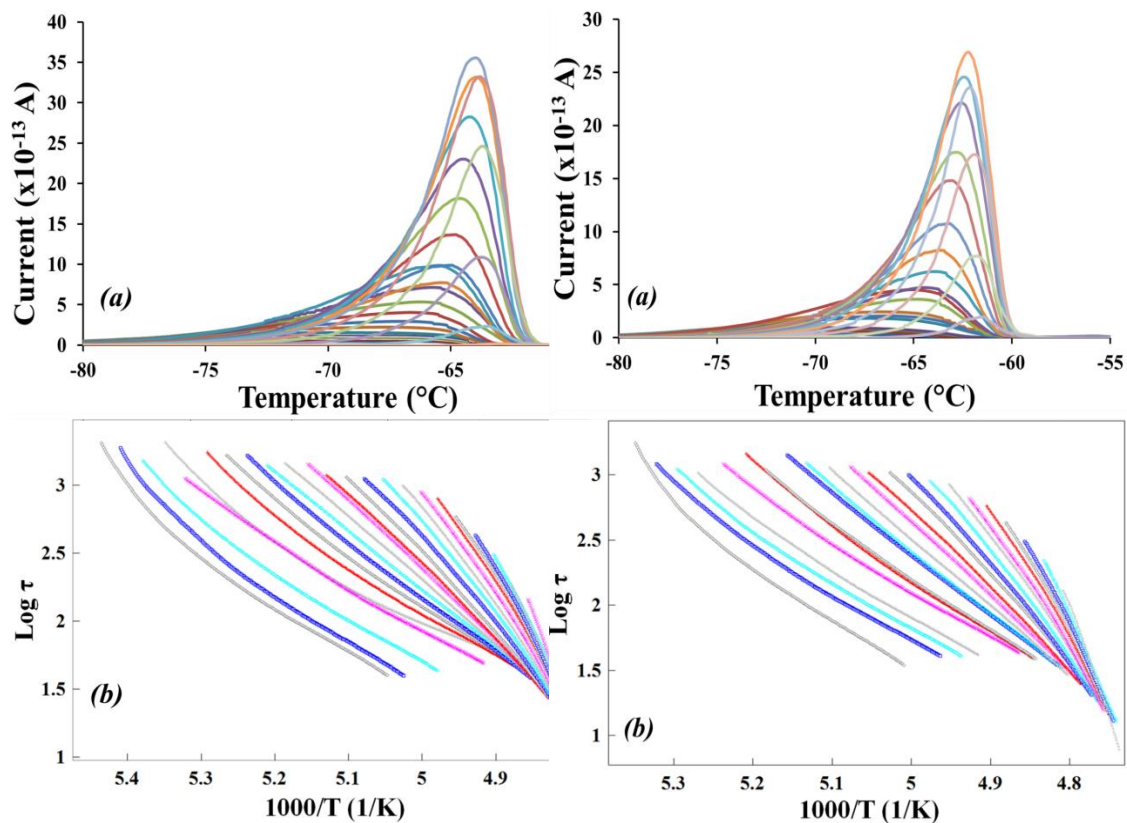


**Figure 4.10** The TW results obtained for PPG 425 (left) and PPG 1000 (right), (a) the TW experimental output showing each discrete relaxation mode under the global TSDC output and (b) the distribution of relaxation times obtained for each TW experimental output.



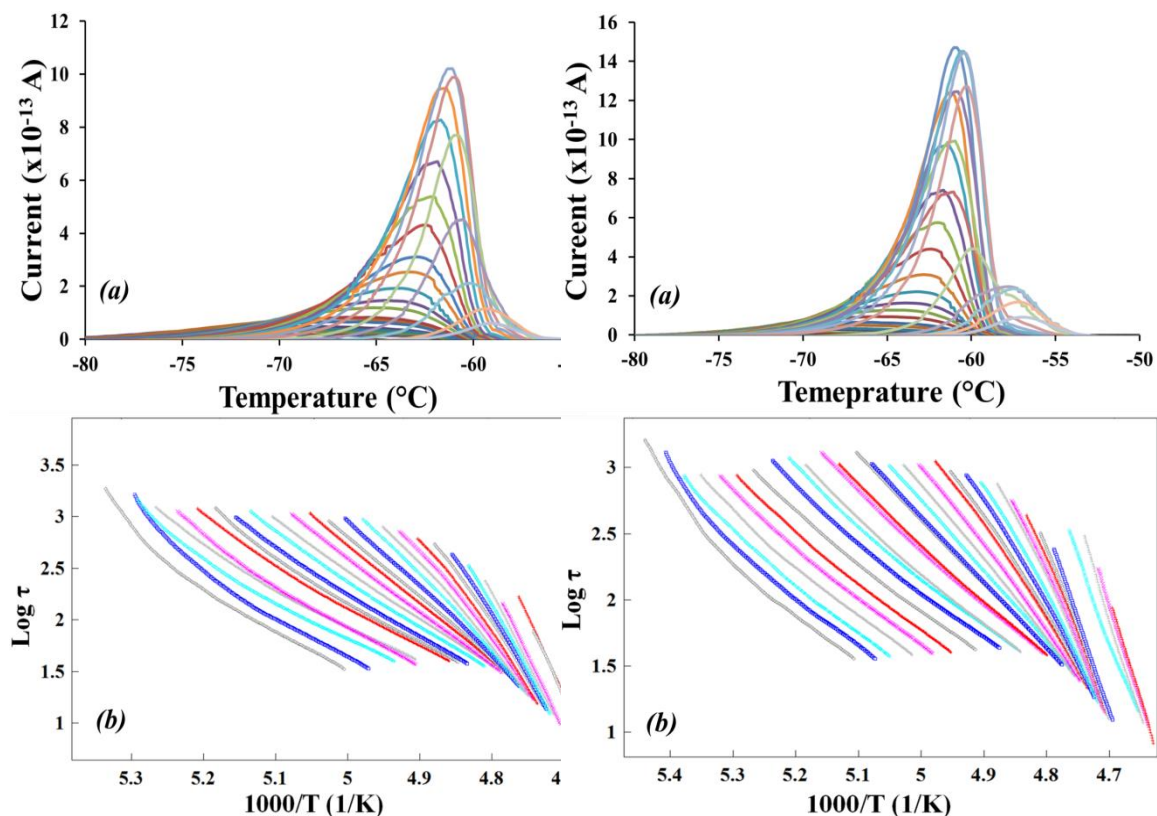


**Figure 4.11** The TW results obtained for PPG 2000 (left) and 2700 (right), (a) the TW experimental output showing each discrete relaxation mode under the global TSDC output and (b) the distribution of relaxation times obtained for each TW experimental output.

The output reveals a second relaxation process (Fig. 4.11 right) on the high temperature side (-60 to -55°C) of PPG 2700 that was not clearly visible in the TSDC experiments, demonstrating the resolving power of this experimental approach. These relaxation processes are designated as  $T_p$  and are believed to be originated from various different processes according to various different researchers. Some researchers propose that the process is due to the release of the excess charge delocalised in the polymer structure, whilst others have attributed  $T_p$  to be a liquid-liquid transition (Vicioso et al. 2010). It has been stated to be universally present for all the polymers in TSC analysis (Ibar 1993). However, the results

presented in this work for PPG contradicts that statement, it demonstrates that this may be true only for high molecular mass polymers, in this case molecular mass  $\geq 2700$  for the PPG.

The total depolarisation current intensity of a TW, when all the conditions are kept constant, arises from the combined result of polarising efficiency at  $T_p$  and the tendency of dipoles to orient back to their temperature equilibrium during the absence of the electric field (i.e. during isothermal depolarisation and cooling steps involved) (Correia et al. 2000). At  $T_p \ll T_g$  due to only a small group of motional modes with low activation energies can be activated. But as the  $T_p$  temperature raises, a greater number of motional modes, including those with higher activation energies are activated which leads to an increase in the current intensity up until the temperature reaches  $T_g$  (where nearly all the high activation energy motional modes can be activated). At temperatures higher than the  $T_g$ , viscosity is lower and molecules have a greater kinetic energy. In this state a greater number of motional modes are accessible and activated during polarisation; however freezing-in of the polarisation becomes difficult for the exact same reason. Lower viscosity and higher kinetic energy allow a significant number of those modes to relax back during the initial depolarisation step at  $T_d$ . The  $T_p$  is therefore an important temperature parameter to quote in addition to the  $T_m$  for TSC  $T_g$  values ( $T_M$ ). The  $T_p$  that results in the highest current intensity obtained for the PPG samples compares well with that obtained from the DSC results. However when the  $T_m$  is considered, there is a difference of  $10^\circ\text{C}$  observed between the  $T_g$  obtained by DSC and TSC (Table 4.4). But the  $T_g$  increases with increasing molecular mass in all cases. The temperature scale in TSC over which a relaxation process occurs gives information about the rate of the molecular relaxation, so an increase in  $T_m$  as molecular mass increases suggests that mobility becomes more restricted as PPG molecular mass increases and this could be due to the increase in viscosity.

**Table 4.4** Glass transition temperatures obtained for PPG 425, 1000, 2000 and 2700 by DSC and TSC.

Sample	DSC $T_g$	TSC	
		$T_p$	$T_M$ ( $^{\circ}C$ )
PPG 425	$-74 \pm 1$	-76	$-64 \pm 1$
PPG 1000	$-72 \pm 1$	-74	$-62 \pm 1$
PPG 2000	$-71 \pm 1$	-73	$-61 \pm 1$
PPG 2700	$-70 \pm 1$	-71	$-61 \pm 1$

#### 4.3.4 High Sensitivity Differential Scanning Calorimetry

The data presented below (Fig. 4.12) was obtained for a series of  $2 \text{ mg mL}^{-1}$  aqueous solutions prepared using PPG samples of differing molecular mass. All experiments were conducted at a scan rate of  $1^{\circ}C \text{ min}^{-1}$ . The transition for PPG 425 could not be observed within the instrument's operational temperature limits because transition temperature range for a  $2 \text{ mg mL}^{-1}$  solution of this PPG is greater than  $100^{\circ}C$ . The transition temperature decreases with increasing molecular mass (Fig. 4.12). This can be explained using the theory presented by Kjellander and Florin. They suggest increased structural constraints with the incorporation of PPG instead of PEO in the water lattice due to the extra  $-CH_3$  in PPG. Increase in the molecular mass and hence the chain length of PPG increases the structural constraints due to the methyl groups in PPG in the formation of PPG-water lattice (Kjellander & Florin 1981). So when the molecular weight increases, phase-separation occurs at a lower temperature due to weaker hydrogen bonding between the water molecules and the ether groups in PPG due to the structural constraints.

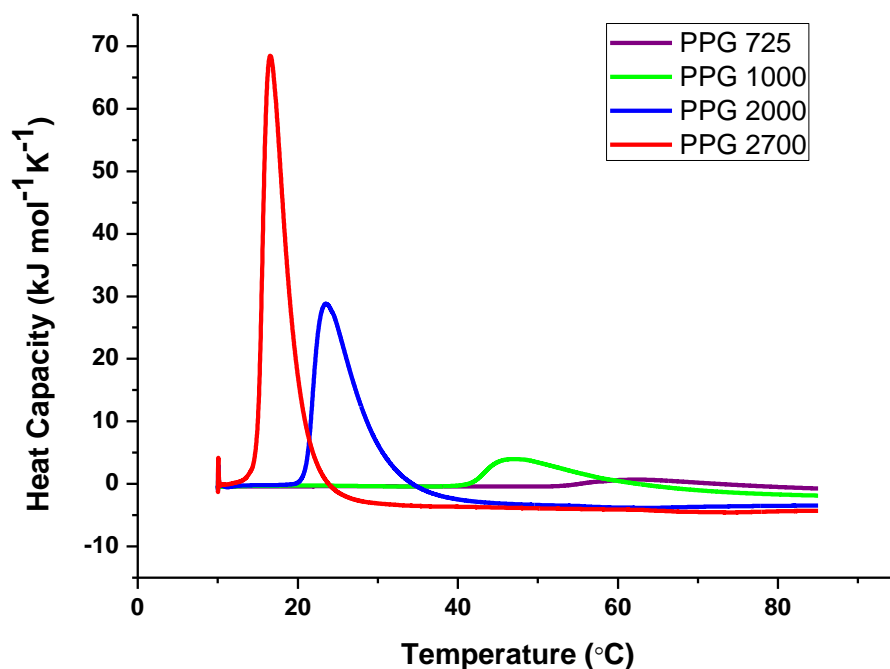


**Figure 4.12** HSDSC output for the change in heat capacity for different molecular mass PPGs as a function of temperature.

In Fig. 4.12, the endothermic transitions indicate that phase transition is entropically driven and that process involves water and possibly involves desolvation or dehydration.

All the thermal traces obtained for the PPG solutions are asymmetric. They possess a steep leading low temperature edge and high temperature steadily reducing tail. This is usually an indication of the aggregation process (Paterson et al. 1997).

A further observation that can be made is that the post-transitional baseline is lower than the pre-transitional baseline for all the PPG samples. The post-transitional baseline represents the heat capacity of the aggregated form, which is lower than the relative heat capacity of the unaggregated unimeric form. PPG molecules as proposed by Kjellander and Florin form an ordered structure with water via hydrogen bonding. The hydrogen bonded structure requires a

high energy to be disrupted and hence the unaggregated structure shows a higher heat capacity. The aggregated form however has minimal or no hydrogen bonding and so these structures would have a lower heat capacity. This makes the  $\Delta C_p$  negative. But the heat capacity change is not the same for all the samples; the change is lower for the lower molecular mass PPGs. The lower molecular mass materials have proportionately more OH groups (Table 4.1) which might remain hydrated after aggregation, hydrogen-bond with water molecules and prevent the coalescence. This is alluded to by the discrete nature of the droplets as shown by HSM images later. This hydration would result in higher heat capacity of the aggregates formed, hence the lower heat capacity change. There is also a possibility that the heat capacity changes are not independent of temperature.

The calorimetric data obtained was fitted to a mass action model using a software package called Scientist (MicroMath). Initial estimates of the thermodynamic parameters were made and fed into the software. It then fits the calorimetric data to a model by reducing the sum of squared residuals to a minimum value and determines the values for  $\Delta H_{vH}$ ,  $\Delta H_{cal}$ ,  $T_{1/2}$ ,  $\Delta C_p$  and  $n$ .

The plots in Figs. 4.13, 4.14, 4.15, 4.16 and 4.17 were obtained by extracting different parameters using the modelling and fitting function using the “Scientist” program.

Figs. 4.13 and 4.14 show good curvilinear relationship between the calorimetric enthalpy and molecular mass ( $R^2 = 0.995$ ) and van't Hoff enthalpy and molecular mass ( $R^2 = 0.995$ ) of PPG, respectively. The heat capacity is negative for this phase-separation reaction. Thus using equation 3.7, if the transition occurs at a higher temperature the enthalpy value is lower. The  $T_{1/2}$  decreases with the increase in molecular mass and shows a curvilinear relationship with molecular mass ( $R^2 = 0.983$ ) (Fig. 4.15) due to a weaker hydrogen bonded PPG-water network for higher molecular mass PPGs. Fig. 4.16 shows an excellent curvilinear relationship between

the change in heat capacity and molecular mass of PPG ( $R^2 = 0.991$ ) due to less  $-OH$  groups present in higher molecular mass samples and lower heat capacity of the aggregates formed. The curvilinear relationship between the  $n$  values and the molecular mass has an  $R^2$  value of 0.902 (Fig. 4.17) and the  $RSD \pm 19\%$ , so it is reasonable to infer that the  $n$  values are independent of molecular mass.

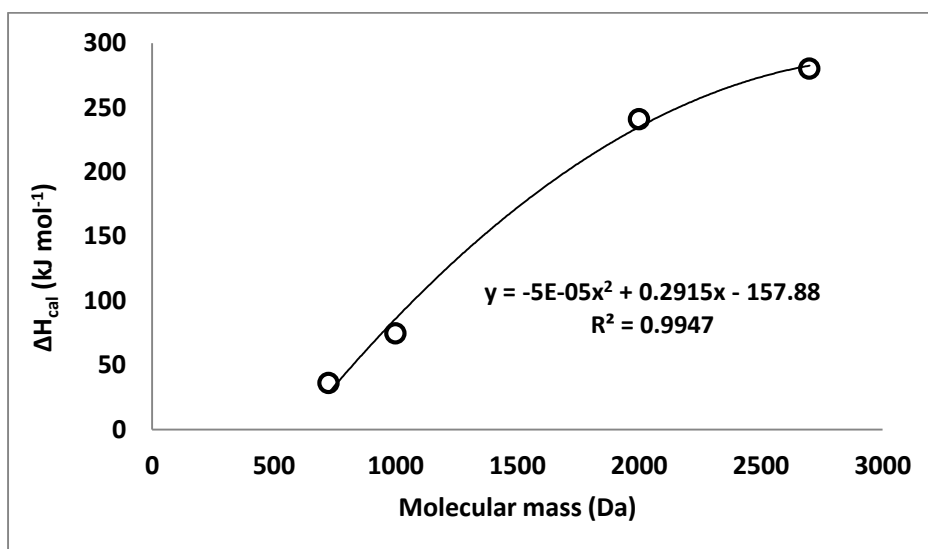


**Figure 4.13** Relationship between the optimised calorimetric enthalpy values and molecular mass of PPG, obtained using the model fitting procedure.

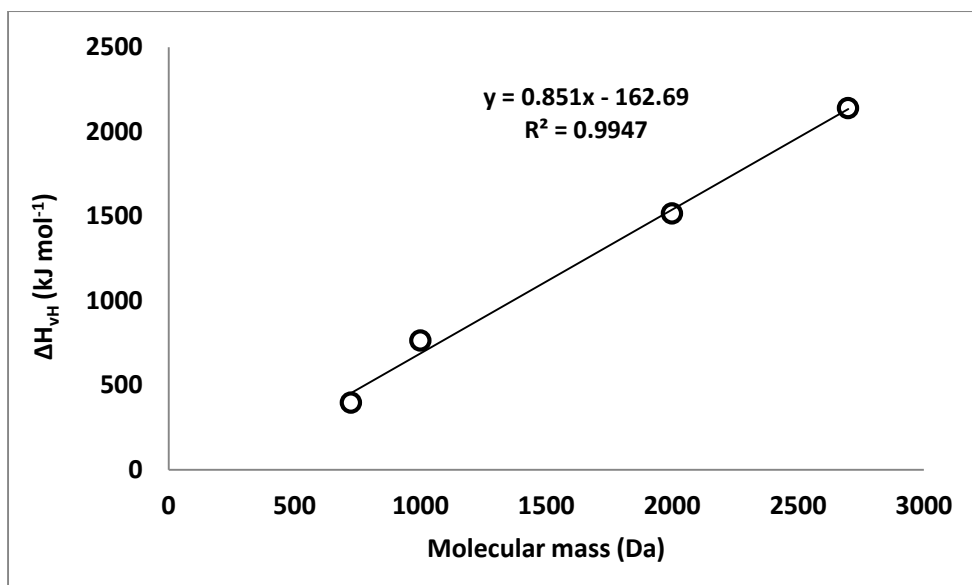


**Figure 4.14** Relationship between the optimised van't Hoff enthalpy values and molecular mass of PPG, obtained using the model fitting procedure.

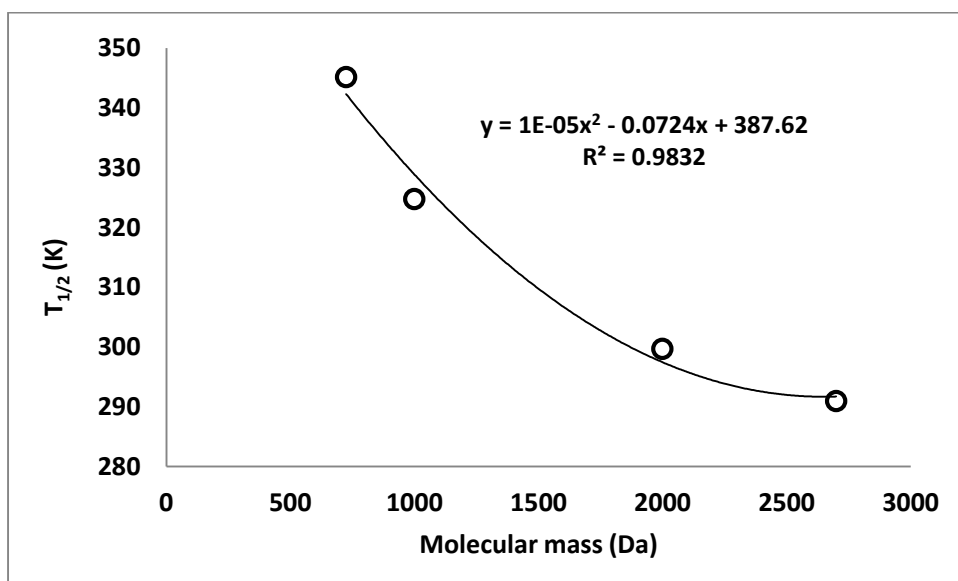


**Figure 4.15** Relationship between the optimised  $T_{1/2}$  values and molecular mass of PPG, obtained using the model fitting procedure.

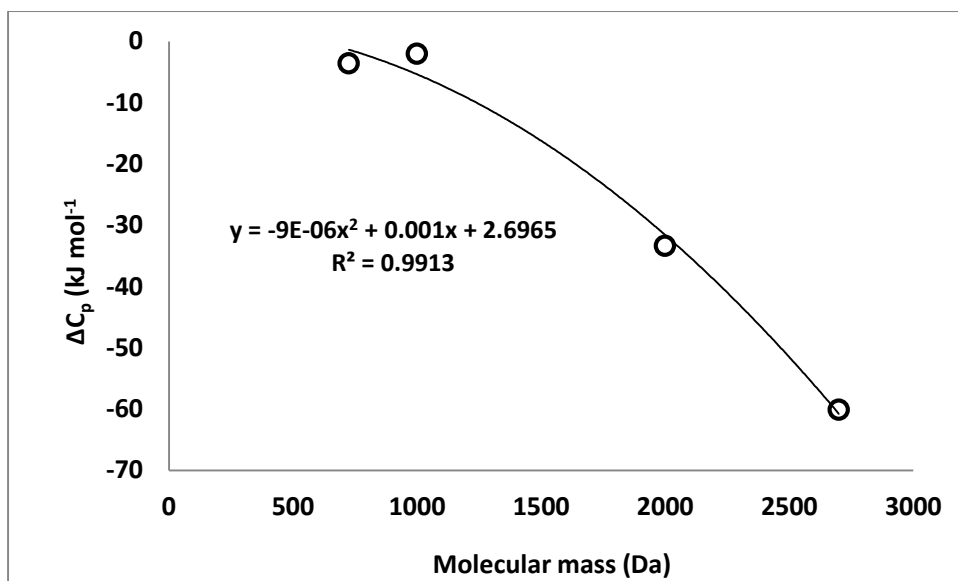


**Figure 4.16** Relationship between the optimised heat capacity change values and molecular mass of PPG, obtained using the model fitting procedure.

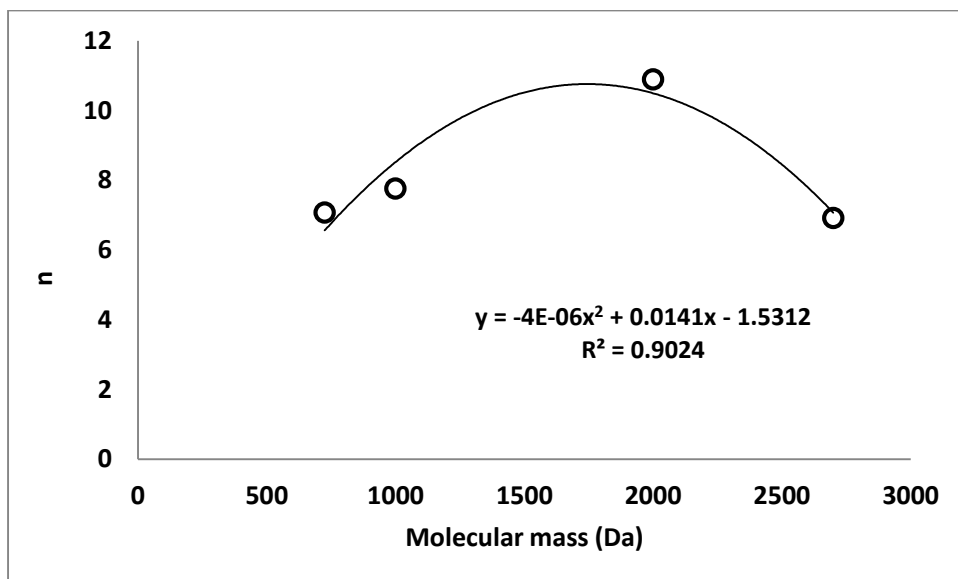
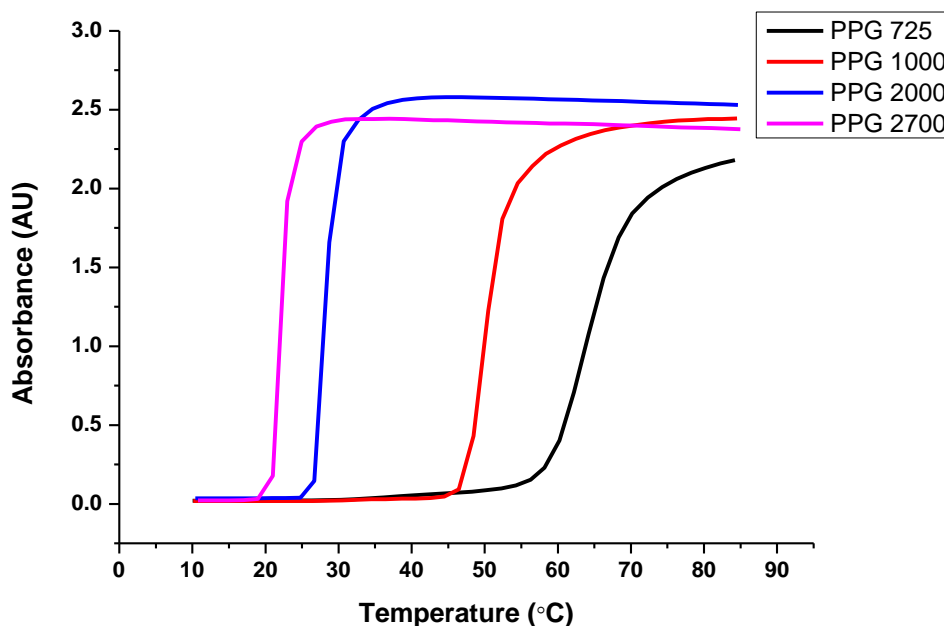


**Figure 4.17** Relationship between the optimised n values and molecular mass of PPG, obtained using the model fitting procedure.



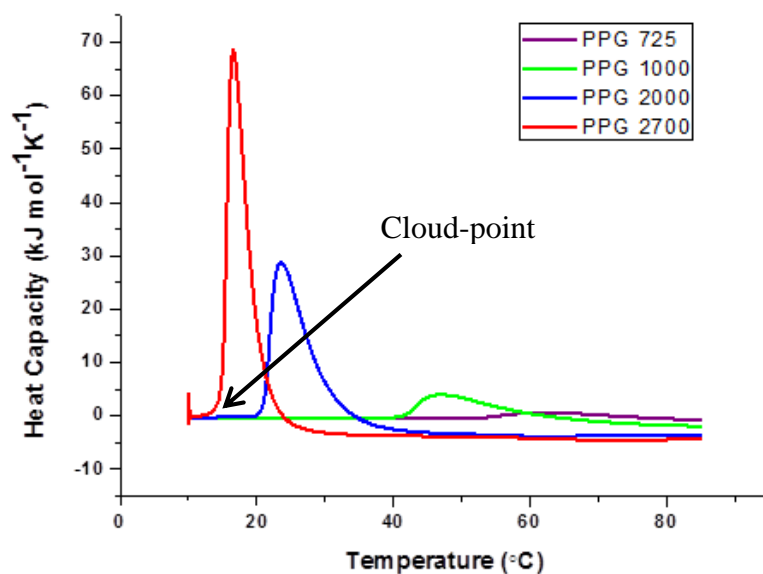
### 4.3.5 Turbidity Measurements using UV-Visible Spectrometry

Fig. 4.18 shows a plot of the spectroscopic data obtained using UV-Visible spectroscopy as a function of molecular mass. It records the temperature at which the solutions become turbid and records the absorbance change as the temperature is further raised.



**Figure 4.18** Increase in absorbance of PPG solutions with temperature.

The cloud-point can also be obtained from the HSDSC measurements. The cloud-point obtained from the HSDSC measurements is the temperature at the start of the endothermic transition (Fig. 4.19); the cloud-point however does not coincide with turbidity measurements. This is because the turbidity data only detects the particles when they are large enough to scatter monochromatic radiation. These particles/molecules attenuate the light passing through the sample and get detected in the visible range of the spectrometer since the wavelength set was 532 nm. So any aggregation occurring below this wavelength, where the solution is not turbid, would not be detected by the spectrometer. But the presence of turbidity and the increase in absorbance is indicative of some de-mixing process which is intimately linked to the aggregation process observed using HSDSC.



**Figure 4.19** Cloud-point at the beginning of the phase-transition peak obtained from the HSDSC data.

The cloud-point obtained using the two techniques: UV-Visible spectroscopy and HSDSC are plotted in Fig. 4.20. The cloud-points obtained using both the techniques follow the same trend with change in molecular mass of the PPG.

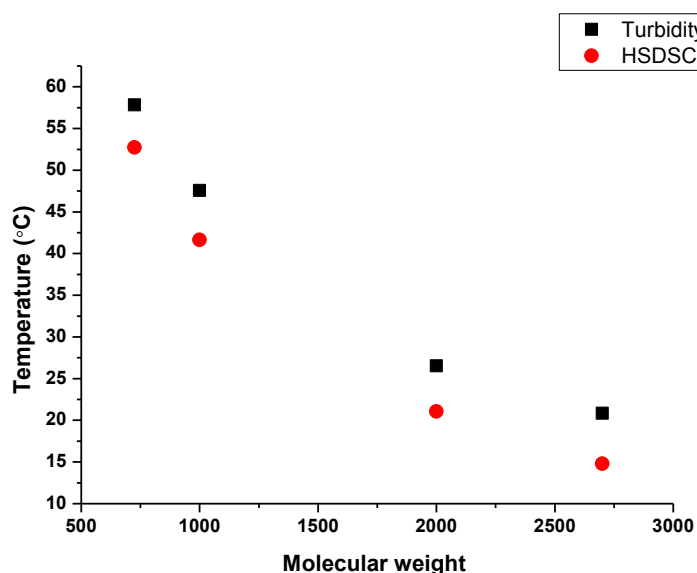


**Figure 4.20** Plot of cloud-points obtained using turbidity and HSDSC measurements.

#### 4.4 Conclusions

This study has helped to delineate the effect of the change in molecular mass of PPG on the glass transition temperature and on the degree of molecular mobility in the glass transition process. TGA results for the different PPG samples showed a difference in the decomposition temperature of PPG 425 compared to the other PPG samples analysed upon heating from ambient to 600°C. DSC was used to characterise the glass transition which was then studied in detail for four PPGs by TSC. Increasing molecular mass increases the glass transition temperature detected by DSC ( $T_g$ ) and by TSC ( $T_M$ ). The degree of molecular mobility is also found to increase with increasing PPG molecular mass, which has been attributed to the increase in the flexibility of the molecule resulting in greater degrees of motional freedom. TW experiments conducted on the four PPGs showed that PPG 425, 1000 and 2000 undergo one global relaxation process however PPG 2700 undergoes an additional relaxation process  $T_p$  after the  $T_M$  which has been attributed to either the release of the excess charge delocalised in the polymer structure or a liquid-liquid transition. The fact that this process is not observed for PPG of molecular mass  $<2700$  indicates that it is not a universal process that occurs in all glass forming polymers, as suggested by some researchers.

HSDSC studies conducted on PPG solutions gave information about the phase-transition temperature range of the solutions and how it changes for different molecular masses. The  $T_m$  of the PPG solution increases with the decrease in the molecular mass of the PPG. The signal obtained using HSDSC indicated that phase-separation occurs via an enthalpically observable aggregation process. The enthalpic component of the transition arises from the disruption of a hydrogen bonded network as evidenced by the negative heat capacity. Turbidity measurements reveal the cloud-point of these solutions which decreases as the molecular mass increases. The increase in absorbance is indicative of phase-separation *via* liquid-liquid de-mixing with aggregates which scatter the monochromatic light passing through the system. This supports

the aggregation process detected by HSDSC. The onset of phase separation, obtained by both the HSDSC and the turbidity data, follow the same trend; however, the temperatures determined by the two techniques do not coincide.

The studies reported in this chapter provide useful information about the thermo-chemical and thermo-physical properties of pure PPG. Important new solution properties were also revealed and some information about the phase-separation behaviour of PPG was gained from this study.

## Chapter 5 : Investigation of Phase Separation in Aqueous Solutions of PPG

### 5.1 Introduction

PPG is the cornerstone of thermally induced micellization in aqueous solutions of pluronic copolymers. This is a result of the hydrophobic aggregation event that occurs in these pluronics with an increase in temperature. Alexandridis et al., (1994) showed the aggregation process in pluronics to be entropically driven and that the micellization enthalpy was endothermic due to diminishing hydrogen-bonding between water and PPG as a function of temperature. Subsequent studies have shown a correlation between the thermodynamic parameters obtained by HSDSC and the PPG content in pluronic solutions; however, no such relationship between the content of PEO and aggregation in pluronics has been established (Beezer et al. 1992; Beezer et al. 1994). The aim of the work presented in this chapter was to investigate, in some detail, the molecular details of the phase separation process for aqueous solutions of PPG ( $M_n \sim 1000$ ) using high sensitivity differential scanning calorimetry (HSDSC), hot stage microscopy (HSM), turbidity measurements made using UV-Visible spectroscopy, dynamic light scattering (DLS), and small-angle neutron scattering (SANS). In addition phase separation of PPG 1000 in  $D_2O$  has also been studied in order to compare and contrast with its behaviour in  $H_2O$ .

Previous research suggests a greater therapeutic effect of the pluronics with higher hydrophobic PPG content such as in L61 than the pluronics with a higher hydrophilic PEO content such as in P85 in anticancer therapy (Melik-Nubarov et al. 1999). The proposed mechanism for this effect might be the different binding abilities of the two different pluronics to the cell membrane. Since the PPG content differs significantly in the two pluronics, PPG might be the reason for the enhanced binding ability to certain cells for pluronics with a greater PPG content. The motivation of the research reported in this chapter is to explore details of the phase

separation process in aqueous PPG solutions with a view to (a) understanding how the phase diagram may be established using HSDSC and (b) how to control the phase separation process via the addition of cosolutes to the aqueous phase.

## 5.2 Experimental

### 5.2.1 Materials

Poly(propylene glycol)  $M_n \sim 1000$  and  $D_2O$  (99.9% D) used in the experiments were purchased from Sigma-Aldrich UK. Deionised water was produced locally in the laboratory. Samples were used as purchased from the manufacturer.

### 5.2.2 Methods

#### 5.2.2.1 High Sensitivity Differential Scanning Calorimetry

A range of PPG aqueous solutions were prepared in deionised water ranging in concentrations between 1-50  $mg\ mL^{-1}$ . A set of samples were also prepared in  $D_2O$  with PPG concentrations of 5, 10, 20 and 30  $mg\ mL^{-1}$ . The samples were equilibrated at the starting temperature for 30 minutes, followed by scanning up and down between 5 and 85 °C at a scan rate of 1°C  $min^{-1}$ .

#### 5.2.2.2 Hot Stage Microscopy

Instrument: HS1 control unit and HS82 microscope hot-stage

Manufacturer: Mettler Toledo, UK

Software (control): Studio Capture

Software (analysis): Studio Capture

An aqueous solution of PPG of 20  $mg\ mL^{-1}$  was prepared and a drop was placed on a glass slide and covered with a cover slide. Observations made under the microscope were recorded by computer software as the sample was heated from 25-60°C at 2°C  $min^{-1}$ .

### 5.2.2.3 UV-Visible Spectroscopy

Samples ranging in concentration from 0.2 to 30 mg mL<sup>-1</sup> of PPG in deionised water were prepared. The blank reference used for these experiments was deionised water. The samples were heated from 10-70°C and absorbance measurements were undertaken every 2°C. The temperature was held at 10 and 70°C for 5 minutes to let the sample equilibrate and the measurements were made at 532 nm wavelength in glass cuvettes. Solutions of PPG in different organic solvents were also studied. These solvents included methanol, propanol, butanol, toluene and dimethyl sulfoxide (DMSO). These solutions were all heated from 10-55°C to prevent boiling of some of the solvents upon heating during the measurements.

### 5.2.2.4 Small-Angle Neutron Scattering

Instrument: LOQ, ISIS, Oxfordshire, UK

Manufacturer: Rutherford Appleton Laboratory, Oxfordshire, UK

Cooling system (internal): JULABO Water Bath, UK

Software (control): Mantid

Software (analysis): SASView

A 20 mg mL<sup>-1</sup> PPG solution was prepared in D<sub>2</sub>O and H<sub>2</sub>O mix. The sample was analysed in a 1 mm path length, UV-spectrophotometer grade, quartz cuvettes (Hellma). This was then placed in the sample holders in a computer-controlled sample chamber. Temperature control was achieved by using a thermostatic circulating bath pumping fluid through the base of the sample chamber to achieve a temperature stability  $\pm 0.5^\circ\text{C}$ .

The scattering data was normalised for the sample transmission and the incident wavelength distribution, corrected for instrumental and sample backgrounds using an empty quartz cell, and for the linearity and efficiency of the detector response.

### 5.2.2.5 Dynamic Light Scattering

Instrument: Zetasizer NanoZS Zen 3600

Manufacturer: Malvern Instruments Ltd.

Software (control): Malvern Zetasizer

Software (analysis): Malvern Zetasizer

1 mg mL<sup>-1</sup> and 2 mg mL<sup>-1</sup> PPG solutions were prepared in water. The samples were analysed using 1 cm path length, quartz cuvettes. Helium-neon laser was used for the measurements with the wavelength of 632.8 nm and the detector was placed at the angle of 90°.

## 5.3 Results and Discussion

### 5.3.1 High Sensitivity Differential Scanning Calorimetry

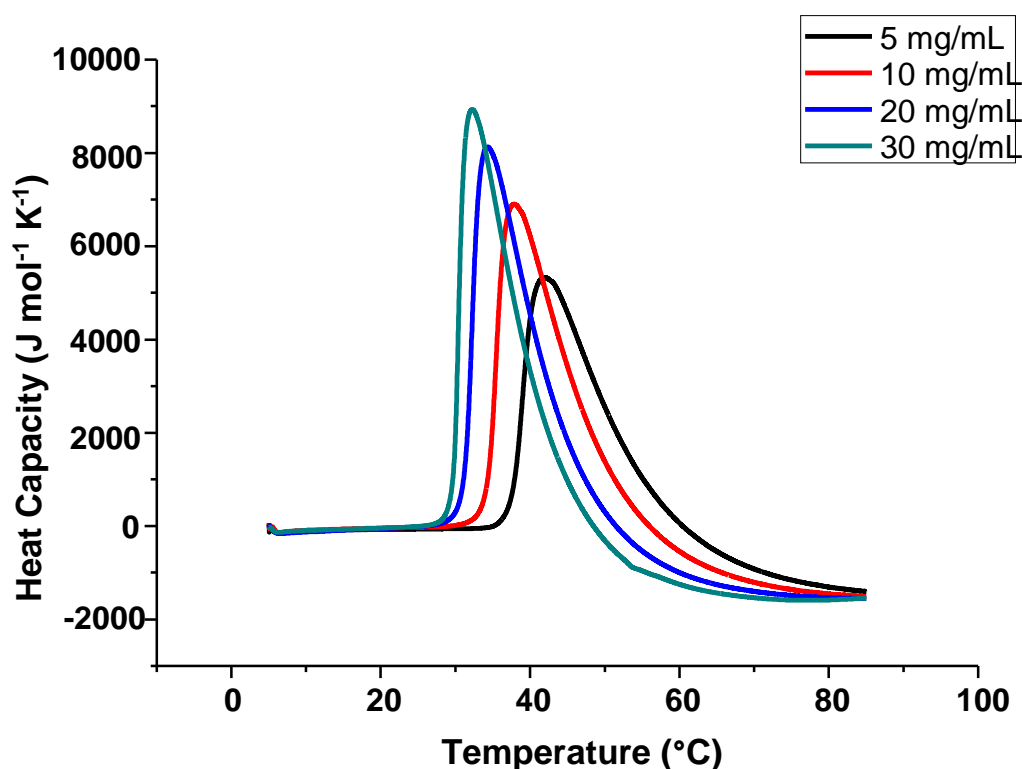
HSDSC is a technique that provides a direct route for the accurate measurements of thermodynamic transitions in dilute aqueous solutions. This technique was used to study the phase-separation of aqueous PPG solutions.

Figure 5.1 shows the HSDSC output for 4 different concentrations of PPG in water as the solutions were heated up to 85°C at 1°C min<sup>-1</sup>. HSDSC does not directly reveal any information about the molecular processes occurring during a transition since it is a macroscopic technique but some initial observations can be made from the HSDSC signals.

T<sub>m</sub> or the phase-transition temperature can be determined as the temperature where the excess heat capacity value is a maximum. The ΔH<sub>vH</sub> or van't Hoff enthalpy is related to the transition width and the shape of the signal and ΔH<sub>cal</sub> or the calorimetric enthalpy is related to the integrated area under the C<sub>p</sub> curve and both are determined in units of kJ mol<sup>-1</sup>. The cooperativity can be estimated from the ΔH<sub>vH</sub>/ΔH<sub>cal</sub> ratio (Ohline et al. 2001). In cooperative



transitions, well before the transition temperature is reached, molecules cooperate and move close to each other. The number of molecules that contribute to these aggregates is called a cooperative unit. Larger cooperative units result in sharper transitions and higher van't Hoff enthalpies because of the higher  $C_p$  maximum value (Sturtevant 1987).  $C_p$  molar heat capacity is in units of  $\text{kJ mol}^{-1} \text{K}^{-1}$ . Samples were scanned at four different scan rates from  $0.1\text{-}2^\circ\text{C min}^{-1}$  for four different concentrations and the lack of scan rate dependence on the calorimetric signals indicate that the process is under strict thermodynamic control and is not kinetically limited.



**Figure 5.1** HSDSC output for different concentrations of aqueous PPG solutions as a function of temperature.

The signals suggest hydrophobe desolvation which that might be due to either intra- or intermolecular hydrophobic association due to conformational changes (Beezer et al. 1994). The endothermic peak shows the absorption of heat due to the loss of water of hydration and

the negative heat capacity for all the signals suggests weakening of the hydrogen bonded structure between PPG and water as the solution is heated up. The heat capacity of hydrogen bonded structure is high, so when the PPG bonded water lattice is heated up, according to Kjellander-Florin theory, if the structure doesn't break fast enough, the unfavourable entropy factors starts to dominate by the disruption of the hydrogen bonded PPG and water lattice and releasing the water molecules to bulk (Kjellander & Florin 1981). This leads to phase-separation. The asymmetry of the signal also indicates an aggregation process whose thermodynamic properties may be described by the mass action model of association accompanied by the dehydration (Paterson et al. 1997). The signals can be interpreted by Kjellander and Florin (1981) model which suggests that PPG is originally confined to a hydrogen bonded network comprising of many water molecules and PPG chains. As the temperature is raised the PPG chains begin to self-associate and water is released from the network to the bulk. The cooperativity of the transitions point to the existence of a network and the ability to fit the HSDSC signal to an aggregation event corroborates the validity of self-association as the temperature increases. The change in the cooperativity with the change in concentration suggests that there are many cooperative units involved in this process.

Another observation that can be made from the signal is that the  $T_m$  increases with the decrease in the concentration of PPG (Table 5.1). If the process can be modelled using the mass action aggregation process and the enthalpy for the process is endothermic. Then with the increase in concentration, the extent of system to form more aggregates will increase. Since the formation of aggregates is an endothermic event, the temperature of the system will drop. So the net result is that as the aqueous PPG concentration increases, the temperature at which phase separation occurs decreases. Also, since all the thermograms obtained for different concentrations show the presence of an aggregation event, all these phase separation events must lie on the same binodal.

The phase separation model suggested by Linse proposes that at high temperatures, the non-polar polymer conformer becomes more populated and the polymer-water interaction becomes less favourable, can also be used to explain the HSDSC signal obtained above. At elevated temperatures, polymer-polymer interactions become more favourable, which leads to polymer aggregation and the water between the polymer chains gets pushed out. This aggregation event is clearly revealed by the HSDSC signal (Carlsson et al. 1995).

Fig. 5.1 also shows that the signal gets smaller as the temperature increases. This is a consequence of the negative heat capacity and can be explained using Kirchhoff's law, Equation 5.1.

$$\Delta H(T) = \Delta H(T_{ref}) + \Delta C_p(T - T_{ref}) \quad (5.1)$$

The effect of the change in concentration on the  $T_m$  can be explained thermodynamically by Eq. 5.2. Because it is an aggregation process, with the increase in number of monomers (X) by increasing the concentration, the extent of aggregation increases. Since aggregation is an endothermic process, it occurs at a lower temperature with an increase in PPG concentration.



**Table 5.1** Change of  $T_m$  with the change in concentration of PPG in aqueous solution.

Concentration (mg mL <sup>-1</sup> )	$T_m$ (°C)
5	41.5
10	37.7
20	34.3
30	32.2

The same experiment was then conducted under the same experimental conditions in D<sub>2</sub>O solutions to ascertain the effect of D<sub>2</sub>O on the phase-separation. The change in  $T_m$  with the

change in PPG concentration in D<sub>2</sub>O solution is shown in Table 5.2. A slightly lower T<sub>m</sub> in D<sub>2</sub>O solutions than H<sub>2</sub>O is observed because it has been suggested by some researchers that the hydrophobic compounds become more hydrophobic in D<sub>2</sub>O, increasing the necessity of the system to phase-separate at a lower temperature (Fig. 5.2).

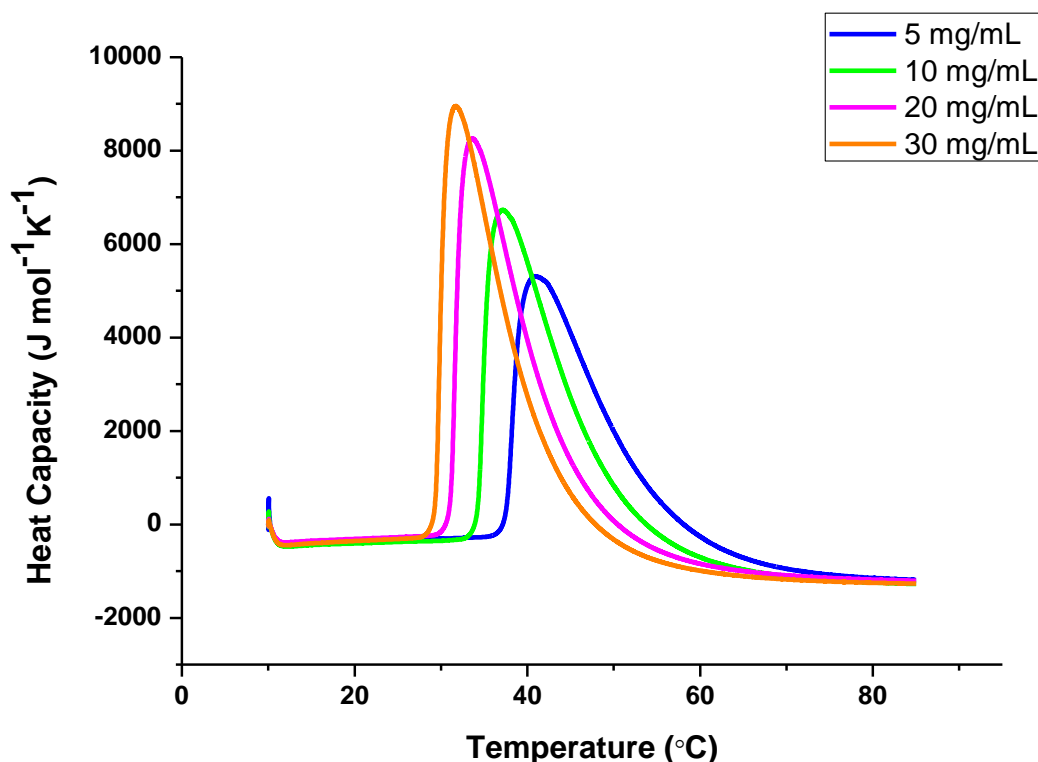


**Figure 5.2** HSDSC outputs for different concentrations of PPG solutions prepared in D<sub>2</sub>O as a function of temperature.

**Table 5.2** Change of T<sub>m</sub> with change in the PPG concentration in the presence of D<sub>2</sub>O.

Concentration ( mg mL <sup>-1</sup> )	T <sub>m</sub> (°C)
5	40.8
10	37.1
20	33.1
30	31.6

It was found that reheating of the aqueous PPG solutions after an initial heating and cooling cycle gave an identical scan to the first heating scan. However when the same experiment was

conducted for the solutions prepared in D<sub>2</sub>O, the second heating scan did not give a similar output to the first scan (Fig. 5.3).

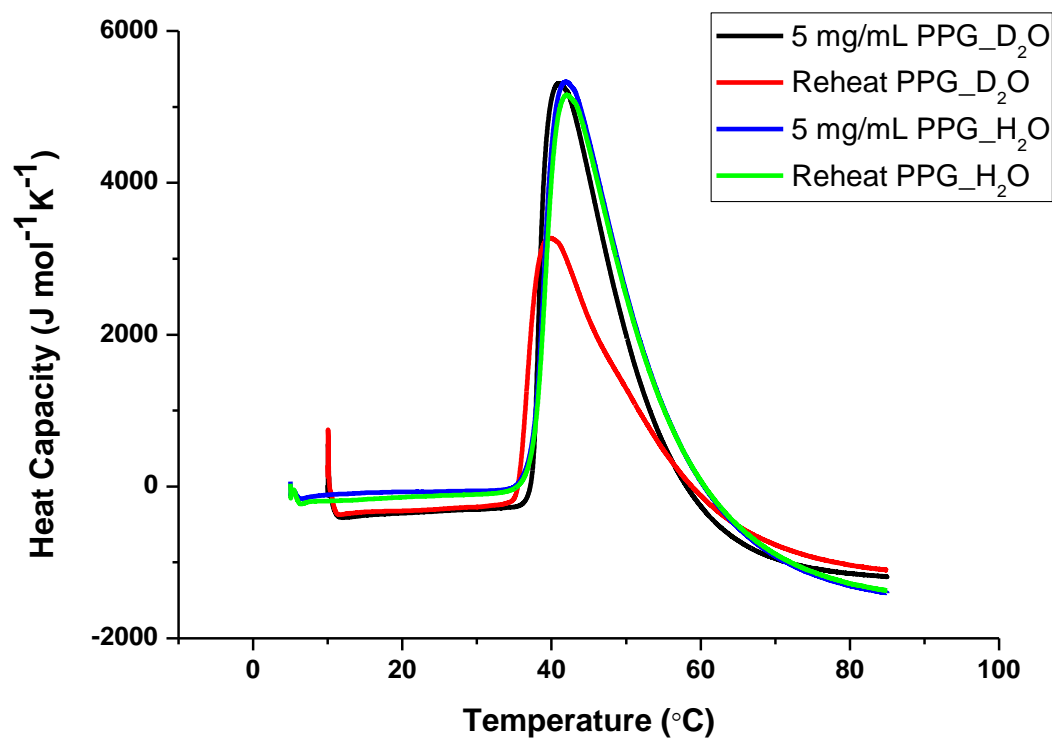


**Figure 5.3** HSDSC data output for the reheating scans for 5 mg mL<sup>-1</sup> PPG in H<sub>2</sub>O and D<sub>2</sub>O solutions at 1°C/min as a function of temperature.

It was found that PPG in D<sub>2</sub>O solutions when heated above the T<sub>m</sub> started to cream (Fig. 5.4). As a result, it was presumed, that when D<sub>2</sub>O solutions were heated in the HSDSC cells, upon cooling down of the solutions, not all the phase-separated PPG went back into the solution and hence the second heating scan did not give a similar thermal output. It showed a lower excess heat capacity change than the first heating scan.

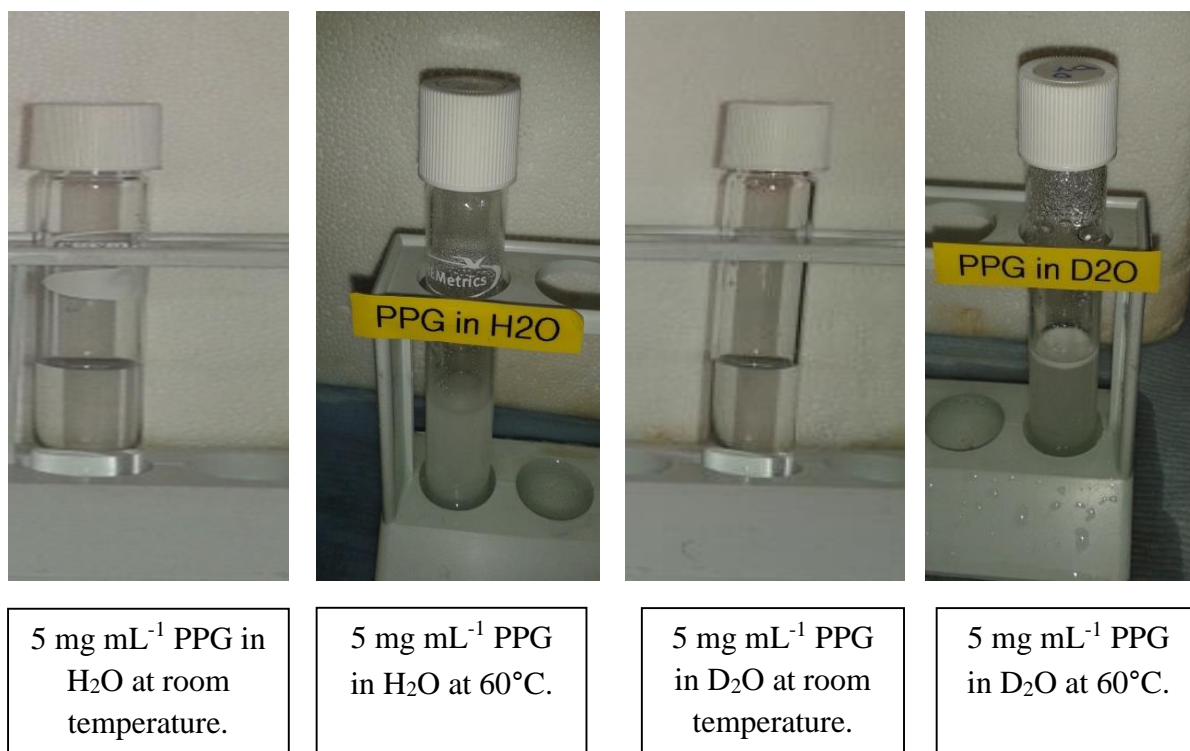


**Figure 5.4** The absence and presence of creaming in PPG in H<sub>2</sub>O and D<sub>2</sub>O solutions, respectively, upon heating.

A detailed study was then conducted to obtain the thermodynamic parameters for the HSDSC output. Nine different concentrations were prepared in water and scanned at  $1^{\circ}\text{C min}^{-1}$  on the HSDSC (Fig. 5.5). The HSDSC output shows that the heat capacity change for low concentrations, i.e. 1 and 2  $\text{mg mL}^{-1}$  is lower than the heat capacity change for the other concentrations. This could be because at such low concentrations, within the temperature range analysed; not all the polymer solution has undergone phase-separation. In other words, aggregate formation is not completed at  $85^{\circ}\text{C}$  for 1 and 2  $\text{mg mL}^{-1}$  PPG solutions. Fig. 5.5 also shows the decrease in  $T_m$  as the concentration of PPG in the solution increases. Asymmetry in the signals and the negative heat capacity is also observed in these thermograms as well.

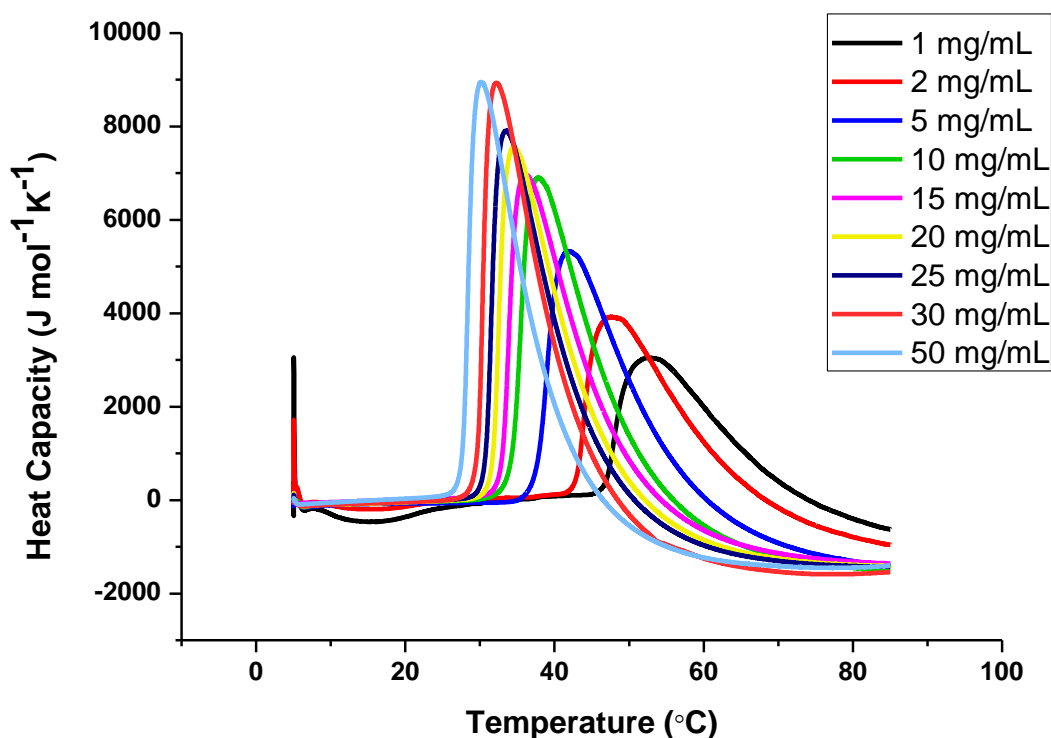


**Figure 5.5** HSDSC data for nine different PPG concentrations in water solutions upon heating at  $1^{\circ}\text{C min}^{-1}$ .

The HSDSC data obtained was modelled using “Scientist” (Table 5.3) and the plots of various parameters including  $\Delta H_{\text{cal}}$ ,  $\Delta H_{\text{vH}}$ , the aggregation number,  $n$ ,  $T_{1/2}$  and  $\Delta C_p$  values are shown in Figs. 5.7- 5.12. Figure 5.6 shows an example of the model fit obtained for aqueous PPG solutions using Scientist. Fig. 5.7 shows that the aggregation number is changing in a curvilinear relationship with the PPG concentration ( $R^2 = 0.951$ ). The cooperativity, can also be calculated using the ratio  $\Delta H_{\text{vH}}/\Delta H_{\text{cal}}$ , which is also increasing upon the increase in concentration of PPG. Fig. 5.8 shows an excellent curvilinear relationship of  $\Delta H_{\text{vH}}$  with the concentration ( $R^2 = 0.995$ ) but the calorimetric enthalpy shows no such relationship with the PPG concentration (Fig. 5.9). According to the Kjellander and Florin model, PPG chains are linked with water in a supramolecular network. Increase in the PPG concentration would result

in more PPG molecules coming close to each other, increasing the  $n$  values. And because there are more PPG molecules, the cooperative units supposedly grow bigger too. For a two-state model, cooperativity of the transition is responsible for  $\Delta H_{\text{vH}}$ . The greater the cooperativity the sharper the transition and hence a larger value of  $\Delta H_{\text{vH}}$  is obtained. With the increase in the concentration of PPG, since the cooperativity is increasing, the  $\Delta H_{\text{vH}}$  will increase too. So the van't Hoff enthalpy increases with concentration much more than the calorimetric enthalpy.

A curvilinear relationship between  $T_{1/2}$  and  $\Delta C_p$  ( $R^2 = 0.98$ ) is also observed (Fig. 5.10). Figs. 5.11 and Fig. 5.12 show a curvilinear relationship between  $\Delta H_{\text{vH}}$  and  $T_{1/2}$  ( $R^2 = 0.96$ ) and between  $\Delta H_{\text{cal}}$  and  $T_{1/2}$  ( $R^2 = 0.955$ ), respectively. The slope of  $\Delta H_{\text{vH}}$  and  $T_{1/2}$  graph gives the value for  $\Delta C_p$  since the first derivative of enthalpy with respect to temperature is heat capacity.

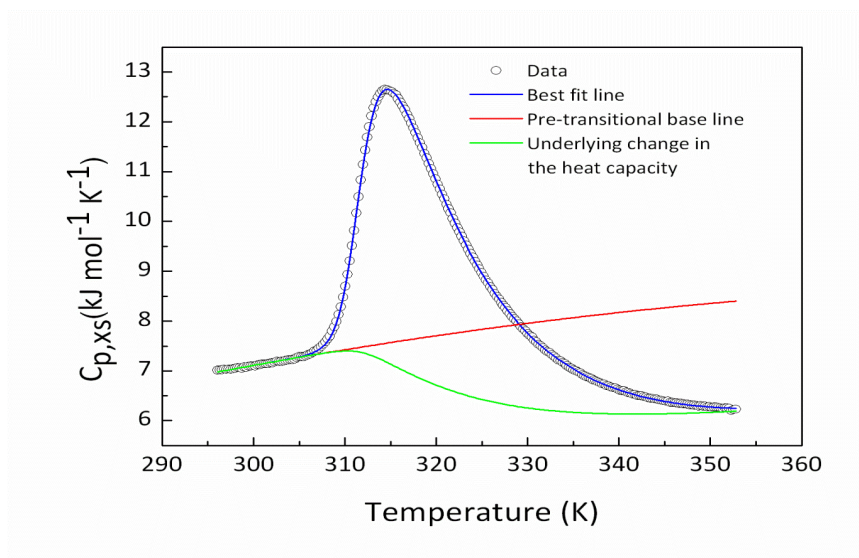


**Figure 5.6** An example of a model fit for the HSDSC output for an aqueous PPG solution obtained using Scientist.



**Table 5.3** HSDSC parameters obtained for aqueous solutions of PPG as a function of concentration.

Concentration (mg mL <sup>-1</sup> )	$\Delta H_{cal}$ (kJ mol <sup>-1</sup> )	$\Delta H_{vH}$ (kJ mol <sup>-1</sup> )	n	T <sub>1/2</sub> (K)	$\Delta C_p$ (kJ mol <sup>-1</sup> K <sup>-1</sup> )
1	76.99	561.19	30	350.3	-15.6
2	94.75	716.05	34	342.3	-19.69
5	106.71	885.35	17	324.6	-15.36
10	115.2	1134.45	19	318.9	-19.36
15	102.84	1396.79	20	315.9	-20.68
20	111.56	1591.92	25	315	-27.83
25	111.48	1670.21	25	313.5	-28.89
30	118.65	1762.44	24	311.7	-31.01
50	114.06	1815.23	25	309.6	-33.96

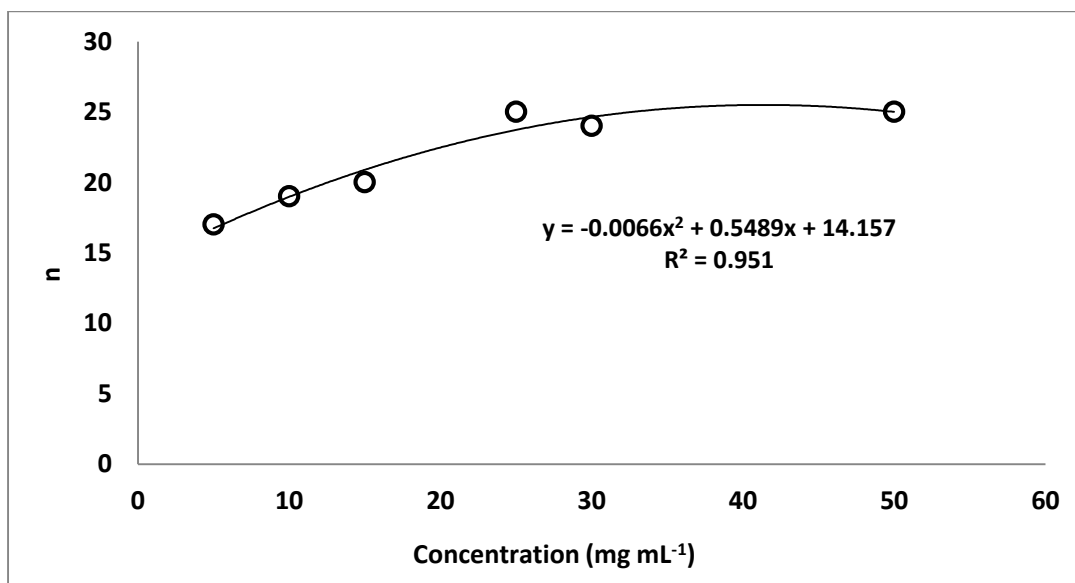


**Figure 5.7** Concentration dependence of PPG on the optimised aggregation number obtained using the model fitting procedure.

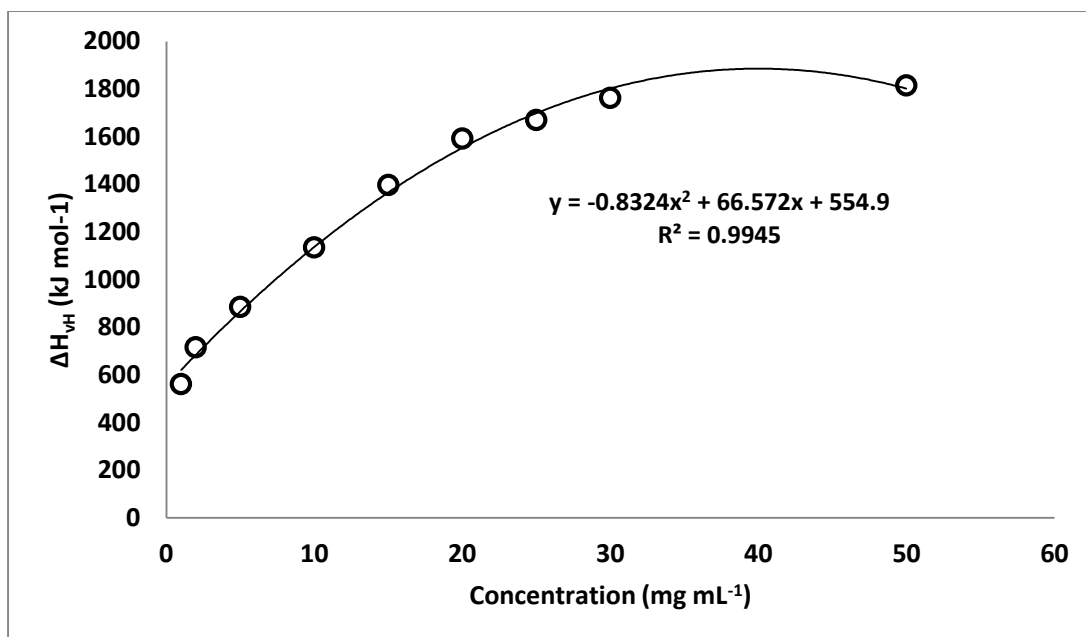


**Figure 5.8** Concentration dependence of PPG on the optimised van't Hoff enthalpy values obtained using the model fitting procedure.

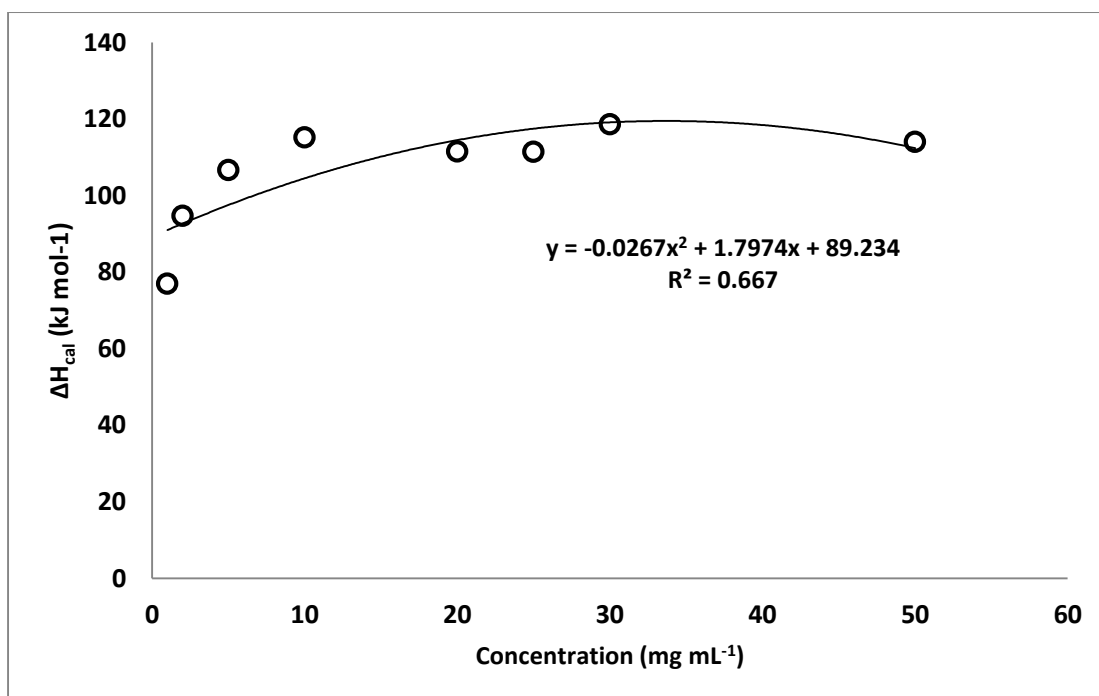


**Figure 5.9** Concentration dependence of PPG on the optimised calorimetric enthalpy values obtained using the model fitting procedure.

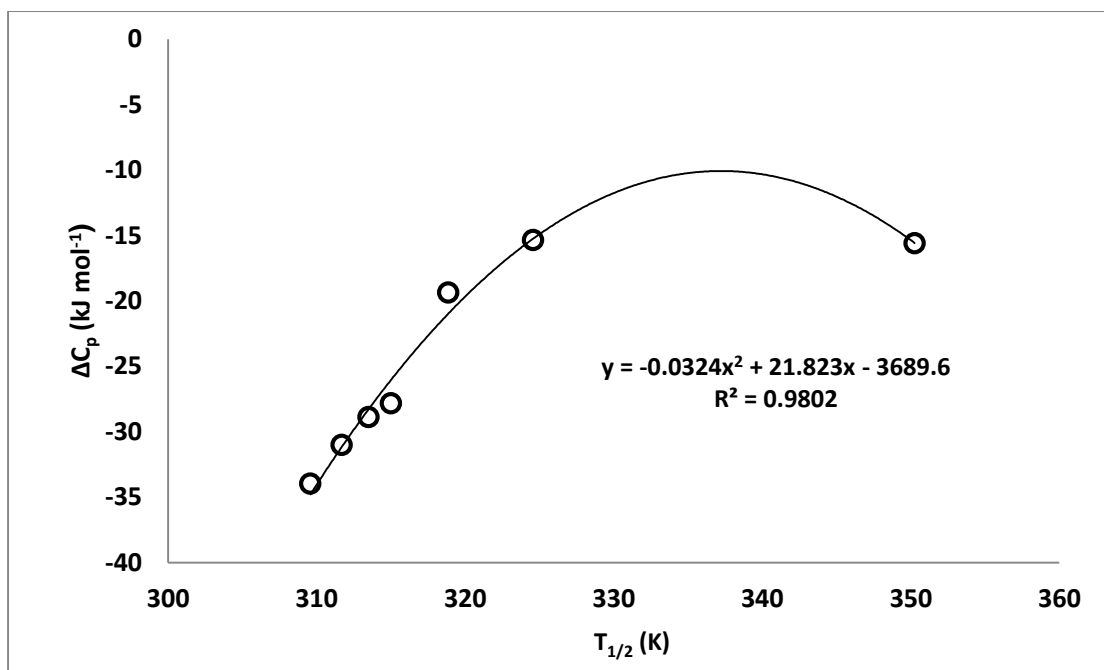


**Figure 5.10** Relationship between the optimised values of  $T_{1/2}$  and the heat capacity change values obtained for PPG, using the model fitting procedure.

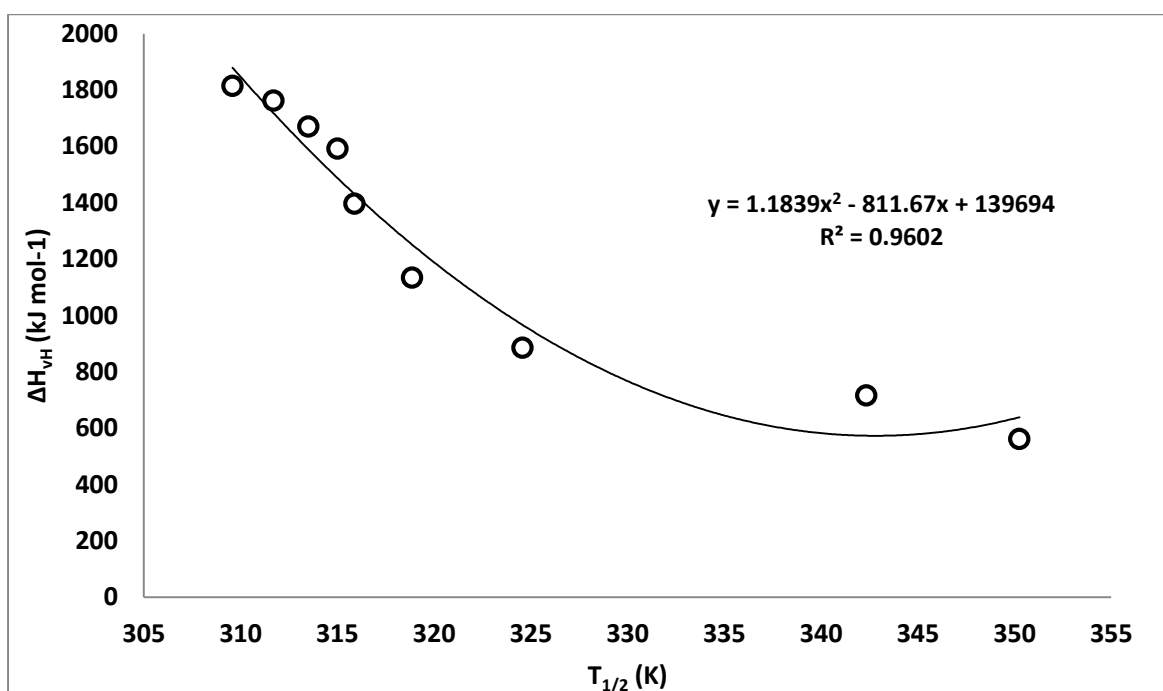


**Figure 5.11** Relationship between the optimised van't Hoff enthalpy values and  $T_{1/2}$  of PPG obtained using the model fitting procedure.

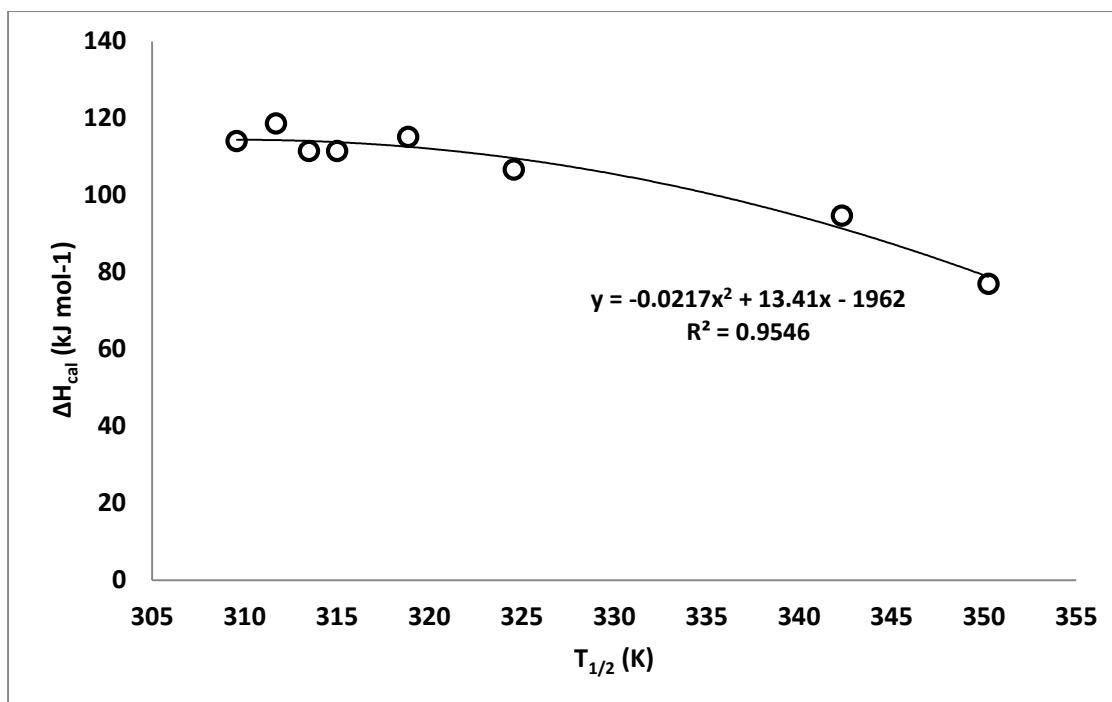


**Figure 5.12** Relationship between the optimised calorimetric enthalpy values and  $T_{1/2}$  of PPG obtained using the model fitting procedure.

The data for the parameters obtained for PPG in  $D_2O$  solutions using Scientist (Table 5.4) are shown in Figs. 5.13, 5.14, 5.15, 5.16, 5.17 and 5.18. Fig. 5.13 and Fig. 5.14 shows an excellent linear relationship between  $\Delta H_{vH}$  and  $T_{1/2}$  ( $R^2 = 0.999$ ) and between  $\Delta H_{cal}$  and  $T_{1/2}$  ( $R^2 = 0.994$ ). The slope of the  $\Delta H_{vH}$  and  $T_{1/2}$  graph gives the value of  $\Delta C_p$  and shows a constant  $\Delta C_p$ . The  $\Delta H_{vH}$  and concentration (Fig. 5.16) and  $\Delta H_{cal}$  and concentration (Fig. 5.17) graphs show a log-linear relationship with  $R^2 = 0.998$  and  $0.983$ , respectively. The concentration dependence of  $n$  graph (Fig. 5.18) and  $T_{1/2}$  and  $\Delta C_p$  (Fig. 5.19) both show a curvilinear relationship with  $R^2 = 0.992$  and  $R^2 = 0.993$ , respectively.

Also, the data obtained for aqueous PPG solutions in  $H_2O$  (Table 5.3) and for PPG in  $D_2O$  (Table 5.4) shows that the  $\Delta H_{cal}$  for PPG in  $H_2O$  solutions is higher than the PPG in  $D_2O$  solutions. However, the  $\Delta H_{vH}$  for the PPG in  $D_2O$  solutions is higher since it depends on the

modelling and the shape of the signal.  $\Delta H_{vH}$  gives information about the cooperativity; higher  $\Delta H_{vH}$  for PPG in in  $D_2O$  solutions is due to higher cooperativity in these solutions.

**Table 5.4** HSDSC parameters obtained for aqueous PPG solutions in  $D_2O$  as a function of concentration.

Concentration (mg mL <sup>-1</sup> )	$\Delta H_{cal}$ (kJ mol <sup>-1</sup> )	$\Delta H_{vH}$ (kJ mol <sup>-1</sup> )	n	$T_{1/2}$ (K)	$\Delta C_p$ (kJ mol <sup>-1</sup> K <sup>-1</sup> )
5	92.13	1314.73	19	320.9	-15.53
10	97.83	1683.25	20	315.9	-17.02
20	102.14	1988.96	21	311.6	-18.17
30	103.67	2171.14	22	309.3	-19.31

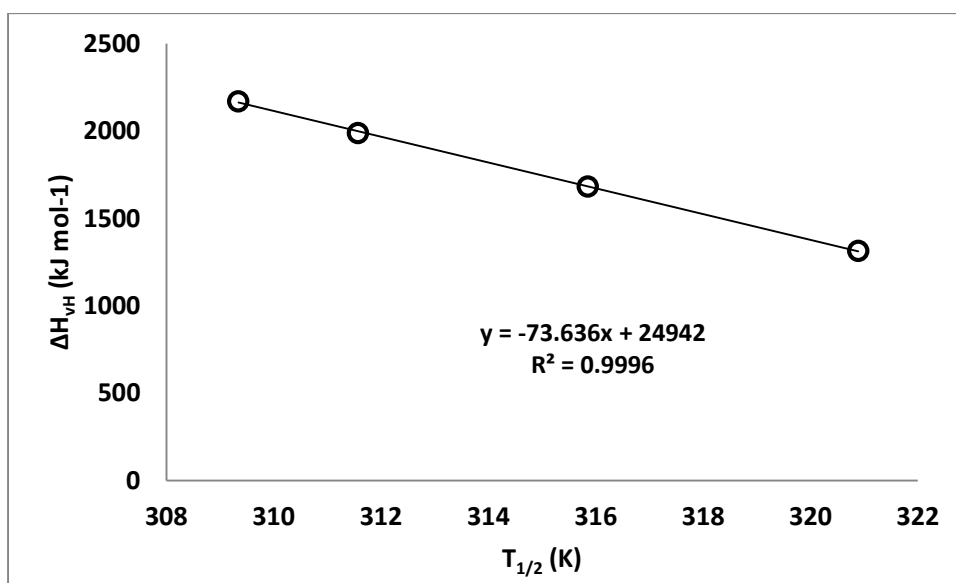


**Figure 5.13** Relationship between the optimised van't Hoff enthalpy values and  $T_{1/2}$  of PPG in  $D_2O$  solutions obtained using the model fitting procedure.

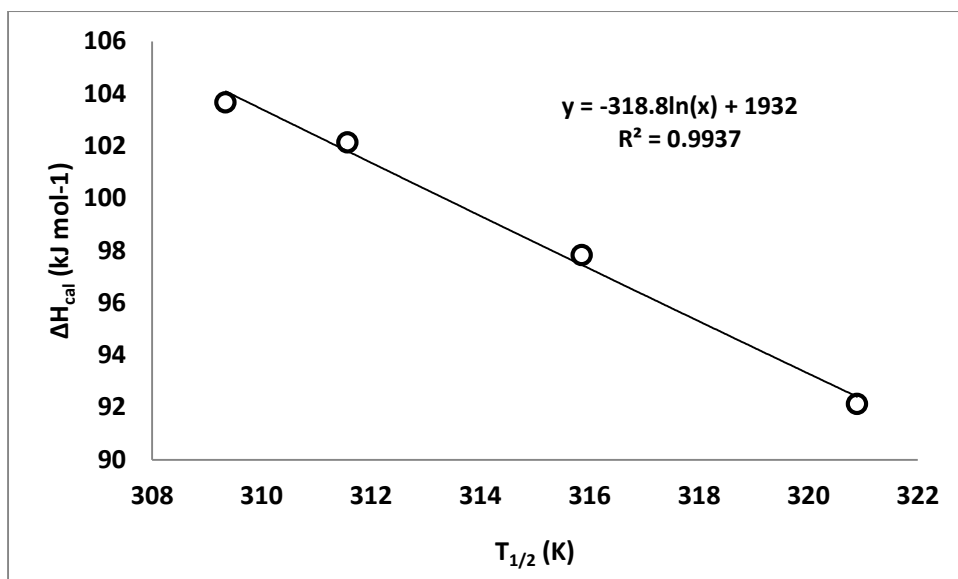


**Figure 5.14** Relationship between the optimised calorimetric enthalpy values and  $T_{1/2}$  of PPG in  $D_2O$  solutions obtained using the model fitting procedure.

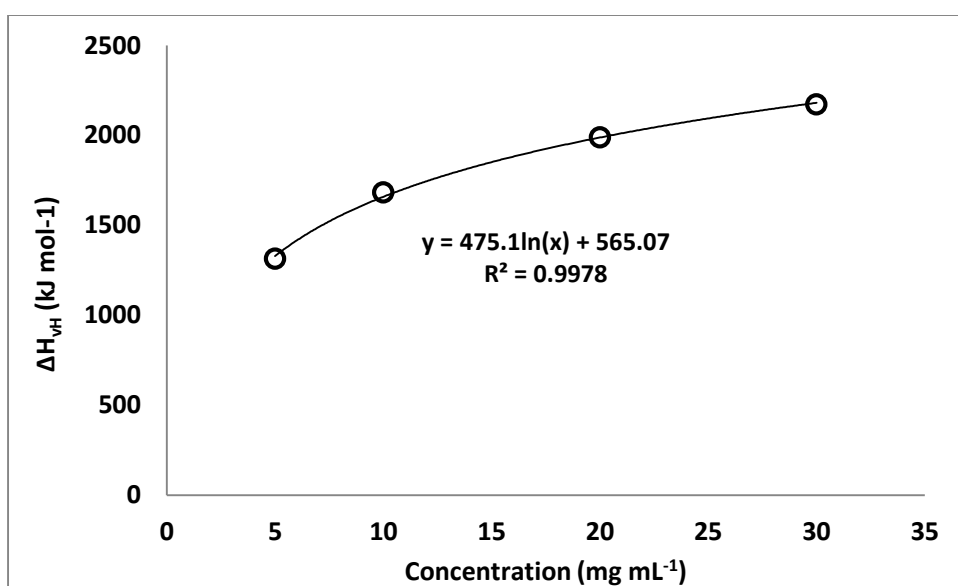


**Figure 5.15** Concentration dependence of the optimised van't Hoff enthalpy values of PPG in  $D_2O$  solutions obtained using the model fitting procedure.

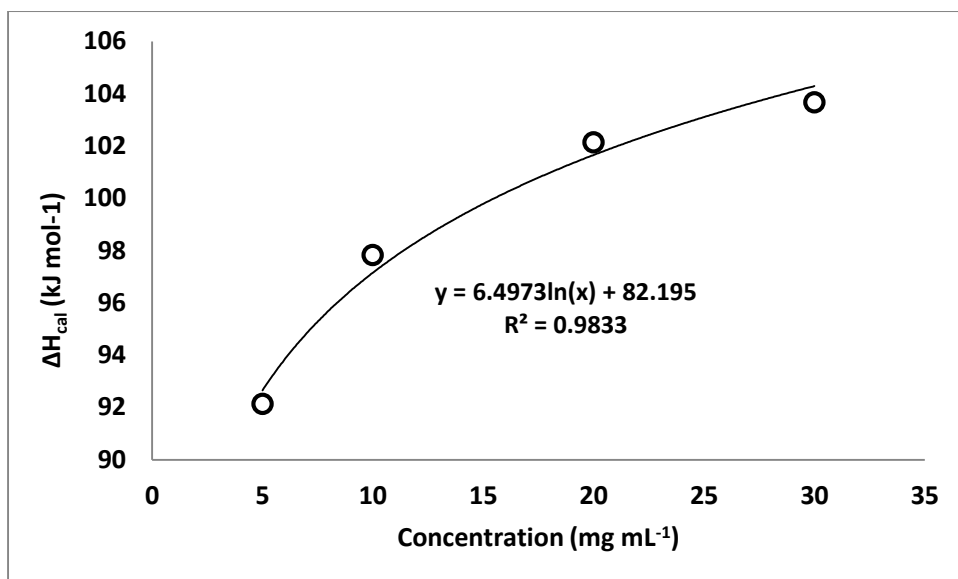


**Figure 5.16** Concentration dependence of the optimised calorimetric enthalpy values of PPG in D<sub>2</sub>O solutions obtained using the model fitting procedure.

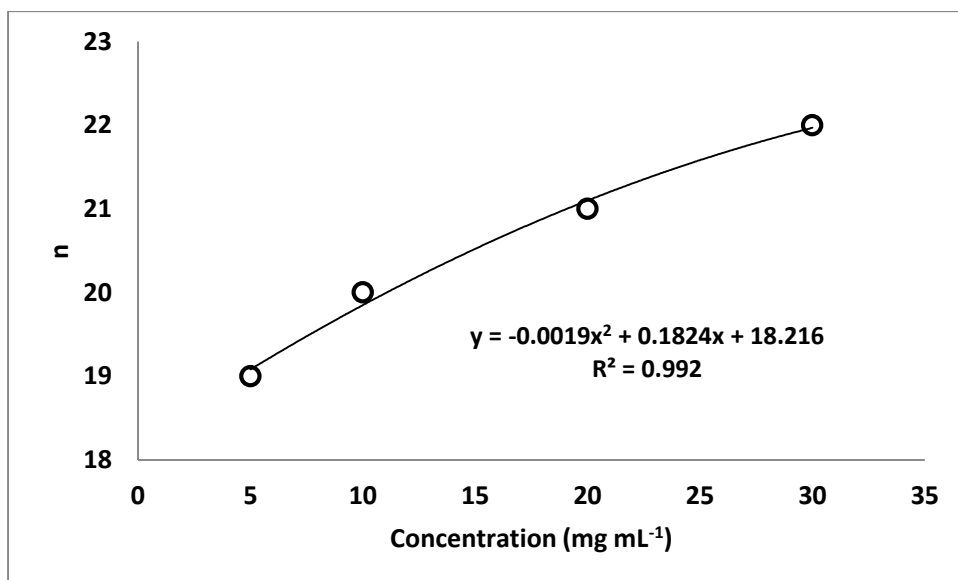


**Figure 5.17** Concentration dependence of the optimised aggregation number of PPG in D<sub>2</sub>O solutions obtained using the model fitting procedure.

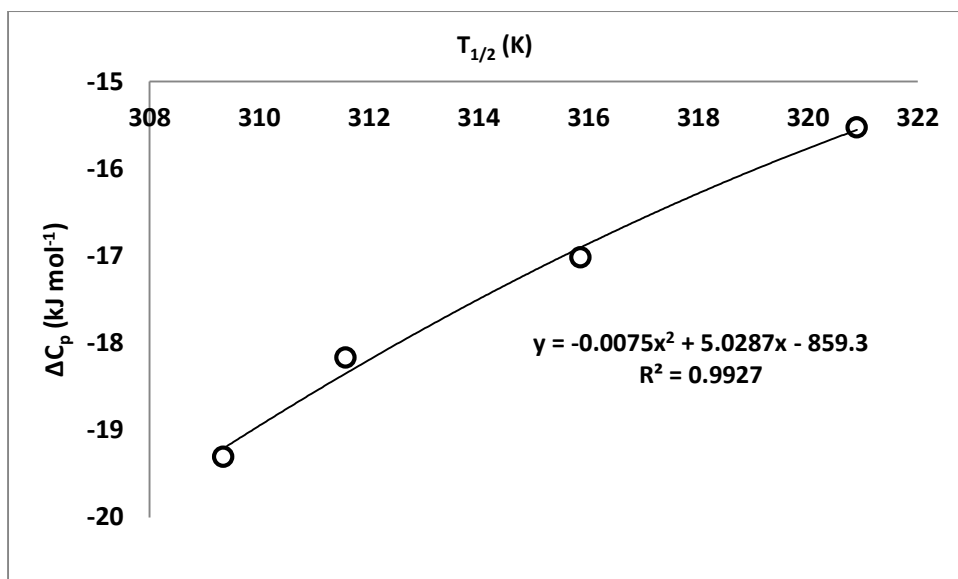


**Figure 5.18** Relationship between the optimised heat capacity values and  $T_{1/2}$  of PPG in  $D_2O$  solutions obtained using the model fitting procedure.

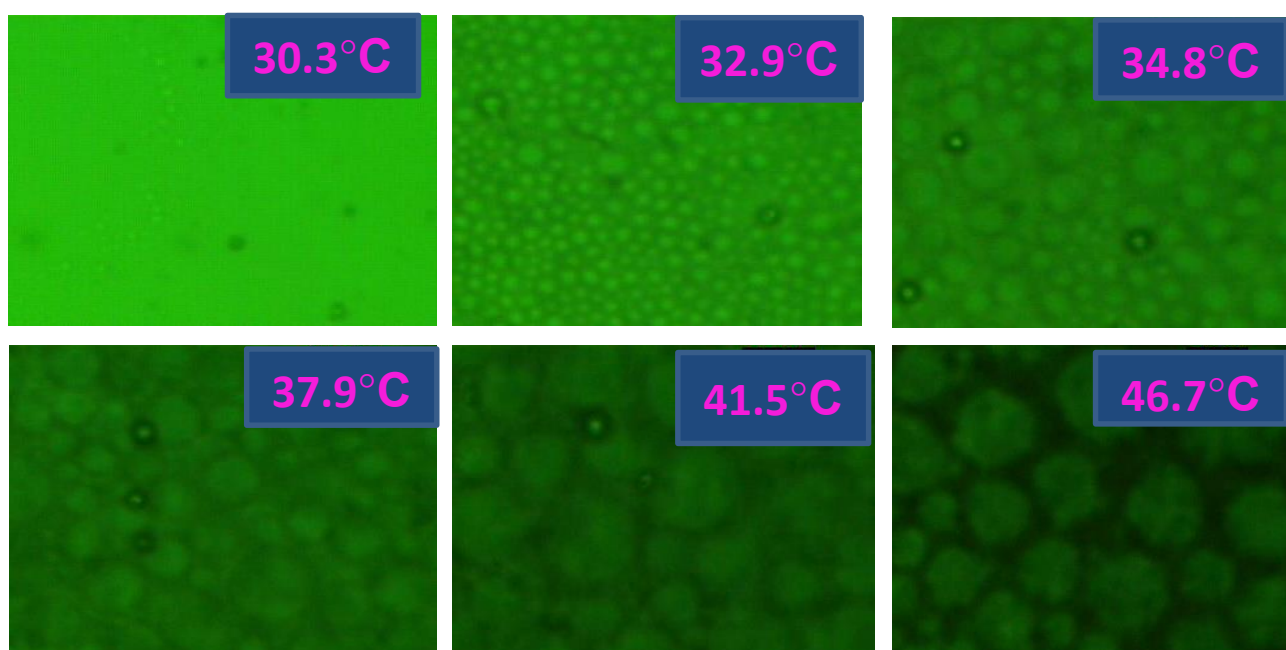
### 5.3.2 Hot Stage Microscopy

Figure 5.14 shows the HSM images taken for a  $20 \text{ mg mL}^{-1}$  PPG solution as it was heated up. The phase-separation process was recorded and the series of events that took place are as follows. As the temperature was increased, the clear solution started to form discrete spherical droplets emerging initially as pinpoints which gradually grow. The droplets grow with increasing temperature but remain distinct. There is no sign of coalescence thus the droplets remain dispersed in the aqueous phase. The observation of growth and the discrete nature of the droplets can be explained by the nucleation and growth model. These observations are consistent with aggregate formation observed using the HSDSC data. For  $20 \text{ mg mL}^{-1}$  solution, this growth of the droplets was observed until about  $42^\circ\text{C}$  after which the image darkens and nothing was visible. This is probably the point where the turbidity is so high that no light could pass through the sample, and so nothing could be recorded. The images here clearly indicate phase-separation occurring in the solution by the formation of well-defined droplets which are formed as a consequence of the initial aggregation process seen in the HSDSC. Also, the



temperature at which these droplets start to form (33-34°C) corresponds to the  $T_m$  of 20 mg mL<sup>-1</sup> obtained using HSDSC (34.4°C). The observation made using HSM is in agreement with our initial hypothesis that the phase-separation in the PPG solution in the metastable region is by the nucleation and growth mechanism. The growth of the droplets can be explained by Ostwald ripening where larger particles are formed because they are thermodynamically and energetically more stable than the smaller particles (Yao et al. 1993). This is because molecules have a higher Laplace pressure in small droplets and a lower Laplace pressure in the larger droplets. So big drops grow at the expense of small drops and eventually disappear.

The repulsion caused between the hydrated terminal -OH groups on the PPG chains might be preventing the coalescence to occur by either bridging or hydrogen bonding with each other.

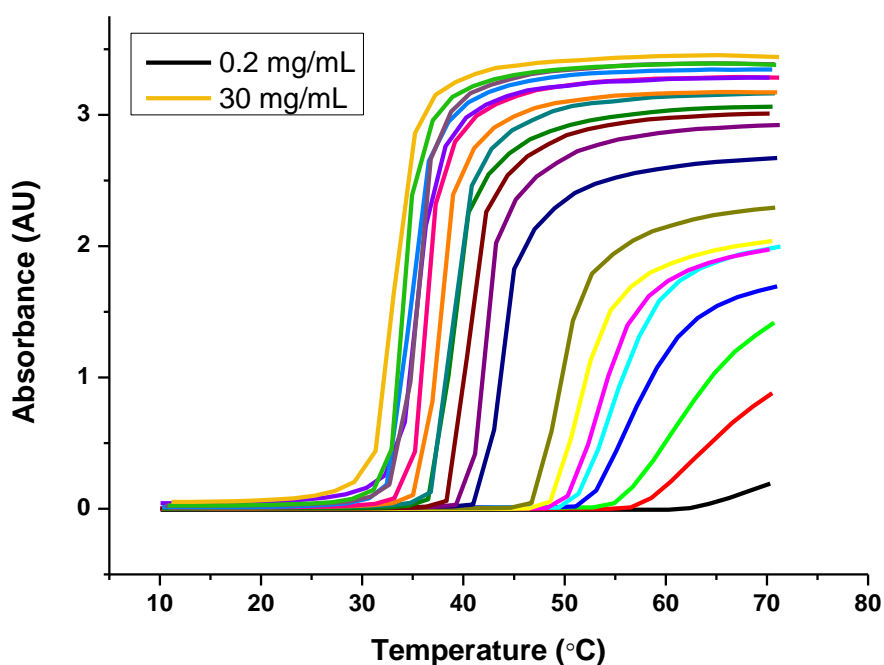


**Figure 5.19** Hot stage microscopy images obtained for 20 mg mL<sup>-1</sup> aqueous PPG solution when heated at 1°C min<sup>-1</sup>.

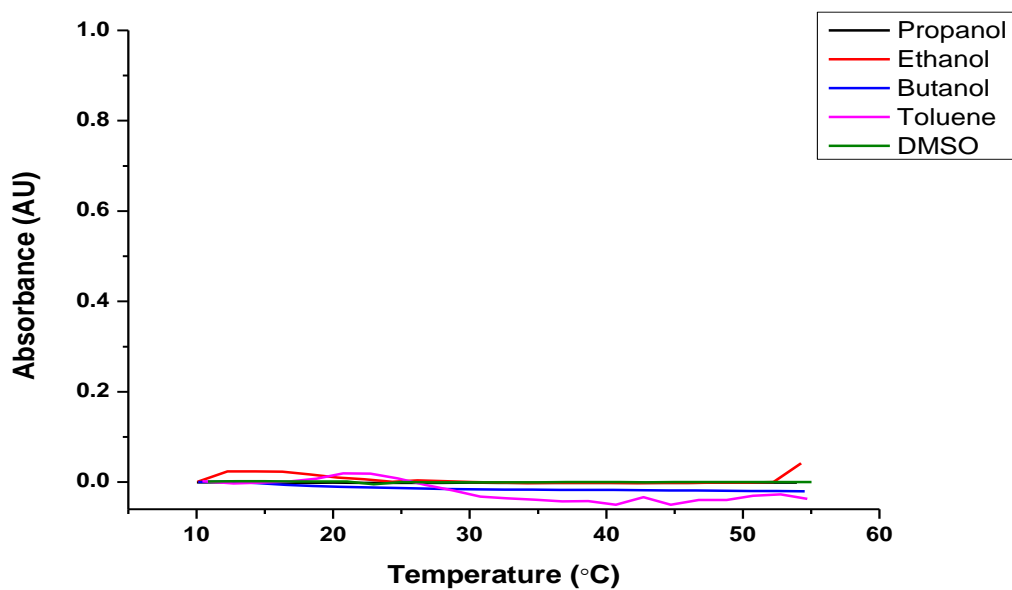
### 5.3.3 Turbidity Measurements using UV-Visible Spectrometer

Fig. 5.20 shows data obtained by UV-Vis spectroscopy for the change in absorbance with temperature as a function of aqueous PPG concentration. The onset of turbidity is taken as being the onset of phase separation. Turbidity measurements were also conducted for 20 mg mL<sup>-1</sup> PPG solutions made up in five organic solvents; propanol, ethanol, butanol, toluene and dimethyl sulfoxide (DMSO). No significant change in absorbance was recorded in these solutions (Fig. 5.16) showing the absence of aggregation/phase-separation of PPG in these solutions.

The data follows the same trend (Fig. 5.17) as the cloud-point data obtained using the HSDSC. Increase in the concentration of PPG in water brings the cloud-point and the transition temperature,  $T_m$  down.



**Figure 5.20** Graph of absorbance against temperature for a number of solutions with different PPG concentrations to measure the cloud-point of the solutions.



**Figure 5.21** Absorbance change with temperature for PPG solutions in different solvents.

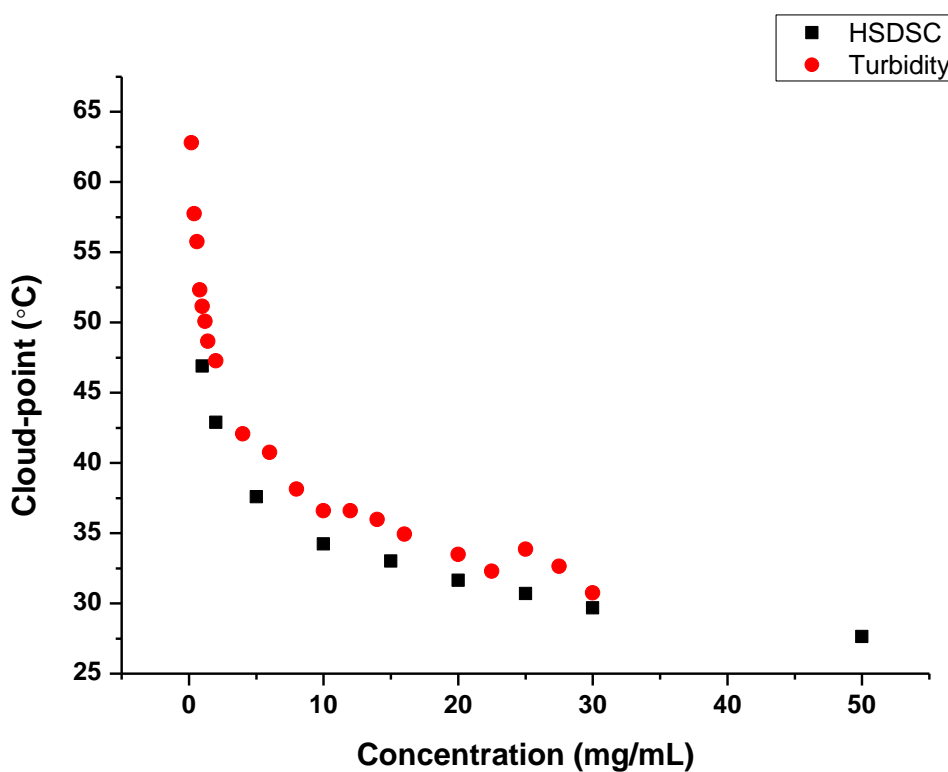


**Figure 5.22** Plots for cloud-points using two techniques: HSDSC and turbidity (UV-Visible spectroscopy).

### 5.3.4 Small-Angle Neutron Scattering

A 20 mg mL<sup>-1</sup> PPG solution was prepared in a mixture of 80% D<sub>2</sub>O and 20% H<sub>2</sub>O. Neutron scattering requires the samples to be prepared in D<sub>2</sub>O instead of H<sub>2</sub>O because of relatively low scattering length density of D<sub>2</sub>O. But a mixture of D<sub>2</sub>O and H<sub>2</sub>O was used to avoid the creaming behaviour of D<sub>2</sub>O in PPG solutions as mentioned above. A solution of PPG prepared in D<sub>2</sub>O was tested in a water bath and no or very little creaming was visibly seen in the test tube upon heating. The output for the SANS data is shown in Fig. 5.18.

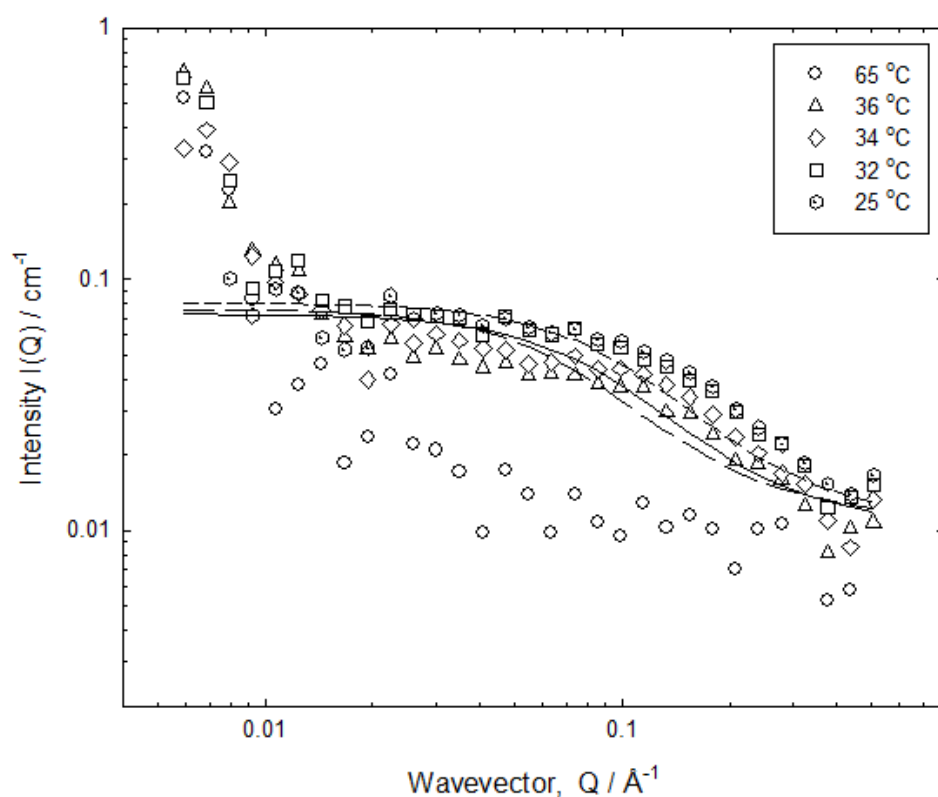


**Figure 5.23** SANS plot for 20 mg mL<sup>-1</sup> PPG solution in a mixture of 80% D<sub>2</sub>O and 20% H<sub>2</sub>O at 6 different temperatures.

To interpret the data, the slope is plotted on a double logarithmic plot. A shape is then adopted; a random coil in this case and scattering is then calculated for different shape dimensions. The three lines shown in the graph above correspond to the scattering intensity predictions of random coils of radii of gyration of 18, 20 and 22 Å, respectively starting from the bottom. The

data does fit the random coil assumption but there is a doubt over the presence of random coil structures for this small polymer.

A change in the scattering pattern can be seen at a temperature above the room temperature. At 32°C, the scattering intensity increases indicating the formation of aggregates at this temperature. Another observation that can be made from the above data is the change in the scattering at 65°C. This data backs up the data obtained from HSDSC and UV-Visible spectroscopy showing the evidence of aggregation.

### 5.3.5 Dynamic Light Scattering

Low concentration solutions of PPG in water were prepared, i.e., 1 mg mL<sup>-1</sup> and 2 mg mL<sup>-1</sup>.

Fig. 5.19 shows the change in the size of the particles in PPG solution as it was heated from 10-55°C.

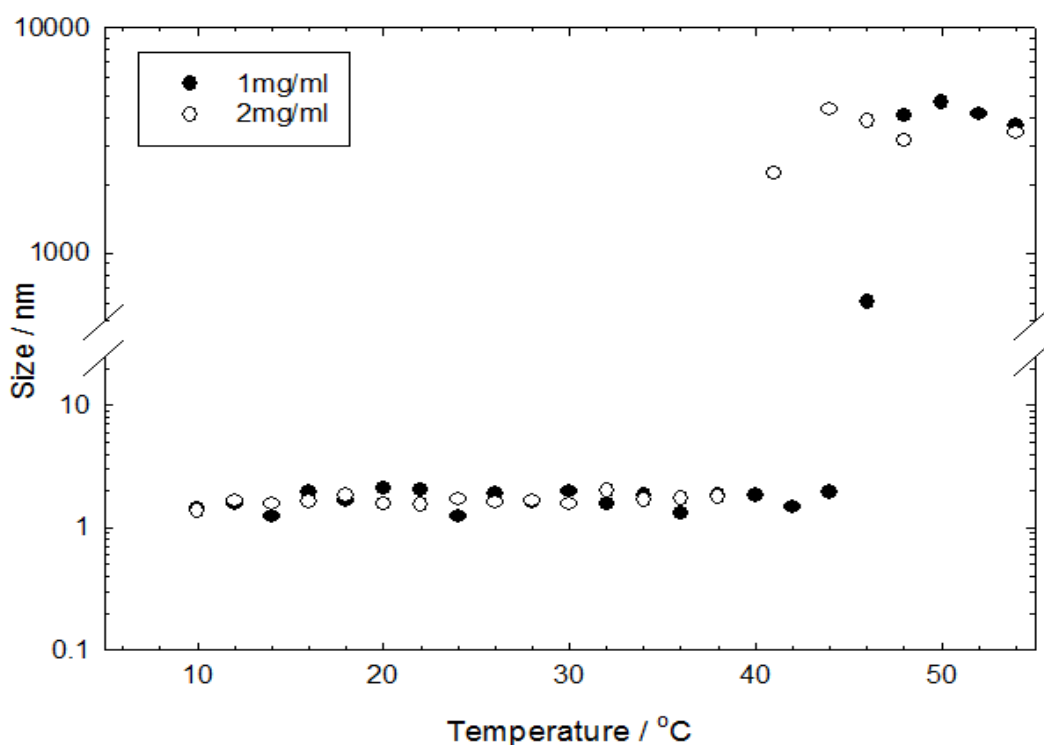


**Figure 5.24** Size of particles as a function of temperature for 1 mg mL<sup>-1</sup> and 2 mg mL<sup>-1</sup> aqueous PPG solutions.

As the solutions are heated, the presence of molecular size species is seen at  $\sim 45^\circ\text{C}$  for the  $1 \text{ mg mL}^{-1}$  solution and at  $\sim 39^\circ\text{C}$  for the  $2 \text{ mg mL}^{-1}$  solution. Average size changes from 1-2 nm to about 4-5  $\mu\text{m}$ . Intermediate size particles of about 1  $\mu\text{m}$  are also observed for  $1 \text{ mg mL}^{-1}$  solution. These are the temperatures around which clouding starts to occur. DLS scatters lights from suspensions and different sized particles have different intensity fluctuations because of the difference in their Brownian motion. The change in the size of the particles upon heating, confirms the formation of aggregates.

#### 5.4 Data Analysis

In order to obtain an analysis that incorporates the concentration dependence of the HSDSC data we use the following analysis.

For an aggregation process the chemical potential of unimers in aqueous solution is given by:

$$\mu_X = \mu_X^o + RT \ln[X] \quad (5.3)$$

Where  $[X]$  is the concentration of unimers,  $\mu_X^o$  is the chemical potential of unimers in pure state and  $\mu_X$  is the chemical potential of unimers in solution. The chemical potential of aggregates is given by:

$$\mu_{X_n} = \mu_{X_n}^o + RT \ln[X_n] \quad (5.4)$$

Where  $[X_n]$  is the concentration of unimers in the aggregates,  $\mu_{X_n}^o$  is the chemical potential of aggregates in their pure state and  $\mu_{X_n}$  is the chemical potential of aggregates in the aggregated formed in solution.

At equilibrium the chemical potential of a unimer in solution is equal to the chemical potential of a unimer in the aggregates:

$$\mu_X = \frac{\mu_{Xn}}{n} \quad (5.5)$$

The chemical potential of the n-mer aggregate is the sum total of the chemical potential all n unimers in the aggregate so we divide the chemical potential of n-mer by n.

Substitution of Equations 5.3 and 5.4 into 5.5 gives:

$$\mu_X^o + RT \ln[X] = \frac{\mu_{Xn}^o + RT \ln[X_n]}{n} \quad (5.6)$$

Rearrangement gives the following expression:

$$\Delta G_{nX \rightarrow Xn} = \mu_{Xn}^o - n\mu_X^o = -RT \left( \ln \frac{[X_n]}{[X]^n} \right) \quad (5.7)$$

Recognising that:

$$\Delta G = -RT \ln K \quad (5.8)$$

We can write the following equilibrium expression for aggregation:

$$K = \frac{[X_n]}{[X]^n} \quad (5.9)$$

This expression is variously referred to as the mass action expression for aggregation and sometimes it is called the closed association model.

The concentrations can be expressed in terms of the extent of transfer of PPG molecules into aggregates  $\alpha(T)$  where  $C_{Total} = [X] + n[X_n]$

$$\alpha(T) = \frac{n[X_n]}{C_{Total}} \quad (5.10)$$

Rearrangement gives:

$$[X_n] = \frac{\alpha(T)C_{Total}}{n} \quad (5.11)$$

The corresponding expression for [X] is given by:

$$[X] = (1 - \alpha(T))C_{Total} \quad (5.12)$$

Substitution into equation 5.9 gives:

$$\frac{\frac{\alpha(T)C_{Total}}{n}}{(1 - \alpha(T))^n C_{Total}^n} = K(T) \quad (5.13)$$

If we define  $C_{ref}$ , which is a reference concentration, then we can define the following expression at  $T_{ref}$  the temperature at which  $\alpha$  is equal to 0.5:

$$K(T_{ref}) = \frac{1}{n0.5^{n-1}C_{ref}^{n-1}} \quad (5.14)$$

The corresponding value for  $K(T)$  at some other concentration,  $C_{Total}$  is given as:

$$K(T) = \frac{\alpha(T)}{n(1 - \alpha(T))^n C_{Total}^{n-1}} \quad (5.15)$$

The following expression can now be written which represents the integral form of the van't Hoff isochore:

$$\frac{K(T)}{K(T_{ref})} = \exp\left(\frac{\Delta H_{vH}}{R}\left(\frac{1}{T_{ref}} - \frac{1}{T}\right) + \frac{\Delta C_p}{R}\left(\ln\left(\frac{T}{T_{ref}}\right) + \frac{T_{ref}}{T} - 1\right)\right) \quad (5.16)$$



Substitution gives:

$$\frac{\alpha(T)0.5^{n-1}C_{ref}^{n-1}}{(1-\alpha(T))^n C_{Total}^{n-1}} = \exp\left(\frac{\Delta H_{vH}}{R}\left(\frac{1}{T_{ref}} - \frac{1}{T}\right) + \frac{\Delta C_p}{R}\left(\ln\left(\frac{T}{T_{ref}}\right) + \frac{T_{ref}}{T} - 1\right)\right) \quad (5.17)$$

We can use the variation of  $\alpha$  in equation 5.17 to fit the cloud point data thereby obtaining the thermodynamic data for the phase separation process. The cloud point data as shown in Fig. 5.25 is a plot of temperature at which phase separation is initially detected optically.

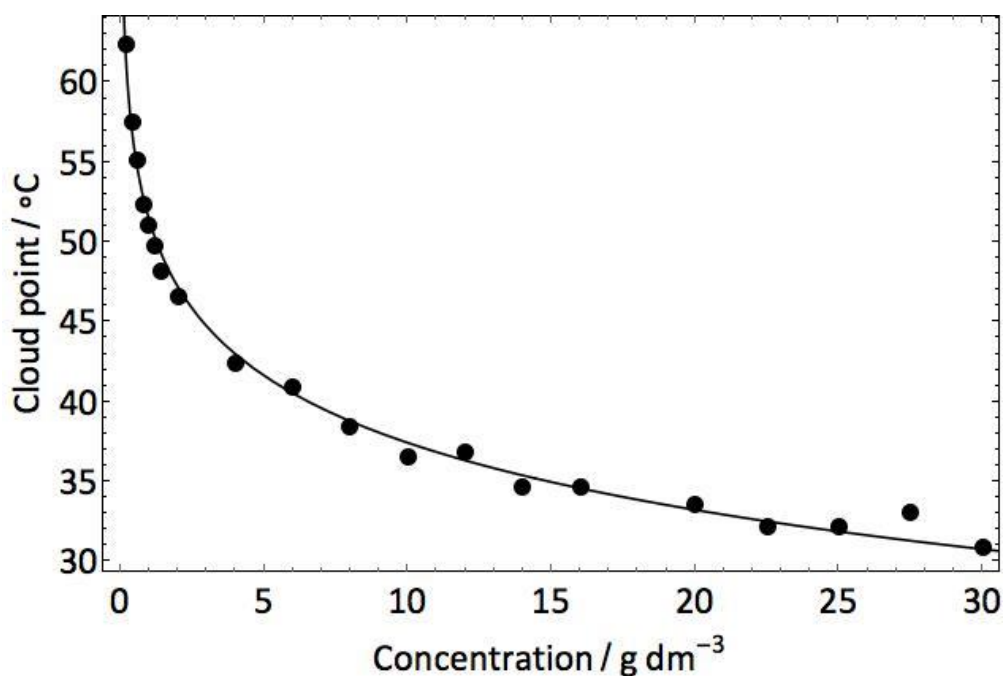


**Figure 5.25** Cloud point data showing a plot of temperature at which phase separation is first detected optically.

The graph shows that if we had a solution consisting of 30 mg mL<sup>-1</sup> of PPG 1000 then as we raise the temperature of this solution it would remain optically clear (transparent) until we reach a temperature of just above 30°C. At that temperature phase separation occurs. As we now raise the temperature, the composition of the aqueous phase is given by the cloud point curve. So using the cloud point/composition data we can calculate  $\alpha$ ; the fraction of PPG that has

phase separated. So we assume that if we started with a  $30 \text{ mg mL}^{-1}$  solution then as we raise the temperature the fraction of phase separated PPG is given by:

$$\frac{30 \left(\frac{\text{mg}}{\text{mL}}\right) - C(T)}{30 \left(\frac{\text{mg}}{\text{mL}}\right)} \quad (5.18)$$

Where  $C(T)$  is the concentration at cloud point temperature  $T$ .

Using a variation of equation 5.17 wherein the reference concentration and the initial concentration of PPG are the same ( $30 \text{ mg mL}^{-1}$ ) which is:

$$\frac{\alpha(T)0.5^{n-1}}{(1 - \alpha(T))^n} = \exp\left(\frac{\Delta H_{vH}}{R}\left(\frac{1}{T_{ref}} - \frac{1}{T}\right) + \frac{\Delta C_p}{R}\left(\ln\left(\frac{T}{T_{ref}}\right) + \frac{T_{ref}}{T} - 1\right)\right) \quad (5.19)$$

We can fit the computed  $\alpha$  values to the temperature data. The fit is shown in Fig. 5.26.

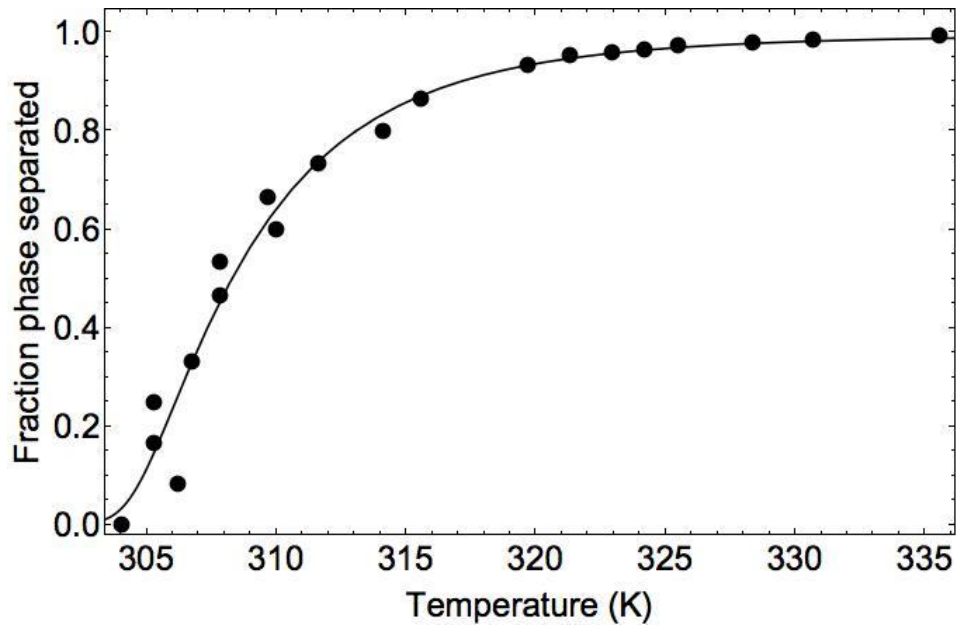


**Figure 5.26** Fit of the computed  $\alpha$  values to the temperature (cloud-point) data.

The following thermodynamic parameters are obtained from the fitting process

$$\Delta H_{vH} = 1406 \text{ kJ mol}^{-1}, T_{ref} = 308.3\text{K}, \Delta C_p = 32.4 \text{ kJ mol}^{-1} \text{ K}^{-1} \text{ and } n = 8.14.$$

Using this data and  $\Delta H_{cal}$  value obtained for  $30 \text{ mg mL}^{-1}$  solution of  $118 \text{ kJ mol}^{-1}$ , we can simulate the HSDSC signal using equation 5.17 and compare the simulations with the actual data obtained by HSDSC (Fig. 5.27).

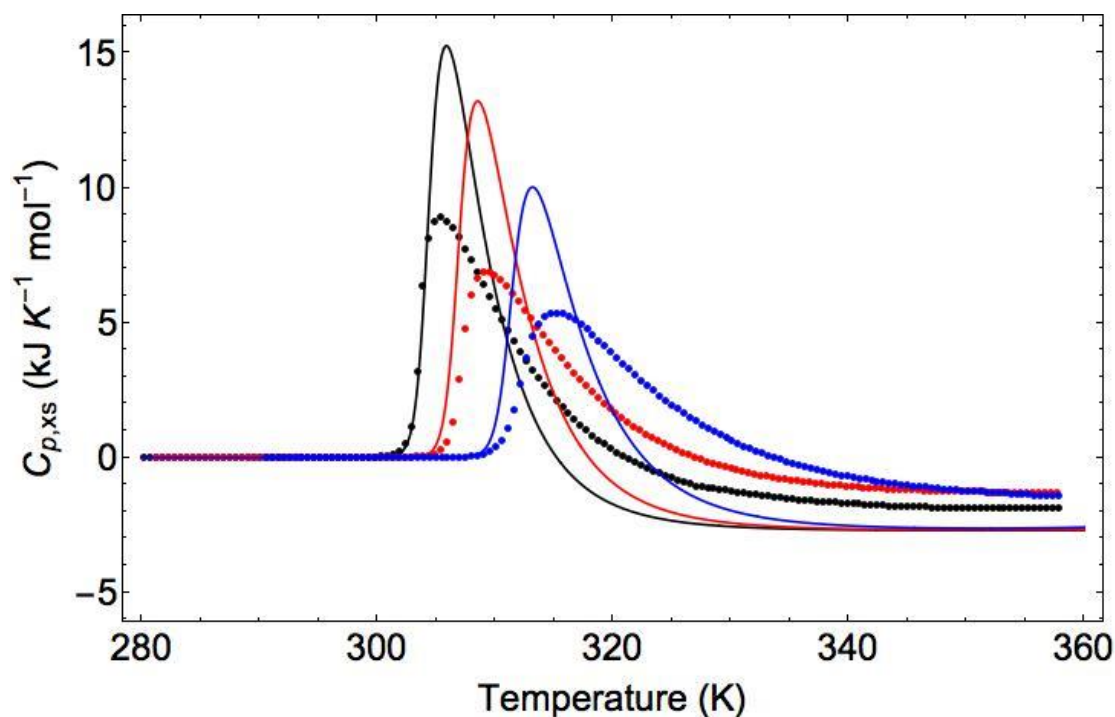


**Figure 5.27** Plot of simulated HSDSC signal using the cloud-point data (solid line) and the actual HSDSC data (dashed line) obtained at  $30 \text{ mg mL}^{-1}$  (in black),  $15 \text{ mg mL}^{-1}$  (in red) and  $5 \text{ mg mL}^{-1}$  (in blue).

The simulations show some correspondence with the data; in particular the simulation for  $30 \text{ mg mL}^{-1}$  and the actual data, which unfortunately is lost at higher temperatures. Even for the other concentrations it is noticeable that the use of equation 5.17 allows the cloud point derived data to correctly predict the start of the phase transition even if the simulations are sharper than the actual HSDSC data. This is due to the fact that the cloud point temperature data reports on

the state of the systems at the start of the transition, which must be similar in every case and is similarly reported by the HSDSC instrument.

But at high concentrations, according to Kjellander and Florin, the PPG water network must be quite extensive and the system should show a high degree of cooperativity that will provide a sharp signal which is evident from the increase in cooperativity values with the increase in concentration obtained using HSDSC data. This explains the high degree of correspondence between the simulation and the HSDSC data obtained for the 30 mg mL<sup>-1</sup> solution. As the concentration decreases this cooperativity decreases and the HSDSC signals become broader. This shows that Equation 5.17 is unable to reproduce the effects of concentration on the HSDSC signal as shown in Figure 5.27. The thermodynamic treatment is only valid if the cooperativity remains the same, which we presume is the case for each specific concentration.

It is also possible to establish a phase diagram using the HSDSC data. The HSDSC model derived data can be used to calculate  $\alpha$  using equation 5.19 for each concentration. Multiplying the obtained  $\alpha$  value by the initial PPG concentration, the concentration of PPG that has phase separated can be obtained using equation 5.10. This term is the mass of PPG that has phase separated divided by the volume of water that was initially used to make up the solution. A plot of this phase-separated PPG as a function of temperature along with the cloud-point curve is shown in Fig. 5.28. The lines that are produced sort of correspond with the cloud point curve particularly at the initial point of phase separation. The reason they do not correspond over the whole concentration range is because the system is changing with initial concentration in terms of aggregation number and cooperative unit size. Also, the cloud point consistently appears at a temperature that is slightly greater than the point at which the HSDSC curves begin to show the onset of phase separation. This is because the experimental optical detection of the cloud point requires the phase separated liquid particles to be of a particular size (in the order of 530 nm). Whereas the temperature (which is detectable by HSDSC) at which phase separation

occurs, the phase-separated particles are much smaller in size as evidenced by the HSM and DLS measurements and are thus optically undetectable.

Another observation that can be made from this data is that the cloud-point curve overestimates the PPG that has phase separated. Thus if we take an example temperature of 320 K and initial aqueous phase concentration of  $30 \text{ mg mL}^{-1}$ , the composition of the aqueous phase system, as described by the cloud point curve, should be approximately  $2 \text{ mg mL}^{-1}$  in PPG. Whereas the HSDSC generated curve suggests that this concentration should be  $7.7 \text{ mg mL}^{-1}$ .

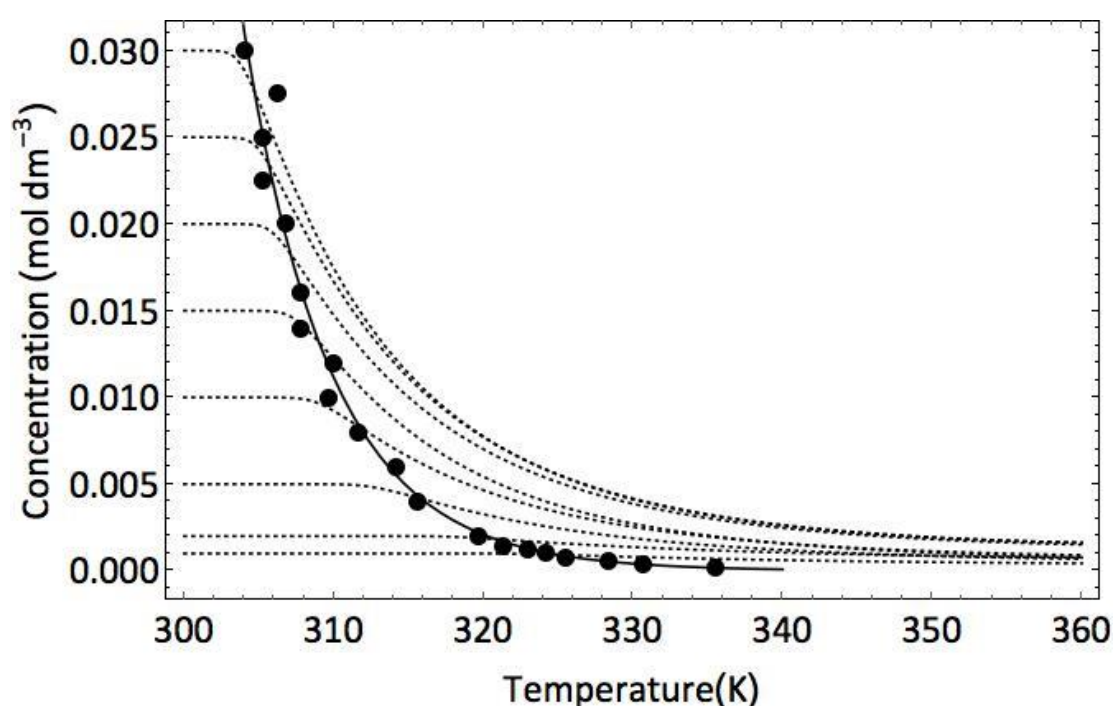


**Figure 5.28** Plot of phase-separated PPG ( $\alpha$ ) as a function of temperature for different concentrations of PPG (dashed lines) along with the cloud-point curve (solid line).

The model fitted data for  $30 \text{ mg mL}^{-1}$  is then plotted with the calorimetric data obtained for  $30 \text{ mg mL}^{-1}$ . These peaks superimpose on each other perfectly well at least within experimental error. However, if equation 5.17 is used to model the HSDSC data for PPG at 5 or  $15 \text{ mg mL}^{-1}$  concentration (Fig. 5.31) the HSDSC data does not correspond to the HSDSC data created using equation 5.19. The same applies for the other two graphs, Figs. 5.29 and 5.30,

where the 5 and 15 mg mL<sup>-1</sup> data are used, respectively, to reproduce the HSDSC data for the other two concentrations.

This suggests that the cloud point data seems to be able to predict when the HSDSC transition should occur but it does not predict the shape of the transitions. However, the HSDSC fitted data at one concentration cannot predict anything about a HSDSC transition at another concentration. This is because the system changes with concentration. The aggregation number and the cooperative unit size change with concentration. However, the transitions are related to the clouding phenomenon. Hence we can conclude that cloud point curve does not necessarily provide an unambiguous phase diagram because the phase diagram as elucidated by HSDSC is concentration dependent.

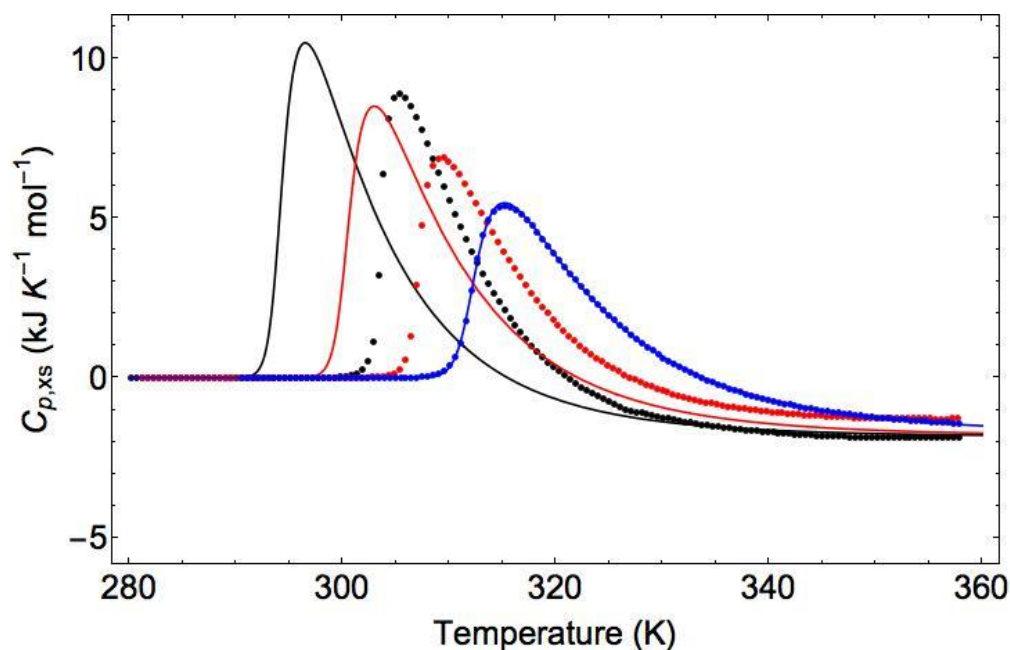


**Figure 5.29** HSDSC simulations (solid line) for 15 mg mL<sup>-1</sup> (in red) and 30 mg mL<sup>-1</sup> (in black) using 5 mg mL<sup>-1</sup> (in blue) (the original HSDSC data is shown in dashed line).

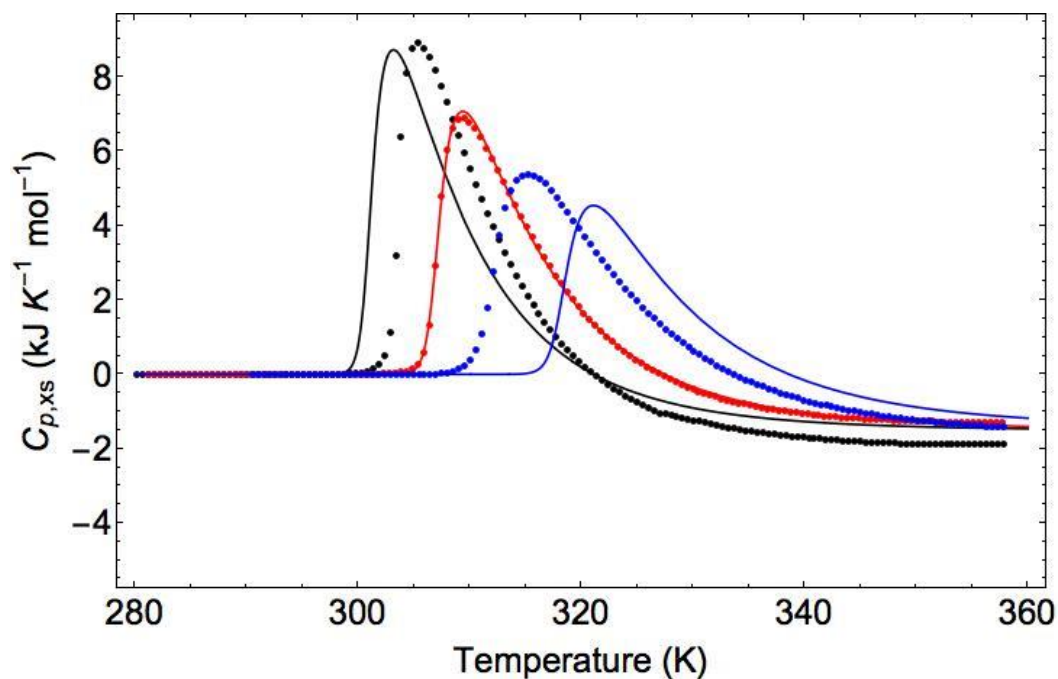


**Figure 5.30** HSDSC simulations (solid line) for 5 mg mL<sup>-1</sup> (in blue) and 30 mg mL<sup>-1</sup> (in black) using 15 mg mL<sup>-1</sup> (in red) (the original HSDSC data is shown in dashed line).

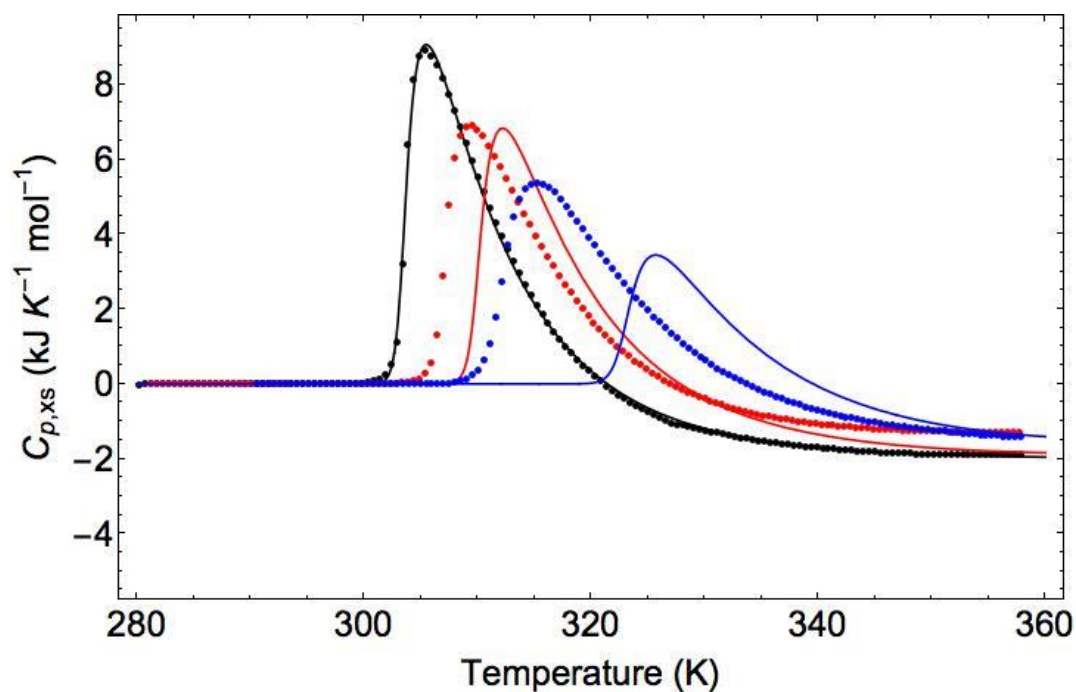


**Figure 5.31** HSDSC simulations (solid line) for 5 mg mL<sup>-1</sup> (in blue) and 15 mg mL<sup>-1</sup> (in red) using 30 mg mL<sup>-1</sup> (in black) (the original HSDSC data is shown in dashed line).

## 5.5 Conclusions

The turbidimetric data indicates that phase separation occurs at a precise temperature which is intimately linked to the onset of the signal obtained by HSDSC. The HSDSC signal indicates that phase separation occurs via formation of aggregates and disruption of a water/PPG network. The formation of aggregates is further corroborated by the SANS measurements. Whilst the formation of discrete droplets of PPG rich phase dispersed in water is confirmed by the DLS data. Moreover the HSM images directly show the formation of droplets which grow in size with an increase in temperature. These droplets are formed as a consequence of the aggregation process seen using HSDSC. This data supports our initial hypothesis of phase-separation of PPG solutions via a nucleation and growth mechanism. Nucleation observed as an aggregation event from the HSDSC and the turbidity data and growth seen in the HSM images. SANS and DLS measurements also suggested formation of bigger size droplets upon heating the sample.

The data obtained for PPG 1000 supports the hypothesis of phase-separation of PPG solutions via nucleation and growth mechanism. The data suggested that the  $T_m$  could be decreased down to room temperature by increasing the PPG concentration. The higher molecular mass PPGs offer a lower  $T_m$  which can be useful for drug delivery purposes. The data analysis shows that there is no unique coexistence line for PPG systems and that the coexistence line derived from cloud point measurements will differ from the coexistence line derived by starting at a specific concentration and raising the temperature.

In the next chapter we examine the effect of cosolutes upon the onset of phase separation in PPG solutions which is part of the programme to learn how to control the phase separation properties of PPG. It is presumed that aggregation upon heating occurs because PPG becomes increasingly hydrophobic as the temperature is raised. The water dispersed phase-separated



droplets which are formed presumably have hydrophobic centres which can be used for the solubilisation/encapsulation of hydrophobic drugs. This potential use of PPG solution for the delivery of drugs will be discussed later in this thesis.

## Chapter 6 Effect of Sugars on the Phase-Transition Temperature of PPG

### 6.1 Introduction

Studies of the LCST behaviour of polymers have been undertaken in the past and have been used as a simple model to study the behaviour of biopolymers, particularly proteins in aqueous systems. LCST/UCST values can be altered by the addition of cosolutes/cosolvents (Heyda & Dzubiel 2014; Zhang et al. 2007; Freitag & Garret-Flaudy 2002; Kathmann et al. 1996; Cowie & McEwen 1974). These may be ionic or non-ionic and they have the effect of either salting in/out effects on the macromolecules (Zhang et al. 2007; Kırıcı & Güner 2001). The aim of this part of the research is to study the effect of five different sugars differing in their stereochemical structure, molecular weight and dielectric properties on the phase-transition temperature ( $T_m$ ) of PPG solutions. Sugars were considered because they are produced from renewable raw-materials, are highly biodegradable and, generally, non-toxic. When used in pharmaceutical formulations, they can lead to the formation of safe biocompatible formulations.

Cosolutes are divided into two types; kosmotropes (also called structure-makers) and chaotropes (also called structure-breakers). Kosmotropes bind water molecules strongly, creating conditions for avoiding denaturation processes, hence called structure makers. Chaotropes bind water molecules weakly relative to the strength of water-water interactions in bulk solution and hence do not stabilise biomolecules; thus they are termed structure-breakers (Barreca et al. 2008; Collins 1997). Kosmotropes exhibit strong interactions compared to the water-water interactions in bulk leading to modification of the water structure and reduction in the entropy of water around these molecules and hence stabilising the protein (Collins & Washabaugh 1985; Collins 1997). Most sugars act as kosmotropes and act as protein stabilizers (Moelbert et al. 2004). Chaotropes however do not have the effect that kosmotropes have in reducing the mobility/entropy of the water molecules around them, but they interfere with the

hydrogen bonds between the water molecules, reducing the protein stability and acting as denaturants (Collins & Washabaugh 1985; Collins 1997).

The way kosmotropes and chaotropes effect is through their influence on solvent rather than the direct interaction between the cosolute/cosolvent and the solute. Water molecules form strong, intermolecular hydrogen bonds and form a highly ordered structure. Addition of a hydrophobic molecule disrupts the hydrogen-bonded structure but at low temperatures the structure rearranges to a cage-like structure. However, at higher temperatures the free energy of the system is decreased by disruption of the ordered water structure and increasing the entropy of the water molecules, and this is the driving force of aggregation of hydrophobic molecules. Hence the hydrophobic interaction between non-polar solute molecules is primarily solvent-induced (Moelbert et al. 2004).

### **Mechanism of the Effect of Kosmotropes and Chaotropes**

Kosmotropes like sucrose are more polar than water and enhance its structure by hydrogen bonding and so they interact with water rather than non-polar solute molecules. This leads to their preferential exclusion from the vicinity of hydrophobic solutes and a net repulsion between the solvent and solute molecules. This leads to solute molecules being pushed together to minimise their exposure to the surface and hydrophobic aggregation. The same process leads to the stabilisation of the native protein structure (Galinski et al. 1997).

Chaotropes like urea; are less polar than water and so they disrupt the water structure. Hence these molecules are excluded from the bulk water, towards the solute particles (preferential binding with the solute particles) (Timasheff 2002b). Their presence leads to an increase in the solvent available for binding the hydrophobic solutes and hence destabilises hydrophobic aggregates, micelles and native protein structures (Timasheff 2002a; Timasheff 2002b).

The Hofmeister series, first noted in 1888 ranks the relative influence of ions on the basis of their physical behaviour on aqueous systems (Hofmeister 1888). Originally it was believed that ions influence macromolecular properties by affecting just the water structure but according to Hofmeister effect, ion-macromolecule interactions as well as the interactions with the water molecules are responsible for the effect on the macromolecular properties (Zhang & Cremer 2006). Fig. 6.1 shows Hofmeister anion series and some of its related properties. Species to the left of  $\text{Cl}^-$  are referred to as kosmotropes and to the right are called chaotropes. Kosmotropes have salting out effects on proteins and macromolecules while chaotropes destabilize the folded proteins and have salting-in behaviour (Zhang & Cremer 2006).

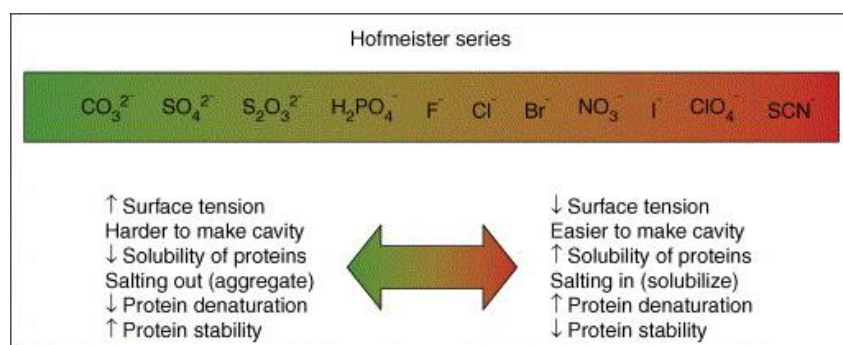


**Figure 6.1** Hofmeister series showing typical ordering of the anion series and some of its related properties (Zhang & Cremer 2006).

So kosmotropes and chaotropes should affect proteins in the opposite way they affect PPG. Globular, water soluble proteins unfold to expose their hydrophobic groups to water and thus increase the heat capacity. PPG aggregates to reduce their exposure to water. Therefore, if a cosolute increases the unfolding temperature of a protein it should reduce the phase separation temperature for PPG.

The effect of sugars on the LCST behaviour of many polymers including PEG (Harris 1992) and on the stabilising effect on proteins (Gerlisma 1968) has been previously studied. The effect

of sugars on the stabilisation of proteins has been explained by preferential hydration of proteins by Timasheff and co-workers (Arakawa & Timasheff 1982; Lee & Timasheff 1981). Addition of sugars to protein-water systems leads to an unfavourable free-energy change which increases with the increase in the protein surface area; hence stabilizing the proteins. Preferential exclusion of the sugars from the vicinity of the protein domains is also responsible for protein stabilization (Lee & Timasheff 1981). McClements showed that the thermal stability of the proteins not only depends on the type of cosolvent but also upon the concentration of cosolvent. The transfer free energy of proteins into cosolvent solution influences protein transitions (McClements 2001). When a cosolvent concentration around protein is lower than in the bulk solution, the cosolvent is said to be ‘preferentially excluded’ and the transfer free energy associated with moving protein from bulk solution to cosolvent solution is unfavourable. However, if the concentration of cosolvent is greater around the protein than in the bulk solution, cosolvent is ‘preferentially accumulated’ and the transfer free energy of the protein is negative (McClements 2001; McClements 2002).

Different sugars exhibit different effects on the LCST of the polymers and the stabilization of proteins depends on their ability to interact with water. Shpigelman et al. studied the effect of different sugars and polyol solutions on the LCST of poly-*N*-isopropylacrylamide (PNIPAM) aqueous solutions (Shpigelman et al. 2008). PNIPAM undergoes a coil-to-globule transition at low concentrations and a CP at high concentrations (Graziano 2000). Shpigelman et al. hypothesised and demonstrated that the already existing theory of ‘differential interaction’ by Timasheff and coworkers; that the effect the sugars have on polymers and proteins is from their interaction with water and not directly through polymer/protein interaction (Arakawa & Timasheff 1982; Lee & Timasheff 1981). Preferential exclusion of sugars from polymer vicinity and preferential hydration has been suggested as the main mechanism for protein stabilisation (Shpigelman et al. 2008). They suggested that the bigger size cosolvents are worse

for polymers in terms of mixing entropy and hence they would reduce the coil-to-globule transition temperature. They also suggested that different sugars affect the water structure differently and this is due to the size and the density of the hydration shell formed around the sugar in aqueous solutions (Shpigelman et al. 2008).

The effect of various sugars on the LCST of thermoresponsive polymers has been studied before by various researchers. The LCST phenomenon of water soluble polymers is dependent upon the hydrophile-hydrophobe balance of polymers. An elevated temperature weakens the hydrogen bond between the water and the polymer leading to dehydration and enhancing the hydrophobic interaction. Kim and co-workers showed the effect of the polymer concentration on the sensitivity of the sugars in affecting the LCST (Kim et al. 1995). Increasing the polymers concentration had a greater effect of saccharides in lowering the LCST. They studied the effect of saccharides on the LCST of pluronics, poly(*N*-isopropylacrylamide) and *N*-isopropylacrylamide copolymers. They studied the effect of saccharides on four pluronic solutions: L31, L62, F68LF and L92. They showed that the saccharides decreased the LCST of these pluronics and the ones that had higher content of PEO showed greater effect of the saccharides on the LCST. They also showed that monosaccharides such as glucose have a greater effect than disaccharides such as maltose in lowering the LCST. They explained that the saccharide effect is down to their effect on the structured water lattice around the polymer as suggested by other researchers mentioned above. Saccharides may enhance the hydrophobic interaction between the polymer chains either by immobilizing the water molecules around them and hence weakening the hydrophobic hydration or by increasing the local order of the water molecules around the polymer and hence increasing the driving force of hydrophobic interaction. Another mechanism proposed by these researchers is that the presence of saccharides may stabilise and increase the non-polar conformations of polymer in solutions of some pluronics and PEO solutions where phase-separation is temperature induced (Florin et al.

1984; Lindman et al. 1990; Karlstroem 1985). Researchers have reported the effect of saccharides on PEO solutions and they reported that the decrease in LCST is due to repulsive interaction between the PEO and glucose (Sjoeberg et al. 1989; Gustafsson et al. 1986). This leads to a predominant partitioning of glucose into the polymer poor phase, thus inducing the phase separation at a lower temperature.

In this chapter, the effect of five sugars; Maltose monohydrate, mannitol, sucrose, trehalose dihydrate and raffinose pentahydrate on PPG 1000 aqueous solution has been analysed using HSDSC measurements along with turbidity data obtained using UV-Visible spectroscopy. This study has not been conducted before and could significantly help in reducing the  $T_m$  of the aqueous PPG solutions to ambient or body temperature.

### **6.1.1 Sugars and their Effect on the Dielectric Constant**

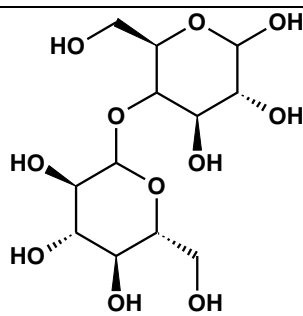
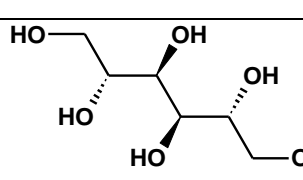
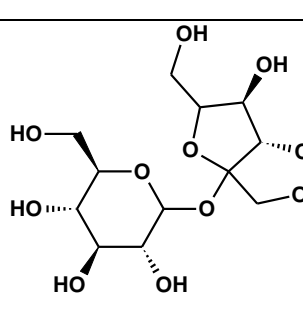
Carbohydrates have a basic chemical structure containing carbon, hydrogen and oxygen. They are one of the main sources of dietary energy and are also known as saccharides. They are classified according to the number of saccharide units they contain as monosaccharides, disaccharides, oligosaccharides and polysaccharides (Brown 2014). Sugars are one of the main types of carbohydrates in the body. The simplest carbohydrates are monosaccharides; made up of single saccharide units. Disaccharides consist of two monosaccharide units, oligosaccharides have 3-10 units and polysaccharides have many units linked together in a chain. Glucose is a monosaccharide and combined with fructose it forms the most common saccharide; sucrose (a disaccharide). It's naturally present in sugar cane, sugar beet and some fruits and is commonly known as sugar. Maltose used in these experiments is also a disaccharide which is made of two glucose units joined together (Cole-Hamilton et al. 1987) and mannitol (a monosaccharide) is a sugar alcohol derived by reduction of mannose. Trehalose is a disaccharide and raffinose is an oligosaccharide made of three monosaccharides (Brown 2014).

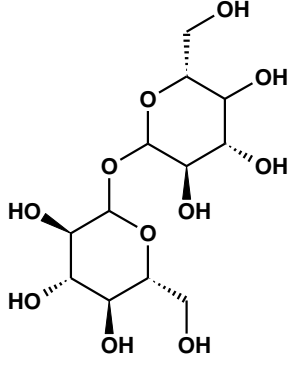
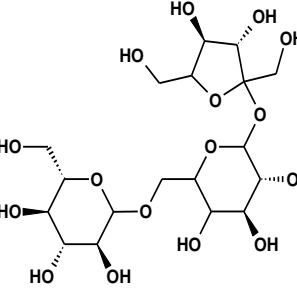
Sugars have the property of modifying the dielectric behaviour of water. Dielectric constant is significant because it can affect the solubility of certain drugs (Fakhree et al. 2010). The hydroxyl groups present in sugars can hydrogen bond with water and stabilise the water and affect the dielectric properties of the sugar solutions. Sugars with more hydroxyl groups accessible for hydrogen-bonding will affect the dielectric constant more since less water is free to respond to the electric field. So increasing the sugar concentration in water generally decreases the dielectric constant (Sahin & Sumnu 2007). The effect of sucrose on decreasing the dielectric constant of ethanol solution has been reported by Abidin et al (2014). They reported a higher dielectric constant for solutions having lower sugar concentration due to availability of more water in these solutions resulting in higher ionic polarization effects. They also analysed the effect of different sugars; sucrose, fructose and glucose on the dielectric constant of ethanol solution (Abidin et al. 2014). Roebuck and Goldblith have also reported the differences in the dielectric constant due to the interaction between monosaccharides like glucose and fructose and a disaccharide like sucrose (Roebuck et al. 1972). Since the hydroxyl groups in monosaccharides are more accessible to the hydrogen-bonding, these solutions would have the lowest dielectric constant compared to the solutions with disaccharides where the hydrogen-bonds formed are not so stable because of the hydroxyl groups exposed to the water. The effect of sugars on the solubility of some solutes has also been studied in the past. Paruta reported solubility of different semi polar solutes in sucrose solutions of varying concentrations. He reported that the solubility of all the solutes studied in his research increased with the increasing sucrose concentration or the decreasing dielectric constant. He explained this might be due to the decreasing polarity of the syrup vehicle as the sugar concentration increases. He concluded that the addition of sucrose or other sugars can enhance the solubility of some drugs. However he suggested that decreased solubility of drugs might be used in the kinetic application for increasing the stability of drug (Paruta 1964). In this study, a



monosaccharide, disaccharides and an oligosaccharide were used. These sugars not only reduce the phase-transition temperature of the solutions but also decrease the dielectric constant of the sugar solutions. Table 6.1 shows some physicochemical properties of the sugars used in this research.

**Table 6.1** Physiochemical properties of the investigated sugars.

Name	Structure and IUPAC name	Molecular formulae	Molecular weight (g/mol)	Melting point (°C)	Solubility (H <sub>2</sub> O) at 20°C
Maltose Monohydrate	 <p><b>.H<sub>2</sub>O</b> 4-O-<math>\alpha</math>-D-Glucopyranosyl-D-glucopyranose</p>	C <sub>12</sub> H <sub>22</sub> O <sub>11</sub> .H <sub>2</sub> O	360.32	102-103	0.2 g/mL
Mannitol	 <p>Hexan-1,2,3,4,5,6-hexol</p>	C <sub>6</sub> H <sub>14</sub> O <sub>6</sub>	182.17	165-167	0.18 g/mL
Sucrose	 <p><math>\alpha</math>-D-Glucopyranosyl <math>\beta</math>-D-fructofuranoside</p>	C <sub>12</sub> H <sub>22</sub> O <sub>11</sub>	342.30	185-187	0.3 g/mL

<p>Trehalose Dihydrate</p>	 <p><b>.2(H<sub>2</sub>O)</b> α-D-Glucopyranosyl α -D-glucopyranoside</p>	<p>C<sub>12</sub>H<sub>22</sub>O<sub>11</sub>.2(H<sub>2</sub>O)</p>	<p>378.33</p>	<p>97-99</p>	<p>0.3 g/mL</p>
<p>Raffinose Pentahydrate</p>	 <p><b>.5(H<sub>2</sub>O)</b> β-D-fructofuranosyl α- D-galactopyranosyl- (1→6)-α -D- glucopyranoside</p>	<p>C<sub>18</sub>H<sub>32</sub>O<sub>16</sub>.5(H<sub>2</sub>O)</p>	<p>594.52</p>	<p>78-80</p>	<p>0.1 g/mL</p>

## 6.2 Experimental

### 6.2.1 Materials

Sucrose  $\geq 99.5\%$ , trehalose dehydrate  $\geq 99.0\%$ , maltose monohydrate  $\geq 99.0\%$ , raffinose pentahydrate  $\geq 99.0\%$  and mannitol  $\geq 99.5\%$  were all obtained from Sigma Aldrich U.K. PPG  $M_n \sim 1000$  obtained from Sigma Aldrich U.K. was used as received. Solutions were prepared using deionised water.

### 6.2.2 Methods

10 mg mL<sup>-1</sup> PPG solutions were used throughout these experiments. A higher stock solution of PPG in water was prepared and then used to prepare sugar in PPG aqueous solutions. Stock solutions of sugars in water were prepared and then used to prepare PPG solutions at different concentrations of sugars; the concentration of PPG was kept constant. The samples were degassed and then analysed using HSDSC with the reference cell containing sugar solutions and the sample cell containing a solution with 10 mg mL<sup>-1</sup> of PPG 1000 solubilized in sugar solutions of the same molarity as in the reference cell. The same solutions were then analysed using turbidity measurements in order to examine the cloud-points.

## 6.3 Results and Discussion

The data obtained for the sugar/PPG samples using HSDSC after the baseline subtraction is shown in Figs. 6.2-6.6.

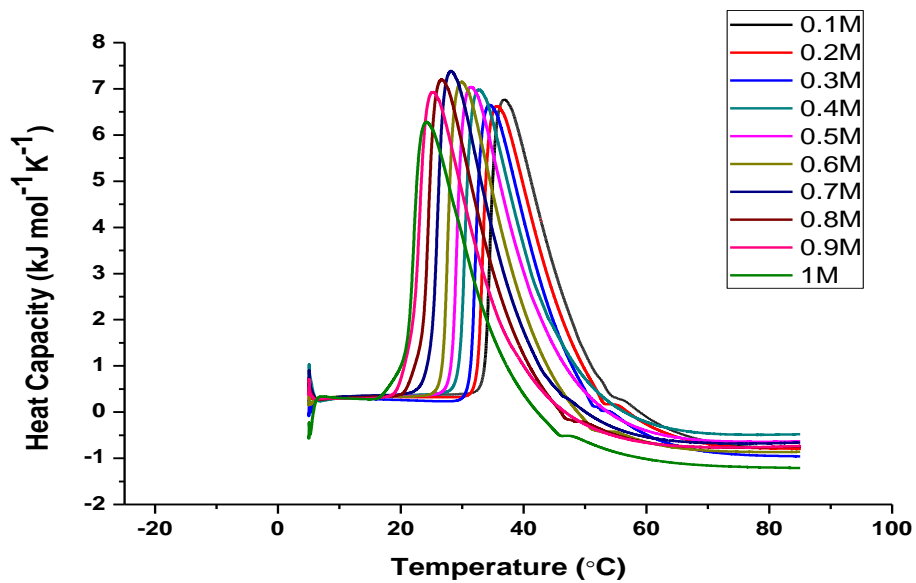


**Figure 6.2** Change in heat capacity of  $10 \text{ mg mL}^{-1}$  PPG solution with the change in the mannitol concentration.

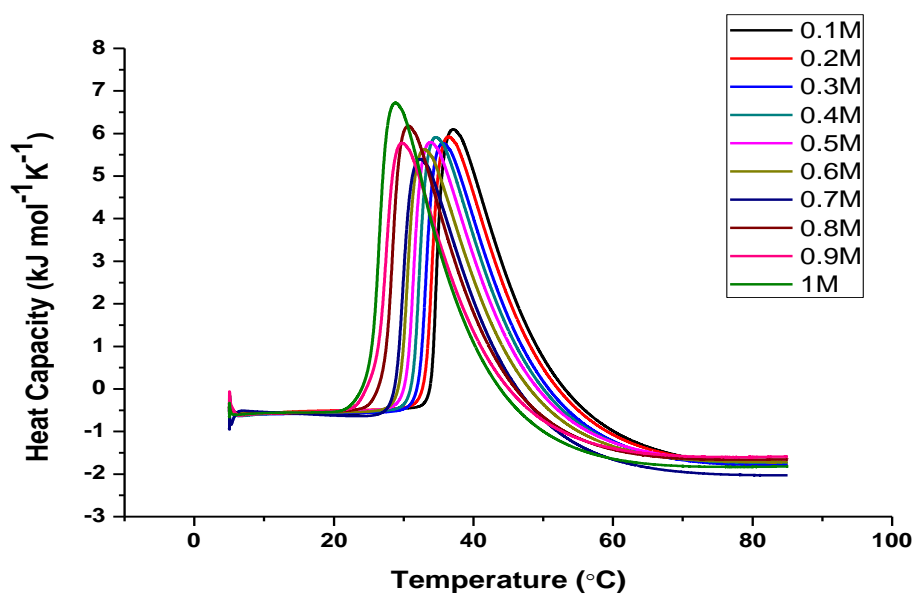


**Figure 6.3** Change in heat capacity of  $10 \text{ mg mL}^{-1}$  PPG solution with the change in the maltose concentration.

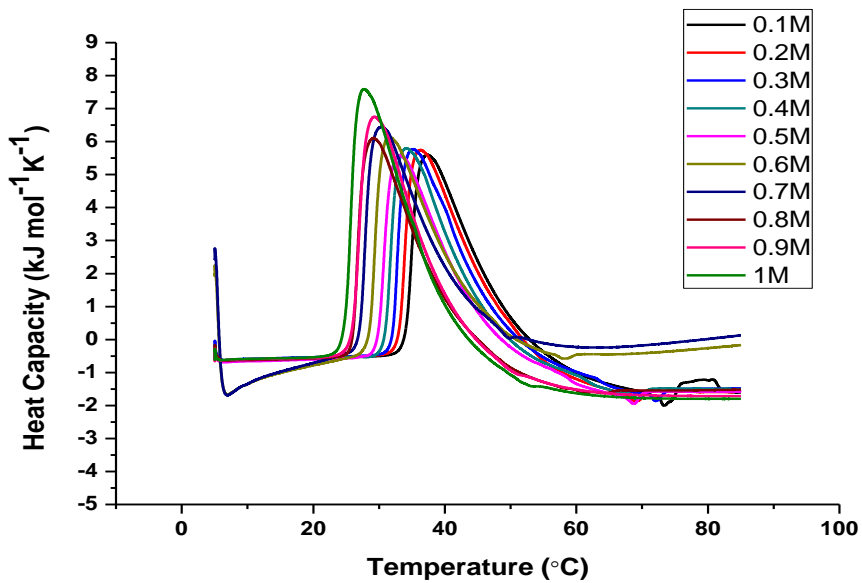


**Figure 6.4** Change in heat capacity of  $10 \text{ mg mL}^{-1}$  PPG solution with the change in the sucrose concentration.

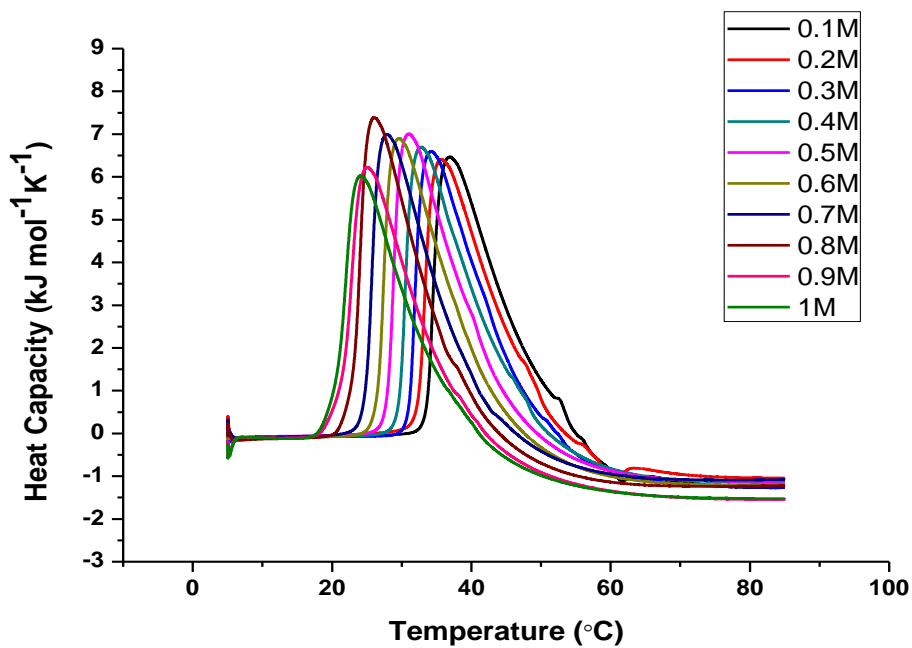


**Figure 6.5** Change in heat capacity of  $10 \text{ mg mL}^{-1}$  PPG solution with the change in the trehalose concentration.

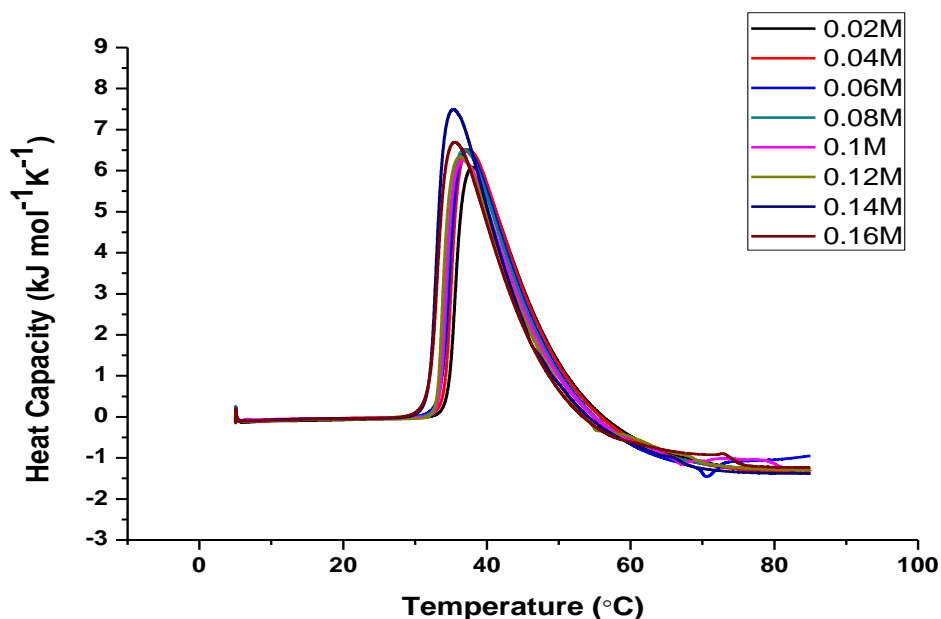


**Figure 6.6** Change in heat capacity of 10 mg mL<sup>-1</sup> PPG solution with the change in the raffinose concentration.

The thermogram above shows that for all five sugars, the increase in sugar concentration decreases the phase-transition temperature ( $T_m$ ). Sugar solutions were made considering their maximum solubility in water.

In Chapter 5, it was established that the change in the  $\Delta C_p$  of the transition for PPG complies with Kirchoff's law. However in the data shown above, the change in the heat capacity is not observed. Shpigelman et al. showed similar data for the increase in glucose concentration in aqueous PNIPAM solution;  $T_m$  decreases but there is no change in the heat capacity (Shpigelman et al. 2008). Endothermic peaks represent that the phase-transition involves water and dehydration. The fact that the heat capacity does not change with the change in sugar concentration indicates that any increase in sugar concentration does not affect the water structure any further, however some other phenomenon must be causing that. It has been proposed by some researchers, that apart from the structuring of water, the presence of sugars

may enhance the population of non-polar conformations in aqueous solutions, where two conformations of polymers exist in a solution; e.g. PEO and pluronics (Lindman et al. 1990; Sjoeborg et al. 1989; Kim et al. 1995). Carlsson and co-workers suggest that PPG, when mixed with water, goes through a conformational change from less polar higher energy conformers to more polar lower energy conformers (Carlsson et al. 1995). So the presence of sugars increasing the non-polar conformations of PPG might be responsible for the decrease in the  $T_m$  of these aqueous solutions. Although no study has been undertaken to determine the effect of the presence of sugars on increasing the non-polar conformations of PPG, we propose that might be the reason for the insignificant change in the heat capacity with the change in sugar concentration.

The decrease in  $T_m$  with the increase in sugar concentration is because the activity of water is decreasing due to the fact that sugar molecules strongly hydrogen bond to water thereby decreasing the amount of water in the bulk. This increases the thermodynamic necessity for PPG to phase separate so as to release water to the bulk and thereby reduce the thermodynamic penalty of having sugar present. Therefore, the presence of sugars in the PPG solution favours the formation of aggregates and to form an aggregate the PPG molecules favour the non-polar conformation forms.

Table 6.2 shows the effect of the change in sugar concentration on the phase-transition temperatures.  $T_m$  for a 10 mg mL<sup>-1</sup> PPG solution in water without the addition of sugar showed a transition temperature of 37.9°C. The data in the Table 6.2 shows that the addition of sugar in any concentration in PPG solution decreases the  $T_m$  but as the concentration of sugar is increased the effect of sugars on the  $T_m$  increases (i.e. lower the  $T_m$ ).



**Table 6.2** Effect of different sugars in varying concentrations on  $T_m$  of aqueous PPG solution.

$T_m$ for $10 \text{ mg mL}^{-1}$ PPG solution without addition of any sugar is $37.9 \text{ }^\circ\text{C}$						
	$T_m$ ( $^\circ\text{C}$ )					
Sugar Concentration (M)	Mannitol	Maltose	Sucrose	Trehalose	Sugar Concentration (M)	$T_m$ ( $^\circ\text{C}$ ) for Raffinose
0.1	37.1	36.8	37.3	36.9	0.02	38.1
0.2	36.6	35.8	36.3	35.7	0.04	37.4
0.3	35.5	34.5	35.2	34.3	0.06	37.2
0.4	34.8	32.7	34.2	32.8	0.08	36.9
0.5	33.7	31.4	33.2	31.0	0.1	36.7
0.6	33.0	29.9	31.6	29.5	0.12	36.3
0.7	32.5	28.1	30.4	27.9	0.14	35.3
0.8	30.7	26.6	29.2	26.1	0.16	35.6
0.9	29.9	25.3	29.2	25.0		
1	28.9	24.2	27.7	24.2		

The data in Table 6.2 shows that the effect of changing concentration of trehalose and maltose has the greatest impact on lowering the phase-transition temperature. The plot of the change in  $T_m$  of the PPG solutions with the addition of sugars in different concentration is shown in Fig. 6.7. The slope is steepest for trehalose and maltose thereby showing the greatest effect upon the  $T_m$ . Raffinose at a concentration of 0.16 M is better at reducing  $T_m$  than any other sugar at similar concentrations but because of the low solubility of raffinose in water, only small amounts of this sugar could be dissolved in the PPG solutions.

The study of the effect of sugars on aqueous PPG solution thus shows that using sugars, a two-phase system can be produced at ambient temperatures.

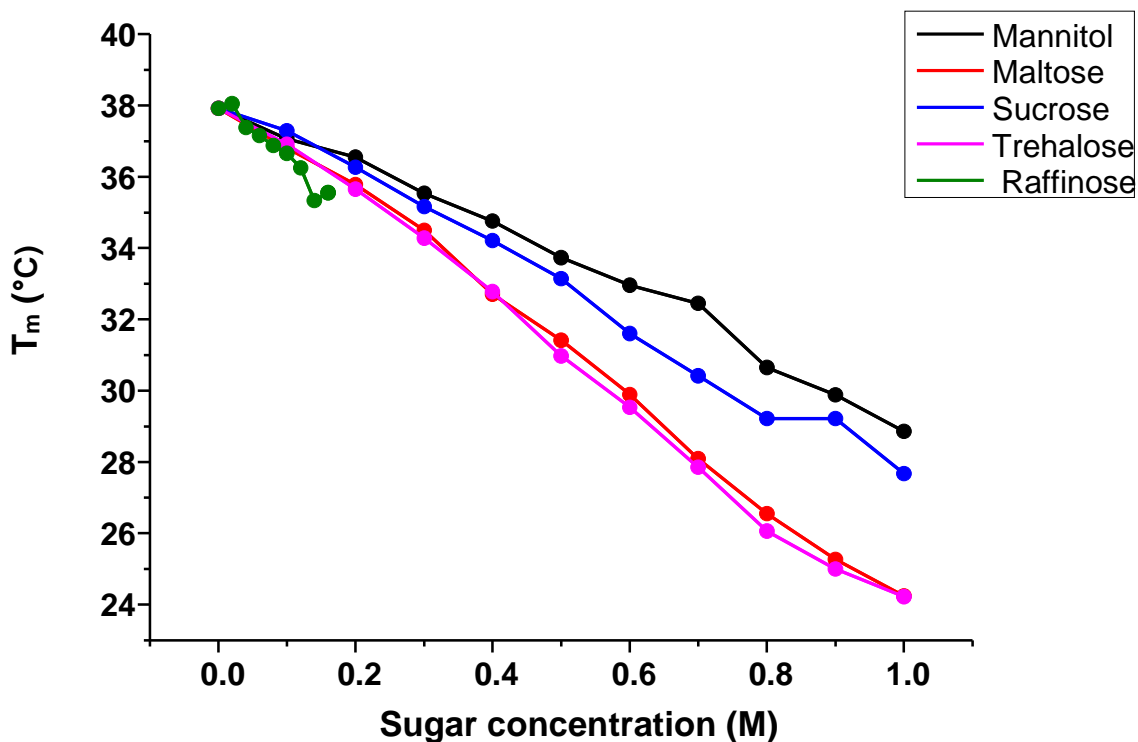


**Figure 6.7** Change in the  $T_m$  of  $10 \text{ mg mL}^{-1}$  PPG solution upon addition of sugars at different concentrations.

Figs. 6.8-6.12 show the change in the absorbance with the change in temperature measured by UV-Visible spectrometry for the different concentrations of sugars. This was used to measure the cloud-point of these solutions. Cloud-point is the point where the solutions start to go turbid. Phase separation is normally noted as the onset of clouding in the aqueous system and cloud points normally lie between the coexistence and spinodal decomposition curves for systems.

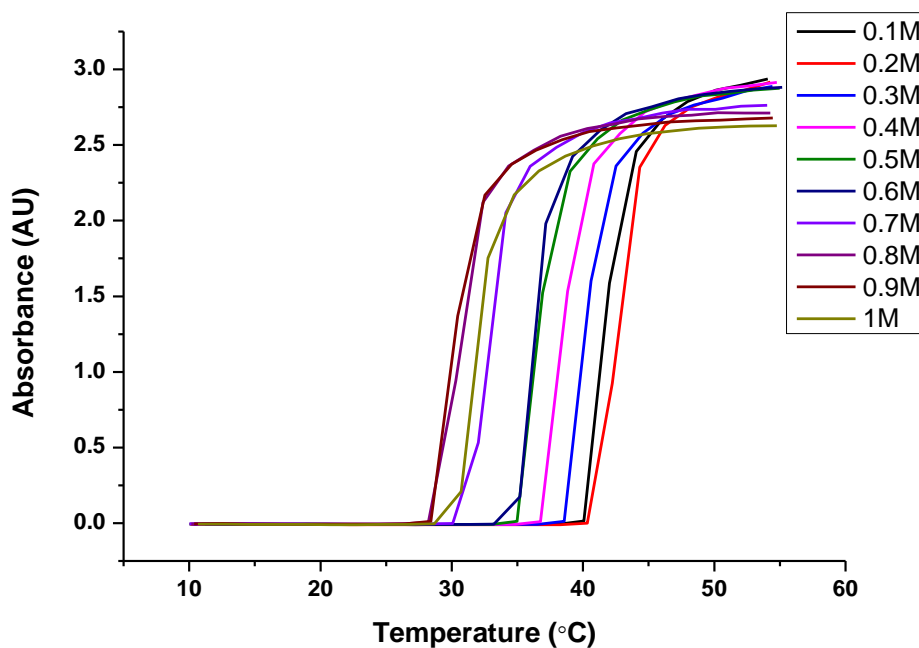


**Figure 6.8** Change in absorbance of the cloud-point data for different concentrations of maltose in  $10 \text{ mg mL}^{-1}$  aqueous PPG solution as a function of temperature.

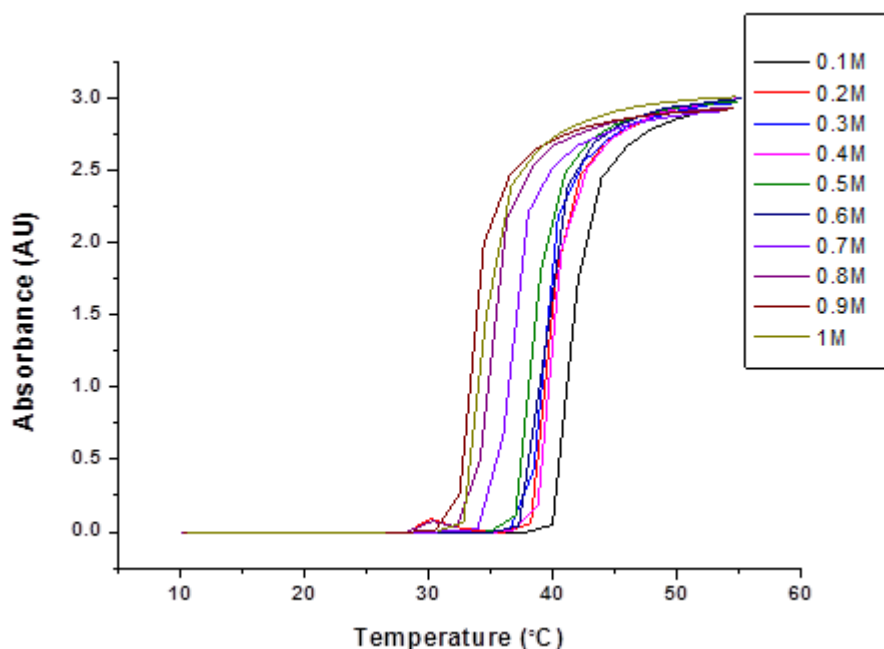


**Figure 6.9** Change in absorbance of the cloud-point data for different concentrations of mannitol in  $10 \text{ mg mL}^{-1}$  aqueous PPG solution as a function of temperature.

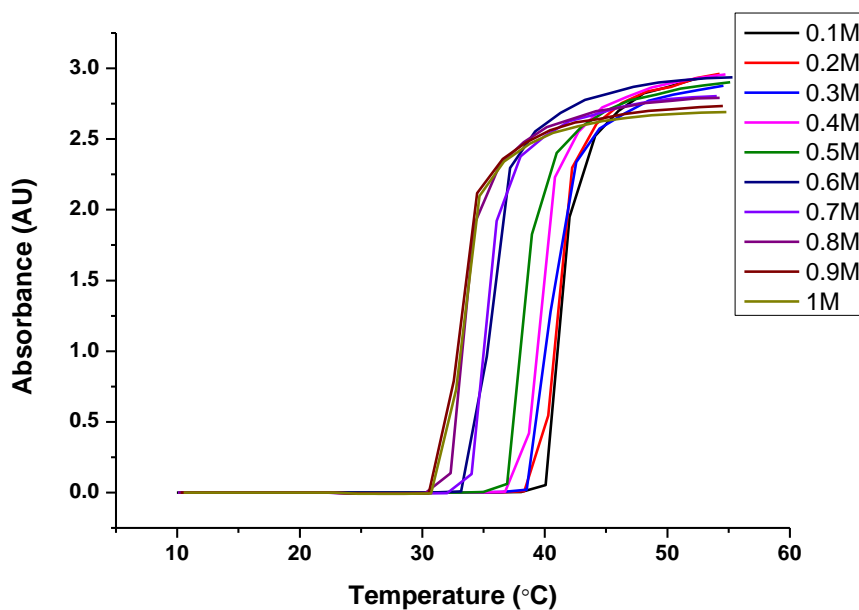


**Figure 6.10** Change in absorbance of the cloud-point data for different concentrations of sucrose in  $10 \text{ mg mL}^{-1}$  aqueous PPG solution as a function of temperature.

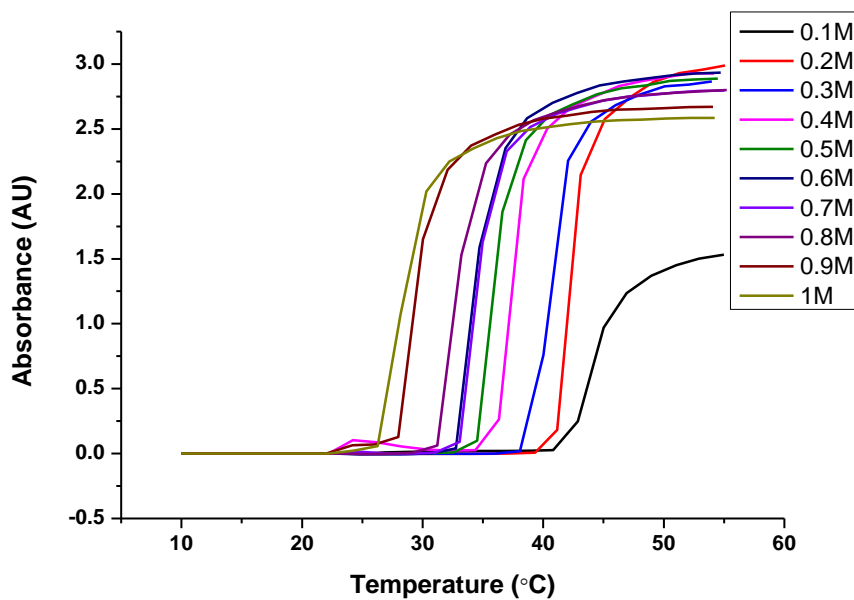


**Figure 6.11** Change in absorbance of the cloud-point data for different concentrations of trehalose in  $10 \text{ mg mL}^{-1}$  aqueous PPG solution as a function of temperature.

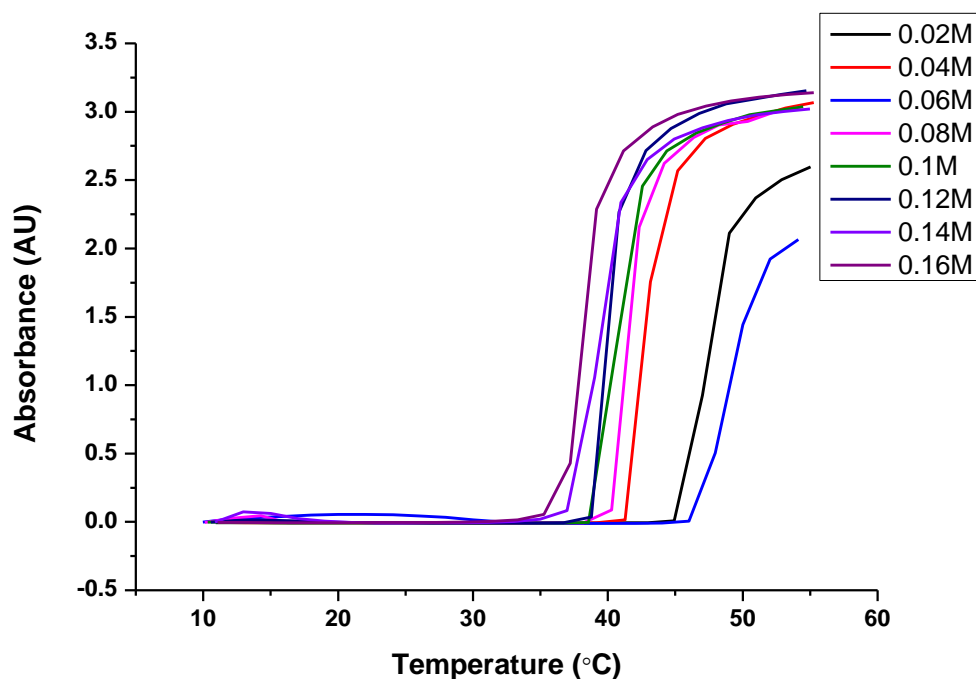


**Figure 6.12** Change in absorbance of the cloud-point data for different concentrations of raffinose in  $10 \text{ mg mL}^{-1}$  aqueous PPG solution as a function of temperature.

The turbidity data obtained was used to find the cloud-point of the solutions. This is the point where the solution starts to go turbid and so the light transmitted is significantly decreased and the absorbance value shows a significant increase. This was obtained by drawing tangents to the start of the transition of the cloud-point data. The cloud-point was also found using the HSDSC again by drawing tangents to find the temperature at the beginning of the HSDSC phase-transition. Tables 6.3 and 6.4 show the change in cloud-points using the two different techniques; turbidity measurements and HSDSC, with the change in the total sugar concentration in the solutions. The data shows that for low concentrations of sugars, the cloud-point is higher than for a solution without the presence of any sugar, but as the concentration of the sugar in the solution increases, the cloud-point temperature decreases.

Fig. 6.13 shows the comparison of the cloud-points obtained using the two techniques. The cloud-point obtained using HSDSC for all the different sugar solutions was lower than the cloud-point obtained using turbidity measurement. This is because the cloud-point measured using HSDSC captures the start of the aggregation process however the turbidity is the point where the aggregates formed are big enough to make the solution go turbid and to be detected by the detector. Trehalose and maltose again seem to have the greatest effect on the phase-separation of the aqueous PPG solutions.

**Table 6.3** Cloud-points measured using turbidity for different sugar concentrations in PPG solutions.

Cloud-point for 10 mg mL <sup>-1</sup> PPG solution without addition of any sugar is 36.5°C						
Sugar Concentration (M)	Cloud-point using turbidity measurements				Sugar Concentration (M)	Cloud-point using turbidity measurements for Raffinose
	Mannitol	Maltose	Sucrose	Trehalose		
0.1	39.9	40.0	40.0	42.2	0.02	45.0
0.2	38.2	40.9	39.8	41.1	0.04	41.3
0.3	38.0	38.6	38.4	39.1	0.06	46.9
0.4	38.6	36.7	38.2	38.1	0.08	40.2
0.5	36.9	34.9	36.8	34.3	0.1	38.5
0.6	37.2	35.0	33.9	32.7	0.12	38.7
0.7	35.2	31.3	33.7	33.0	0.14	37.4
0.8	33.7	28.7	32.2	31.1	0.16	36.7
0.9	32.2	28.4	31.5	27.9		
1	32.7	30.5	31.7	26.3		

**Table 6.4** Cloud-points measured using data obtained from HSDSC for different sugar

concentrations in PPG solutions.

Cloud-point for 10 mg mL <sup>-1</sup> PPG solution without addition of any sugar by HSDSC is 34.5°C						
Sugar Concentration (M)	Cloud-point using HSDSC				Sugar Concentration (M)	Cloud-point using HSDSC for Raffinose
	Mannitol	Maltose	Sucrose	Trehalose		
0.1	33.7	33.7	34.0	33.7	0.02	34.6
0.2	32.7	32.2	32.9	32.3	0.04	34.2
0.3	31.9	31.2	32.0	31.0	0.06	33.7
0.4	31.4	29.4	30.9	29.6	0.08	33.4
0.5	30.7	28.3	29.8	27.9	0.1	33.4
0.6	28.3	26.3	28.8	26.5	0.12	33.0
0.7	28.3	24.2	27.1	24.8	0.14	31.9
0.8	27.6	23.5	26.0	23.0	0.16	31.9
0.9	24.8	21.2	26.0	21.3		
1	24.5	20.7	24.7	20.4		

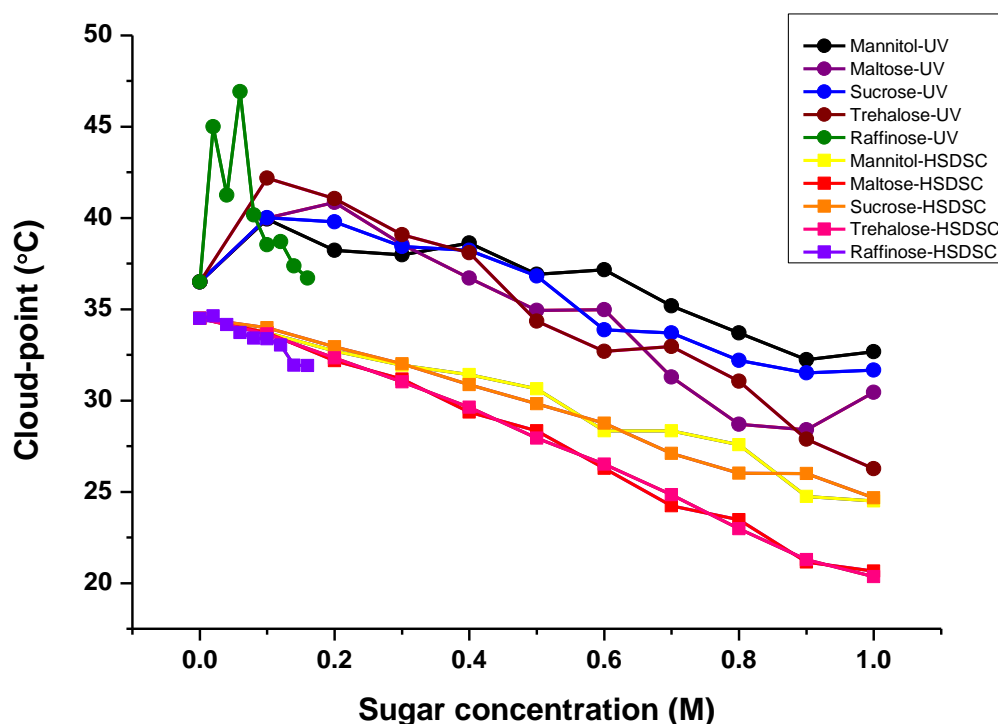


**Figure 6.13** Change in the cloud-point obtained using turbidity and HSDSC measurements of the aqueous PPG solutions with the addition of different concentrations of sugars.

The data obtained for these sugars was then fitted to a two-state transition model using Scientist software to obtain the value of the change in  $T_{1/2}$ , the aggregation number ( $n$ ), van't Hoff enthalpy change ( $\Delta H_{vH}$ ), calorimetric enthalpy change ( $\Delta H_{cal}$ ) and the change in the excess heat capacity ( $\Delta C_p$ ) for the different sugar solutions. These values were substituted in Equation 6.1 to find the value of  $\alpha$ .  $\alpha$  gives the indication of the progress of the reaction, in other terms, the amount of PPG that has undergone phase-separation.

$$\frac{\alpha(T)0.5^{n-1}}{(1 - \alpha(T))^n} = \exp \left( \frac{\Delta H_{vH} \left( \frac{T_1}{2} \right)}{R} \left( \frac{1}{\frac{T_1}{2}} - \frac{1}{T} \right) + \frac{\Delta C_p \left( \frac{T_1}{2} \right)}{R} \left( \ln \left( \frac{T}{\frac{T_1}{2}} \right) + \frac{T_1}{2} - T \right) \right) \quad (6.1)$$

$R$  in this equation is the gas constant.

Table 6.5 shows the change in the aggregation number for the PPG solutions as the sugar concentration changes. Aggregation number seems to decrease with the increasing sugar concentration in the solutions. The data shows that keeping the PPG concentration constant but changing the sugar concentration has the same effect on the  $T_m$  of the system as increasing the total PPG concentration in solution but the effect of  $n$  seems to be opposite. Increasing the PPG concentration increases  $n$  but increasing the sugar concentration with a constant PPG concentration decreases  $n$ .



**Table 6.5** Change in aggregation number with the change in sugar concentration in aqueous PPG solutions.

n for 10 mg mL <sup>-1</sup> PPG solution without addition of any sugar by HSDSC is 19						
Sugar Concentration (M)	Change in n				Sugar Concentration (M)	Change in n for Raffinose
	Mannitol	Maltose	Sucrose	Trehalose		
0.1	35	27	38	40	0.02	27
0.2	28	25	38	31	0.04	30
0.3	26	23	35	32	0.06	34
0.4	27	26	33	33	0.08	29
0.5	24	27	36	27	0.1	31
0.6	23	23	28	24	0.12	26
0.7	21	17	23	22	0.14	28
0.8	18	16	34	19	0.16	16
0.9	14	14	21	15		
1	16	17	27	16		

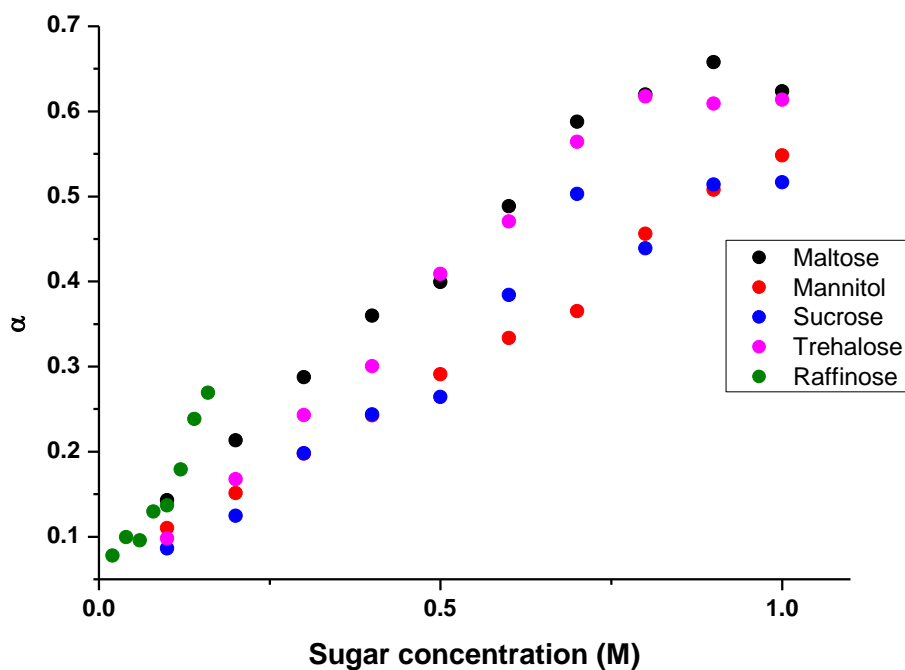
The data in this chapter shows that sugars reduce the  $T_m$  of the aqueous PPG solutions. The cloud-point and the  $T_{1/2}$  data shows that for the low concentration sugars, the cloud-point and the  $T_{1/2}$  is slightly higher than the temperature of PPG solution without the addition of any sugar. This could be because at low sugar concentrations, the sugar molecules are not concentrated enough to change the water structure around the polymer. But as the concentration of sugar increases, the  $T_m$  values are decreased due to the hydrophobic interactions mentioned earlier.

Table 6.6 shows the  $\alpha$  values at different sugar concentrations and Fig. 6.14 shows the plot of the change in  $\alpha$  value with the change in the concentration of the sugar added. The data shows that the amount of phase-separated PPG increases with the increase in the sugar concentration but the effect on the change in the amount of the phase-separated PPG is greatest upon the addition of maltose and trehalose. This is also in agreement with the greatest effect of maltose and trehalose on reducing the  $T_m$  of the PPG solution. Raffinose also has a great effect on

increasing the amount of the PPG phase-separation upon heating, but the low solubility makes the use of this sugar non-ideal.

**Table 6.6** Change in  $\alpha$  value for different sugars with the change in the sugar concentration.

Sugar Concentration (M)	Maltose	Mannitol	Sucrose	Trehalose	Sugar Concentration (M)	Raffinose
0.1	0.14	0.11	0.09	0.10	0.02	0.08
0.2	0.21	0.15	0.12	0.17	0.04	0.10
0.3	0.29	0.20	0.20	0.24	0.06	0.10
0.4	0.36	0.24	0.24	0.30	0.08	0.13
0.5	0.40	0.29	0.26	0.41	0.1	0.14
0.6	0.49	0.33	0.38	0.47	0.12	0.18
0.7	0.59	0.36	0.50	0.56	0.14	0.24
0.8	0.62	0.46	0.44	0.62	0.16	0.27
0.9	0.66	0.51	0.51	0.61		
1	0.62	0.55	0.52	0.61		



**Figure 6.14** Amount of phase-separated PPG ( $\alpha$ ) for different sugars with the change in the total sugar concentration.

Addition of sugars should also decrease the dielectric constant of the solutions by decreasing the polarity of these solutions, but this has not been tested in this research. The effect exhibited by raffinose should be lower than other sugars since raffinose is an oligosaccharide but mannitol being a monosaccharide should have a greater effect in lowering the dielectric constant. No work has been undertaken in this research to support this statement but work done by other researchers suggests the validity of this statement (Roebuck et al. 1972). Research has also shown that the solubility of semi-polar drugs increases in solutions with low dielectric constant, since they have low polarity (Paruta 1964), so the ability of sugars to change the dielectric constant can be utilised in solubility studies.

#### **6.4 Conclusions**

The research conducted here shows that sugars can be added to aqueous PPG solutions to decrease the  $T_m$  of aqueous two-phase system to ambient. HSDSC signals obtained for these systems with addition of sugars show asymmetry with a negative change in heat capacity showing aggregation and disruption of the hydrogen bonded network. The values of  $\alpha$  obtained show an increase in the amount of phase-separated PPG with an increase in the sugar concentration as the temperature increases. Sugars upon addition to these systems hydrate themselves to form large entities. They are kosmotropic, structure making, and thus favour the formation of aggregates for molecules like PPG via hydrophobic interaction. The greater the amount of sugar added to the system, the lower would be the amount of water in the bulk due to the fact that sugar molecules strongly hydrogen bond to water and form hydration shells around them. This decrease in entropy is compensated by the release of water to the bulk via phase separation of PPG. So the presence of sugars in the PPG systems increases the necessity of the system to phase-separate. The cloud-point data showed a demixing process which is linked to aggregation showed by HSDSC due to the increase in the absorbance which means big particles are formed which attenuate the monochromatic light passing through the sample.

The cloud-point decreased with an increase in concentration of sugar; again showing the effect of sugars as kosmotropes on the aqueous PPG systems.

Trehalose and maltose have a greater effect on reducing the  $T_m$  and increasing the amount of phase-separated PPG over the other two sugars; mannitol and sucrose. Raffinose however has the greatest effect but is non-ideal due to its high cost and low solubility.

The data obtained in this research fits in with previous studies of the effects of sugars upon LCST in other polymer systems such as pluronics, PNIPAM and PEG. The effect of two saccharides; maltose and glucose was studied in a set of pluronics and PNIPAM solutions. The effect of sugars on  $T_m$  increased in general with the increase in sugar concentration which is what was observed in this research (Kim et al. 1995). The effect of various sugars on the cloud-point of aqueous PEG solutions has also been studied and the presence of sugars seems to decrease the cloud-point of these solutions (Sjoeberg et al. 1989). The effect of glucose on the DSC transitions of aqueous PNIPAM solutions has also been studied where glucose seemed to have an effect on the  $T_m$  but the effect on the heat capacity change of the transition with the increase in glucose concentration was not observed (Shpigelman et al. 2008) which is similar to the HSDSC data found in this research.

Hence we can conclude that sugars are capable of reducing the  $T_m$  and increasing the amount of phase-separation in aqueous solutions of PPG. The effect of sugars on the solubility of drugs in these two-phase systems is yet to be studied together with dielectric studies on PPG solutions with the addition of sugars.

## Chapter 7 : Use of PPG as a Solubilising Agent for Naphthalene

### 7.1 Introduction

The majority of clinically used drugs display their short half-lives in the bloodstream and high overall clearance rates. More than 80% of the drugs available in the market are small molecular weight molecules; these drugs typically interact via multiple binding sites and diffuse rapidly all over the body without selectivity. Therefore, a relatively small amount of the drug reaches the target site, while the non-selective distribution in the body leads to undesired side effects. The applied dose of the drug is reduced to avoid these side effects, thus the full therapeutic potential of the drug is not achieved. The foregoing disadvantages are especially pronounced with drugs that exhibit a narrow therapeutic index. Furthermore, many of the drugs are hydrophobic and therefore have limited aqueous solubility. In relation to such drugs “polymeric architectures” may provide a solution in relation to their delivery because of their resemblance to natural carriers such as serum lipoproteins (Gupta et al. 2012, Kim & Lee 2001). Improving the therapeutic index of drugs via the use of new drug-delivery concepts is a major driving force in polymer therapeutics (Duncan 2003; Gros et al. 1981). Polyether based amphiphiles have been used successfully as drug delivery vehicles because of their beneficial effects such as low toxicity, good chemical stability, high water solubility and other reasons (Gupta et al. 2012). This work tests the use of an aqueous two phase PPG system as a solubilizing agent for a hydrophobic compound naphthalene.

Thermoresponsive amphiphilic poly(ethylene oxide)-poly(propylene oxide) block copolymers have been broadly studied as hydrosolubilisers for poorly water-soluble drugs (Passerini et al. 2002; Shin & Cho 1997; Kadam et al. 2009). The hydro-solubilisation of drugs is strongly dependent upon the formation of micelles (Dong et al. 2004). In particular, more hydrophobic derivatives having low EO/PO ratio show higher solubilisation capacity. The PPG block plays an important role in the micellisation process as it is driven by the entropy gain and the free

energy of micellization. The release of the water molecules that hydrate the PPG leads to the entropy gain (Alexandridis et al. 1994). The formation of micelles or aggregates provides a hydrophobic environment that is dispersed throughout the aqueous phase where hydrophobic compounds can be transferred which increases the apparent aqueous solubility of these hydrophobic compounds/drugs. Previous HSDSC studies together with the other experiments conducted show the ability of PPG to form aggregates in water upon heating. In this Chapter the use of PPG as a potential solubilizing agent to increase the solubility of a model hydrophobic drug is reported.

In this study, naphthalene was used as a model hydrophobic organic compound to study the effect of PPG on the solubility of naphthalene as a function of temperature. Naphthalene has been used in the study because the naphthalenediimide (NDI) scaffold is present in many anti-cancer agents that interact with DNA as intercalators and so it serves as a simple model drug to test the change in solubility with the formation of PPG aggregates (Milelli et al. 2012). Naphthalene (Fig. 7.1) is very hydrophobic and hence the solubility in water is very low at room temperature, ranging between 30-40 mg L<sup>-1</sup> (Mitchell 1926) at 25°C.

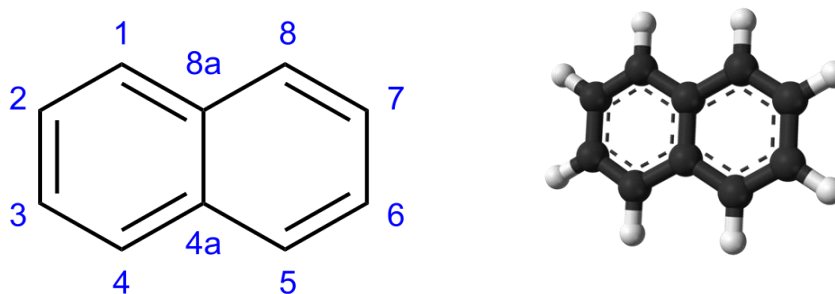


**Figure 7.1** Structure of naphthalene.

Enhancement of naphthalene solubility has been studied previously in the aqueous solutions of several poly(ethylene oxide)-poly(propylene oxide)-poly(ethylene oxide) triblock copolymers

by various researchers (Horský & Walterová 2005; Su & Liu 2003; Paterson et al. 1999). These block copolymers differ from each other in terms of the block sizes which changes their HLB index. It has been shown that the incorporation of the naphthalene inside the core of the micelles formed by these block copolymers are responsible for the increase of the solubility of naphthalene. The formation of micelles by block copolymers creates a hydrophobic environment dispersed throughout the aqueous phase into which hydrophobic organic compounds (HOC's) are able to transfer. This increases their apparent aqueous solubility. However some research also suggests that the interaction between these block copolymers and naphthalene at concentrations below the CMC is also responsible for its solubility enhancement (Paterson et al. 1999). Paterson et al. (1999) studied the enhancement in solubility of naphthalene in various aqueous copolymer solutions that had the same length of the PO block but varying EO block lengths. They studied P103, P105 and P108 copolymers where the hydrophobicity decreased in the order of P103>P105>P108 and the solubility enhancement decreased in the same order. They concluded that the hydrophilicity of the copolymers played a role in the solubility of HOC and more hydrophilic compounds produced a slightly less favourable environment for the solubility of these drugs (Paterson et al. 1999). Hurter and Hatton (1992) have also shown that hydrophobicity leads to the increase in the solubility of hydrophobic drug. Modelling studies also demonstrated that as the fraction of EO increases, with the PO composition being held constant, the micellar size decreased because of the reduction in the core size and the aggregation numbers. Since the solubility of naphthalene is only confined to the hydrophobic core of the polymeric micelles a decrease in the core size would lead to the reduction of the naphthalene solubility (Paterson et al. 1999). It has also been reported that systems undergoing phase-separation dramatically enhance the solubility of naphthalene. Phase-separation reflects the formation of a large number of micelles or aggregates just below this temperature. So systems undergoing phase-separation (clouding)

have a high solubilisation capacity. L92 which has a EO content of 20% and a fairly large PO block is the most effective polymeric surfactant for enhancing the solubility of naphthalene (Rosen 1989). In this research the effect of the aggregation of PPG on the solubility of naphthalene was assessed. PPG solutions phase separates in water upon heating which led to an examination of whether or not this phase separation has an effect on the change in the solubility of naphthalene.

The solubilisation properties of polymeric micelles are usually expressed in terms of micelle-water partition coefficients defined as the ratio between the concentration of the solubilize inside the micelle to the concentration of the solubilize that is molecularly dispersed in the aqueous phase. The solubilisation capacity can be expressed either in the form of the volume or mass fraction of the solubilize in the micellar core, as the number of moles solubilized per gram of hydrophobic block or as the molar solubilisation ratio (MSR); that is the molar ratio of the moles of the guest molecule to the moles of polymer molecules in the aggregate (Nagarajan 2001; Riess 2003).

## **7.2 Experimental**

### **7.2.1 Materials**

PPG  $M_n \sim 1000$  (Sigma Aldrich, U.K.) was used as received. Naphthalene (99% grade) was obtained from Sigma Aldrich, U.K. and used as received. Polymer solutions were prepared using deionised water. Acetonitrile (ACN) (HPLC grade, Cat. No. A/0627/17, Batch: 0619526) was obtained from Fisher Scientific, U.K. A degassing station was used (Millipore) with a HVLP filter of 0.45  $\mu\text{m}$ .



## 7.2.2 Methods

### 7.2.2.1 High Performance Liquid Chromatography

Instrument: Agilent, 1200 Infinity Series. Auto sampler: Agilent Technologies, 1100 Series.

Pump: Isocratic. Detector: VWD 1200 series.

Manufacturer: Agilent Technologies

Software (control & analysis): Agilent Chemstate B.03.01(317)

The solubilisation experiments were carried out by preparing saturated solutions of naphthalene. A stock solution of  $1000 \mu\text{g mL}^{-1}$  of naphthalene in acetonitrile was used to make the standards for the calibration on HPLC.  $1, 3$  and  $5 \text{ mg mL}^{-1}$  solutions of PPG in water were prepared in deionised water and naphthalene was added to these solutions. Saturation was inferred from the continuing presence of a separate solid naphthalene crystalline phase upon heating of the samples using a thermostatically controlled water bath. These samples were shaken at 100 rpm in a temperature controlled shaker for 4 hours. Samples were collected at various temperature points and 1 mL supernatant of each sample was collected and inserted into an empty vial. 1 mL of ACN was washed through the pipette tip and added into the sample collected to stabilise the naphthalene solution. Each temperature controlled point was repeated 3 times. A separate set of saturated naphthalene solutions in deionised water were also prepared. These solutions were also collected as a function of temperature with each temperature point being repeated 3 times. These samples were then analysed using HPLC with a variable wavelength detector at 254 nm which was set for naphthalene detection. The column used for HPLC experiments was XTerra® RP 18,  $3.5 \mu\text{m}$  particle size, 4.6 mm x150 mm column was used. The mobile phase, 70% ACN and 30% water, was degassed prior to starting the experiments because the HPLC detector is sensitive to gas bubbles in the mobile phase. Prior to the measurements, the purge valve was opened for 5 min at  $2 \text{ mL min}^{-1}$  flow rate to

allow the removal of any leftover residues from the previous experiments. The valve was then closed and the flow rate was decreased to 0.5 mL min<sup>-1</sup> for 10 min and then increased to 1.0 mL mL<sup>-1</sup> for 20 min for stabilization. The injection volume used was 20 µL, experiments were conducted at room temperature using a run time of 4.5 min.

### 7.3 Results and Discussion

Table 7.1 shows the data obtained for the solubility of naphthalene at three different PPG concentrations. The data for each of the PPG solutions (1, 3 and 5mg mL<sup>-1</sup>) was plotted as the ratio of the total solubility of naphthalene in the PPG solution to the solubility of naphthalene in water solution (Figs. 7.2, 7.3 and 7.4). Fig. 7.2 shows a clear break in the data for the 1 mg mL<sup>-1</sup> solution at about 42°C signifying the boundary between the phase-separated system and the homogeneous (one) phase system. No such boundaries occur at the other concentrations of PPG (Figs. 7.3 and 7.4) as the onset of phase separation occurs at lower temperatures than the temperature used for analysis.

**Table 7.1** Apparent naphthalene concentration in aqueous PPG solutions as a function of PPG concentration and temperature.

Temperature (°C)	1 mg mL <sup>-1</sup> PPG solution	3 mg mL <sup>-1</sup> PPG solution	5 mg mL <sup>-1</sup> PPG solution	Water (No PPG)
	Concentration of naphthalene (µg mL <sup>-1</sup> )			
30	40.45	37.23	44.03	40.41
35	48.31	67.64	99.02	50.93
38	62.02	163.4	310.59	54.82
40	61.53	122.7	218.51	56.59
42	82.18	211.08	324.17	70.06
45	121.16	297.57	484.92	80.87
48	165.69	465	563.42	86.43
52	241.15	665.82	908.73	93.14
65	584.73	1550.91	1759.6	140.57
70	906.62	2219.29	2110.4	173.63

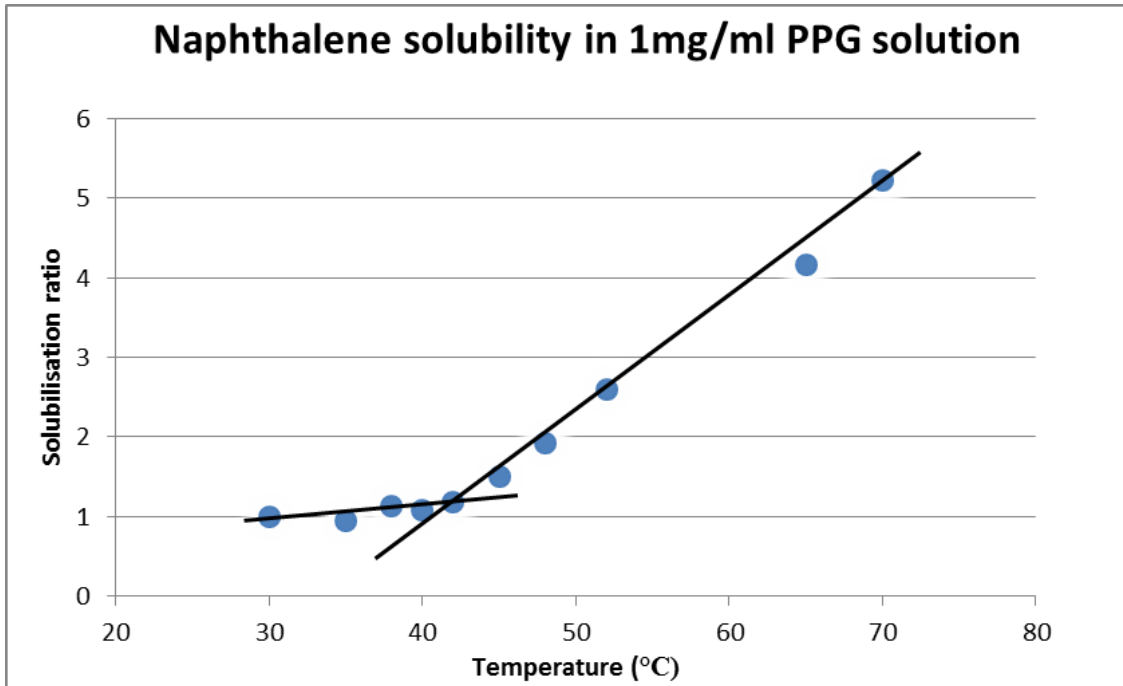


**Figure 7.2** Data obtained for naphthalene solubilisation in 1 mg mL<sup>-1</sup> solution of PPG.

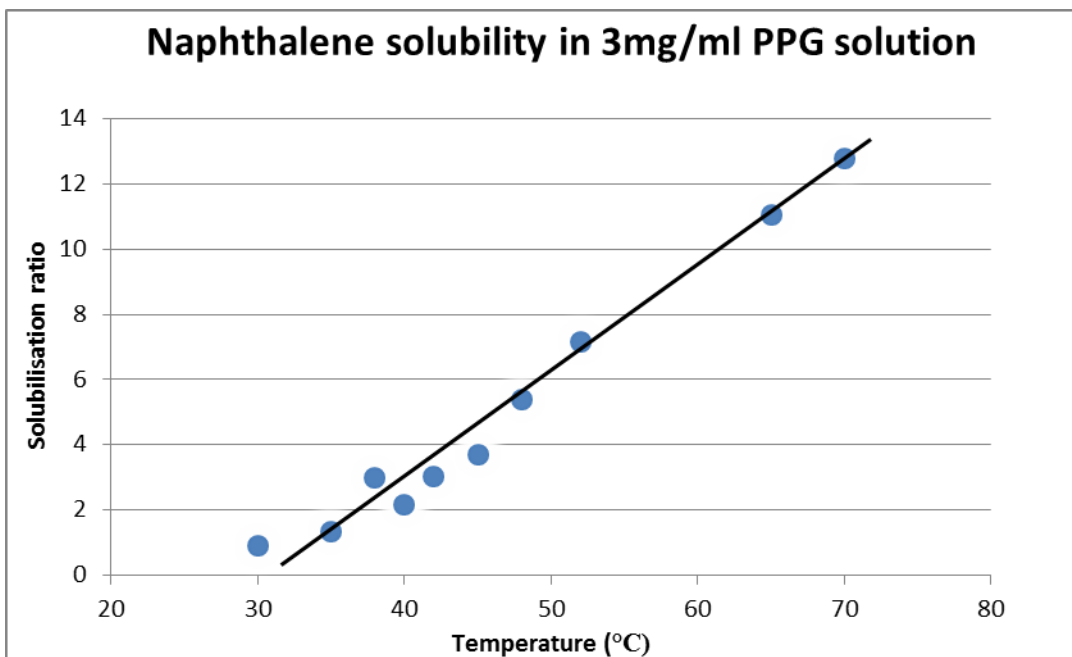


**Figure 7.3** Data obtained for naphthalene solubilisation in 3 mg mL<sup>-1</sup> solution of PPG. The data point at 30°C is part of the low temperature pre-phase separation data.

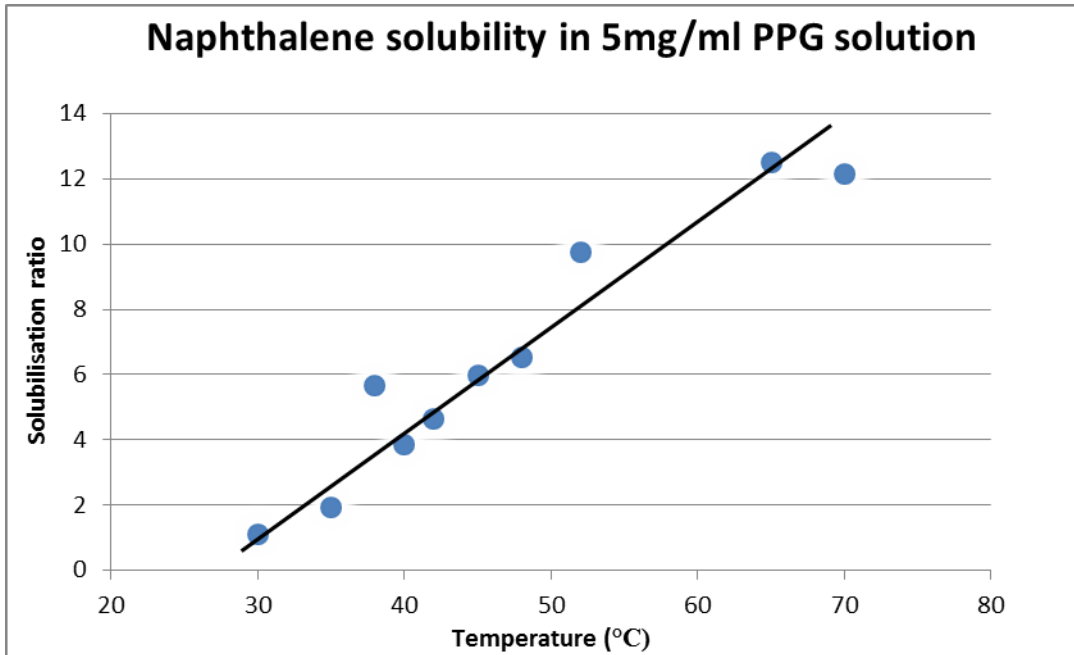


**Figure 7.4** Data obtained for naphthalene solubilisation in 5 mg mL<sup>-1</sup> solution of PPG. The data point at 70°C was treated as an outlier.

Data for naphthalene solubility in 1 mg mL<sup>-1</sup>, and use the following model can describe the solubilisation of naphthalene in aqueous solutions of PPG:

$$S^* = S_{aq} + S_{PPG} \frac{n_{PPG}}{V_w} \quad (7.1)$$

$S^*$  represents the apparent aqueous solubility of naphthalene in the aqueous two-phase system (it has the units of mole of naphthalene per unit volume of water).  $S_{aq}$  is the aqueous saturated solubility of naphthalene (it has the units of mole of naphthalene per unit volume of water).  $S_{PPG}$  is the solubility of naphthalene in the separated PPG phase. The last term, which denotes the moles of phase separated PPG per unit volume of water is included to make the second term dimensionally consistent with the units of the other two terms.

We can obtain an expression for  $S_{PPG}$ :

$$K_P = \frac{S_{PPG}}{S_{aq}} \quad (7.2)$$

or

$$S_{PPG} = K_P \times S_{aq}$$

$K_P$  is the equilibrium constant or partition coefficient for the equilibrium distribution of naphthalene between water and the separated PPG phase.

Substituting equation 7.2 into 7.1 gives:

$$S^* = S_{aq} + K_P \times S_{aq} \frac{n_{PPG}}{V_w} \quad (7.3)$$

If we divide equation 7.3 by  $S_{aq}$ , we obtain expression 7.4 for the solubility enhancement  $\frac{S^*}{S_{aq}}$ :

$$\frac{S^*}{S_{aq}} = 1 + K_P \frac{n_{PPG}}{V_w} \quad (7.4)$$

The final term  $\frac{n_{PPG}}{V_w}$  is given by equation 7.5:

$$\frac{n_{PPG}}{V_w} = C\alpha \quad (7.5)$$

Where  $\alpha$  is the fraction of PPG that has undergone phase separation and C is the original aqueous concentration of PPG.

$\alpha$  is an unknown term in the above equation and its values can be obtained from the thermodynamic parameters we have measured for PPG phase separation in previous chapters. If the temperature induced phase separation of PPG is thermodynamically controlled and phase separation can be described by an aggregation process, a value for  $\alpha$  can be obtained in the following way.

$$K(T) = \frac{[x_n]}{[x]^n} = \frac{\frac{C\alpha}{n}}{(C(1-\alpha))^n} \quad (7.6)$$

$K(T)$  is the equilibrium constant and n is the aggregation number.

The temperature dependence of the equilibrium constant is given by the van't Hoff expression 7.7:

$$K(T) = \left( \frac{\partial \left( \frac{\Delta H_{vH} + \Delta C_p(T - T_{ref})}{RT^2} \right)}{\partial T} \right)_{nP} \quad (7.7)$$

$\Delta H_{vH}$  is the van't Hoff enthalpy,  $\Delta C_p$  is the heat capacity change for the process (the difference between the heat capacity of the system before and after phase separation and  $T_{ref}$  is a reference temperature (the temperature at which half the PPG molecules have undergone phase separation).

Integration of equation 7.7 gives equation 7.8:

$$\frac{K(T)}{K(T_{ref})} = \exp \left( \frac{\Delta H_{vH}}{R} \left( \frac{1}{T_{ref}} - \frac{1}{T} \right) + \frac{\Delta C_p}{R} \left( \ln \left( \frac{T}{T_{ref}} \right) + \frac{T_{ref}}{T} - 1 \right) \right) \quad (7.8)$$

The expression  $\frac{K(T)}{K(T_{ref})}$  can be reduced down to give equation 7.9:

$$\frac{K(T)}{K(T_{ref})} = \frac{\frac{C\alpha}{n}}{(C^n)(1-\alpha)^n} \frac{0.5C}{\frac{n}{(C^n)}} \quad (7.9)$$

Combining 7.8 and 7.9 gives:

$$\frac{\alpha(0.5)^{n-1}}{(1-\alpha)^n} = \exp \left( \frac{\Delta H_{vH}}{R} \left( \frac{1}{T_{ref}} - \frac{1}{T} \right) + \frac{\Delta C_p}{R} \left( \ln \left( \frac{T}{T_{ref}} \right) + \frac{T_{ref}}{T} - 1 \right) \right) \quad (7.10)$$

Before the effect of temperature can be simulated in relation to the solubilisation of naphthalene, it must be noted that  $K_p$  the partition coefficient is also temperature dependent. Assuming that the heat capacity term for the partitioning is negligible over the temperature of the experiment, then;

$$K_P(T) = K_P(298.15) \times \exp\left(\frac{\Delta H_{vH}}{R} \left(\frac{1}{298.15} - \frac{1}{T}\right)\right) \quad (7.11)$$

in which 298.15K is the reference temperature.

Fig. 7.5 shows a simulated output using random guess values. The enthalpy for partitioning is assumed to be endothermic with a value of 30 kJ mol<sup>-1</sup>, which seems too high. The partition coefficient is assumed to be 4, which seems too low. However it gives output similar to that in Fig. 7.1.

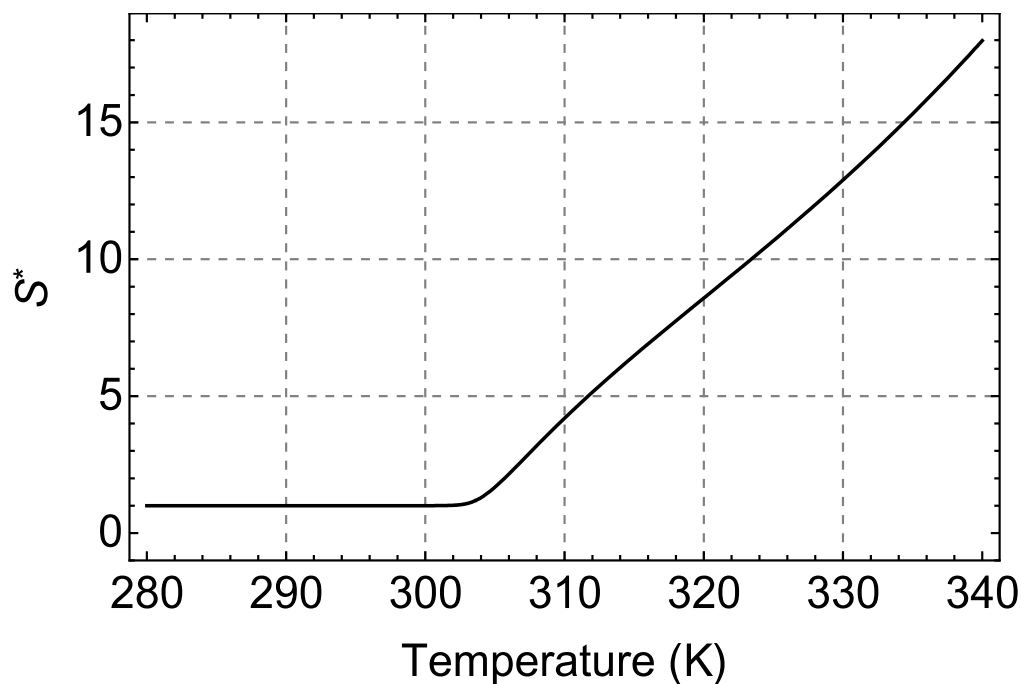


**Figure 7.5** A simulated output for the effect of temperature on the apparent aqueous solubility of naphthalene in the two-phase system for 1 mg mL<sup>-1</sup> PPG solution using the two-state aggregation model.

The measurements conducted by HSDSC (Chapter 5) for the different concentrations of aqueous solutions of PPG gave information about the onset temperature for the phase-

separation phenomenon in these systems. The data for 1 mg mL<sup>-1</sup> PPG solution by HSDSC gave an onset temperature of around 45°C for the aggregation transition. The solubility enhancement data for 1 mg mL<sup>-1</sup> PPG solution (Fig. 7.2) shows a break and solubility enhancement between the 42 and 45°C. There is a slight increase in the solubility below the onset of phase-separation, suggesting that the unimeric/unaggregated chains of PPG might also be binding with the naphthalene increasing the total apparent solubility in the non-phase separated system. This is because naphthalene is a hydrophobic organic compound which probably favours the interaction with hydrophobic PPG molecules compared to the polar water molecules. But as the solution is heated up to a temperature where it starts phase separating due to the disruption of the water-PPG lattice and PPG rich droplets start to appear and grow. This process involves the exclusion of water from around the polymer chains according to the model proposed by Carlsson and Linse, where the PPG conformation changes from non-polar high energy conformation upon mixing with water to polar low energy conformations. But as the solution is heated, polymer chains aggregate and become non-polar (Carlsson et al. 1995). This transition must form spaces or voids from which water molecules are excluded. These are the spaces where naphthalene molecules are accommodated, increasing the apparent aqueous solubility of the PPG solution. The simulated output (Fig. 7.5) obtained using the solubility model above for 1 mg mL<sup>-1</sup> PPG solution gave a similar output as the experimental data (Fig. 7.2). The simulated output used the mass-action aggregation model to obtain the value for  $\alpha$ , the rate of progression of the reaction. Since both the experimental for solubility enhancement and the simulated data for apparent aqueous solubility enhancement follow the same trend, the increase in naphthalene solubility can be attributed to the formation of aggregates. However, the temperature break in the simulated data where the solubility enhancement occurs is a lot lower than the experimental data; that's because the initial



assumptions made for the partitioning parameters to simulate the solubility curve are different to the actual partitioning parameters.

#### 7.4 Conclusions

The data obtained for 1 mg mL<sup>-1</sup> aqueous PPG solution shows an increase in the solubility of naphthalene with the increase in temperature but a break in the solubility enhancement at about 42°C can be observed. This temperature corresponds to the temperature where the aggregation process starts, observed from the HSDSC analysis for 1 mg mL<sup>-1</sup> PPG solution. This data was then used to simulate an output for the apparent aqueous solubility of naphthalene for a 1 mg mL<sup>-1</sup> solution. Since the simulated output is similar to the experimental output, this suggests that the phase-separation process and the enhancement of solubility due to partitioning must be thermodynamically controlled and due to formation of aggregates. The two-state aggregation model was used to simulate the data suggesting that formation of aggregates must be responsible for the solubility enhancement of naphthalene. The data obtained for 2 mg mL<sup>-1</sup> and 5 mg mL<sup>-1</sup> showed an increase in the solubility enhancement for naphthalene too but since the phase-separation starts at a much lower temperature for these concentrations, not enough data points were available for the low temperature pre-phase separated region to show a break in the solubility data. This study suggests that two-phase PPG system could be used as a solubilizing agent to enhance the solubility of the hydrophobic compound naphthalene. Use of this system to enhance solubility of hydrophobic drugs is yet to be tested.

## CONCLUSIONS

The work presented herein demonstrates that it is possible to obtain a phase-diagram for PPG using HSDSC data. The physico-chemical information obtained from the thermal analytical techniques for different molecular masses of pure PPG (Chapter 4) provides a valuable database that has been missing in the literature. The investigation on the solutions of different molecular masses of PPG (Chapter 4), PPG  $M_n \sim 1000$  (Chapter 5), effect of certain solutes on aqueous PPG solutions (Chapter 6) and the effectiveness of the use PPG as a solubilizing agent for naphthalene (Chapter 7), has helped to determine detailed information about the phase-separation behaviour of PPG solutions. The effect of the change of temperature, scan rate, concentration, different solvents and cosolutes on the phase-separation behaviour of PPG has been investigated. An attempt has been made to explain the phase-separation behaviour of PPG solutions based on existing phase-separation model by various researchers and the model suggested by Kjellander and Florin commends to the data obtained for the phase-separation of PPG systems. Use of sugars as cosolutes has been effective in lowering the phase-transition temperature of PPG solutions; with the effect of certain sugars on lowering the  $T_m$  more than the others. The study involving naphthalene dissolution in PPG solutions has shown the capability of phase-separated PPG solution to significantly enhance naphthalene solubility.

Chapter 4 reported the physico-chemical and the solution properties of PPGs of molecular masses  $M_n \sim 425, 725, 1000, 2000$  and  $2700$ . TGA studies helped to ascertain the stability of PPGs;  $M_n \sim 425$  was found to be least stable out of the PPGs examined because of the lowest decomposition temperature of  $293 \pm 1^\circ\text{C}$ . DSC studies showed that liquid PPG samples generate an amorphous form upon cooling to  $-90^\circ\text{C}$ . The heat flow signal obtained from MDSC helped in the determination of  $T_g$  (reversing signal) and showed enthalpy relaxation (non-reversing signal) exhibited by the samples.  $T_g$  of PPGs increases with an increase in molecular

mass, with  $T_g$  values between  $-74$  to  $-70^\circ\text{C}$ . The enthalpy relaxation decreases with the increase in molecular mass due to the higher viscosity of the higher molecular mass PPGs. A TSDC study was conducted on four PPGs out of the five; the output shows a glass transition relaxation process. The current intensity decreases and the temperature of the current maxima increases with an increase in the molecular mass, which gives information about molecular mobility. The experiments revealed a significant contribution of the hydroxyl groups in the total polarisation. Upon normalisation of the polarisation on the basis of number of moles of PPG used, a greater molecular mobility for larger molecular mass PPGs was observed. TW experiments showed a second relaxation process;  $T_p$  after the  $T_M$  observed for PPG 2700 which was not detected in other PPGs.

HSDSC signals for the PPGs can be fitted to a mass action aggregation model similar to ones that are used to describe micellar aggregation. The HSDSC signal reveals an aggregation process upon heating of the polymer solutions, which is the precursor of phase-separation. These aggregates become larger with temperature; the increase in size of the aggregates is a calorimetrically silent process. The  $T_m$  of the PPGs increases with a decrease in their molecular mass which is explained using Kjellander and Florin theory. Turbidity data further supported the hypothesis for an aggregation process, and the cloud-point decreases with an increase in molecular mass.

Chapter 5 reveals important phase-separation properties of PPG 1000 solutions. HSDSC signals indicate aggregation (asymmetry in the signal) with hydrophobe desolvation (larger pre-transitional heat capacity over the post-transitional heat capacity). The data is scan rate independent which reveals that the process is thermodynamically (and not kinetically) controlled. The  $T_m$  decreases with an increase in PPG concentration which was explained using the Kjellander and Florin model. Hydrogen bonds in water-PPG lattice network upon heating

start to disrupt which is also seen by the turbidimetric data. The hypothesis of the phase-separation of PPGs by nucleation and growth is supported by the HSDSC and the turbidity data (which shows aggregation/nucleation) together with the HSM data where formation of discrete droplets which grow bigger in size (growth) was observed. DLS and SANS data further supports phase-separation by formation of PPG rich droplets dispersed in water. The HSDSC and turbidity data was used to find the concentration dependence on the phase-diagram for PPG in solution.

Chapter 6 reports the effect of five different sugars on the  $T_m$  and the phase-separation of PPG solutions. This study was conducted in order to assess if the  $T_m$  of the aqueous phase-separated two phase PPG 1000 system could be reduced to around ambient temperature by the addition of sugar molecules. Sugars act as kosmotropes; they reduce the  $T_m$  of the aqueous PPG solutions due to the preferential interaction of water with sugars and are also believed to increase the non-polar conformations of the polymer. Data suggests that the addition of sugars increase the activity of PPG or reduces the activity of water by reducing the amount of water available in bulk for hydrogen-bonding with PPG (by sugar's preferential interaction with water), thus promoting aggregation of PPG. The data in this chapter reveals a greater effect of raffinose compared to the other sugar molecules; maltose and trehalose seem to have the greatest effect on the  $T_m$  of PPG 1000 and they increase the extent of phase-separation (suggested from the  $\alpha$  values). But raffinose, which displays poor solubility, is not an ideal sugar for reducing the  $T_m$ .

Chapter 7 reports the use of an aqueous two phase system created upon heating the PPG solution, for solubilizing naphthalene; 1, 3 and 5 mg mL<sup>-1</sup> aqueous PPG solutions were used to solubilize the model hydrophobic compound naphthalene. The use of PPG increases the solubility of naphthalene in all three PPG solutions but the data for 1 mg mL<sup>-1</sup> shows a clear

solubility enhancement break at about 42°C which corresponds to the start of the HSDSC transition, i.e. where the PPG 1000 system first starts to aggregate. The simulated output obtained using the two-state aggregation model for this data showed the same trend in increasing the apparent aqueous solubility of naphthalene as the experimental output indicating the role of phase-separation in increasing the solubility of naphthalene.

## FUTURE WORK

- **Use of PPG 2700 and study of its phase-separation behaviour.** In the study conducted in this project, PPG 1000 was used and its solution properties were investigated. Chapter 4 reveals the lower transition temperature of PPG 2700. Use of sugars in lowering the  $T_m$  of PPG 2700 could be effective in creating an aqueous two-phase system at ambient temperature at lower PPG concentration.
- **Investigate the effect of sugar addition on naphthalene solubility in the aqueous PPG solutions.** The effect of solubility enhancement of naphthalene using PPG 2700 in the presence of sugars could also be investigated. This would be an extensive study where the effect of the sugars in decreasing the  $T_m$  of PPG 2700 would be initially investigated using HSDSC and turbidity measurements. The sugar which displayed the greatest effect would then be used to further investigate the solubility enhancement of naphthalene as a function of temperature.
- **Test the solubility of hydrophobic drugs in aqueous PPG systems.** The efficiency of PPG systems for solubility enhancement of hydrophobic drugs - such as the anti-cancer drugs paclitaxel and/or curcumin - could be useful in determining the potential use of these systems as drug delivery systems.
- **Examine the HSDSC properties of mixtures of PPGs of different molecular mass with pluronics.** HSDSC studies in aqueous solution in order to assess the phase transition properties would be interesting from a theoretical perspective in relation to the individual species.
- **Investigate the effects of chaotropic agents, such as urea, guanidinium hydrochloride and salts (e.g. NaCl), and other kosmotropic agents.** Such experiments would be conducted purely from a theoretical perspective in order to gain

further knowledge relating to the phase behaviour of PPGs of different molecular mass in the presence of co-solutes using e.g. HSDSC, turbidity and NMR measurements.

## REFERENCES

- Abidin, Z.Z., Omar, F.N. & Biak, D.R.A., Dielectric Characterization of Ethanol and Sugar Aqueous Solutions for Potential Halal Authentication.
- Abolghassemi Fakhree, M.A. et al., 2010. The Importance of Dielectric Constant for Drug Solubility Prediction in Binary Solvent Mixtures: Electrolytes and Zwitterions in Water + Ethanol. *AAPS PharmSciTech*, 11(4), pp.1726–1729. Available at: <http://www.ncbi.nlm.nih.gov/pmc/articles/PMC3011073/>.
- Alakhov, V.Y. et al., 1996. Hypersensitization of Multidrug Resistant Human Ovarian Carcinoma Cells by Pluronic P85 Block Copolymer. *Bioconjugate Chemistry*, 7(2), pp.209–216. Available at: <http://dx.doi.org/10.1021/bc950093n>.
- Alexandridis, P., Holzwarth, J.F. & Hatton, T.A., 1994. Micellization of Poly(ethylene oxide)-Poly(propylene oxide)-Poly(ethylene oxide) Triblock Copolymers in Aqueous Solutions: Thermodynamics of Copolymer Association. *Macromolecules*, 27, pp.2414–2425.
- Alexandridis, P. & Lindman, B., 2000. *Amphiphilic Block Copolymers: Self-Assembly and Applications*, Elsevier Science. Available at: <https://books.google.co.uk/books?id=HsUuCbPeiUUC>.
- Alfrey, T. & Gurnee, E.F., 1967. *Organic Polymers*, Prentice-Hall. Available at: <https://books.google.co.uk/books?id=wSJRAAAAMAAJ>.
- Alivisatos, A.P., 1996. Perspectives on the physical chemistry of semiconductor nanocrystals. *The Journal of Physical Chemistry*, 100(31), pp.13226–13239.
- Anon, 2012a. Polypropylene glycol [MAK Value Documentation, 1998]. In *The MAK-Collection for Occupational Health and Safety*. Wiley-VCH Verlag GmbH & Co. KGaA, pp. 272–285. Available at: <http://dx.doi.org/10.1002/3527600418.mb2532269kske0010>.
- Anon, 2012b. *Processing and Finishing of Polymeric Materials*, Wiley. Available at: <http://books.google.co.uk/books?id=rVMGfS572WMC>.
- Antonijević, M., 2012. No Title. *European Pharmaceutical Review Magazine*, Issue 3.
- Arakawa, T. & Timasheff, S.N., 1982. Stabilization of protein structure by sugars. *Biochemistry*, 21(25), pp.6536–6544.
- Association, C.G., 1999. *Handbook of Compressed Gases*, Springer US. Available at: <https://books.google.co.uk/books?id=WSLULtCG9JgC>.
- Bailey, F.E. & Koleske, J. V, 1976. *Poly(ethylene oxide)*, Academic Press. Available at: <https://books.google.co.uk/books?id=ptAvAQAAIAAJ>.



- Barreca, D. et al., 2008. Spectroscopic investigation of structure-breakers and structure-makers on ornithine carbamoyltransferase. *Food Chemistry*, 106(4), pp.1438–1442.
- Batrakova, E. V et al., 1996. Anthracycline antibiotics non-covalently incorporated into the block copolymer micelles: in vivo evaluation of anti-cancer activity. *British Journal of Cancer*, 74(10), pp.1545–1552. Available at: <http://www.ncbi.nlm.nih.gov/pmc/articles/PMC2074856/>.
- Batrakova, E. V & Kabanov, A. V, 2008. Pluronic block copolymers: evolution of drug delivery concept from inert nanocarriers to biological response modifiers. *Journal of controlled release : official journal of the Controlled Release Society*, 130(2), pp.98–106. Available at: <http://www.pubmedcentral.nih.gov/articlerender.fcgi?artid=2678942&tool=pmcentrez&rendertype=abstract> [Accessed February 19, 2014].
- Beal, R.E. & Coolants, A.C.D.-15 on E., 1986. *Engine Coolant Testing: Second Symposium : Second International Symposium on Engine Coolants and Their Testing, Philadelphia, Pennsylvania, 9-10 April 1984*, ASTM. Available at: <https://books.google.co.uk/books?id=L87djnkVrsC>.
- Beezer, A.E. et al., 1994. An investigation of dilute aqueous solution behavior of poly (oxyethylene)+ poly (oxypropylene)+ poly (oxyethylene) block copolymers. *Langmuir*, 10(11), pp.4001–4005.
- Beezer, A.E. et al., 1992. High-sensitivity differential scanning microcalorimetry of phase transitions in dilute solutions of poly (oxyethylene)+ poly (oxypropylene)+ poly (oxyethylene) block copolymers. *Journal of Chemical Research. Synopses*, (7), pp.236–237.
- Binks, B. & Furlong, D., 1999. *Modern characterization methods of surfactant systems*, CRC Press.
- Bjoerling, M., Karlstroem, G. & Linse, P., 1991. Conformational adaption of poly(ethylene oxide): A carbon-13 NMR study. *The Journal of Physical Chemistry*, 95, pp.6706–6709. Available at: <http://pubs.acs.org/doi/abs/10.1021/j100170a060>.
- Brown, A., 2014. *Understanding Food: Principles and Preparation*, Cengage Learning. Available at: <http://books.google.co.uk/books?id=Mt7KAgAAQBAJ>.
- Brumberger, H., Stein, R.S., and Powell, R., 1968. Light scattering. *Science and Technology*, pp.34–42.
- Burdock, G.A., 1997. *Encyclopedia of Food and Color Additives*, CRC Press. Available at: <https://books.google.co.uk/books?id=JAVvqWBsBK0C>.
- Canuto, S., 2010. *Solvation Effects on Molecules and Biomolecules: Computational Methods and Applications*, Springer. Available at: <https://books.google.co.uk/books?id=GT9oPnAEkEQC>.

- Cao, Y. et al., 2007. Poly(N-isopropylacrylamide)–chitosan as thermosensitive in situ gel-forming system for ocular drug delivery. *Journal of Controlled Release*, 120(3), pp.186–194. Available at:  
<http://www.sciencedirect.com/science/article/pii/S0168365907002349>.
- Carlsson, M., Hallen, D. & Linse, P., 1995. Mixing enthalpy and phase separation in a poly(propylene oxide)-water system. *Journal of the Chemical Society, Faraday Transactions*, 91(14), pp.2081–2085. Available at:  
<http://dx.doi.org/10.1039/FT9959102081>.
- Chanda, M. & Roy, S.K., 2006. *Plastics Technology Handbook, Fourth Edition*, CRC Press. Available at: [https://books.google.co.uk/books?id=CF\\_-xp9iKHcC](https://books.google.co.uk/books?id=CF_-xp9iKHcC).
- Cheluguet, E.L. et al., 1994. Liquid-liquid equilibrium of aqueous mixtures of poly(propylene glycol) with sodium chloride. *Journal of Chemical & Engineering Data*, 39(1), pp.127–130. Available at: <http://dx.doi.org/10.1021/jc00013a036>.
- Cheremisinoff, N.P., 2003. *Industrial Solvents Handbook, Revised And Expanded*, CRC Press. Available at: <https://books.google.co.uk/books?id=HNpMvao75tkC>.
- Chiou, C.T. & Manes, M., 1986. Application of the Flory–Huggins theory to the solubility of solids in glyceryl trioleate. *Journal of the Chemical Society, Faraday Transactions 1: Physical Chemistry in Condensed Phases*, 82(1), pp.243–246.
- Chiu, M.H. & Prenner, E.J., 2011. Differential scanning calorimetry: An invaluable tool for a detailed thermodynamic characterization of macromolecules and their interactions. *Journal of Pharmacy and Bioallied Sciences*, 3, pp.39–59.
- Codex, I.M.C.F.C., 2003. *Food Chemicals Codex*, National Academies Press. Available at: <http://books.google.co.uk/books?id=k7Mk7-SUIKkC>.
- Cole-Hamilton, I., Livermore, A. & Watson, J., 1987. *Food and Nutrition in Practice*, Heinemann Educational. Available at:  
[http://books.google.co.uk/books?id=T\\_TZI26Zt70C](http://books.google.co.uk/books?id=T_TZI26Zt70C).
- Collins, K.D., 1997. Charge density-dependent strength of hydration and biological structure. *Biophysical Journal*, 72(1), pp.65–76.
- Collins, K.D. & Washabaugh, M.W., 1985. The Hofmeister effect and the behaviour of water at interfaces. *Quarterly Reviews of Biophysics*, 18(04), pp.323–422.
- Cooper, A., Nutley, M.A. & Wadood, A., 2000. Differential scanning microcalorimetry. *Protein-ligand interactions: Hydrodynamics and calorimetry*, pp.287–318.
- Correia, N.T. et al., 2000. Molecular motions in molecular glasses as studied by thermally stimulated depolarisation currents (TSDC). *Chemical Physics*, 252, pp.151–163.
- Cowie, J.M.G., 1991. *No Title* 2nd Editio., Spain: Chapman & Hall. Available at:  
<http://books.google.co.in/books?id=Dt1QAwbXfE0C&printsec=frontcover&dq=polyme>

rs&hl=en&sa=X&ei=uu3LUrXUD8HTrQfqzoCoCA&redir\_esc=y#v=onepage&q=poly  
mers&f=false.

- Cowie, J.M.G. & McEwen, I.J., 1974. Upper and lower critical solution temperatures in the cosolvent system acetone(1)+ diethyl ether(2)+ polystyrene(3). *Journal of the Chemical Society, Faraday Transactions 1: Physical Chemistry in Condensed Phases*, 70(0), pp.171–177. Available at: <http://dx.doi.org/10.1039/F19747000171>.
- Craig, D.Q.M. & Reading, M., 2014. *Thermal Analysis of Pharmaceuticals*, Taylor & Francis. Available at: <https://books.google.co.uk/books?id=CCsRJfmnsqAC>.
- Daniels, C.A., 1989. *Polymers: Structure and Properties*, Taylor & Francis. Available at: <https://books.google.co.uk/books?id=SwsNbiMDqzcC>.
- Dege, G.J., Harris, R.L. & MacKenzie, J.S., 1959. Terminal Unsaturation in Polypropylene Glycol. *Journal of the American Chemical Society*, 81(13), pp.3374–3379. Available at: <http://dx.doi.org/10.1021/ja01522a056>.
- Dill, K. & Bromberg, S., 2010. *Molecular Driving Forces: Statistical Thermodynamics in Biology, Chemistry, Physics, and Nanoscience*, Taylor & Francis Group. Available at: <http://books.google.co.uk/books?id=1gYPBAAAQBAJ>.
- Dissado, L.A. & Fothergill, J.C., 1992. *Electrical Degradation and Breakdown in Polymers*, P. Peregrinus. Available at: <http://books.google.co.uk/books?id=8Tm7dH99-XEC>.
- Dong, J., Chowdhry, B.Z. & Leharne, S.A., 2004. Solubilisation of polyaromatic hydrocarbons in aqueous solutions of poloxamine T803. *Colloids and Surfaces A: Physicochemical and Engineering Aspects*, 246, pp.91–98.
- Duncan, R., 2003. The dawning era of polymer therapeutics. *Nat Rev Drug Discov*, 2(5), pp.347–360. Available at: <http://dx.doi.org/10.1038/nrd1088>.
- Fehrenbacher, U. et al., 2000. The kinetics of the early stage of dispersion polymerization in supercritical CO<sub>2</sub> as monitored by turbidimetric measurements, 1. Method. *Macromolecular Chemistry and Physics*, 201(13), pp.1532–1539. Available at: [http://dx.doi.org/10.1002/1521-3935\(20000801\)201:13<1532::AID-MACP1532>3.0.CO](http://dx.doi.org/10.1002/1521-3935(20000801)201:13<1532::AID-MACP1532>3.0.CO).
- Fenby, D. V, 1987. Heat: its measurement from Galileo to Lavoisier. *Pure Appl Chem*, 59(1), pp.91–100.
- Florin, E., Kjellander, R. & Eriksson, J.C., 1984. Salt Effects on the Cloud Point of the Poly (ethylene oxide ) + Water System. *Journal of the Chemical Society, Faraday Transactions 1*, 80, pp.2889–2910. Available at: <http://xlink.rsc.org/?DOI=f19848002889>.
- Flory, P.J., 1953. *Principles of Polymer Chemistry*, Cornell University Press. Available at: <http://books.google.co.uk/books?id=CQ0EbEkT5R0C>.

- Flory, P.J., 1942. Thermodynamics of High Polymer Solutions. *The Journal of Chemical Physics*, 10(1).
- Freiberg, S. & Zhu, X.X., 2004. Polymer microspheres for controlled drug release. *International Journal of Pharmaceutics*, 282(1), pp.1–18.
- Freire, E., 1995. Differential Scanning Calorimetry. In B. Shirley, ed. *Protein Stability and Folding SE - 9. Methods in Molecular Biology*<sup>TM</sup>. Humana Press, pp. 191–218. Available at: <http://dx.doi.org/10.1385/0-89603-301-5%3A191>.
- Freitag, R. & Garret-Flaudy, F., 2002. Salt effects on the thermoprecipitation of poly-(N-isopropylacrylamide) oligomers from aqueous solution. *Langmuir*, 18(9), pp.3434–3440.
- Gabbott, P., 2008. *No Title* P. Gabbott, ed., Blackwell. Available at: [http://books.google.co.uk/books?hl=en&lr=&id=1u4v\\_tGUEQoC&oi=fnd&pg=PP2&dq=Gabbott+calorimetry&ots=lHOybRGYjP&sig=9nnvQIDnLOYXIwhJ0Cpw5MDbBgC#v=onepage&q=Gabbott+calorimetry&f=false](http://books.google.co.uk/books?hl=en&lr=&id=1u4v_tGUEQoC&oi=fnd&pg=PP2&dq=Gabbott+calorimetry&ots=lHOybRGYjP&sig=9nnvQIDnLOYXIwhJ0Cpw5MDbBgC#v=onepage&q=Gabbott+calorimetry&f=false).
- Galaev, I. & Mattiasson, B., 2007. *Smart Polymers: Applications in Biotechnology and Biomedicine, Second Edition*, CRC Press. Available at: <https://books.google.co.uk/books?id=lJ5MfrfohuYC>.
- Galinski, E.A. et al., 1997. The Kosmotropic (Structure-Forming) Effect of Compensatory Solutes. *Comparative Biochemistry and Physiology Part A: Physiology*, 117(3), pp.357–365. Available at: <http://www.sciencedirect.com/science/article/pii/S0300962996002757>.
- Gedde, U., 1995. *Polymer Physics*, Springer. Available at: <http://books.google.co.uk/books?id=lEm3fC7XdnkC>.
- Gerlsma, S., 1968. Reversible denaturation of ribonuclease in aqueous solutions as influenced by polyhydric alcohols and some other additives. *Journal of Biological Chemistry*, 243(5), pp.957–961.
- Goldburg, W.I., 1999. Dynamic light scattering. *American Journal of Physics*, 67(12), pp.1152–1160.
- Goldstein, R.E., 1984. On the theory of lower critical solution points in hydrogen-bonded mixtures stretching bands of meso-tetraphenylporphine and vibrational., *Journal of Chemical Physics*, 80 (10), pp.5340–5341.
- Graziano, G., 2000. On the temperature-induced coil to globule transition of poly-N-isopropylacrylamide in dilute aqueous solutions. *International Journal of Biological Macromolecules*, 27(1), pp.89–97. Available at: <http://www.sciencedirect.com/science/article/pii/S0141813099001221>.
- Gros, L., Ringsdorf, H. & Schupp, H., 1981. Polymeric Antitumor Agents on a Molecular and on a Cellular Level? *Angewandte Chemie International Edition in English*, 20(4), pp.305–325. Available at: <http://dx.doi.org/10.1002/anie.198103051>.

- Gupta, S. et al., 2012. Polyether based amphiphiles for delivery of active components. *Polymer (United Kingdom)*, 53, pp.3053–3078.
- Gustafsson, Å., Wennerström, H. & Tjerneld, F., 1986. Aqueous polymer two-phase systems in biotechnology. *Fluid Phase Equilibria*, 29(0), pp.365–371. Available at: <http://www.sciencedirect.com/science/article/pii/0378381286850361>.
- Haines, P.J., 2002. *Principles of thermal analysis and calorimetry*, Royal Society of Chemistry.
- Hannay, N., 2013. *Changes of State*, Springer US. Available at: <http://books.google.co.uk/books?id=rlrhBwAAQBAJ>.
- Harris, J.M., 1992. *Poly(Ethylene Glycol) Chemistry: Biotechnical and Biomedical Applications*, Springer. Available at: <http://books.google.co.uk/books?id=UheNFtAB7cAC>.
- Hempstead, C. & Worthington, W., 2005. *Encyclopedia of 20th-Century Technology*, Taylor & Francis. Available at: <https://books.google.co.uk/books?id=2ZCNAgAAQBAJ>.
- Heyda, J. & Dzubielia, J., 2014. Thermodynamic Description of Hofmeister Effects on the LCST of Thermosensitive Polymers. *The Journal of Physical Chemistry B*, 118(37), pp.10979–10988. Available at: <http://dx.doi.org/10.1021/jp5041635>.
- Hofmeister, F., 1888. Zur Lehre von der Wirkung der Salze. *Archiv für experimentelle Pathologie und Pharmakologie*, 24(4-5), pp.247–260. Available at: <http://dx.doi.org/10.1007/BF01918191>.
- Horský, J. & Walterová, Z., 2005. Solubility of naphthalene in aqueous solutions of poly(ethylene glycol)–poly(propylene glycol)–poly(ethylene glycol) triblock copolymers and (2-hydroxypropyl)cyclodextrins. *Colloid and Polymer Science*, 283(9), pp.1033–1040. Available at: <http://dx.doi.org/10.1007/s00396-004-1268-z>.
- Horvath, C.G., Preiss, B.A. & Lipsky, S.R., 1967. Fast liquid chromatography. Investigation of operating parameters and the separation of nucleotides on pellicular ion exchangers. *Analytical Chemistry*, 39(12), pp.1422–1428.
- Huber, J.F.K. & Hulsman, J.A.R.J., 1967. A study of liquid chromatography in columns, the time of separation. *Analytica Chimica Acta*, 38(0), pp.305–313. Available at: <http://www.sciencedirect.com/science/article/pii/S0003267001805924>.
- Huggins, M.L., 1942. Some Properties of Solutions of Long-chain Compounds. *The Journal of Physical Chemistry*, 46(1), pp.151–158. Available at: <http://dx.doi.org/10.1021/j150415a018>.
- Hutchinson, J.M., 1995. Physical aging of polymers. *Progress in Polymer Science*, 20(4), pp.703–760. Available at: <http://www.sciencedirect.com/science/article/pii/007967009400001I>.

- Ibar, J.P., 1993. *Fundamentals of thermal stimulated current and relaxation map analysis*, SLP Press. Available at: <http://books.google.co.uk/books?id=BcVQAAAAAYAAJ>.
- Inoue, T. & Yamashita, K., 2006. Aggregation behavior of polypropylene oxide with electric charges at both ends in aqueous solution. *Journal of Colloid and Interface Science*, 300(2), pp.774–81. Available at: <http://www.ncbi.nlm.nih.gov/pubmed/16690076> [Accessed March 8, 2014].
- Isis, Neutron Training Course Manual.
- James C. Gerdeen, P.D.P.E. & Ronald A. L. Rorrer, P.D.P.E., 2011. *Engineering Design with Polymers and Composites, Second Edition*, Taylor & Francis. Available at: <https://books.google.co.uk/books?id=C2aGmT5f0NkC>.
- Jiang, Q. & Wen, Z., 2011. *Thermodynamics of Materials*, Springer. Available at: <https://books.google.co.uk/books?id=3TfJOP2kd6YC>.
- Kabanov, A. V et al., 1992. Pluronic micelles as a tool for low-molecular compound vector delivery into a cell: effect of Staphylococcus aureus enterotoxin B on cell loading with micelle incorporated fluorescent dye. *Biochemistry International*, 26(6), pp.1035–1042. Available at: <http://europepmc.org/abstract/MED/1632800>.
- Kabanov, A. V et al., 2002. Pluronic® block copolymers: novel functional molecules for gene therapy. *Advanced Drug Delivery Reviews*, 54(2), pp.223–233. Available at: <http://www.sciencedirect.com/science/article/pii/S0169409X02000182>.
- Kabanov, A. V et al., 1989. The neuroleptic activity of haloperidol increases after its solubilization in surfactant micelles: Micelles as microcontainers for drug targeting. *FEBS Letters*, 258(2), pp.343–345. Available at: <http://www.sciencedirect.com/science/article/pii/0014579389816898>.
- Kadam, Y. et al., 2011. Micelles from PEO-PPO-PEO block copolymers as nanocontainers for solubilization of a poorly water soluble drug hydrochlorothiazide. *Colloids and surfaces. B, Biointerfaces*, 83(1), pp.49–57. Available at: <http://www.ncbi.nlm.nih.gov/pubmed/21123038> [Accessed February 19, 2014].
- Kadam, Y., Yerramilli, U. & Bahadur, A., 2009. Solubilization of poorly water-soluble drug carbamezapine in Pluronic® micelles: Effect of molecular characteristics, temperature and added salt on the solubilizing capacity. *Colloids and Surfaces B: Biointerfaces*, 72(1), pp.141–147. Available at: <http://www.sciencedirect.com/science/article/pii/S0927776509001271>.
- Karlstroem, G., 1985. A new model for upper and lower critical solution temperatures in poly(ethylene oxide) solutions. *The Journal of Physical Chemistry*, 89(23), pp.4962–4964. Available at: <http://dx.doi.org/10.1021/j100269a015>.
- Karlstrom, G., 1985. A New Model for Upper and Lower Critical Solution Temperatures in Poly(ethylene oxide) Solutions. *Journal of Physical Chemistry*, 89, pp.4962–4964.

- Kathmann, E.E., White, L.A. & McCormick, C.L., 1996. Water-soluble copolymers. 68. Polyelectrolytes of N-vinylformamide with sodium 3-acrylamido-3-methylbutanoate, sodium 2-acrylamido-2-methylpropanesulfonate, and sodium acrylate: solution behavior. *Macromolecules*, 29(16), pp.5273–5278.
- Kato, M. et al., 1990. International Solvent Extraction Conference. *Kyoto, Japan*.
- Keatch, C.J., 1969. *An introduction to thermogravimetry*, London: Heyden & Sons.
- Kim, S.Y. & Lee, Y.M., 2001. Taxol-loaded block copolymer nanospheres composed of methoxy poly(ethylene glycol) and poly( $\epsilon$ -caprolactone) as novel anticancer drug carriers. *Biomaterials*, 22(13), pp.1697–1704. Available at: <http://www.sciencedirect.com/science/article/pii/S0142961200002921>.
- Kim, Y.-H. et al., 1995. Saccharide Effect on the Lower Critical Solution Temperature of Thermosensitive Polymers. *Macromolecules*, 28, pp.939–944. Available at: <http://pubs.acs.org/doi/abs/10.1021/ma00108a022>.
- Kırcı, B. & Güner, A., 2001. Effect of phenolic cosolutes on the main parameters, phase separation and theta temperature of dilute aqueous poly(N-vinyl-2-pyrrolidone) solutions. *European Polymer Journal*, 37(2), pp.361–365. Available at: <http://www.sciencedirect.com/science/article/pii/S0014305700001063>.
- Kirkland, J.J., 1969. Controlled surface porosity supports for high-speed gas and liquid chromatography. *Analytical Chemistry*, 41(1), pp.218–220.
- Kirkland, J.J., 1968. High-performance ultraviolet photometric detector for use with efficient liquid chromatographic columns. *Analytical Chemistry*, 40(2), pp.391–396.
- Kissa, E., 1999. *Dispersions: Characterization, Testing, and Measurement*, Taylor & Francis. Available at: <http://books.google.co.uk/books?id=0AueaypD1BwC>.
- Kjellander, R. & Florin, E., 1981. Water structure and changes in thermal stability of the system poly(ethylene oxide)-water. *Journal of the Chemical Society, Faraday Transactions 1: Physical Chemistry in Condensed Phases*, 77(9), pp.2053–2077. Available at: <http://dx.doi.org/10.1039/F19817702053>.
- Krupka, T.M. et al., 2007. Effect of Intratumoral Injection of Carboplatin Combined with Pluronic P85 or L61 on Experimental Colorectal Carcinoma in Rats. *Experimental Biology and Medicine*, 232 (7), pp.950–957. Available at: <http://ebm.sagepub.com/content/232/7/950.abstract>.
- Kulshreshtha, A.K. & Vasile, C., 2003. *Handbook of Polymer Blends and Composites*, Rapra Technology. Available at: <https://books.google.co.uk/books?id=tJ8kjN3Z4HkC>.
- LaKind, J.S. et al., 1999. A review of the comparative mammalian toxicity of ethylene glycol and propylene glycol. *CRC Critical Reviews in Toxicology*, 29(4), pp.331–365.
- Lee, J.C. & Timasheff, S.N., 1981. The stabilization of proteins by sucrose. *Journal of Biological Chemistry*, 256(14), pp.7193–7201.

- Liechty, W.B. et al., 2010. Polymers for drug delivery systems. *Annual Review of Chemical and Biomolecular Engineering*, 1, p.149.
- Lindman, B. et al., 1990. Nonionic polyhers and surfactants-some anomalies in temperature dependence and in interactions with ionic surfactants. *Advances in Colloid and Interface Science*, 32(2), pp.183–203.
- Maeda, H. & Matsumura, Y., 1988. Tumoritropic and lymphotropic principles of macromolecular drugs. *Critical Reviews in Therapeutic Drug Carrier Systems*, 6(3), pp.193–210.
- Maniar, G.N. & Abrams, H., 1974. Metallography--A practical tool for correlating the structure and properties for materials.
- McClements, D.J., 2001. Estimation of steric exclusion and differential interaction contributions to protein transfer free energies in aqueous cosolvent solutions. *Food Hydrocolloids*, 15(4–6), pp.355–363. Available at: <http://www.sciencedirect.com/science/article/pii/S0268005X01000455>.
- McClements, D.J., 2002. Modulation of Globular Protein Functionality by Weakly Interacting Cosolvents. *Critical Reviews in Food Science and Nutrition*, 42(5), pp.417–471. Available at: <http://dx.doi.org/10.1080/20024091054210>.
- McElhaney, R.N., 1982. The use of differential scanning calorimetry and differential thermal analysis in studies of model and biological membranes. *Chemistry and Physics of Lipids*, 30(2–3), pp.229–259. Available at: <http://www.sciencedirect.com/science/article/pii/0009308482900536>.
- Melik-Nubarov, N.S. et al., 1999. Interaction of tumor and normal blood cells with ethylene oxide and propylene oxide block copolymers. *FEBS letters*, 446(1), pp.194–8. Available at: <http://www.ncbi.nlm.nih.gov/pubmed/10100641>.
- Milelli, A. et al., 2012. Structure-activity relationships of novel substituted naphthalene diimides as anticancer agents. *European Journal of Medicinal Chemistry*, 57, pp.417–428.
- Mitchell, S., 1926. CLXXI.-A method for determining the solubility of sparingly soluble substances. *Journal of the Chemical Society (Resumed)*, 129(0), pp.1333–1336. Available at: <http://dx.doi.org/10.1039/JR9262901333>.
- Moelbert, S., Normand, B. & De Los Rios, P., 2004. Kosmotropes and chaotropes: modelling preferential exclusion, binding and aggregate stability. *Biophysical Chemistry*, 112(1), pp.45–57.
- Myers, R., 2003. *The Basics of Chemistry*, Greenwood Press. Available at: <http://books.google.co.uk/books?id=oS50J3-IfZsC>.
- Nagarajan, R., 2001. Solubilization of “Guest” molecules into polymeric aggregates. *Polymers for Advanced Technologies*, 12, pp.23–43.



- Narten, A.H., 1972. Liquid Water: Atom Pair Correlation Functions from Neutron and X-Ray Diffraction. *The Journal of Chemical Physics*, 56(11), pp.5681–5687.
- Nicholson, J.W., 2012. *The Chemistry of Polymers* 2nd editio., Royal Society of Chemistry. Available at: [http://books.google.co.uk/books?id=5XFST69cX\\_YC](http://books.google.co.uk/books?id=5XFST69cX_YC).
- Ohline, S.M. et al., 2001. Differential Scanning Calorimetric Study of Bilayer Membrane Phase Transitions. A Biophysical Chemistry Experiment. *Journal of Chemical Education*, 78(9), p.1251.
- Owusu-Ware, S., 2013. *Understanding correlations between secondary relaxations and thermal behaviour of biologically relevant molecules*. PhD thesis, University of Greenwich. Available at: <http://gala.gre.ac.uk/id/eprint/11388>.
- Paruta, A.N., 1964. Solubility of several solutes as a function of the dielectric constant of sugar solutions. *Journal of Pharmaceutical Sciences*, 53(10), pp.1252–1254.
- Passerini, N. et al., 2002. Preparation and characterisation of ibuprofen–poloxamer 188 granules obtained by melt granulation. *European Journal of Pharmaceutical Sciences*, 15(1), pp.71–78. Available at: <http://www.sciencedirect.com/science/article/pii/S092809870100210X>.
- Paterson, I. et al., 1997. Thermodynamic Model Fitting of the Calorimetric Output Obtained for Aqueous Solutions of Oxyethylene– Oxypropylene–Oxyethylene Triblock Copolymers. *Langmuir*, 13(8), pp.2219–2226. Available at: <http://dx.doi.org/10.1021/la960432g>.
- Paterson, I.F., Chowdhry, B.Z. & Leharne, S.A., 1999. Investigations of naphthalene solubilization in aqueous solutions of ethylene oxide-b-propylene oxide-b-ethylene oxide copolymers. *Langmuir*, 15, pp.6187–6194.
- Pecora, R., 1985. *Dynamic light scattering: applications of photon correlation spectroscopy*, Springer.
- Price, D.M., Hourston, D.J. & Dumont, F., 2000. Thermogravimetry of Polymers., pp.8094–8105
- Privalov, P.L. & Gill, S.J., 1987. Stability of protein structure and hydrophobic interaction. *Advances in Protein Chemistry*, 39, pp.191–234.
- Qiu, L.Y. & Bae, Y.H., 2006. Polymer architecture and drug delivery. *Pharmaceutical research*, 23(1), pp.1–30. Available at: <http://www.ncbi.nlm.nih.gov/pubmed/16392022> [Accessed August 19, 2014].
- Riess, G., 2003. Micellization of block copolymers. *Progress in Polymer Science (Oxford)*, 28, pp.1107–1170.
- Rijcken, C.J.F. et al., 2007. Triggered destabilisation of polymeric micelles and vesicles by changing polymers polarity: an attractive tool for drug delivery. *Journal of Controlled Release : Official Journal of the Controlled Release Society*, 120(3), pp.131–48.

Available at: <http://www.ncbi.nlm.nih.gov/pubmed/17582642> [Accessed February 20, 2014].

- Ringsdorf, H., 1975. Structure and properties of pharmacologically active polymers. In *Journal of Polymer Science: Polymer Symposia*. Wiley Online Library, pp. 135–153.
- Robeson, L.M., 2007. Polymer blends. *Hanser, Munich*, pp.109–210.
- Roebuck, B.D., Goldblith, S.A. & Westphal, W.B., 1972. DIELECTRIC PROPERTIES OF CARBOHYDRATE-WATER MIXTURES AT MICROWAVE FREQUENCIES. *Journal of Food Science*, 37(2), pp.199–204. Available at: <http://dx.doi.org/10.1111/j.1365-2621.1972.tb05816.x>.
- Rosen, M.J., 1989. *Surfactants and Interfacial Phenomena*, Wiley. Available at: <http://books.google.co.uk/books?id=pNVTAAAAMAAJ>.
- Sadeghi, R. & Jamehbozorg, B., 2008. Effect of temperature on the salting-out effect and phase separation in aqueous solutions of sodium di-hydrogen phosphate and poly(propylene glycol). *Fluid Phase Equilibria*, 271(1-2), pp.13–18. Available at: <http://linkinghub.elsevier.com/retrieve/pii/S037838120800215X> [Accessed December 14, 2014].
- Sahin, S. & Sumnu, S.G., 2007. *Physical Properties of Foods*, Springer. Available at: [http://books.google.co.uk/books?id=-QEfJ\\_U9tAAC](http://books.google.co.uk/books?id=-QEfJ_U9tAAC).
- Salamone, J.C., 1996. *Polymeric Materials Encyclopedia, Twelve Volume Set*, Taylor & Francis. Available at: [https://books.google.co.uk/books?id=j7ZbmIE\\_\\_EwC](https://books.google.co.uk/books?id=j7ZbmIE__EwC).
- Schick, C., 2009. Differential scanning calorimetry (DSC) of semicrystalline polymers. *Analytical and Bioanalytical Chemistry*, 395, pp.1589–1611.
- Shin, S.-C. & Cho, C.-W., 1997. Physicochemical Characterizations of Piroxicam-Poloxamer Solid Dispersion. *Pharmaceutical Development and Technology*, 2(4), pp.403–407. Available at: <http://dx.doi.org/10.3109/10837459709022639>.
- Shpigelman, A. et al., 2008. Saccharide-structure effects on poly N-isopropylacrylamide phase transition in aqueous media; Reflections on protein stability. *Journal of Polymer Science Part B: Polymer Physics*, 46(21), pp.2307–2318.
- Sjoeberg, A., Karlstroem, G. & Tjerneld, F., 1989. Effects on the cloud point of aqueous poly(ethylene glycol) solutions upon addition of low molecular weight saccharides. *Macromolecules*, 22, pp.4512–4516. Available at: <http://pubs.acs.org/doi/abs/10.1021/ma00202a023>.
- Slepnev, V.I. et al., Alakhov VYu, and Kabanov AV. 1992. *Micelles of poly (oxyethylene)-poly (oxypropylene) block copolymer (pluronic) as a tool for low-molecular compound delivery into a cell. Phosphorylation of intracellular proteins with micelle incorporated [ $\gamma$ - $^{32}P$ ] ATP. Biochem. Internat*, 26, pp.587–595.

- Sperling, L.H., 2005. *Introduction to Physical Polymer Science*, Wiley. Available at: <https://books.google.co.uk/books?id=i7HMbG9MwnIC>.
- Staff, A., 2011. *Operational Control of Coagulation and Filtration Processes, 3rd Ed. (M37)*, American Water Works Association. Available at: [https://books.google.co.uk/books?id=IS\\_MI2Jx1QsC](https://books.google.co.uk/books?id=IS_MI2Jx1QsC).
- Sturtevant, J.M., 1987. Biochemical applications of differential scanning calorimetry. *Annual Review of Physical Chemistry*, 38(1), pp.463–488.
- Su, Y. & Liu, H., 2003. Temperature-dependent solubilization of PEO-PPO-PEO block copolymers and their application for extraction trace organics from aqueous solutions. *Korean Journal of Chemical Engineering*, 20(2), pp.343–346. Available at: <http://dx.doi.org/10.1007/BF02697250>.
- Sutherland, A.J., 2002. Quantum dots as luminescent probes in biological systems. *Current Opinion in Solid State and Materials Science*, 6(4), pp.365–370.
- Timasheff, S.N., 2002a. Protein-solvent preferential interactions, protein hydration, and the modulation of biochemical reactions by solvent components. *Proceedings of the National Academy of Sciences of the United States of America*, 99(15), pp.9721–9726. Available at: <http://www.ncbi.nlm.nih.gov/pmc/articles/PMC124992/>.
- Timasheff, S.N., 2002b. Thermodynamic binding and site occupancy in the light of the Schellman exchange concept. *Biophysical Chemistry*, 101–102(0), pp.99–111. Available at: <http://www.sciencedirect.com/science/article/pii/S0301462202001886>.
- Torchilin, V.P., 2001. Structure and design of polymeric surfactant-based drug delivery systems. *Journal of Controlled Release*, 73(2–3), pp.137–172. Available at: <http://www.sciencedirect.com/science/article/pii/S0168365901002991>.
- Tripathy, T. & De, B.R., 2008. Making Sense About Dipole Moments. *Journal of Physical Sciences*, 12(2008), pp.155–172.
- Turnhout, J. va., 1975. *Thermally stimulated discharge of polymer electrets*, Amsterdam: Elsevier.
- Urbain, G. & Boulanger, C., 1912. Sur une balance-laboratoire à compensation électromagnétique à l'étude des systèmes qui dégagent des gaz avec une vitesse sensible. *Compt. rend*, 154, pp.347–349.
- Venne, A. et al., 1996. Hypersensitizing effect of pluronic L61 on cytotoxic activity, transport, and subcellular distribution of doxorubicin in multiple drug-resistant cells. *Cancer Research*, 56(16), pp.3626–3629.
- Verdonck, E., Schaap, K. & Thomas, L.C., 1999. A discussion of the principles and applications of Modulated Temperature DSC (MTDSC). *International Journal of Pharmaceutics*, 192(1), pp.3–20. Available at: <http://www.sciencedirect.com/science/article/pii/S0378517399002677> [Accessed April 20, 2014].

- Vicioso, M.T., Ramos, J.J.M. & Diogo, H.P., 2010. Molecular dynamics of an epoxy resin studied by Thermally Stimulated Depolarization Currents. *Journal of Non-Crystalline Solids*, 356, pp.2858–2864.
- Vyazovkin, S. et al., 2011. ICTAC Kinetics Committee recommendations for performing kinetic computations on thermal analysis data. *Thermochimica Acta*, 520(1-2), pp.1–19. Available at: <http://www.sciencedirect.com/science/article/pii/S0040603111002152> [Accessed March 25, 2014].
- Ward, M. a. & Georgiou, T.K., 2011. Thermoresponsive Polymers for Biomedical Applications. *Polymers*, 3(4), pp.1215–1242. Available at: <http://www.mdpi.com/2073-4360/3/3/1215/> [Accessed March 23, 2014].
- Van de Witte, P. et al., 1996. Phase separation processes in polymer solutions in relation to membrane formation. *Journal of Membrane Science*, 117(1-2), pp.1–31. Available at: <http://linkinghub.elsevier.com/retrieve/pii/0376738896000889>.
- Yao, J.H. et al., 1993. Theory and simulation of Ostwald ripening. *Physical Review B*, 47(21), p.14110.
- Zafarani-Moattar, M.T., Emamian, S. & Hamzehzadeh, S., 2008. Effect of Temperature on the Phase Equilibrium of the Aqueous Two-Phase Poly(propylene glycol) + Tripotassium Citrate System. *Journal of Chemical & Engineering Data*, 53(2), pp.456–461. Available at: <http://dx.doi.org/10.1021/jc700549u>.
- Zahedi, P. et al., 2012. Recent advances in drug delivery strategies for treatment of ovarian cancer. *Expert Opinion on Drug Delivery*, 9, pp.567–583.
- Zhang, Y. et al., 2007. Effects of Hofmeister anions on the LCST of PNIPAM as a function of molecular weight. *The Journal of Physical Chemistry C*, 111(25), pp.8916–8924.
- Zhang, Y. & Cremer, P.S., 2006. Interactions between macromolecules and ions: the Hofmeister series. *Current Opinion in Chemical Biology*, 10(6), pp.658–663. Available at: <http://www.sciencedirect.com/science/article/pii/S1367593106001517>.

## APPENDICES

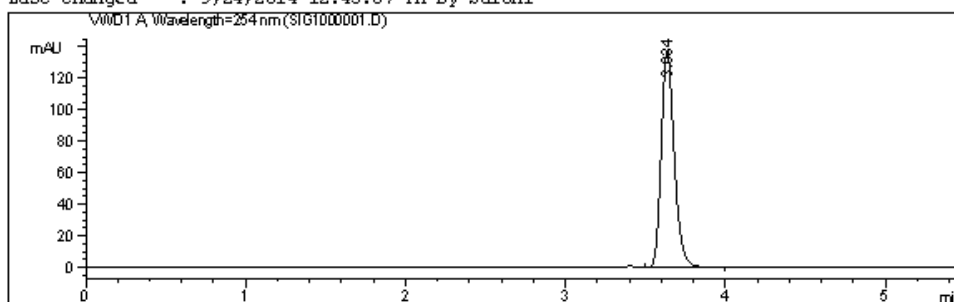
Examples of chromatograms for the study of naphthalene solubility in aqueous PPG solutions are attached below. Three samples for each temperature point were prepared and each sample examined twice by HPLC. The chromatograms shown below are for the following samples:

- 1) Water solution saturated with naphthalene at 42°C.
- 2) Aqueous 1 mg mL<sup>-1</sup> PPG solutions saturated with naphthalene at 42°C.

# 1) Water Solution Saturated with Naphthalene at 42°C.

Data File C:\CHEM32\...\NAPHTHALENES\DEF\_LCNAPHTHALENES\_2 2014-09-25 13-46-30\SIG1000001.D  
Sample Name: w\_42c

```
=====
Acq. Operator   : Saloni                      Seq. Line :    1
Acq. Instrument : Instrument 1                Location  : Vial 1
Injection Date  : 9/25/2014 1:48:05 PM      Inj       :    1
                                           Inj Volume: 20 µl
Sequence File   : C:\Chem32\1\DATA\NAPHTHALENES\DEF_LCNAPHTHALENES_2 2014-09-25 13-46-30\DEF_LCNAPHTHALENES_2.S
Method          : C:\Chem32\1\DATA\NAPHTHALENES\DEF_LCNAPHTHALENES_2 2014-09-25 13-46-30\DEF_LCNAPHTHALENES.M
Last changed    : 9/24/2014 12:45:07 PM by Saloni
=====
```



## Area Percent Report

```
=====
Sorted By      :      Signal
Multiplier     :      1.0000
Dilution       :      1.0000
Use Multiplier & Dilution Factor with ISTDs
=====
```

Signal 1: WWD1 A, Wavelength=254 nm

Peak #	RetTime [min]	Type	Width [min]	Area mAU *s	Height [mAU]	Area %
1	3.634	VB	0.0860	778.20105	138.37019	100.0000

Totals :                    778.20105 138.37019

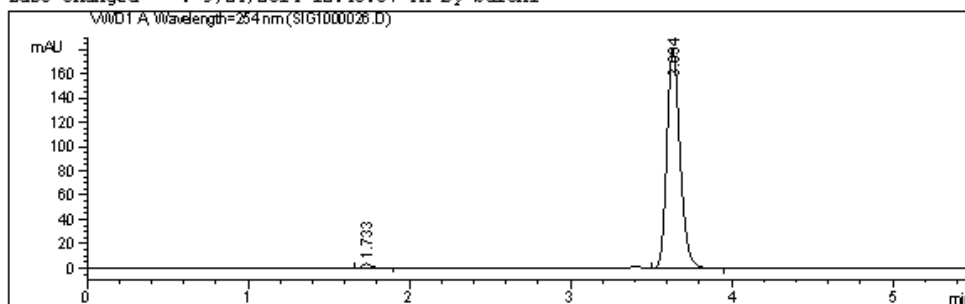
```
=====
*** End of Report ***
=====
```

## 2) Aqueous 1 mg mL<sup>-1</sup> PPG Solutions Saturated with Naphthalene at 42°C.

Data File C:\CHEM32\1\DATA\NAPHTHALENES\DEF\_LCNAPHTHALENES\_2 2014-09-24 12-45-09\SIG1000026.D  
 Sample Name: 1\_42a

```

=====
Acq. Operator   : Saloni                      Seq. Line : 13
Acq. Instrument : Instrument 1                Location  : Vial 13
Injection Date  : 9/24/2014 3:55:46 PM      Inj       : 2
                                           Inj Volume: 20 µl
Sequence File   : C:\Chem32\1\DATA\NAPHTHALENES\DEF_LCNAPHTHALENES_2 2014-09-24 12-45-
                  09\DEF_LCNAPHTHALENES_2.S
Method          : C:\Chem32\1\DATA\NAPHTHALENES\DEF_LCNAPHTHALENES_2 2014-09-24 12-45-
                  09\DEF_LCNAPHTHALENES.M
Last changed    : 9/24/2014 12:45:07 PM by Saloni
  
```



### Area Percent Report

```

=====
Sorted By      : Signal
Multiplier     : 1.0000
Dilution       : 1.0000
Use Multiplier & Dilution Factor with ISTDs
  
```

Signal 1: VWD1 A, Wavelength=254 nm

Peak #	RetTime [min]	Type	Width [min]	Area mAU *s	Height [mAU]	Area %
1	1.733	EB	0.0649	15.71187	3.74956	1.5121
2	3.634	VB	0.0863	1023.39258	181.16539	98.4879

Totals : 1039.10445 184.91495

\*\*\* End of Report \*\*\*

## **Gel Permeation Chromatography to Estimate the Molecular Mass of PPGs**

Gel permeation chromatography (GPC) was performed on PPG samples to estimate their molecular mass. GPC is a type of size exclusion chromatography used to separate analytes based on their size. So the smaller analytes are retained for longer inside the pores of the column and hence have a longer retention time and the bigger analytes have a shorter retention time.

Instrument: Gel Permeation Chromatography 1100 series

Manufacturer: Agilent Technologies, UK

Column: Styragel HR1 7.8 x 300 mm column, Waters, UK

Software: Chemstation A.10.02 (1757)

Tetrahydrofuran: Inhibitor-free, Chromasolv Plus, for HPLC,  $\geq 99.9\%$ , Sigma Aldrich, UK

Calibration standards: Polystyrene standard kit, Waters, UK

Samples were prepared in tetrahydrofuran (THF). Flow rate of  $1 \text{ ml min}^{-1}$  was used to run the samples with the column temperature of  $22^\circ\text{C}$  and pressure of 23 bar. The polarity of refractive index detector (RID) was positive and only the signal from RID detector (signal 1) was used to estimate the retention time of PPG samples.  $20 \text{ mg mL}^{-1}$  PPG samples used were prepared THF. Calibration standards were prepared in THF at a concentration of 0.05% w/v. Due to the lack of appropriate instrumentation and the columns; the molecular mass could only be estimated relative to the polystyrene calibration standards. Five polystyrene calibration standards were used to estimate the relative average molecular mass of PPGs used in this research. Polydispersity and the actual molecular mass could not be calculated due to the lack



of appropriate instrumentation and software. The chromatograms for the GPC standards and PPG samples are shown below.

The molecular masses obtained using GPC shown in the Table on page 216 may not correspond to the actual PPG molecular mass because of the possible inappropriate standards used for the experiments in relation to the chromatographic columns available and the software required for the analysis of the actual PPG molecular mass.

# Chromatograms for THF and Polystyrene Standards

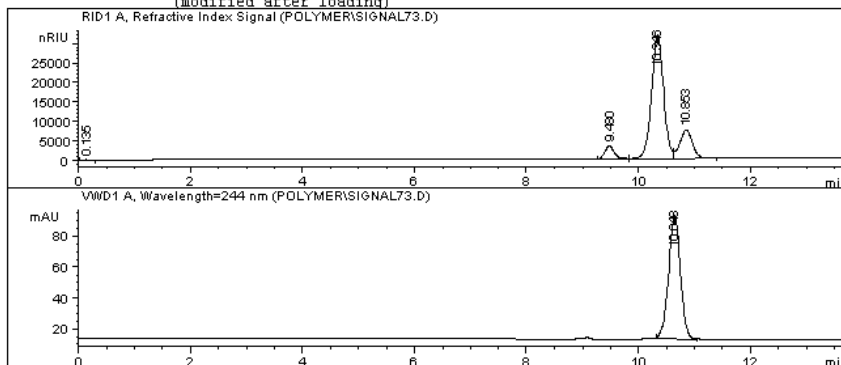
Data File C:\HPCHEM\1\DATA\POLYMER\SIGNAL73.D

Sample Name: THF

RID -ve Polarity, flow 1.0ml/min Pressure 23bar  
 column Waters hrl 7.8x300mm column  
 column at 22 deg C  
 sample in 20thf

```

=====
Injection Date : 11/26/2014 11:45:15 AM
Sample Name   : THF                               Location  : -
Acq. Operator : Saloni
Acq. Instrument : GPC
Method        : C:\HPCHEM\1\METHODS\POLYMER.M
Last changed  : 11/26/2014 10:16:11 AM by Saloni
                (modified after loading)
    
```



### Area Percent Report

```

=====
Sorted By      : Signal
Multiplier    : 1.0000
Dilution      : 1.0000
Use Multiplier & Dilution Factor with ISTDs
    
```

Signal 1: RID1 A, Refractive Index Signal

Peak #	RetTime [min]	Type	Width [min]	Area [nRIU*s]	Height [nRIU]	Area %
1	0.135	BP	0.0812	359.38464	70.29302	0.0564
2	9.480	PV	0.1963	4.34456e4	3406.35059	6.8222
3	10.346	VV	0.2324	4.77496e5	3.16038e4	74.9802
4	10.853	VB	0.2434	1.15528e5	7369.13770	18.1412

Totals : 6.36829e5 4.24496e4

Results obtained with enhanced integrator!

Signal 2: VWD1 A, Wavelength=244 nm

Peak #	RetTime [min]	Type	Width [min]	Area [mAU*s]	Height [mAU]	Area %
1	10.648	BB	0.2257	1179.58850	80.08638	100.0000

Totals : 1179.58850 80.08638

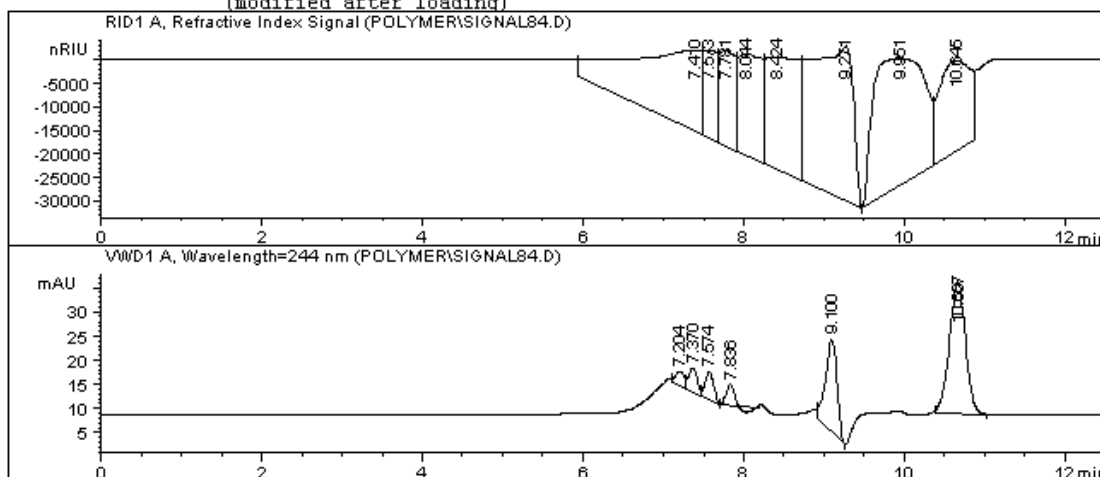
GPC 11/26/2014 11:59:04 AM Saloni

Page 1 of 2

RID +ve Polarity. flow 1.0ml/min Pressure 23bar  
 column Waters hrl 7.8x300mm column  
 column at 22 deg C  
 sample in 20thf

```

=====
Injection Date : 11/26/2014 3:26:21 PM
Sample Name    : STD580
Acq. Operator  : Saloni
Acq. Instrument : GPC
Method         : C:\HPCHEM\1\METHODS\POLYMER.M
Last changed   : 11/26/2014 3:00:55 PM by Saloni
                  (modified after loading)
    
```



=====  
 Area Percent Report  
 =====

```

Sorted By      : Signal
Multiplier     : 1.0000
Dilution       : 1.0000
Use Multiplier & Dilution Factor with ISTDs
    
```

Signal 1: RID1 A, Refractive Index Signal

Peak #	RetTime [min]	Type	Width [min]	Area [nRIU*s]	Height [nRIU]	Area %
1	7.410	BV	0.6819	9.82273e5	1.74699e4	17.9427
2	7.573	VV	0.1624	2.20431e5	1.88470e4	4.0265
3	7.781	VV	0.1992	2.85696e5	2.02461e4	5.2187
4	8.044	VV	0.2649	4.29007e5	2.17335e4	7.8364
5	8.424	VV	0.3641	6.66777e5	2.39189e4	12.1797
6	9.271	VP	0.4694	1.17885e6	3.29348e4	21.5333
7	9.951	VV	0.7376	1.18690e6	2.67687e4	21.6804
8	10.645	VV	0.4196	5.24588e5	1.91097e4	9.5824

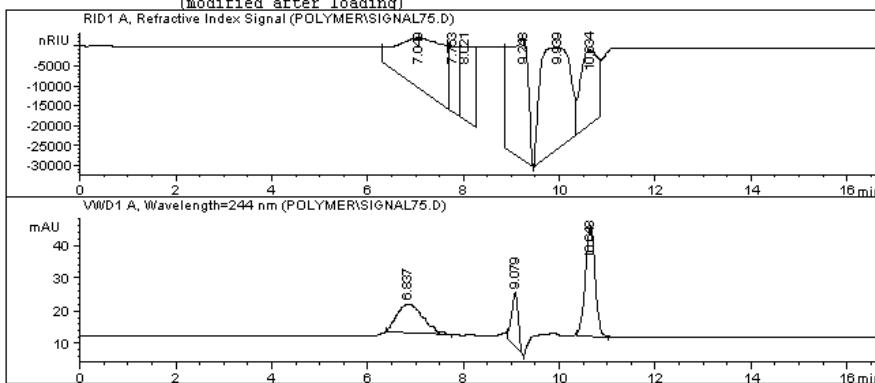
Totals : 5.47451e6 1.81029e5

Results obtained with enhanced integrator!

RID +ve Polarity, flow 1.0ml/min Pressure 23bar  
 column Waters hrl 7.8x300mm column  
 column at 22 deg C  
 sample in 20thf

```

=====
Injection Date : 11/26/2014 12:18:33 PM
Sample Name    : STD 860
Acq. Operator  : Saloni
Acq. Instrument : GPC
Method         : C:\HPCHEM\1\METHODS\POLYMER.M
Last changed   : 11/26/2014 12:16:51 PM by Saloni
                (modified after loading)
    
```



Area Percent Report

```

Sorted By      : Signal
Multiplier     : 1.0000
Dilution       : 1.0000
Use Multiplier & Dilution Factor with ISTDs
    
```

Signal 1: RID1 A, Refractive Index Signal

Peak #	RetTime [min]	Type	Width [min]	Area [nRIU*s]	Height [nRIU]	Area %
1	7.049	BV	0.9743	9.14383e5	1.24376e4	22.7682
2	7.753	VV	0.1950	2.30729e5	1.63332e4	5.7452
3	8.021	VB	0.2782	3.83490e5	1.83607e4	9.5489
4	9.248	BP	0.3879	8.83014e5	3.06504e4	21.9871
5	9.939	VV	0.7268	1.11885e6	2.57733e4	27.8594
6	10.634	VV	0.3978	4.85585e5	1.89831e4	12.0911

Totals : 4.01605e6 1.22538e5

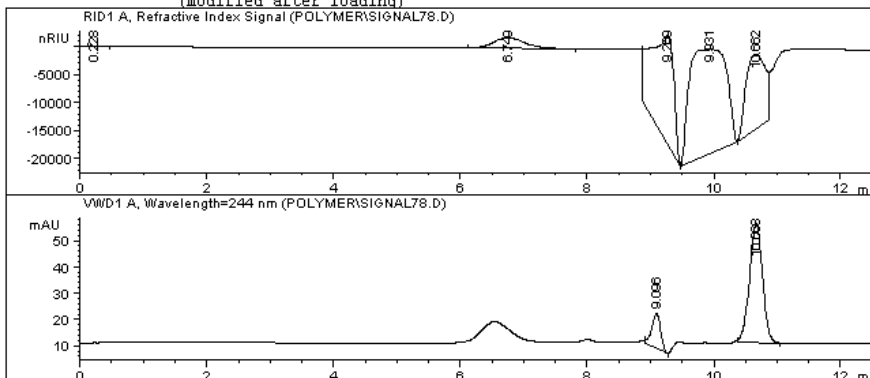
Results obtained with enhanced integrator!

Signal 2: VWD1 A, Wavelength=244 nm

RID +ve Polarity, flow 1.0ml/min Pressure 23bar  
 column Waters hrl 7.8x300mm column  
 column at 22 deg C  
 sample in 20chf

```

=====
Injection Date : 11/26/2014 1:09:44 PM
Sample Name    : STD1320
Acq. Operator  : Saloni
Acq. Instrument : GPC
Method         : C:\HPCHEM\1\METHODS\POLYMER.M
Last changed   : 11/26/2014 12:16:51 PM by Saloni
                (modified after loading)
    
```



Area Percent Report

```

Sorted By      : Signal
Multiplier     : 1.0000
Dilution       : 1.0000
Use Multiplier & Dilution Factor with ISTDs
    
```

Signal 1: RID1 A, Refractive Index Signal

Peak #	RetTime [min]	Type	Width [min]	Area [nRIU*s]	Height [nRIU]	Area %
1	0.228	BB	0.2044	507.68765	34.86436	0.0326
2	6.749	BP	0.5128	6.15300e4	1873.49377	3.9477
3	9.269	BP	0.3333	4.60891e5	1.91055e4	29.5701
4	9.931	VP	0.6899	7.49959e5	1.86333e4	48.1162
5	10.662	VV	0.3440	2.85752e5	1.33888e4	18.3334

Totals : 1.55864e6 5.30361e4

Results obtained with enhanced integrator!

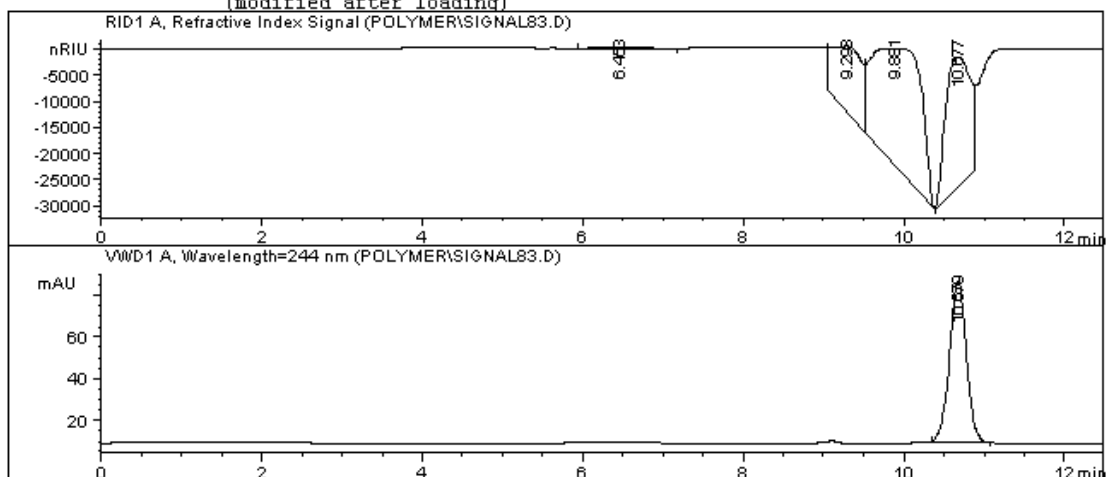
Signal 2: VWD1 A, Wavelength=244 nm

Peak #	RetTime [min]	Type	Width [min]	Area [mAU*s]	Height [mAU]	Area %
1	9.096	BP	0.1504	128.97200	13.19966	16.4072
2	10.668	BB	0.2223	657.09943	45.52182	83.5928

RID +ve Polarity. Flow 1.0ml/min Pressure 23bar  
 column Waters hrl 7.8x300mm column  
 column at 22 deg C  
 sample in 20thf

```

=====
Injection Date : 11/26/2014 3:10:45 PM
Sample Name    : STD1860
Acq. Operator  : Saloni
Acq. Instrument : GPC
Method         : C:\HPCHEM\1\METHODS\POLYMER.M
Last changed   : 11/26/2014 3:00:55 PM by Saloni
                  (modified after loading)
    
```



Area Percent Report

```

Sorted By      : Signal
Multiplier     : 1.0000
Dilution       : 1.0000
Use Multiplier & Dilution Factor with ISTDs
    
```

Signal 1: RID1 A, Refractive Index Signal

Peak #	RetTime [min]	Type	Width [min]	Area [nRIU*s]	Height [nRIU]	Area %
1	6.453	PP	0.4004	1837.08179	73.30029	0.0994
2	9.293	BV	0.3663	3.31317e5	1.26407e4	17.9293
3	9.881	VP	0.7211	9.73201e5	2.22880e4	52.6649
4	10.677	VV	0.3481	5.41557e5	2.49718e4	29.3064

Totals : 1.84791e6 5.99737e4

Results obtained with enhanced integrator!

Signal 2: VWD1 A, Wavelength=244 nm

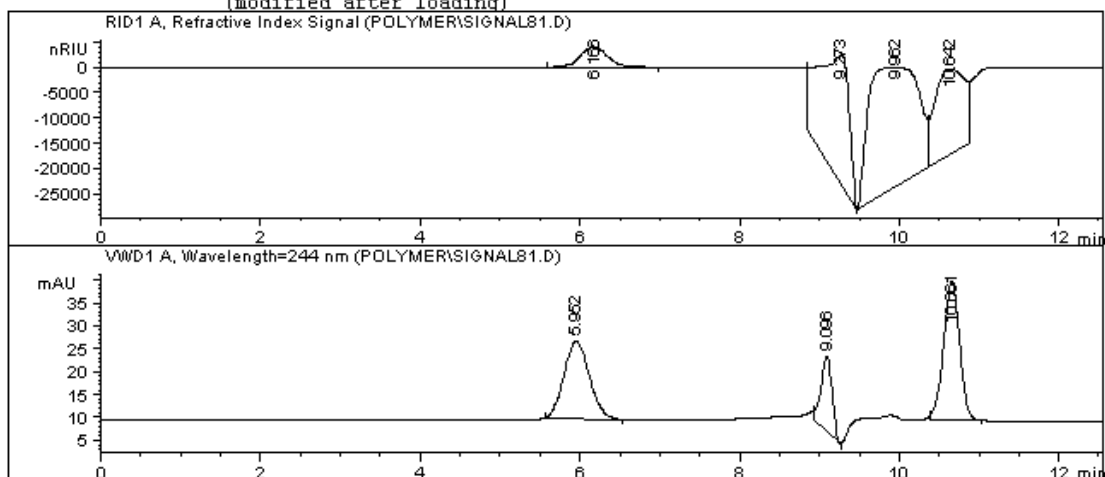
Peak #	RetTime [min]	Type	Width [min]	Area mAU*s	Height [mAU]	Area %
1	10.679	BB	0.2281	1149.11768	77.61272	100.0000

Totals : 1149.11768 77.61272

RID +ve Polarity. Flow 1.0ml/min Pressure 23bar  
 column Waters hrl 7.8x300mm column  
 column at 22 deg C  
 sample in 20thf

```

=====
Injection Date : 11/26/2014 2:42:50 PM
Sample Name    : STD2780                      Location   : -
Acq. Operator  : Saloni
Acq. Instrument : GPC
Method         : C:\HPCHEM\1\METHODS\POLYMER.M
Last changed   : 11/26/2014 12:16:51 PM by Saloni
                (modified after loading)
    
```



=====  
 Area Percent Report  
 =====

```

Sorted By      : Signal
Multiplier     : 1.0000
Dilution       : 1.0000
Use Multiplier & Dilution Factor with ISTDs
    
```

Signal 1: RID1 A, Refractive Index Signal

Peak #	RetTime [min]	Type	Width [min]	Area [nRIU*s]	Height [nRIU]	Area %
1	6.166	BB	0.3650	9.54384e4	4059.41113	4.3368
2	9.273	BP	0.3493	6.44830e5	2.52905e4	29.3019
3	9.962	VV	0.7237	1.02029e6	2.34464e4	46.3634
4	10.642	VV	0.4063	4.40083e5	1.67291e4	19.9979

Totals : 2.20065e6 6.95254e4

Results obtained with enhanced integrator!

Signal 2: VWD1 A, Wavelength=244 nm

Peak #	RetTime [min]	Type	Width [min]	Area mAU*s	Height [mAU]	Area %
1	5.952	BB	0.3463	376.35977	16.86462	39.2776
2	9.096	BP	0.1493	159.27824	16.45590	16.6226
3	10.661	BB	0.2176	422.56610	30.10189	44.0998

# Chromatograms for 20 mg mL<sup>-1</sup> PPG Samples

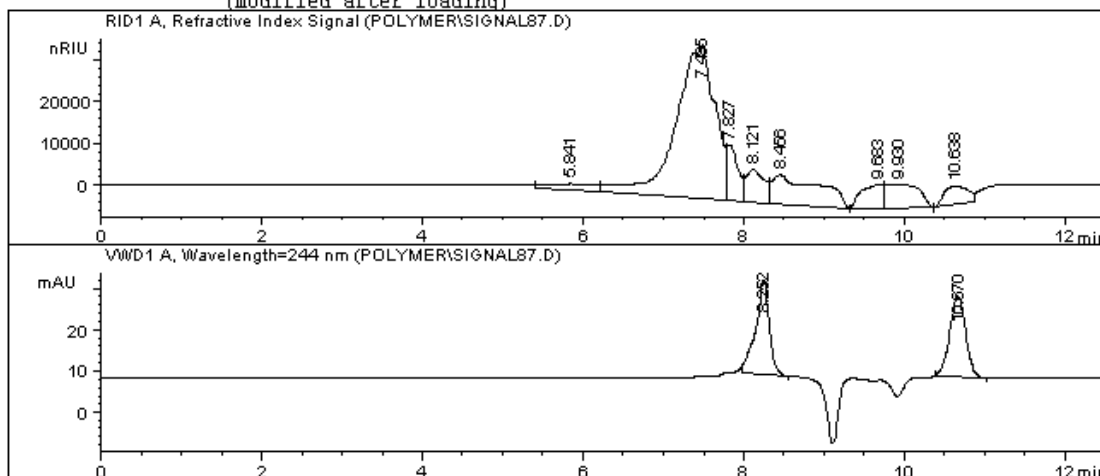
Data File C:\HPCHEM\1\DATA\POLYMER\SIGNAL87.D

Sample Name: PPG 425 20MGML

RID +ve Polarity. Flow 1.0ml/min Pressure 23bar  
 column Waters hrl 7.8x300mm column  
 column at 22 deg C NEW THF  
 sample in 20thf

```

=====
Injection Date   : 11/26/2014 4:24:28 PM
Sample Name     : PPG 425 20MGML           Location  : -
Acq. Operator  : Saloni
Acq. Instrument : GPC
Method         : C:\HPCHEM\1\METHODS\POLYMER.M
Last changed   : 11/26/2014 3:00:55 PM by Saloni
                (modified after loading)
  
```



## Area Percent Report

```

=====
Sorted By       : Signal
Multiplier     : 1.0000
Dilution       : 1.0000
Use Multiplier & Dilution Factor with ISTDs
  
```

Signal 1: RID1 A, Refractive Index Signal

Peak #	RetTime [min]	Type	Width [min]	Area [nRIU*s]	Height [nRIU]	Area %
1	5.841	BV	0.5684	5.68756e4	1352.48108	2.5779
2	7.485	VV	0.4230	1.24710e6	3.66408e4	56.5256
3	7.827	VV	0.1444	1.29406e5	1.32193e4	5.8654
4	8.121	VV	0.2214	1.20603e5	7710.56836	5.4664
5	8.456	VP	0.5149	2.87796e5	6989.90186	13.0446
6	9.683	VV	0.2619	1.02825e5	5486.01318	4.6606
7	9.930	VP	0.4998	1.66186e5	5493.04346	7.5325
8	10.638	VV	0.3478	9.54634e4	4483.75586	4.3270

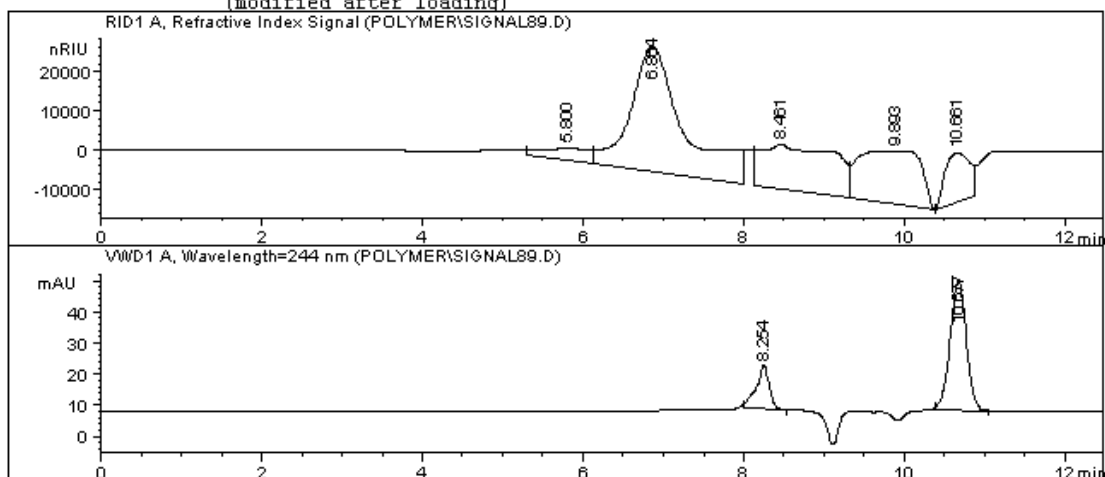
Totals : 2.20625e6 8.13759e4

Results obtained with enhanced integrator!



RID +ve Polarity. Flow 1.0ml/min Pressure 23bar  
 column Waters hrl 7.8x300mm column  
 column at 22 deg C NEW THF  
 sample in 20thf

=====  
 Injection Date : 11/26/2014 4:53:15 PM  
 Sample Name : PPG 725 20MGML Location : -  
 Acq. Operator : Saloni  
 Acq. Instrument : GPC  
 Method : C:\HPCHEM\1\METHODS\POLYMER.M  
 Last changed : 11/26/2014 3:00:55 PM by Saloni  
 (modified after loading)



=====  
 Area Percent Report  
 =====

Sorted By : Signal  
 Multiplier : 1.0000  
 Dilution : 1.0000  
 Use Multiplier & Dilution Factor with ISTDs

Signal 1: RID1 A, Refractive Index Signal

Peak #	RetTime [min]	Type	Width [min]	Area [nRIU*s]	Height [nRIU]	Area %
1	5.800	BV	0.5851	1.22520e5	2969.00684	3.7042
2	6.864	VB	0.6551	1.45584e6	3.18000e4	44.0153
3	8.461	BV	0.8146	7.43897e5	1.12511e4	22.4907
4	9.893	VP	0.7630	7.19264e5	1.36189e4	21.7459
5	10.661	VV	0.3517	2.66057e5	1.22991e4	8.0439

Totals : 3.30758e6 7.19381e4

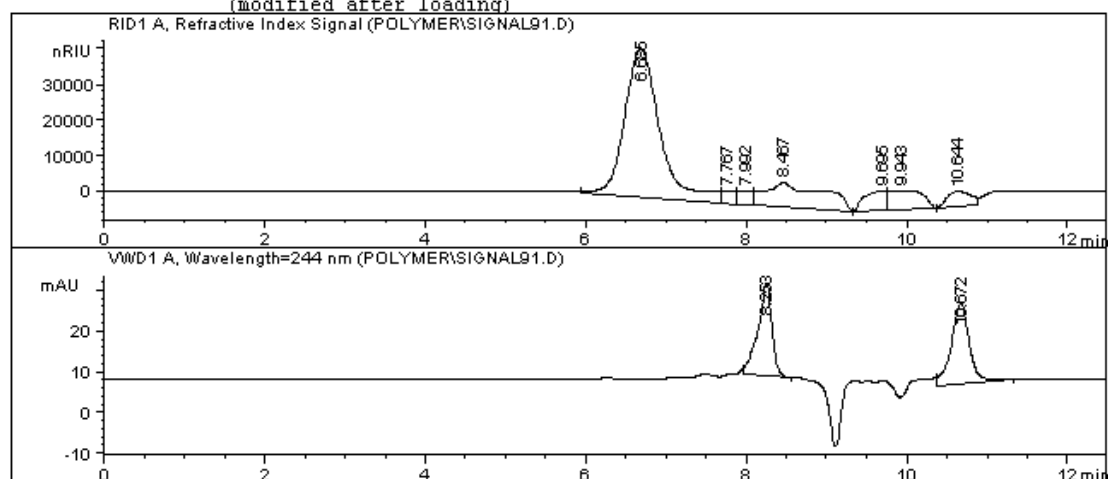
Results obtained with enhanced integrator!

Signal 2: VWD1 A, Wavelength=244 nm

Peak #	RetTime [min]	Type	Width [min]	Area mAU *s	Height [mAU]	Area %
1	8.254	BP	0.1678	161.33434	13.86514	21.5535
2	10.677	BB	0.2195	587.19519	41.36869	78.4465

RID +ve Polarity. Flow 1.0ml/min Pressure 23bar  
 column Waters hrl 7.8x300mm column  
 column at 22 deg C NEW THF  
 sample in 20thf

=====  
 Injection Date : 11/26/2014 5:21:02 PM  
 Sample Name : PPG 1000 20MGML Location : -  
 Acq. Operator : Saloni  
 Acq. Instrument : GPC  
 Method : C:\HPCHEM\1\METHODS\POLYMER.M  
 Last changed : 11/26/2014 3:00:55 PM by Saloni  
 (modified after loading)



=====  
 Area Percent Report  
 =====

Sorted By : Signal  
 Multiplier : 1.0000  
 Dilution : 1.0000  
 Use Multiplier & Dilution Factor with ISTDs

Signal 1: RID1 A, Refractive Index Signal

Peak #	RetTime [min]	Type	Width [min]	Area [nRIU*s]	Height [nRIU]	Area %
1	6.685	BV	0.4689	1.29346e6	4.18128e4	62.4824
2	7.767	VV	0.1628	3.96136e4	3487.42163	1.9136
3	7.992	VV	0.1714	4.62396e4	3821.19434	2.2337
4	8.467	VP	0.6273	3.50088e5	6940.77588	16.9114
5	9.695	VV	0.2622	1.00408e5	5348.38428	4.8503
6	9.943	VP	0.4973	1.55561e5	5179.71826	7.5145
7	10.644	VV	0.3475	8.47529e4	3985.26685	4.0941

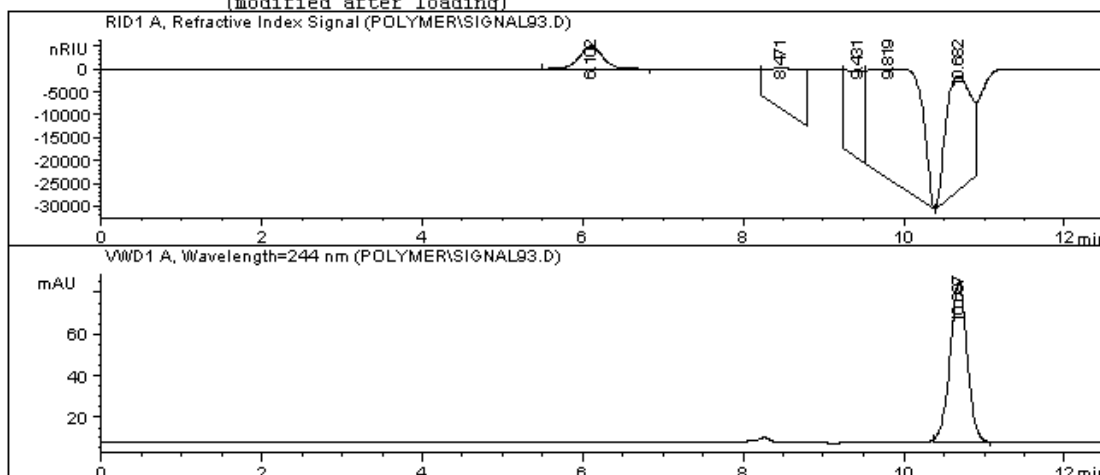
Totals : 2.07013e6 7.05756e4

Results obtained with enhanced integrator!

RID +ve Polarity. Flow 1.0ml/min Pressure 23bar  
 column Waters hrl 7.8x300mm column  
 column at 22 deg C NEW THF  
 sample in 20thf

```

=====
Injection Date : 11/26/2014 5:49:08 PM
Sample Name    : PPG 2000 20MGML           Location : -
Acq. Operator  : Saloni
Acq. Instrument : GPC
Method         : C:\HPCHEM\1\METHODS\POLYMER.M
Last changed   : 11/26/2014 3:00:55 PM by Saloni
                (modified after loading)
    
```



=====  
 Area Percent Report  
 =====

```

Sorted By      : Signal
Multiplier     : 1.0000
Dilution       : 1.0000
Use Multiplier & Dilution Factor with ISTDs
    
```

Signal 1: RID1 A, Refractive Index Signal

Peak #	RetTime [min]	Type	Width [min]	Area [nRIU*s]	Height [nRIU]	Area %
1	6.102	BB	0.3152	9.82747e4	4829.65674	4.1683
2	8.471	BB	0.4594	3.10100e5	8604.25488	13.1528
3	9.431	BV	0.2084	2.99667e5	1.91598e4	12.7103
4	9.819	VP	0.7514	1.11231e6	2.40443e4	47.1782
5	10.682	VV	0.3524	5.37321e5	2.47735e4	22.7903

Totals : 2.35767e6 8.14115e4

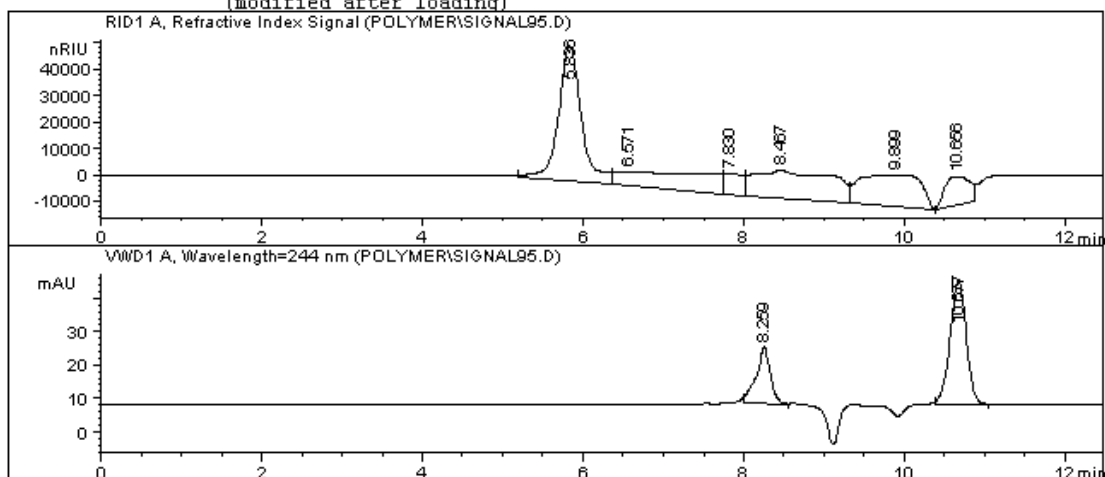
Results obtained with enhanced integrator!

Signal 2: VWD1 A, Wavelength=244 nm

Peak #	RetTime [min]	Type	Width [min]	Area mAU *s	Height [mAU]	Area %
1	10.687	BB	0.2284	1143.62988	77.10846	100.0000

RID +ve Polarity. Flow 1.0ml/min Pressure 23bar  
 column Waters hrl 7.8x300mm column  
 column at 22 deg C NEW THF  
 sample in 20thf

=====  
 Injection Date : 11/26/2014 6:16:56 PM  
 Sample Name : PPG 2700 20MGML Location : -  
 Acq. Operator : Saloni  
 Acq. Instrument : GPC  
 Method : C:\HPCHEM\1\METHODS\POLYMER.M  
 Last changed : 11/26/2014 3:00:55 PM by Saloni  
 (modified after loading)



=====  
 Area Percent Report  
 =====

Sorted By : Signal  
 Multiplier : 1.0000  
 Dilution : 1.0000  
 Use Multiplier & Dilution Factor with ISTDs

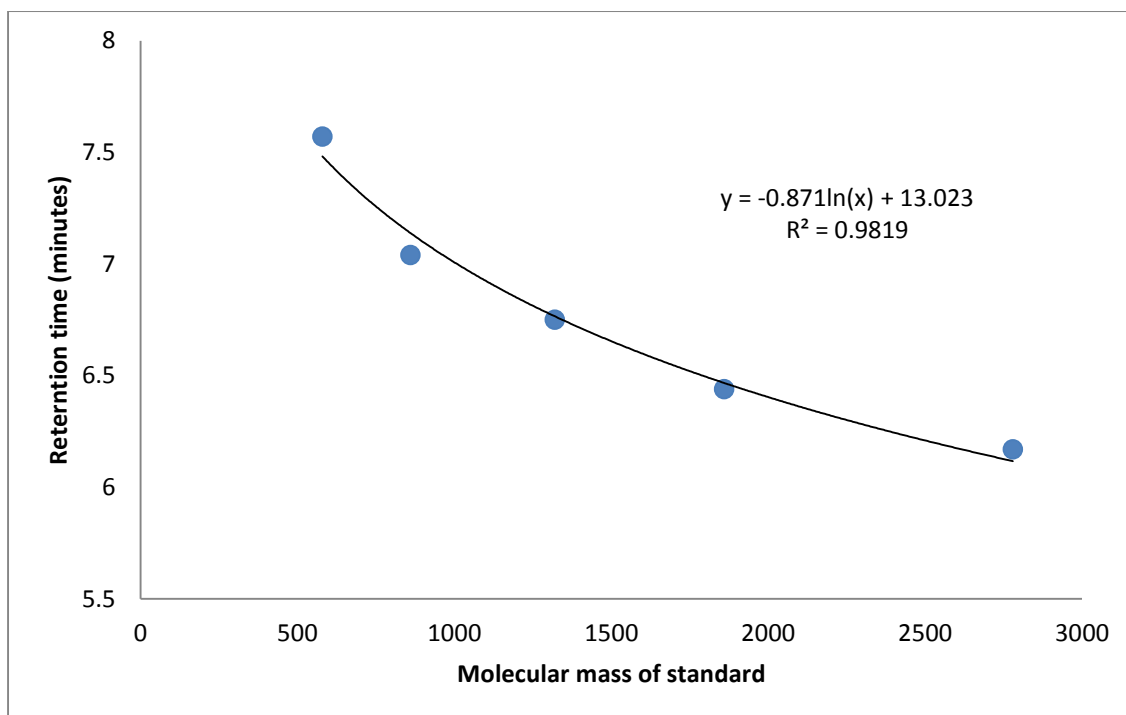
Signal 1: RID1 A, Refractive Index Signal

Peak #	RetTime [min]	Type	Width [min]	Area [nRIU*s]	Height [nRIU]	Area %
1	5.836	BV	0.3024	1.04398e6	5.12532e4	32.2327
2	6.571	VV	1.2661	4.95654e5	5146.74072	15.3032
3	7.830	VV	0.2228	1.18905e5	7368.51465	3.6712
4	8.467	VV	0.8364	7.17613e5	1.04975e4	22.1561
5	9.899	VP	0.7543	6.25936e5	1.20222e4	19.3256
6	10.656	VV	0.3540	2.36806e5	1.08479e4	7.3113

Totals : 3.23890e6 9.71360e4

Results obtained with enhanced integrator!

Signal 2: VWD1 A, Wavelength=244 nm



Appendix 1. Calibration of molecular mass of polystyrene standards against the retention time.

Using the calibration curve above for the standards, the relative estimated average molecular mass of PPG samples is shown in the Table below.

Molecular mass provided by the manufacturer (Da)	Calculated relative average molecular mass (Da)
425	574
725	1183
1000	1455
2000	2831
2700	3816